

https://dspace.org/

Estimating Resistance and Performance of Earthing Systems Electrode in Variably Saturated Soil Conditions

Nnamdi, Onyedikachi Samuel

2024

University of the Witwatersrand, Johannesburg

https://hdl.handle.net/10539/45433

Nnamdi, Onyedikachi Samuel . (2024). Estimating Resistance and Performance of Earthing Systems Electrode in Variably Saturated Soil Conditions [PHD thesis, University of the Witwatersrand, Johannesburg]. WIReDSpace.

Downloaded from a DSpace repository. https://dspace.org/

UNIVERSITY OF THE WITWATERSRAND

Doctor of Philosophy in Engineering

Estimating Resistance and Performance of Earthing Systems Electrode in Variably Saturated Soil Conditions

Onyedikachi Samuel Nnamdi

Supervisor: Prof Chandima Gomes

A thesis submitted to the Faculty of Engineering and Built Environment, University of the Witwatersrand, in partial fulfilment of the requirements for the award of the degree of Doctor of Philosophy in Engineering.

September 2024



Declaration

I, **Onyedikachi Samuel Nnamdi**, declare that this thesis titled "**Estimating Resistance and Performance of Earthing Systems Electrode in Variably Saturated Soil Conditions**", and the contents presented in it are my unaided work. I confirm that this work was performed while I was a candidate for a research degree at the University of the Witwatersrand, Johannesburg. I declare that this thesis is being submitted for the degree of Doctor of Philosophy in Engineering at this University. That to the best of my knowledge, it has not been presented before for any degree or examination at any other university.

Signature: 

Date: 26/09/2024

Abstract

The design and determination of post-installed resistance of earthing systems are significantly influenced by subsoil resistivity profiles, which are prone to seasonal variations due to environmental and climatic changes. These fluctuations can compromise operational safety and reliability of transmission systems, necessitating periodic monitoring of earthing installations as recommended by national and international standards. However, compliance with these recommendations is often impractical due to the vast number of earthing installations and associated costs. To address this challenge, this thesis proposes a novel multiphysics earthing model that integrates hydraulic and electrical properties of subsoil and earthing enhancement materials (EEMs) with climatic parameters to predict earthing resistance under varying conditions. The model, developed by coupling partial differential equations governing electric current dispersion and fluid retention in porous media, is validated through COMSOL Multiphysics® simulations of vertical earth rods in single and double subsoil layers. The results demonstrate that earthing resistance variation is dependent on subsoil texture, water content, and distribution of soil water potential, which determines subsoil resistivity. The proposed method achieves a relative error range of 2.72% to 6.53% and 1.47% compared to analytical and finite element method solutions, ensuring accuracy and validity. This innovative approach enables site-specific and climate-adaptive assessments of EEM effectiveness, facilitating informed decisions for earthing improvements in diverse conditions, and ultimately optimising material selection and recommendation for various soils and climates.

Dedication

I dedicate this work to two extraordinary individuals who have been my pillars of strength. To my mother, Mrs. Ijeoma Victoria Samuel, whose vision for my education and unwavering support have shaped me into the person I am today. Your selflessness and guidance have been a constant source of inspiration, and I am forever grateful. To my beloved wife, Prisca Funa Samuel, whose love, encouragement, and partnership have brought joy and fulfilment to my life. You are my rock, my confidante, and my best friend. Thank you for being my everything.

Acknowledgements

I extend my deepest gratitude to those who have supported me throughout this academic journey.

First and foremost, I am grateful to Nnamdi Azikiwe University Awka for approving my study leave and sponsoring my research grant from the Tertiary Education Trust Fund (TetFund) between 2018 and 2020.

I am indebted to my supervisor, Prof Chandima Gomes, for his unwavering guidance, counsel, and encouragement. His dedication to my success has been a constant source of inspiration, and I am forever grateful. My thanks also go to Eskom High Voltage Centre for Excellence at the University of the Witwatersrand (Wits) for their financial support, which enabled me to secure research materials, devices, and attend conferences.

I also wish to express my sincere appreciation to the immediate past Head of School, Prof Estelle Trengove, for providing me with valuable opportunities and exposures.

I would like to thank the following individuals for their contributions: Mr Sifiso, Mr Philip, Mr Ronnett, Mr Abraham, and Mr Jabu at the Wits High Voltage Laboratory; Mrs Mumtaz Adams, Mrs Jeanine, and Mrs Jeanne for their administrative support; Mrs Tumelo Sithole for her assistance at the geotechnical laboratory; Mr Uzor Okafor for his kindness and hospitality; and Mr Austine Onyeabor (Daddy Angie) and his family for their warmth and generosity.

I also appreciate the support and encouragement from Dr Peter Oviroh, Dr Samuel Olaniran, Dr Zee, and Mr Philip; Dr Gideon Nnachi and his family; and Dr Abi.

My heartfelt thanks go to my family: my son, Chivunirim, and his sister, Chimubaram, for being my motivation; my sister, Mrs Jemimah Gabriel, and her family; my brother, Mr Palmtree, and his family; my mother, for her unwavering support and prayers; my mother-in-law; and my sister-in-law, Mrs Chimuanya Sarah Ezeh. To my lovely wife, Prisca Ifunanya Onyedikachi, I am grateful for her partnership and support. Together, we will always succeed.

Finally, I give glory, honour, worship, and praise to Almighty God, who has supplied me with grace, protection, and provision throughout this journey.

List of Research Publications

[1] S.N. Onyedikachi, C. Gomes, and J. van Coller, “Equations for Predicting the Volumetric Water Content affecting the Resistivity of Soil in the Vicinity of a Driven Earth Electrode in Variably Saturated Homogeneous Soil,” in *2022 36th International Conference on Lightning Protection (ICLP)*, Cape Town, South Africa: IEEE, Oct. 2022, pp. 1–6. doi:10.1109/ICLP56858.2022.9942536.

[2] O.S. Nnamdi and G. Chandima, “New Method for Modelling Seasonal Variation in Resistance and Performance of Earthing Systems,” *Energies*, 16(19): 7002, Oct. 2023, doi:10.3390/en16197002.

[3] S.N. Onyedikachi and C. Gomes, "Modelling Performance Variation of Earthing Enhancement Materials in Different Soils and Conditions," *2024 32nd Southern African Universities Power Engineering Conference (SAUPEC)*, Stellenbosch, South Africa, 2024, pp. 1-6, doi:10.1109/SAUPEC60914.2024.10445044.

Table of Contents

Title Page i
Declaration ii
Abstract iii
Dedication iv
Acknowledgements v
List of Research Publications vi
Table of Contents vii
List of Tables xi
List of Figures xiii
List of Mathematical Symbols xvi
List of SI Units xviii
List of Acronyms and Abbreviations xix
Chapter 1 - Introduction, Problem Statement, and Research Aim 1
1.0 Introduction 1
1.1 Research Motivation 5
1.2 Significance of Research 5
1.3 Research Problem 6
1.4 Research Questions 6
1.5 Research Aim and Objectives 7
1.6 Limitations of Research 8
1.7 Outline of Chapters 9
Chapter 2 - Literature Review and Mathematical Modelling of Proposed Method 11
2.0 Introduction 11
2.1 Seasonality of Subsoil Condition 11
2.1.1 Factors Influencing Seasonality of Earthing Resistance 12
2.1.2 Implications of Seasonality on Safe Potential Limits 12
2.2 Limitations of the IEC 62561 Standard 13
2.2.1 Research in Earthing Enhancement Materials Applications 13
2.2.2 Performance Variation of Earthing Enhancement Materials 14
2.3 Methods of Estimating the Seasonal Variation of Soil Resistivity 14
2.3.1 Methods Using Factors and Artificial Intelligence 15
2.3.2 Limitations of Existing Methods 15
2.4 Need for Paradigm Shift 16
2.4.1 Soil Water Retention and Resistivity 16
2.4.2 Hydro-Geophysical Models of Earthing Systems 17
2.5 Soil Composition, Property and Energy State 17
2.5.1 Composition of Soil and Subsoil 17
2.5.2 Soil Water Content 19

2.5.3 Soil Resistivity and Water Content 20
2.5.4 Modelling Electrical Current Flow in Subsoil 21
2.5.5 Energy State of Soil Water 23
2.5.6 Force of Fluid Flow in Unsaturated Soil 24
2.6 Soil Suction 24
2.6.1 Relationship Between Suction and Pressure Head 25
2.6.2 Suction Profile of Subsoil 26
2.6.3 External Influence on Soil Suction 26
2.7 Atmospheric Description of Climates 27
2.7.1 Parameters for Modelling Climatic Conditions 27
2.7.2 Relative Humidity and Subsoil Suction 28
2.8 Water Flow in Porous Medium 29
2.8.1 Coefficient of Permeability of the Soil 30
2.8.2 Modelling Fluid Flow in Unsaturated Porous Medium 30
2.8.3 Soil Water Characteristics Curve 32
2.8.4 Hydraulic Conductivity of Porous Medium 35
2.8.5 Equations of Water Retention 36
2.9 Multiphysics Coupling of Fluid and Electric Current Flows in Subsoil 37
2.10 Definition of Terms 39
Chapter 3 - Research Methodology and Simulation Modelling of Proposed Method 40
3.0 Introduction to Research Methodology 40
3.1 Model Development 40
3.2 Hydro-Geoelectric Earthing Modelling in COMSOL Multiphysics® 42
3.2.1 Geometric Modelling of Earthing Electrode in the Subsoil 43
3.2.2 Definition Branch of the Model Builder 45
3.2.3 Physics Interfaces 47
3.2.4 Multiphysics Coupling Equation 49
3.2.5 Modelling Assumptions 49
3.2.6 Initial Condition 50
3.2.7 Boundary Conditions 50
3.2.8 Geometric Discretisation 52
3.2.9 Study Modes and Solvers 54
3.2.10 Modelling Hydraulic and Electrical Parameters 55
3.2.11 Post-Processing Analysis and Validation 56
3.2.12 Modelling Cases and Scenarios 58
Chapter 4 - Effect of Soil Texture and Hydraulic Properties on Resistance and Performance of Earthing Systems 60
4.0 Introduction 60
4.1 Simulation of Hydro-Geophysical Earthing Modelling 60
4.1.1 Subsoil Resistivity 63

4.1.2 Model Validation 64
4.1.3 Distribution of Ground Electric Potential 65
4.2 Model Sensitivity....68
4.2.1 Effect of Infinite Element Domain....69
4.2.2 Effect of the Width of Infinite Element Domain 70
4.2.3 Effect of Infinite Element Domain on Ground Surface Electric Potential....71
4.2.4 Effect of Infinite Element Domain on Earthing Resistance....72
4.2.5 Effective Size of Subsoil Domain Width 74
4.3 Hydro-Geophysical Earthing Modelling with Earthing Enhancement Materials in Single-Layer Subsoil 77
4.3.1 Effect of Volume of Earthing Enhancement Material 82
4.3.2 Resistance Reduction of Earthing Enhancement Materials in Single-Layer Subsoils....84
4.4 Hydro-Geophysical Earthing Modelling of Two-Layer Subsoil....85
4.4.1 Resistivity of Sublayers in Two-Layer Subsoil Model....86
4.4.2 Resistance of Earthing System in Two-Layer Subsoil Model 87
4.4.3 Resistance Reduction of Earthing Enhancement Materials in Two-Layer Subsoils....89
Chapter 5 - Equation Formulation Water Content Variation Within the Region of Influence of Vertical Earth Electrodes....97
5.0 Sphere of Influence of Earth Electrode 97
5.1 Volume of the Sphere of Influence of Earth Electrode 97
5.1.1 Effects of the Region of Influence and Soil Domain on Earthing Modelling in Single-Layer Subsoil 98
5.1.2 Effects of the Region of Influence and Soil Domain on Earthing Modelling in the Two-Layer Subsoil 100
5.2 Formulation of Gradient Function of Water Content 102
5.2.1 Profile of Soil Water Under Suction 102
5.2.2 Predicting Volumetric Water Content in Variably Saturated Region of Influence of Rod in Single-Layer Subsoil....105
5.2.3 Predicting Volumetric Water Content in Variably Saturated Region of Influence of Rod in Two-Layer Subsoil....109
5.3 Application in Single-Layer Subsoil Model....114
5.3.1 Estimating Gradient Function 114
5.3.2 Prediction of Volumetric Water Content Within Region of Influence of Vertical Earth Rod in Single-Layer Subsoil 116
Chapter 6 - Performance of Earthing Systems in Different Soils and Climates 118
6.0 Introduction 118
6.1 Spatial and Temporal Changes of Subsoil Suction 118
6.1.1 Estimating Diffusion Coefficient, α....119
6.1.2 Estimating Climate Frequency, nf 120
6.2 Modelling Climate-Based Variation of Soil Suction....120
6.2.1 Limits of Suction at Soil Depth....122
6.2.2 Maximum Change of Soil Suction....123

6.2.3 Critical Coefficients of Periodic Suction Expression....123
6.2.4 Equations of Subsoil Suction Profile of Climates With Two Seasons....124
6.3 Application: Formulations of Temporal Variation of Suction in Different Climates....127
6.4 Application: Earthing System Performance in Different Climatic Zones....133
6.4.1 Earthing System Without EEM in Single and Double-Layer Subsoils....136
6.4.2 Earthing System With EEM in Single- and Double-Layer Subsoils....139
Chapter 7 - Conclusion and Recommendations....143
7.0 Conclusion....143
7.1 Research Contributions....144
7.2 Research Limitation....145
7.3 Recommendation for Future Research....145
References....146
Appendices....157
Appendix A: Tables A1 to A26....157
Appendix B....183
Appendix B1: Components and forms of energy state of soil water....183
Appendix B2: Chain rule and derivative of the SWRC....184

List of Tables

Table 3.1: Models of single-layer, double-layer, and triple-layer subsoils consisting of the combinations of clay, silty and sandy textured soils. 44
Table 3.2: Input and output mesh statistics for 2D axisymmetric of vertical earth rod in homogeneous soil and 3D model of earthing grid in homogeneous soil....53
Table 3.3: Hydraulic and electrical parameters of three soil textures for earthing subsoil modelling. 55
Table 3.4: Hydraulic and electric parameters of earthing enhancement materials (EEM) 55
Table 3.5: Summary of model cases for the proposed method of earthing design and resistance evaluation and prediction....59
Table 4.1: Comparing the subsoil volumetric resistivity derived from the proposed model 64
Table 4.2: Comparing the resistance of the proposed model to models in literature....65
Table 4.3: Transition and residual suction values and corresponding volumetric water contents derived suction transition width and transition gradient....79
Table 4.4: Descriptive statistics for percentage resistance reduction of two-layer subsoil models for three top layer depths 91
Table 4.5: Descriptive statistics of percentage resistance reduction of EEM I and EEM II in two-layer silty-sandy clay subsoil....95
Table 6.1: Analytical description of surface suction during wet and dry seasons in sub-humid, arid and semi-arid climatic zones....128
Table 6.2: Descriptive statistics of resistivity of clay, silty, and sandy clay soils in sub-humid, arid, and semi-arid climates. 136
Table 6.3: Descriptive statistics of resistance of earthing rod in clay, silty, and sandy clay soils under sub-humid, arid, and semi-arid climates. 138
Table 6.4: Descriptive statistics of resistance reduction of earthing enhancement materials (EEM I and EEM II) in silty and sandy clay soils under sub-humid and arid climates. 142
Table A1: Measured values of water content and resistivity for EEM I....157
Table A2: Post-simulation computed resistance Re (Ω) of earthing rod in a single layer and corresponding volumetric water content, subsoil resistivity and soil suction....158
Table A3: Mesh statistics for soil domain showing infinite element domain (IED) 159
Table A4: Effect of width of infinite element domain on earthing resistance 160
Table A5: Effect of infinite element domain on ground surface electric potential....161
Table A6: Effect of subsoil size with infinite element size on subsoil water content and resistivity)....162
Table A7: Effect of size of subsoil domain on hydro-geophysical earthing modelling....163
Table A8: Sensitivity of subsoil depth on the simulation earthing modelling....164
Table A9: Resistance reduction different earthing enhancement materials in single layer silty and sandy clay subsoils for varying degrees of saturation....165
Table A10: Suction-induced variability of soil layer resistivity for clayey, silty and sandy clay as top and bottom layer subsoils....166
Table A11: Volumetric water contents of soil textures as top and bottom layer soils....167
Table A12: Resistance vertical earth rod in single- and two-layer subsoils 168
Table A13: Volumetric water contents within the subsoil domain and region of influence of vertical rod of three single-layer subsoils....169
Table A14: Resistance of vertical earth rod relative to the subsoil domain and region of influence of vertical rod of three single-layer subsoils....170
Table A15: Resistance of vertical earth rod relative to the region of influence and presence of infinite element domain for two two-layer subsoil models....171
Table A16: Coefficients of regression and corresponding coefficient of determination for minimum water content for silty subsoil....172
Table A17: Water content gradient function coefficients and minimum volumetric water content valid for less than 10.5 m depth of single-layer subsoil 173
Table A18: Coefficients of the regression of water content for subsoil depth of 0.1 m 174

Table A19: Water content gradient function coefficients for 0.1 m to 10.5 m depth of single-layer silty subsoil 175
Table A20: Comparison of resistance evaluated from gradient function and hydro-geophysical earthing model 176
Table A21: Coefficients of the expanded Fourier series from the equation of soil suction of three climates.....177
Table A22: Climatic frequency (nf) and soil diffusion coefficient (α) for different time scale 178
Table A23: Daily variation of the volumetric water content of silty, sandy clay and clay subsoils in sub-humid, arid, and semi-arid climates 179
Table A24: Resistivity of silty, sandy clay, and clayey subsoils in sub-humid, arid, and semi-arid climates.....180
Table A25: Daily variation of ground surface suction and corresponding resistivity of two earthing enhancement materials in sub-humid, arid and semi-arid climates 181
Table A26: Effect of earthing enhancement materials on the daily variation of resistance of vertical earth rod in silty and sandy clay soils under sub-humid and arid climates 182

List of Figures

Figure 2.1: Soil Texture Triangle Classification based on World Reference Base for Soil Resources (WRB) 18
Figure 2.2: Schematic diagram showing a vertical section of the subsoil from the ground surface to the unconfined saturated zone through the unsaturated or vadose zone 19
Figure 2.3: Soil water retention curve as a semi-logarithmic plot of volumetric water content (θ) versus suction (ψ) showing critical regions and points 33
Figure 2.4: Soil water retention curve as a semi-logarithmic plot of soil suction (ψ) against the degree of saturation (Sd) showing critical regions and points....33
Figure 3.10: Mesh plot of 2D axisymmetric vertical earth rod in single-layer subsoil showing good quality mesh element in green colour....54
Figure 4.1: Soil water retention curves for sandy clay, silty and clay soils.....61
Figure 4.2: Graphical variation of electric conductivity of sandy clay, silty and clay soil with volumetric water content....61
Figure 4.3: Soil suction resistivity curve of sandy clay, silty and clay soils....62
Figure 4.4: Resistance of vertical earth rod in single-layer clay, silty, and sandy clay subsoils 64
Figure 4.5: Distribution of ground surface electric potential on clay, silty, and sandy clay subsoils under saturation conditions 66
Figure 4.6: Ground surface distribution of electric potential on clay, silty, and sandy clay soils under field capacity (-33 kPa) conditions....66
Figure 4.7: Ground surface distribution of electric potential on clay, silty, and sandy clay subsoils under permanent wilting point suction (-1500 kPa) condition....67
Figure 4.8: Comparison of ground surface electric potential at distance of 7.5 m from earth rod in clay, silty, and sandy clay subsoils at saturation and field capacity suctions....67
Figure 4.9: Comparison of ground surface electric potential of 7.5 m from earth rod in clay, silty, and sandy clay subsoils at field capacity and permanent wilting point suctions 68
Figure 4.10: Distribution of mesh element of hydro-geophysical vertical earthing rod in different single-layer subsoil models....69
Figure 4.11: Plot of electric potential on the ground surface for subsoil model at field capacity suction....71
Figure 4.12: Plot of electric potential on the ground surface for subsoil model at permanent wilting point suction 71
Figure 4.13: Plot of electric potential on the ground surface for subsoil model....72
Figure 4.14: Percentage difference histogram of simulation and analytical earthing resistance of vertical rod in three subsoil domain widths....74
Figure 4.15: Plot of the ratio of electric potential to subsoil width against subsoil width for pressure head at field capacity and permanent wilting point 74
Figure 4.16: Distribution of ground surface electric potential for different width of subsoils under permanent wilting point suction....75
Figure 4.17: Percentage difference of simulation and analytical derived resistance for vertical earthing rod in single-layer soil without infinite element domain....76
Figure 4.18: Water retention curves of silty and sandy clay subsoils with earthing enhancement materials....78
Figure 4.19: Plot of electric conductivity against volumetric water content for silty and sandy clay subsoils, and two earthing enhancement materials....80
Figure 4.20: Plots showing the variation of electric conductivity of soil and earthing enhancement materials (EEMs) with volumetric water content 80
Figure 4.21: Variation of percentage resistance reduction of 0.1152 m radius of two earthing enhancement materials in sandy clay and silty subsoils 81
Figure 4.22: Variation of percentage resistance reduction of 0.32256 m radius of two earthing enhancement materials in sandy clay and silty soils....82
Figure 4.23: Percentage resistance reduction of different radii of two earthing enhancement materials in sandy clay subsoil under different soil suctions....82
Figure 4.24: Percentage resistance reduction different radii of two earthing enhancement materials in silty subsoil under different soil suctions....83

Figure 4.25: Effect of diameter of earthing enhancement materials on the percentage resistance reduction in sandy clay subsoil 83
Figure 4.26: Effect of diameter of earthing enhancement materials on the percentage resistance reduction in silty subsoil 84
Figure 4.27: Plot of percentage resistance reduction against radius of earthing enhancement materials in single-layer sandy clay and silty subsoils 85
Figure 4.28: Suction-induced variability of soil resistivity in top and bottom layers of two-layer subsoil model 86
Figure 4.29: Comparison of volumetric water content in single layer, against sandy clay sublayer above and below clay subsoil layer 87
Figure 4.30: Variation of resistance of vertical earth rod in single and two-layer subsoils with top layer depth of 1.4 m 88
Figure 4.31: Effect of topsoil depth on the resistance of 3 m long vertically driven earth rod in two-layer (sandy clay-silty) subsoil 89
Figure 4.32: Suction resistivity curve of sandy clay and silty subsoils and two earthing enhancement materials (EEM I and EEM II) 90
Figure 4.33: Comparison of resistance reduction performance of two 0.1152 m radius earthing enhancement materials (EEM I and EEM II) around a vertical earth rod relative to the resistance of earth rod without earthing enhancement 90
Figure 4.34: Soil suction induced percentage resistance reduction variation of two earthing enhancement materials 92
Figure 4.35: Soil suction induced percentage resistance reduction variation of an earthing enhancement materials (EEM I) around a vertical earth rod in two double-layer subsoils 93
Figure 4.36: Soil suction induced percentage resistance reduction variation of two separate earthing enhancement materials (EEM II) around a vertical earth rod in two double-layer subsoils 93
Figure 4.37: Soil suction induced percentage resistance reduction variation of two earthing enhancement materials around a vertical earth rod in a double-layer (silty-sandy clay) subsoil 94
Figure 4.38: Soil suction induced percentage resistance reduction variation of two earthing enhancement materials (EEM I and EEM II) of different radius around a vertical earth rod in a double-layer (silty-sandy clay) subsoil of 0.8 m depth of top subsoil layer. 96
Figure 5.1: Annotated 3D view of earthing model showing the region of influence of vertical earth rod 98
Figure 5.2: Percentage difference of volumetric water contents in entire domain and region of influence of subsoil on the vertical earth rod and the corresponding earthing resistances for single-layer subsoil 99
Figure 5.3: Percentage difference of volumetric water contents in entire subsoil domain and region of influence of the vertical earth rod and the corresponding earthing resistances for different depths of topsoil of a double-layer subsoil 101
Figure 5.4: Percentage difference of volumetric water contents in entire subsoil domain and region of influence of the vertical earth rod and the corresponding earthing resistances for two different depths of topsoil of two double-layer subsoil 101
Figure 5.5: Region of influence of vertical earth rod showing saturated and unsaturated zones of the subsoil ..106
Figure 5.6: 2D cross-sectional view of the region of influence of vertical earth rod in two-layer subsoil model 110
Figure 5.7: 2D cross-sectional view the region of influence of vertical earth rod in a two-layer showing the saturation depth 112
Figure 5.8: 2D cross-sectional view the region of influence of vertical earth rod in a two-layer showing the saturation depth 113
Figure 5.9: Regression plot determining the coefficients of the water content gradient function $\theta s(z)$ at soil depth (z) due to pressure head at $z = zs$ 115
Figure 6.1: Time plot of surface suction for predominantly arid climate. 124
Figure 6.2: Illustrative surface suction-time plot of a predominantly humid climate. 126
Figure 6.3: Typical wet and dry seasonal cycle in sub-humid, arid and semi-arid climates. 127
Figure 6.4: Typical daily variation of ground surface suction in sub-humid, arid and semi-arid climates 129
Figure 6.5: Daily variation of suction from ground surface to depth of constant suction in sub-humid climate 130

Figure 6.6: Daily variation of suction from ground surface to depth of constant suction in arid climate. 130
Figure 6.7: Daily variation of suction from ground surface to depth of constant suction in semi-arid climate ..131
Figure 6.8: Daily variation of suction at depth exhibiting constant suction in sub-humid, arid, and semi-arid climates 131
Figure 6.9: Profile of monthly ground surface and subsurface suctions in a sub-humid climate 132
Figure 6.10: Profile of monthly ground surface and subsurface suctions in arid climate.....132
Figure 6.11: Profile of monthly ground surface and subsurface suctions in a semi-arid climate 133
Figure 6.12: Daily variation of surface suction and volumetric water content of clay, silty and sandy clay subsoils in sub-humid climate.....134
Figure 6.13: Daily variation of surface suction and volumetric water contents of clay, silty and sandy clay subsoils in arid climate.....134
Figure 6.14: Daily variation of surface suction and volumetric water contents of clay, silty and sandy clay subsoils in semi-arid climate.....135
Figure 6.15: Daily variation of resistance of vertical rod in silty, clay, and sandy clay subsoils under (a) sub-humid, ((b) arid, and (c) semi-arid climates.....137
Figure 6.16: Daily variation of resistance of vertical rod of silty, clay, and sandy clay single-layer subsoils under arid climate.....138
Figure 6.17: Daily variation of resistance of vertical rod without and with earthing enhancement materials (EEM I and EEM II) each of radius 115.2 mm in single-layer silty subsoil under sub-humid climate 140
Figure 6.18: Daily variation of resistance of vertical rod without and with earthing enhancement materials (EEM I and EEM II) each of radius 115.2 mm in single-layer silty subsoil under arid climate 140
Figure 6.19: Daily variation of resistance of vertical rod without and with earthing enhancement materials (EEM I and EEM II) each of radius 115.2 mm in single-layer sandy clay soil under sub-humid climate.....141
Figure 6.20: Daily variation of resistance of vertical rod without and with earthing enhancement materials (EEM I and EEM II) each of radius 115.2 mm in single-layer sandy clay soil under arid climate.....141

List of Mathematical Symbols

β ..... saturation index or exponent

a_z, b_z, c_z .....coefficients of water content gradient function

I_f ..... current dissipated from earth electrode

V_m ..... electric potential at the edge of earthing enhancement material

V_{sat} .....volume of saturated portion of region of influence of electrode

V_{ui}, V_{si} volumes of unsaturated and saturated portions within the region of influence of *earth electrode in* ith *layer*

X_θ, X_{se} ..... dummy variables assigned for domain probe average water content and effective saturation

α_h (m^{-1}) .....inverse of suction at air entry poin

α_s .....Gardner soil characteristic

ρ_1, ρ_2 .....resistivity of top and bottom layers of two-layer subsoil

ρ_l ($kg \cdot m^{-3}$) .....density of liquid in soil

$\partial h_p/\partial z$ ..... pressure head gradient in subsoil

$\partial\theta/\partial z$ ..... water content gradient

$d\theta/dh_p$ .....derivative of water retention curve

$\Delta U(z)_{max}$ ..... maximum suction change at any depth, z

$\Delta\theta_{tr} = \theta_t - \theta_r$ ..... width of transition volumetric water content

$\Delta\psi_{tr}$ .....suction transition width or width of transition suction

A_σ ..... product of liquid conductivity and porosity coefficients

C [L^{-1}] ..... specific water capacity of the soil

D_1, D1 or h_1 .....depth of top layer of subsoil

d_s ..... depth of subsoil

d_u ..... depth of unsaturated soil portion of region of influence of earth electrode

E_{ir} ..... electric field strength at r horizontal distance from the electrode in the ith layer

$Econ(X_\theta)$, $Econ(X_{se})$ dummy variable for electric conductivity in terms of average water content and effective saturation

h_a ..... bubbling pressure or suction

h_{pwp} ..... pressure head at permanent wilting point

h_s, h_r .....pressure head at saturated and residual water contents

i ..... index of subsoil layer

$K(h_p)$, $K(\theta)$ .....unsaturated hydraulic conductivity as function of pressure head and water content

k_c ..... reflection coefficient between adjacent layers of subsoil

l ..... connectivity-tortuosity coefficient (pore-connectivity parameter)

L_r ..... length of earth rod

ɱ ..... cementation factor

m_c .....index of non-zero Fourier coefficients of sinusoidal suction function

$\vec{n}$ .....normal vector

n, m: .....van Genuchten soil water retention model fitting parameters

n_f (cycle/year) ..... seasonal frequency

q .....flux or flow rate of water in a porousmedium

R_{e12} ..... resistance of earth electrode in two-layer subsoil

r_r ..... radius of earth rod

S_{se} ..... dummy variable for effective saturation

t .....time

u ..... flux vector

$U(z,t)$ .....spatial and temporal variation of suction at any depth, z and time, t

$U_0, U_1, U_2, \ldots$: .....Fourier coefficients of sinusoidal suction function

U_a .....amplitude of surface suction (pF)

U_e .....constant or equilibrium suction

v ..... flow velocity

V ..... voltage

V_E .....voltage at surface of earth electrode

V_{Ei} ..... electric potential at surface of earth electrode in the i^{th} subsoil layer

V_i .....volume of i^{th} layer within the region of influence of earth electrode

V_{ri} ….. electric potential at a horizontal distance r from the electrode surface in the i^{th} layer

W_{cs} .....dummy variable for average water content

z_{es} .....active zone or penetration depth

z_s ..... depth of saturation or aturation depth

z_v ..... depth of region of influence of electrode

α [L^2/T] ..... diffusion coefficient

$\theta_{(z=0.1m)}$ .....water content at depth of 0.1 m

θ_a ..... ratio of volume integral of gradient function to volume of subsoil

$\theta_{ae}, \theta_{fc}, \theta_{ip}, \theta_{wp}$ .... volumetric water content at air entry point, field capacity, inflexion point, and wilting point

θ_{ave} .....average volumetric water content partially or unsaturated soil

θ_{min} .....minimum water content

θ_u ..... unsaturated water content gradient function

θ_a .....water content at z depth

κ_r ..... relative permeability

μ (Pa.s) ..... dynamic viscosity of fluid

ρ_{roi} ..... resistivity of soil in region of influence of earth electrode

σ_i ..... electric conductivity of soil in the i^{th} sublayer

$\psi_{ae}, \psi_{fc}, \psi_{ip}, \psi_{wp}, \psi_r$ soil suction at air entry point, field capacity, inflexion point, wilting point, and residual state

List of SI Units

The seven base units

Name	Symbol	Quantity
second	s	time
metre	m	length
kilogram	kg	mass
ampere	A	electric current
kelvin	K	thermodynamic temperature
mole	mol	amount of substance
candela	cd	Luminous intensity

Twenty-two coherent derived units

Name	Symbol	Quantity	In SI base units
radian	rad	plane angle	m/m
steradian	sr	solid angle	m^2/m^2
hertz	Hz	frequency	s^{-1}
newton	N	force, weight	kg m s^{-2}
pascal	Pa	pressure, stress	kg m^{-1} s^{-2}
joule	J	energy, work, heat	kg m^2 s^{-2}
watt	W	power, radiant flux	kg m^2 s^{-3}
coulomb	C	electric charge	s A
volt	V	electric potential, voltage, emf	kg m^2 s^{-3} A^{-1}
farad	F	capacitance	kg^{-1} m^{-2} s^4 A^2
ohm	Ω	resistance, impedance, reactance	$kg{\cdot}m^2{\cdot}s^{-3}{\cdot}A^{-2}$
siemens	S	electrical conductance	$kg^{-1}{\cdot}m^{-2}{\cdot}s^3{\cdot}A^2$
weber	Wb	magnetic flux	$kg^{-1}{\cdot}m^{-2}{\cdot}s^3{\cdot}A^2$
tesla	T	magnetic flux density	$kg{\cdot}s^{-2}{\cdot}A^{-1}$
henry	H	inductance	$kg{\cdot}m^2{\cdot}s^{-2}{\cdot}A^{-2}$
degree Celsius	°C	temperature relative to 273.15 K	K
lumen	lm	luminous flux	$cd{\cdot}m^2/m^2$
lux	lx	illuminance	$cd{\cdot}m^2/m^4$
becquerel	Bq	activity referred to a radionuclide (decays per unit time)	s^{-1}
gray	Gy	absorbed dose (of ionising radiation)	$m^2{\cdot}s^{-2}$
sievert	Sv	equivalent dose (of ionising radiation)	$m^2{\cdot}s^{-2}$
katal	kat	catalytic activity	$mol{\cdot}s^{-1}$

List of Acronyms and Abbreviations

2D: ..... Two-Dimensional
3D: ..... Three-Dimensional
AC/DC: ..... Alternating Current and Direct Current
ANN: ..... Artificial Neural Network
ASTM: ..... American Society for Testing and Materials
CDEGS: ..... Current Distribution, Electromagnetic and Grounding System
CEC: ..... Cation Exchange Capacity
CMDE: ..... Coupled Multiphysics Differential Equation
CY: ..... Clayey Soil
EC: ..... Electric Currents
EEM: ..... Earthing Enhancement Material
FC: ..... Field Capacity
FEM: ..... Finite Element Method
GRNN: ..... Generalised Regression Neural Networks
IEC: ..... Internaltional Electrotechnical Commission
IED: ..... Infinite Element Domain
IEEE: ..... Institute of Electrical and Electronics Engineers
MUMPS: ..... Multifrontal Massively Parallel Sparse
PARDIS: ..... Parallel Sparse Direct Solver
PDE: ..... Partial Differential Equation
pH: ..... Potential of Hydrogen
PSD: ..... Pore Size Distribution
RE: ..... Richards' Equation
ROI: ..... Region of Influence of Earth Electrode
RSCC: ..... Resistivity Suction Characteristic Curve
RWCC: ..... Resistivity Water Characteristic Curve
SC: ..... Sandy Clay Soil
SCI: ..... Suction Compression Index
SRC: ..... Suction Resistivity Curve
ST: ..... Silty Soil
STP: ..... Standard Temperature and Pressure
SWCC: ..... Soil Water Characteristic Curve
SWP: ..... Soil Water Potential
SWRC: ..... Soil Water Retention Curve
T: ..... Temperature
TFR: ..... Tower Footing Resistance
TMI: ..... Thornthwaite Moisture Index
VES: ..... Vertical Electrical Survey
V: ..... Voltage
WAP: ..... Water Acceptance Potential
WRC: ..... Water Retention Curve
WT: ..... Water Table

Chapter 1 - Introduction, Problem Statement, and Research Aim

1.0 Introduction

For reliable power system operation and the safe dissipation of fault and surge currents through buried earthing systems, maximum permissible earthing resistance values are specified by the appropriate standards. Typically, these recommended values are low but vary depending on the specific application. During the design stage, it is necessary to determine the soil resistivity at the intended earthing site to select the appropriate earthing composition and size to achieve the target resistance.

However, soil resistivity undergoes significant seasonal changes due to the alternation between wet and dry periods. This change can lead to high earthing resistance values, which may cause hazardous electrical conditions and disrupt operations [1]. To mitigate such risks, IEEE (the Institute of Electrical and Electronics Engineers) Standard 81 recommends routine monitoring of earthing resistance to identify sites prone to high and unacceptable resistance [2].

To address high soil resistivity, conductive earthing compounds have been used for years to improve earthing in areas with high resistivity and contact resistance. Section 7 of the IEC (International Electrotechnical Commission) 62561 standard recommends various tests for selecting earthing enhancement materials (EEMs), including tests for resistivity, pH (potential of hydrogen), leaching, and sulphur content [3]. A compound is deemed suitable for earthing enhancement if it has low resistivity (smaller than the native soil), a pH of 7, no leaching, and a 2% sulphur content. However, while the standard outlines selection criteria to ensure low resistance, prevent soil contamination, and minimise corrosion, it lacks information on matching EEMs to different soils and climate zones to ensure optimal earthing resistance. Without this information, the selection of EEMs may be subjective, potentially resulting in suboptimal, redundant, expensive, or inefficient earthing designs.

The performance of an earthing system is significantly affected by the resistivity of the surrounding soil and any EEM present [4]. To determine the ground's resistivity profile, a vertical electrical survey (VES) - a non-destructive technique with Wenner and Schlumberger variants - is used. Although supplementary data such as soil texture, structure, type, temperature, and water content can be acquired through on-site inspection, measurement, or laboratory analysis of soil samples, only resistivity is used in the current methodology of earthing design. This means that important soil parameters like temperature, clay, chemical,

and water content are ignored in deciding the type, composition, configuration, and size of the earthing terminal. Even though the resistance of the earthing design meets the specification for the application, the resistance measured post-installation is not fixed and experiences seasonal variations, potentially reaching unacceptably high values [5]. Since the size, composition, and configuration of the earthing terminal remain the same, these seasonal variations in earthing resistance are attributed to the rate and extent of changes in soil resistivity.

Ground resistivity variability is both spatial and temporal. Spatial variation arises from differences in geological composition, structure, sub-layer texture, and the depth from the ground surface to the water table. Temporal variation, or seasonal variation, exists due to environmental and climatic influences. While spatial variation is accommodated by different compositions, sizes, or configurations of earthing designs in different locations, accommodating temporal variation is challenging. Current methods used to account for seasonal changes in resistivity or resistance include artificial neural network (ANN) techniques, correlation, or correction factors [6], [7], [8], [9]. These methods use meteorological rainfall data and resistivity or resistance measurements within an area at a particular time or season to estimate corresponding values at another time or season. However, recognising the limitations of correction and correlation factors, Wang et al. recommend considering the influence of terrain, ground condition, and soil parameters for earthing design and resistance estimations [10].

Generally, soil resistivity is affected by various factors such as clay and chemical contents, salinity, compaction, porosity, water content, and temperature [7], [11], [12], [13]. At unsaturation, soil resistivity is influenced by additional factors including soil texture, porosity, fluid composition, counter-ion content, salinity, crack properties, surface conduction of double layers, mineralisation, permeability or compaction, ionic content of pore fluids, vertical thickness or depth, soil structure, and cross-sectional area of the conductive path [6], [14], [15], [16], [17], [18]. Amongst these variables, temperature and water content exhibit greater susceptibility to climatic and environmental impacts and are sometimes used as modelling variables for resistivity. For instance, Andolfato et al. utilised the temperature-resistivity correlation to develop a time-dependent numerical model capable of predicting soil resistivity at any temperature and time[13]. Under direct current flows, the impact of water content on soil conductivity is more significant than that of temperature [19]. Recently, Wang and colleagues reported that soil water exerts considerable influence on resistivity and some properties of unsaturated soil, including, but not limited to, porosity, compaction, and salinity

[10]. Hence, it is plausible to describe the seasonal fluctuations of ground resistivity solely by considering the variability of soil water content due to environmental and climatic influences.

The condition of the ground is influenced by weather and climate, which determine the extent of dryness or wetness of the soil and the energy state of soil water [20]. The energy state of soil water, denoted by the soil water potential (SWP), describes the total energy that potential soil water experiences. SWP may be expressed in energy per unit weight or hydraulic head. Under certain assumptions or conditions, the hydraulic head may be reduced and expressed in terms of the pressure head, its most dominant component [21]. With the unit of length, the pressure head represents the potential energy or pressure exerted by the weight of water in the soil. Another term representing the energy exerted on soil water is soil suction. As soil loses water, tension or negative pressure is exerted on water within the soil pores, referred to as soil suction. Soil suction, measured in units of pressure, represents the forces that hold water within the soil pores against gravitational forces. Although pressure head and soil suction refer to different aspects of the hydraulic behaviour of soil, their magnitudes are equal but have opposite signs. Therefore, the energy state of soil water can be described by either pressure head or soil suction.

Despite the earthing system being buried in an infinite soil medium, the earthing resistance is primarily determined by the resistivity of a finite volume of soil surrounding the buried earthing system. The water content, suction, and resistivity of the ground surface and superficial sublayers are more susceptible to atmospheric and environmental changes due to their proximity and contact with the atmosphere [7], [13], [22]. For example, in a recent study, Mohamad Nasir et al. reported that during winter, up to 1.5 m depth of soil is frozen, revealing the extent to which soil resistivity is impacted by seasonal changes [10]. The ground surface suction is a cumulative reflection of the atmosphere's and environment's influence on the ground. Precipitation, melting snow, and defrosting ice lead to wet conditions that decrease the ground surface suction, while dry conditions resulting from evaporation or prolonged loss of soil water and freezing temperatures increase ground surface suction [5], [6], [23], [24]. At any time, the net effect of wet and dry conditions influences the suction profile from the highest value at the ground surface to the lowest at the water table.

Various empirical formulas have been proposed, particularly by Archie and Waxman-Smith, establishing the relationship between soil resistivity and the water content or degree of saturation of soil [25], [26], [27], [28], [29]. The soil water characteristic curve (SWCC) or soil water retention curve (SWRC) is a graphical relationship between soil water content and either

soil pressure head or matric suction. SWRCs are unique for different soil textures and can be used to determine soil properties such as hydraulic conductivity, shear strength, water storage, and compressibility of unsaturated soils. To provide a mathematical description of SWRC, retention formulas have been proposed that express water content in terms of suction or pressure head and other fitting parameters.

Kong et al. used the existing SWCC and the resistivity water characteristic curve (RWCC) they formulated to propose a resistivity suction characteristic curve (RSCC) [20]. Their effort established an implicit tripartite correlation between resistivity, soil suction, and water content [20], [30], [31], [32]. The recent multi-disciplinary numerical modelling of corrosion processes in subterranean metal pipes due to differential aeration by Azoor and colleagues illustrates the profound implications of this implicit relationship in engineering applications [33].

Following a field study conducted for over four years on four EEMs, Androvitsaneas et al. [5] concluded that the quantity, duration, and period (time window) of rainfall determine the amount of water available to the ground and that the material memory (water retention capacity) influenced the performance of the EEMs [5]. This is consistent with observations made by Androvitsaneas et al. [34] on five EEMs. Although none of these reports quantified water retention capacity, its mention provides insight into one of the unnamed variables affecting the performance of the EEMs [35].

These observations are consistent with empirical field data involving earthing systems in clay- and sand-rich soils. The superior water retention capacity of clay-rich soils enables earthing systems buried in them to have low resistance values and experience minimal variations over different seasons. However, the inferior water retention capabilities of sandy soils result in high earthing resistance. This basis allows us to conclude that, like soils, the water content of EEMs is subject to external (climate and environmental) influences, which can result in significant seasonal variation in their resistivity [5].

Consequently, given the impact of climate and seasonal variations on soil resistivity and earthing resistance, the inclusion of hydraulic properties of soil, specifically water retention characteristics and hydraulic conductivity, should be considered in the design of earthing systems, the estimation of resistance, and the prediction of resistance values.

1.1 Research Motivation

The seasonal variation in earthing resistance, largely influenced by the water retention characteristics of the soil or soil-EEM pair, poses a significant challenge in the prediction of resistance and for reliable power system operation. The electrolytic nature of current flow within the ground makes these characteristics critical, as they control the rate and extent of seasonal changes in earthing resistance. Despite the distinct electrical properties exhibited by each combination of soil and EEM, there has been insufficient research on identifying the optimal combination that achieves the greatest reduction in resistance while exhibiting minimal seasonal variation.

Understanding the dynamics of soil moisture is essential for addressing this challenge. The amount of water available to the soil is regulated by moisture exchanges between the soil and the atmosphere, influenced by atmospheric conditions, seasonal periods, and cycles. These exchanges are cumulatively modelled as soil suction. By modelling soil suction as a sinusoidal function of climate parameters, soil depth, and time, we can approximate suction at various depths and times. This, in turn, allows us to determine the corresponding water content and resistivity of the soil using the SWCC and empirical functions connecting water content and resistivity.

The distinct water-suction correlations and water retention characteristics of each soil or EEM necessitate a robust methodology for evaluating and forecasting earthing resistance. This approach is crucial for assessing the performance of conductive earthing backfills (EEMs) and predicting ground potential rise across different timescales (hourly, daily, or monthly). By incorporating these factors, this research aims to enhance the efficiency and reliability of earthing design, addressing the impact of climate and seasonal variations on soil resistivity and earthing resistance.

1.2 Significance of Research

The research is significant for several reasons:

1. Innovative approach and enhanced prediction

   Existing methods for predicting seasonal changes in earthing resistance, including correlation factors and artificial neural networks (ANNs), use general rainfall data and historical soil resistivity measurements. However, these approaches frequently neglect important local factors such as vegetation, topography, and soil texture, which influence

water retention and soil resistivity. The proposed method takes a more precise approach by quantifying the amount of water retained in the subsoil and not just rainfall on the subsoil surface. While rainfall and runoff impact large areas, the amount of water infiltrated and retained depends on the hydraulic conductivity and water retention characteristics of the subsoil. Employing an approach not explored before in earthing design and practice, the new method will provide insight for seasonal earthing performance assessment and enhance the accuracy of earthing resistance predictions for specific locations.

2. Effective application of earthing enhancement materials

By quantifying and using actual water content to determine resistivity, the method has potential of estimating the effectiveness of EEMs across different soil types and climatic conditions, leading to improved efficient and cost-effective earthing system designs, reducing the risk of failures and enhancing safety.

3. Alternative to routine earthing resistance monitoring

The proposed method provides a convenient alternative to physical measurement at earthing sites. Utility companies will be able to assess earthing resistance deviations while saving resources, time and personnel.

1.3 Research Problem

Existing methods for predicting seasonal variations in earthing resistance primarily rely on meteorological precipitation data, which does not account for the actual soil condition or its degree of saturation. This leads to potential inaccuracies in predicting earthing resistance. The challenge is to develop a more precise approach that accurately quantifies soil water content and its retention characteristics to better predict and evaluate seasonal changes in earthing resistance.

1.4 Research Questions

How can soil water content and its retention characteristics be accurately quantified to predict and evaluate seasonal variations in earthing resistance of transmission and distribution towers, and how does this approach compare to existing methods that rely solely on meteorological precipitation data?

The four sub-questions are formulated to address the issues of quantifying soil water content, modelling soil resistivity variability, assessing seasonal resistance changes, and evaluating EEM performance across different conditions.

1. How can the water content of the subsoil and its retention characteristics be accurately quantified to predict seasonal variations in earthing resistance for transmission and distribution towers?
2. How can the variability of subsoil resistivity for different soils and climates be modelled to reflect the impacts of atmospheric and seasonal weather conditions?
3. How can the hydraulic and water retention properties of EEMs be utilised to model their performance across different soils and climate zones, and what additional criteria should be considered for selecting EEMs to ensure optimal performance in high-resistivity soils?
4. What additional selection criteria can be recommended in selecting earthing enhancement materials for optimal performance in high-resistivity soils?

1.5 Research Aim and Objectives

The aim of this research is to develop a comprehensive methodology for accurately predicting and evaluating seasonal variations in earthing resistance of transmission and distribution towers. This will be achieved by quantifying subsoil water content and retention characteristics, modelling subsoil resistivity variability, and determining the performance of EEMs across different subsoil profiles and climates. This aim will be achieved through the following objectives:

1. To demonstrate a new method for quantifying the water retention in subsoil, enabling the prediction of seasonal variations in earthing resistance for transmission and distribution towers.
2. To create models that represent and predict the variability of subsoil resistivity under different conditions of subsoil.
3. To incorporate hydraulic properties of EEMs in modelling and evaluating their performance in different soils, soil conditions and climates.
4. To investigate the impact the variation within the sphere of influence of earthing conductors and predict its water content at any condition at the subsoil surface.
5. To identify additional criteria for applying EEMs for optimal performance in high soil resistivity location and climate.

By achieving these objectives, the research aims to enhance the understanding and accuracy of estimating earthing system resistance without physical measurements and improve the selection and effectiveness of EEMs in different soils, and environmental and climate conditions.

1.6 Limitations of Research

1. Comparison Constraints

The research encountered obstacles in comparing the anticipated earthing resistance using the developed models with those derived from meteorological precipitation data due to constraints in data availability and the intricate nature of correlating precipitation data directly to soil resistivity changes.

2. Data Limitations

The investigation depended on multiphysics simulation models to forecast soil resistivity fluctuations based on water content and retention characteristics under evolving atmospheric conditions. The precision and relevance of these forecasts are inherently restricted by the nature and specificity of the accessible data on soil properties and atmospheric conditions.

3. Model Assumptions

The multiphysics simulation models utilised in this study presume steady-state conditions and uniformity in soil composition for each subsoil layer, which may not represent the intricacies and diversities present in real-world scenarios. This could impact the general applicability of the conclusions.

4. Hydraulic Properties

Although the research integrated hydraulic properties like water retention and soil suction, it overlooked other potential factors that could impact earthing resistance, such as soil temperature, chemical composition, compaction, salinity, and root systems of vegetation, which could also fluctuate with atmospheric conditions.

5. Validation Limitations

The validation of the projected earthing resistance was executed through comparisons with analytical formulas and simulation models that excluded hydraulic properties. This method,

while beneficial, does not entirely validate the predictive precision of the new models against real-world observations.

6. Temporal and Spatial Variability

The study might not have comprehensively captured the temporal and spatial variability of soil and atmospheric conditions over prolonged periods and diverse geographical regions. This limitation could undermine the reliability of the proposed models in forecasting earthing resistance under varying circumstances.

7. External Influences

External influences such as human activities, alterations in land use, and severe weather occurrences like drought, snow and ice covers, were not explicitly factored into the models. These elements could significantly influence soil properties and earthing resistance, thereby impacting the accuracy of the forecasts.

1.7 Outline of Chapters

Chapter One: Introduction, Problem Statement, and Research Aim

This chapter provides a comprehensive introduction to the research, outlining the background, research problem, and key research questions. It details the research aim, objectives, significance, and limitations of the study.

Chapter Two: Literature Review and Derivation of Existing Formulas

This chapter presents a review of relevant literature on evaluating earthing resistance under seasonal variations. It includes the formulation and refinement of critical equations from fundamental principles, such as Richard's equation for fluid flow in unsaturated porous media, equations for water retention characteristics, empirical equations relating to conductivity-water content, and the equation for electric flow in conductive media. It also covers the analytical formulation of the coupled computational electromagnetic model for earthing resistance.

Chapter Three: Research Methodology and Modelling of Proposed Method

This chapter describes the research methodology based on multiphysics modelling of the proposed hydro-geoelectric method in COMSOL Multiphysics® software. It shows the numerical application and coupling of the partial differential equations governing the two physics that describes the proposed method.

Chapter Four: Effect of Soil Texture and Hydraulic Properties on Resistance and Performance of Earthing Systems

This chapter examines the impact of soil texture and hydraulic properties on the resistance and performance of earthing systems. It involves modelling earthing system terminals (electrodes) in single (homogeneous) and double subsoil layers, both with and without EEMs. The chapter analyses how variations in earthing resistance and ground potentials are affected by current dispersion from the surface of the earthing electrode under steady-state conditions, evaluating the effectiveness of EEMs based on their capacity for resistance reduction compared to native soil.

Chapter Five: Equation Formulation Water Content Variation Within the Region of Influence of Vertical Earth Electrodes

This chapter explores the region of influence, also known as the sphere of influence, surrounding vertical earth electrodes. It presents equations for estimating volumetric water content and analyses how this impacts resistivity and earthing resistance in single- and double-layer subsoils at various soil suction levels.

Chapter Six: Performance of Earthing Systems in Different Soils and Climates

This chapter focuses on hydro-geoelectric modelling of vertical earth rods and rod-beds with EEMs in both single-layer and two-layer soils. It evaluates the performance of these systems across different degrees of saturation in both steady and time-dependent states. The efficiency of EEMs is assessed using the concept of percentage resistance reduction, and the effects of EEM volume and water retention characteristics on resistance reduction and ground potential are discussed for various soil types and conditions.

Chapter Seven: Conclusion and Recommendations

The final chapter summarises the key findings of the research and provides recommendations based on the study's results. It offers insights into the implications of the findings and suggests areas for future research.

Chapter 2 - Literature Review and Mathematical Modelling of Proposed Method

2.0 Introduction

This chapter explores the factors that drive seasonal changes in the resistivity of the subsoil and the impact of these changes on earthing systems, particularly those that use earthing-enhancing materials. Following this, it critiques the limitations of the IEC 62561 standard. The chapter reviews current methods for evaluating seasonal changes in earthing resistance, highlighting their limitations and the need for a new approach. It further delves into the composition of subsoil and the effects of soil types on water content, energy states, and responses to climatic and environmental conditions. The chapter concludes by discussing the fundamental principles required to develop hydro-geophysical models of earthing systems, including the formulation and modification of partial differential equations to simulate water flow and electric current dispersion in a porous conductive medium and the impact of water retention and hydraulic conductivity properties of the medium.

2.1 Seasonality of Subsoil Condition

Significant research has been dedicated to understanding the variability of subsoil conditions and their influence on earthing resistance and performance. While safety assessments have predominantly focused on the implications of seasonal changes, the primary variable driving and predicting the seasonality of subsoil resistivity has been identified as quantity and condition of water in the subsoil, which varies with time and location.

The temporal and spatial variability of subsoil resistivity significantly impacts the design and performance analysis of earthing systems. While spatial variations are typically addressed in earthing designs, temporal variations are often inadequately accounted for, leading to changes in resistance and performance post-installation. Temporal variability of subsoil resistivity is largely attributed to seasonal climate or weather conditions, which influence water exchange between the atmosphere and subsoil through infiltration and evaporation. Precipitation increases subsoil water content and electrical conductivity, while evaporation reduces it. The water table (WT) - the uppermost level of groundwater - serves as a reference point for assessing water movement and subsoil saturation. The WT delineates the unsaturated Vadose zone from the saturated region below it. Variations in the Vadose zone's saturation change moisture profiles and matric suction in the subsoil [20]. The ground surface, as the interface between the subsoil and atmosphere, is particularly sensitive to climatic and environmental conditions affecting subsoil resistivity [7], [13]. For example, the increase in subsoil water

content caused by precipitation, snowmelt, and ice thawing reduces ground surface suction, while dry conditions resulting from evapotranspiration increases ground surface suction.

2.1.1 Factors Influencing Seasonality of Earthing Resistance

The seasonality of subsoil resistivity and its impact on earthing resistance is influenced by the type of earthing electrode, soil condition, and soil type [36]. The depth at which an earthing electrode is buried affects how seasonal changes impact its resistance. Horizontal strips and earth grids, typically buried within the Vadose zone, are more susceptible to seasonal changes than vertical earthing rods, which are driven deeper. In regions where the subsoil freezes to a depth of 1.5 metres [10] or 6 metres, as observed in Southern China [37], the resistance of earthing grids positioned above these depths is significantly affected. The rate, intensity, and duration of water exchange between the subsoil and atmosphere are critical factors regulating seasonal subsoil conditions. Increased precipitation raises subsoil water content and saturation, thereby enhancing electrical conductivity until saturation is reached. Excess water is typically drained within two to three days post-rainfall, followed by evapotranspiration that further de-saturates the subsoil. The rate at which the subsoil de-saturates determines the variation of its resistivity. Rainfall is a key indicator of climate conditions, but it does not fully capture the ability of the subsoil to accept water, which is influenced by factors such as fissures, vegetation, and topography [36]. The water acceptance potential (WAP) indicates the likelihood of water from precipitation processes to pond, drain, or runoff on the ground surface [3]. By regulating the rate and frequency of water retention and release in the subsoil, climate-weather factors control the energy state of soil water and provide a definite description of soil condition [5], [38].

2.1.2 Implications of Seasonality on Safe Potential Limits

Climate-induced seasonality can lead to high earthing resistance and poor performance, necessitating corrective measures [23]. Safety assessments focus on parameters such as resistance, step and touch potentials, ground potential rise, and lightning performance of the tower footing resistance (TFR) [10], [13], [38], [39]. Abdullah et al. conducted a study using 12 to 18 months of soil resistivity, earthing resistance, rainfall, and subsoil water content measurements at various depths (1 m, 3 m, 5 m) to assess the impact of seasonal variations on substation earthing systems. Their findings, supported by simulation-based assessments using current distribution, electromagnetic, and grounding system (CDEGS) software, revealed that

seasonal variations could cause step and touch potentials exceeding safe limits, despite meeting initial design specifications [8], [38].

2.2 Limitations of the IEC 62561 Standard

The IEC 62561 and other relevant standards do not offer guidance on several key aspects for selecting earthing enhancement for optimal resistance reduction in high-resistivity soils. Specifically, these standards do not:

1. Provide recommendations for the optimal dimensions and distribution of EEMs.
2. Define criteria for effective resistance reduction of EEMs.
3. Suggest appropriate distribution of EEMs and space between adjacent earth electrodes with EEMs.
4. Address the long-term impact of EEMs on the performance of earthing electrodes.
5. Evaluate the performance and efficiency of EEMs across various soil types, and subsoil condition and climate zones.

These limitations are significant following the inclination of researchers in these areas, underscoring their relevance in the earthing system design and applications.

2.2.1 Research in Earthing Enhancement Materials Applications

The determination of the ideal quantity and distribution of EEMs to achieve effective performance, characterised by resistance reduction, has been extensively researched. This research has led to a variety of recommendations. For instance, Kutter and Lange (1967) suggested a minimum volume of 0.02 m^3 of bentonite slurry per metre length of earthing strip to effectively eliminate contact resistance [40]. Field experiments by Okyere and Eduful demonstrated that EEMs positioned within the critical areas of the earthing system provided superior resistance reduction [41]. Further, Eduful, Cole, and Okyere found that using four vertical rods in parallel resulted in the optimal resistance reduction [42].

In terms of determining the quantity of EEMs needed in critical areas, Chen et al. observed that resistance reduction increased with the amount of EEM up to a maximum value. Beyond this point, additional increments in EEM quantity produced only marginal or insignificant reductions in resistance [43]. Thus, identifying the optimal quantity or volume of EEMs has become a key focus of research.

A significant approach involves determining the optimal dimensions of the auger hole or pit for the conductive backfill, with extensive use of optimisation techniques. For example, studies

have developed optimisation models to define the optimal size, configuration, and distribution of EEM around earthing electrodes [44], [45]. Alternatively, Trifunovic employed the concept of the knee point, rather than optimisation, to derive a mathematical expression that best represents the optimal volume of EEM for square earthing loops, given a specific target percentage resistance reduction [46].

2.2.2 Performance Variation of Earthing Enhancement Materials

Earthing systems enhanced with conductive materials (EEM) are also subject to seasonal variations, which can affect their performance in high-resistivity or poor contact environments [5]. A study evaluating six EEMs over a year found that only one of these compounds maintained consistent resistance. The other five compounds exhibited varying degrees of resistance reduction, with one commercial compound performing thirteen times worse relative to the performance of the bare electrode used as reference [35].

The suitability of low-resistivity compounds for earthing enhancement varies across soil types and climate conditions. Galvan D. et al. observed that soil type and other variables significantly impact the effectiveness of EEMs [35]. Another study found that the choice of earthing enhancement compound should match the soil type to optimise performance and minimise material failure [34]. Androvitsaneas et al. [5] suggested considering external influences when selecting EEMs for areas with high-resistivity and poor contact.

2.3 Methods of Estimating the Seasonal Variation of Soil Resistivity

The phenomenon of seasonal variation in earthing resistance has been the subject of considerable research, which attributes these variations primarily to changes in soil conditions, notably the moisture content and the liquid-solid phase transitions of water within the soil [5], [13], [23], [47], [48], [49], [50]. The level of subsoil water, which fluctuates with rainfall and temperature, is significantly influenced by meteorological conditions. Given that groundwater sources contribute less to soil moisture compared to precipitation, weather conditions are the principal determinant of soil water content [38].

Water, as a constituent of the soil, exhibits superior thermal and electrical conductivity than the gaseous and solid constituents. This characteristic renders it a critical factor in determining soil electrical conductivity. Research indicates that the effect of water on soil resistivity is more pronounced than that of temperature [11], [20], [36], [51]. Additionally, soil water influences various soil properties, including porosity, compaction, and salinity [11]. Due to its high thermal conductivity, water is more sensitive to temperature fluctuations, which can induce

phase changes or heat latency. Consequently, water content governs the primary mechanism of electrical conduction in soil and is inversely proportional to the electrical resistivity of unsaturated soil [11], [20], [51].

2.3.1 Methods Using Factors and Artificial Intelligence

In predictive modelling of earthing resistance, meteorological records such as rainfall data are commonly employed to estimate property and parameter variations attributed water content. Two principal methodologies are utilised: those based on correlation or correction factors [6], [8], [9], and those employing artificial neural networks (ANNs) [7], [48], [49]. These methodologies typically involve the analysis of historical data on soil resistivity, earthing resistance, and rainfall from meteorological stations.

For instance, Kizhlo and colleagues conducted a statistical correlation analysis between grounding resistance and various meteorological parameters, including temperature, pressure, and humidity. Their study led to a recommendation for periodic inspections of grounding systems [49]. Similarly, investigations conducted by Christy Thomas for Eskom in South Africa produced location-specific correction factors for soil resistivity, reflecting monthly rainfall variability [8]. Androvitsaneas et al. [5] proposed correlation factors to predict the temporal evolution of earthing resistance. Additionally, Madikizela et al. in 2022 suggested correction factors for estimating monthly earthing grid resistance based on data collected from the Eastern Cape province, South Africa [9]. Despite their utility, methods reliant on correction factors can yield site-specific estimations that may be inaccurate, potentially leading to design or performance issues [39].

In contrast, Androvitsaneas et al. [48] modelled seasonal variation as a sinusoidal time function, incorporating this model into an ANN framework that utilised rainfall data as an input variable to predict resistance changes in vertical earthing rods [7], [48], [49]. ANN models typically incorporate soil resistivity measurements taken at various distances (1 and 2 m) from the earthing electrode, historical rainfall data, and average earthing resistance of the preceding week. S. Anbazhagan proposed an enhancement to ANN accuracy through the application of the generalised regression neural networks (GRNN) approach [52].

2.3.2 Limitations of Existing Methods

S. Anbazhagan emphasised the need for investigating the significance of input variables used in ANN training and resistance prediction [52]. Coelho et al. noted that while cumulative rainfall improves prediction accuracy, significant variations in apparent resistivity can occur

due to decreased soil moisture following a period of no rainfall [22]. Coelho et al. also observed that although moisture substantially affects soil resistivity in every subsoil layer, it is the topmost layer that is most sensitive to weather conditions. Abdullah et al. found a direct correlation between the highest and lowest values of soil resistivity and amount of rainfall [38]. Although resistance, subsoil resistivity, and rainfall data are commonly used in these methods, Kizhlo et al. have observed that incorporating geological properties and meteorological parameters can lead to improved design and resistance estimation of predictive models [52].

2.4 Need for Paradigm Shift

In 2019, Datsios and Mikropoulos observed that the effects of soil properties on the low-frequency spectra of soil electrical properties had not been adequately explored [53]. Despite the recommendations by Laver and Griffiths in 2001 for improving earthing design and installation in response to temporal variations in soil resistivity [36], two decades later, Andolfato et al. noted the continued lack of standardised techniques for modelling seasonal effects on earthing systems [13].

2.4.1 Soil Water Retention and Resistivity

Current methods of evaluating subsoil resistivity changes due to water content rely on indirect measures from rainfall data. The assumption that soil resistivity variations can be inferred from precipitation intensity is a common thread in both methodologies. However, this assumption oversimplifies the complex relationship between rainfall and soil resistivity. Soil resistivity is more significantly influenced by the quantity of water retained within the subsoil than by the amount of rainfall on the surface.

A more accurate approach involves quantifying subsoil water content using geotechnical parameters such as permeability and hydraulic conductivity [36], although these hydraulic properties, along with porosity and compaction, determine water retention and influence changes in resistivity. For instance, soil compaction affects water infiltration rates and can significantly alter resistivity measurements [54]. Similarly, soil porosity influences the capacity for water retention and its distribution within the soil matrix [55]. However, the influence of these hydraulic properties is often ignored in developing predictive models of earthing resistance.

From the foregoing, besides the criteria specified by the IEC 65261-7 standard, a material is considered suitable for earthing enhancement if it achieves lower contact resistance with the earthing conductor, has superior water retention, and offers less restriction to electric current

flow than the surrounding native soil under identical conditions. These features are essential for EEMs to achieve earthing improvements in areas with high-resistivity or poor soil-electrode contact. For example, the earthing performance of sandy soils, which are problematic in earthing applications, can be improved by increasing their humus content to achieve higher water retention [6].

2.4.2 Hydro-Geophysical Models of Earthing Systems

To address the limitations of current methods, the development of hydro-geophysical models is proposed. These models integrate hydraulic and electrical properties of the subsoil. For example, by incorporating the property of hydraulic conductivity, the movement and retention of water through and by each layer of the subsoil can be determined [56]. The proposed method uses the uniqueness of texture and hydraulic characteristics of soil in the subsoil layers to quantify soil water retention under any condition of soil. This is achieved by applying established geotechnical formulations of parameters such as permeability, hydraulic conductivity, and soil water retention characteristics. Since the water content and water retention characteristics of earthing enhancement materials can be described quantitatively, this method provides a potential basis for comparative performance analysis of earthing enhancement materials across different climates, soil conditions, and high-resistivity soil types.

The mathematical form of the model incorporates partial differential equations that govern water flow in porous media and electric current dissipation in conductive media to predict soil water content, degree of saturation, resistivity, and earthing resistance under any climatic condition. The equations are formulated to account for soil heterogeneity and boundary conditions of the earthing conductor surface and subsoil domain. For instance, using Richards' equation, which models fluid flow in unsaturated porous media, the water content of the subsoil can be determined by specifying pressure or suction at the top boundary of the subsoil.

2.5 Soil Composition, Property and Energy State

This section presents a discussion on the composition, properties, and energy state of the soil, which are fundamental in formulating the hydro-geophysical model of earthing systems.

2.5.1 Composition of Soil and Subsoil

Soil consists of three volumetric constituents: air, water, and solid grains. The spaces or pores between the soil grains are filled with either air or water, or a combination of both. A typical soil sample contains solid aggregates or grains of various sizes, with these pores determining the state of the soil. Soil grains can be categorised into three sizes: coarse sand grains (0.05 to

2 mm), fine silt grains (0.002 to 0.05 mm), and finer clay grains (less than 0.002 mm). Soil texture describes the percentage composition of clay, silt, and sand within the soil. As shown in Figure 2.1, there are twelve classifications of soil texture according to the World Reference Base for Soil Resources (WRB) [57].

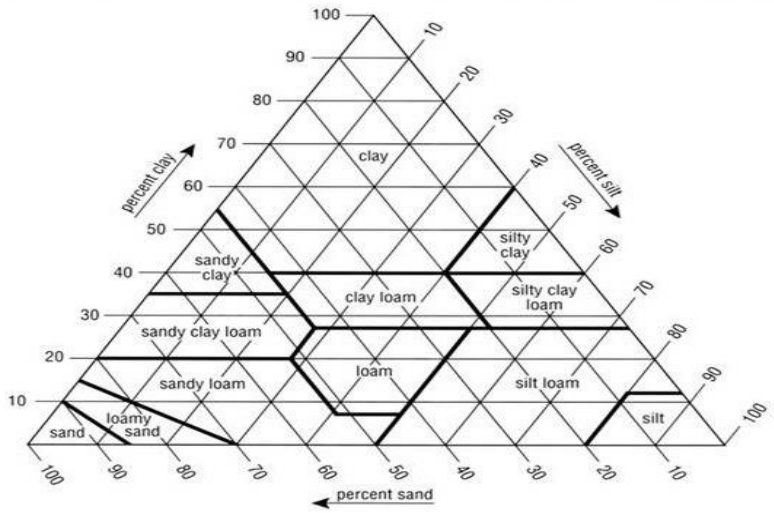


Figure 2.1: Soil Texture Triangle Classification based on World Reference Base for Soil Resources (WRB)

Source: [57].

Grain size distribution determines the space between adjacent grains and hence the pore size, distribution, and connectivity. Finer grains result in smaller but more numerous soil pores, whereas coarse grains have larger but fewer pores. The content of these pores determines the soil's state of saturation. Soil is considered saturated when the pores are filled with water alone, unsaturated when filled with air only, and partially saturated when both air and water coexist in the soil pores.

Except for driven rods targeting the water table, earthing conductors are buried within a region of the subsoil known as the vadose zone. The vadose zone, also referred to as the unsaturated zone, is the region of soil and rock between the land surface and the water table where the pores are partially filled with water and partially filled with air. This zone is characterised by a mixture of water, air, and soil grains and is a critical area for water movement, storage, and interaction with the atmosphere. Water, air and solid grains are the constituents of soil. A schematic view of the vadose zone, relative to the ground surface and water table, is shown in Figure 2.2.

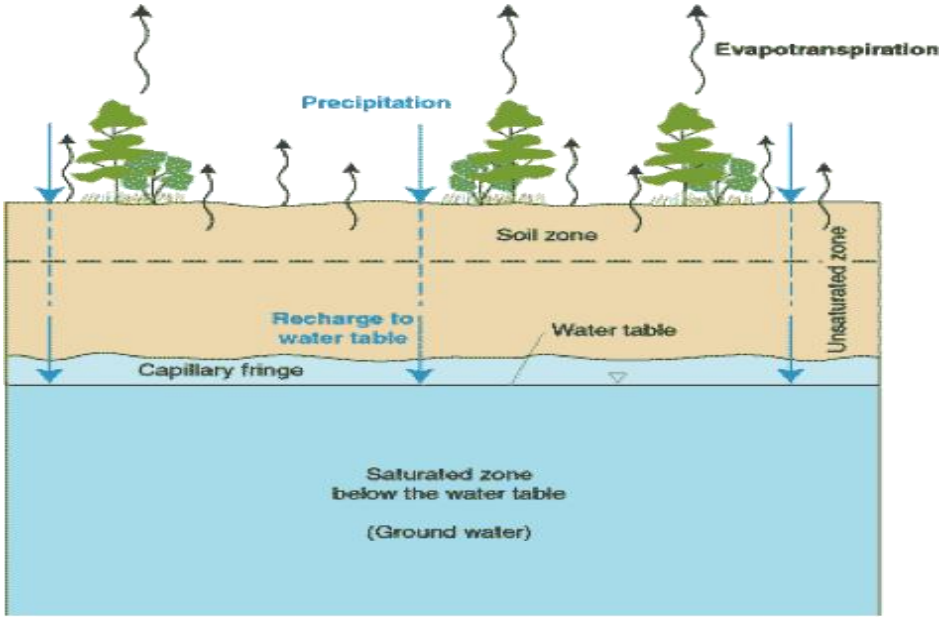


Figure 2.2: Schematic diagram showing a vertical section of the subsoil from the ground surface to the unconfined saturated zone through the unsaturated or vadose zone

Source: [58].

The vadose zone can be multilayered, with each layer having a unique structure, texture, morphology, and chemical properties [59]. The relative position and composition of each sublayer determines the volumetric response of the subsoil to external climate and environmental influences and the impact of the subsoil on earthing system resistance and performance.

2.5.2 Soil Water Content

The total soil volume V_t comprises the volumes of air (gas) V_a, water (liquid) V_w, and solid grains V_s. The sum of V_w and V_w equals the volume of pores V_v. The relative volume of water in the soil can be described in two forms: the volumetric water content θ and the degree of saturation S_d. Volumetric water content is the ratio of the volume of water to the volume of soil, as expressed in Equation 2.1:

$$\theta = \frac{V_w}{V_t} \tag{2.1}$$

Saturated and residual water contents are the extreme states of water content that soil can attain under atmospheric conditions. Residual water content is an extreme state of unsaturation where no additional water can be extracted from the soil without decomposing. The volumetric components of saturated and unsaturated water contents are denoted with θ_s and θ_r respectively.

The factors that affect the water content of soil are: (i) total porosity, (ii) pore size distribution and connectivity, and (iii) energy status of soil water. Porosity ϕ, expressed in Equation 2.2 as the ratio of the volume of voids to the volume of soil, is closely related to volumetric water content:

$$\phi = \frac{V_v}{V_t} \tag{2.2}$$

Soil porosity influences the amount of water that can be retained within the volume. When water fills the pores, the soil medium is said to be saturated; otherwise, it is unsaturated or partially saturated. The degree of saturation S_d indicates the extent of soil saturation and is expressed as the ratio of the volume of water to the volume of voids in the soil, as shown in Equation 2.3:

$$S_d = \frac{V_w}{V_v} \tag{2.3}$$

At saturation, $\phi = \theta_s$, because the volume of water equals the volume of voids or $V_w = V_v$. The relationship between θ, S_d and, ϕ is expressed in Equation 2.4:

$$S_d = \frac{\theta}{\phi} \tag{2.4}$$

$0 \leq S_d \leq 1$ is the valid range of S_d, where 0 and 1 represent the respective extremes of unsaturated and saturated states. The normalised form of the degree of saturation, is known as effective saturation S_e. It is sometimes used to describe water retention under various conditions. S_e relates to the volumetric water content θ, saturated volumetric water content θ_s, and residual volumetric water content θ_r, as expressed in Equation 2.5 [56]:

$$S_e = \frac{\theta - \theta_r}{\theta_s - \theta_r} \tag{2.5}$$

2.5.3 Soil Resistivity and Water Content

The property of the soil that enables the ease of electric current flow is electrical conductivity (σ) the inverse of resistivity. Numerous empirical formulas have been proposed to describe the relationship between water content and the electrical conductivity of porous media. These formulas are utilised in various applications in geophysics, agriculture, and soil sciences [13], [25], [26], [27], [28], [29]. For instance, Archie's equation is widely used in geological exploration to identify liquid deposits underground. The formula proposed by Waxman-Smith has been employed to estimate water content from electrical resistivity measurements taken for

landslide monitoring [60]. Kazmi et al. used laboratory and field measurements to establish a nonlinear quantitative relationship between electrical resistivity and water content for silty and sandy soils at a depth of 3 metres [27]. Khafizov et al. expanded the resistivity-water content function by incorporating a mineral concentration variable and suggested that the reliability of earthing design could be improved using such functions [61].

Unlike saturated soil, the resistivity of unsaturated soil is influenced by several factors, including soil texture, porosity, fluid composition, counter-ion content, salinity, crack properties, surface conduction of double layers, mineralisation, permeability, ionic content of pore fluids, temperature, vertical thickness or depth, soil structure, and the cross-sectional area of the conductive path [5], [15], [16], [17], [18], [20]. The relative ease of measuring soil resistivity facilitates the estimation of various soil properties such as compaction, dry density, friction angle, and organic and water contents from their correlation with resistivity [62], [63].

Archie's equation, formulated from empirical laws, provides a relationship between water content or degree of saturation and electrical conductivity in a porous medium. For unsaturated and partially saturated soil, Archie's equation is expressed in terms of porosity (ϕ), surface conductivity (σ_s) of fine-grained soils, and the electrical conductivity (σ_w) of the liquid in the porous medium, as shown in Equation 2.6:

$$\sigma = \sigma_w \phi^{\mathfrak{m}} (S_d)^{\beta} + \sigma_s \tag{2.6}$$

where $\mathfrak{m}$ is the cementation factor, β is the saturation index, and $\beta \gg \mathfrak{m}$.

2.5.4 Modelling Electrical Current Flow in Subsoil

The finite size of earthing electrodes relative to the infinite volume of the ground within which they are buried allows the modelling of earthing electrodes as point sources of fault, surge, or lightning currents. The dispersion of current (I_f) from the surface of an earthing electrode into the soil is governed by Ohm's law, which is expressed in terms of current density **(J)** (A/m^2), electric field strength (E**)** (V/m), and electrical conductivity (σ) (S/m) of the soil, as shown in Equation 2.7:

$$J = \sigma E \tag{2.7}$$

To describe electric current flow in a variably saturated soil volume or ground, it is important to understand the relationship between electrical conductivity and water content of the medium,

as well as the current density or electric potential at any point within the medium. Equation 2.8 describes the relationship between the electric potential (V_p) and electric field at any point:

$$E = -\nabla V_p \tag{2.8}$$

The gradient operator, ∇ in 3D space is expressed in Cartesian $(\mathrm{x}, \mathrm{y}, \mathrm{z})$, Cylindrical (r_c, φ, z), and Spherical $(r_s, \varphi, \vartheta)$ as

$$\nabla = \begin{cases} \frac{\partial}{\partial x}\hat{\imath} + \frac{\partial}{\partial y}\hat{\jmath} + \frac{\partial}{\partial z}\hat{k} & (\mathrm{x}, \mathrm{y}, \mathrm{z}) \\ \frac{\partial}{\partial r_c}\hat{r_c} + \frac{1}{r}\frac{\partial}{\partial \varphi}\hat{\varphi} + \frac{\partial}{\partial z}\hat{z} & (r_c, \varphi, z) \\ \frac{1}{r_s}\frac{\partial}{\partial r}\hat{r} + \frac{1}{r_s \sin\varphi}\frac{\partial}{\partial \varphi}\hat{\varphi} + \frac{1}{r_s \sin\vartheta}\frac{\partial}{\partial \vartheta}\hat{\vartheta} & (r_s, \varphi, \vartheta) \end{cases} \tag{2.9}$$

where x, y, z are the distances of a point from the centre of the electrode in the directions of unit vectors $\hat{\imath}$, $\hat{\jmath}$ and $\hat{k}$; r_c represents the radial distance of the point from the central axis of the cylinder in the direction of unit vector $\hat{r_c}$; φ is the azimuthal angle in the direction of unit vector $\hat{\varphi}$; r_s represents the radial distance from the centre in the direction of unit vector $\hat{r_s}$; φ is the polar angle in the direction of unit vector $\hat{\varphi}$; and ϑ is the azimuthal angle in the direction of unit vector $\hat{\vartheta}$.

Substituting for E in Equation 2.7 and performing the divergence operation gives Equation 2.10:

$$\nabla \cdot J = -\sigma \nabla^2 V_p \tag{2.10}$$

The differential Equation 2.10 is the Laplacian form of electric potential that relates electric potential to the divergence of current density. Using appropriate initial and boundary conditions, its solution for steady- or time-dependent states describes the dissipation of electric current in the conductive medium. The product term $\nabla^2 V_p$ can be expressed as a function of the radial distance r from the centre of the sphere. Since $r = \sqrt{x^2 + y^2 + z^2}$, then $\nabla^2 V_p$ in spherical coordinates is expressed in Equation 2.11 as:

$$\nabla^2 V_p = \frac{1}{r^2}\frac{\partial}{\partial r}\left(r^2 \frac{\partial V_p}{\partial r}\right) + \frac{1}{r^2 \sin\varphi}\frac{\partial}{\partial \varphi}\left(\sin\varphi \frac{\partial V_p}{\partial \varphi}\right) + \frac{1}{r^2 \sin^2\varphi}\frac{\partial^2 V_p}{\partial \vartheta^2} \tag{2.11}$$

Alternatively, $\nabla^2 V_p$ can be expressed as a function of the radial distance r from the cylindrical axis. Since $r = \sqrt{x^2 + y^2}$, then $\nabla^2 V_p$ in cylindrical coordinates is expressed in Equation 2.12 as:

$$\nabla^2 V_p = \frac{1}{r}\frac{\partial}{\partial r}\left(r\frac{\partial V_p}{\partial r}\right) + \frac{1}{r^2}\frac{\partial^2 V_p}{\partial \varphi^2} + \frac{\partial^2 V_p}{\partial z^2} \tag{2.12}$$

Under isotropic conditions $\partial V_p/\partial\varphi = 0$, then, the cylindrical form of $\nabla^2 V_p$ reduces to the form in Equation 2.13 as:

$$\nabla^2 V_p = \frac{1}{r}\frac{\partial}{\partial r}\left(r\frac{\partial V_p}{\partial r}\right) + \frac{\partial^2 V_p}{\partial z^2} \tag{2.13}$$

2.5.5 Energy State of Soil Water

The energy state of soil water, influenced by capillarity and adsorption, is approximated by soil water potential (SWP), denoted as (ψ). This potential is also referred to as capillary potential, soil water suction, negative pressure, or water tension [64]. Soil water potential measures the energy status of soil water, expressed in units of pressure (for example, kilopascals or kPa) or energy per unit volume. It describes the movement and retention of water in the soil, accounting for osmotic, gravitational, pressure, and matric potentials [21].

Matric potential, a key component of SWP, represents the potential energy exerted by water within the soil pores. It arises from capillary action within the pores, adhesive forces between water and soil solids, and cohesive forces between water molecules. This potential is crucial for indicating the availability and movement of water in unsaturated soil. The total soil water potential (ψ_T) is the sum of gravitational (ψ_g), matric (ψ_m), and pressure (ψ_p) potentials, as shown in Equation 2.14:

$$\psi_T = \psi_m + \psi_g + \psi_p \tag{2.14}$$

The total energy (E) due to the water phase at any point is the sum of gravitational, pressure, and velocity energy components. This relationship is mathematically expressed in Equation 2.15:

$$E = m_w\left[g \cdot z + \frac{u_w}{\rho_w} + \frac{(v_z)^2}{2}\right] \tag{2.15}$$

Here, m_w (kg) is the mass of water in soil pores, g (m/s^2) is gravitational acceleration, u_w is pore-water pressure, v_z is the flow rate in the z-direction, and ρ_w is the density of water.

When expressed as energy per unit weight of water ($m_w g$), Equation 2.15 transforms into Equation 2.16, taking the form of total head (H) [L], also known as the potential head or hydraulic head:

$$H = z + \frac{u_w}{g \cdot \rho_w} + \frac{(v_z)^2}{2g} \tag{2.16}$$

In unsaturated flow, the velocity term is relatively negligible, so H is approximated by Equation 2.17 as the sum of the gravitational or elevation head (z) and pressure head (h_p):

$$H = z + h_p \tag{2.17}$$

The hydraulic head and its components are measurable quantities with units of length. Elevation head (z) is the distance between the datum (water table) and the elevation of a point of interest in the soil.

2.5.6 Force of Fluid Flow in Unsaturated Soil

The driving force of water flow in unsaturated soil can be described using an arbitrary datum, such as the water table, in terms of the energy gradient between two points in the soil. The hydraulic head gradient (∇H) is the fundamental potential responsible for driving water flow in both saturated and unsaturated soils, and represents the difference between the hydraulic head of two points [21].

For unsaturated flow above the water table, the origin of the ordinate axis is the ground surface, oriented downward. In this condition and orientation, the magnitude of the elevation head is typically in the order of metres, while the pressure head is in the order of hundreds of metres. Therefore, the total water potential or hydraulic head (H) is approximated by Equation 2.18:

$$H \approx h_P \tag{2.18}$$

The pressure head represents the height of a column of water that would produce equal pressure at a given point. In hydrogeology, pressure potential may be expressed in terms of pressure head rather than potential energy per unit weight to describe water flow in pressurised or confined systems.

2.6 Soil Suction

Soil suction is the energy required to extract a unit volume of water from the soil [65]. The application of unsaturated soil mechanics in engineering design and practice relies on the ability to quantify or measure soil suction. Soil suction consists of matric suction (ψ_m) and osmotic suction (ψ_o). The roles of matric and osmotic suctions in the mechanical behaviour of unsaturated soil differ. Matric suction relates to the air-water interface, whereas osmotic suction is associated with the concentration of salt in the pore-water and the diffuse double

layer around clay particles. Matric suction is more closely associated with unsaturated soil water flow due to capillary rise. The total soil suction (ψ) is represented in Equation 2.19:

$$\psi = \psi_m + \psi_o \tag{2.19}$$

Osmotic suctionψ_o is given by the formula $\psi_o = RT_kC_s$ (kPa), where $R = 8.314\ \text{Jmol}^{-1}\text{K}^{-1}$ is the universal gas constant, T_k is the absolute temperature in kelvin (K), and C_s is the sum of molar concentration in solution (mol/L).

Krahn and Fredlund demonstrated that total suction and matric suction are congruent, especially at higher degrees of saturation [66]. This implies that changes in total suction are almost entirely due to changes in matric suction. Except where the salt concentration in the soil significantly changes, climate and environmental changes affect matric suction more than osmotic suction. Therefore, it is more appropriate to model unsaturated soil water flow with matric suction rather than total suction [21].

Soil pores, analogous to capillary tubes, can allow the rise of water to displace air and saturate the soil pores or allow air to displace water as the soil desaturates [21]. The pressures exerted by air and water in the soil pores are known as pore-air pressure (u_a) and pore-water pressure (u_w) respectively. The difference between the pore pressures is called soil matric suction (ψ_m), as expressed in Equation 2.20:

$$\psi_m = (u_a - u_w) \tag{2.20}$$

Since the air pressure at the air-water interface is typically atmospheric ($u_a = 0$ kPa), matric suction is approximately the negative value of pore-water pressure:

$$\psi_m \approx -u_w \tag{2.21}$$

Changes in environmental and climatic conditions at the ground surface are responsible for variations in pore-water pressure in the subsoil [21]. Downward (infiltration) water flux increases the degree of saturation of soil, while upward (evaporation) flux reduces it. The net flux of infiltration and evaporation produces variations in the matric suction of the soil.

2.6.1 Relationship Between Suction and Pressure Head

The interaction between the constituents of soil - solid grains, water, and air - leads to adsorption and capillarity, causing water in an unsaturated soil matrix to exert tension or negative pressure, known as matric suction [67]. Matric suction represents the difference between pore-air pressure and pore-water pressure within the soil matrix. This suction indicates

the energy required to extract a unit volume of water from unsaturated soil [68]. In practical terms, soil suction measures the soil's affinity to retain water and provides insights into soil parameters influenced by soil water content [68].

The energy state of soil water can be described by soil suction, also called matric or capillary suction. ψ_s represents the strength of the attraction of water molecules to a medium, allowing water to be held tightly within soil pores under high tension or negative pressure [67]. Matric suction is influenced by water content, pore size distribution, and soil texture. ψ_s is measured in units of pressure (Pa). Although describing different parameters, ψ_s and h_P are related as shown in Equation 2.22:

$$h_P = -\psi_s / g\rho_w \tag{2.22}$$

2.6.2 Suction Profile of Subsoil

The water table, defined as the topmost surface of groundwater, is a convenient reference depth to mark soil water movement and energy. It divides the soil column into two regions: an upper soil region with discontinuous water pores (unsaturated or partially saturated soil) and a lower region of continuous water volume (fully saturated soil). At this depth, the pressure potential is marked as zero. The potential in the unsaturated region is negative, while it is positive in the saturated region. The negative pressure in the unsaturated soil region is called suction, matric, or tension pressure potential.

As water from saturated soil is lost by draining under the forces of gravity or evaporation, a profile of soil suction is developed. Soil suction varies within the unsaturated vadose zone, being highest at the ground surface and decreasing with depth towards the water table. When comparing a large range of suction values, the pF suction scale is convenient for expressing suction. The pF suction scale is the common logarithm of the suction (ψ) expressed in centimetres (cm) of water, as shown in Equation 2.23. Suction or pressure in kPa can be converted to cm using 1 kPa equal to 10.19716 cm of water.

$$p\mathrm{F} = \log_{10} \psi \tag{2.23}$$

2.6.3 External Influence on Soil Suction

The vadose zone, a partially saturated soil region, lies between the ground surface and the water table. The degree of saturation ranges from 100% to 0%, with corresponding pore-fluid pressures of 0 kPa and -106 kPa, respectively. By controlling the depth of the groundwater table, atmospheric conditions at the ground surface influence the thickness and degree of

saturation of the vadose zone in the subsoil. Even the smallest amount of air, including occluded air bubbles, makes the soil pore fluid compressible and therefore unsaturated [21]. Because the vadose zone is subjected to negative pore-water pressure, it is commonly referred to as an unsaturated or partially saturated soil zone in the geotechnical field. As the suction of the subsoil changes, distinct zones of saturation are formed, such as the fringe zone, an intermediary region above the water table with the highest degree of saturation in the vadose zone.

2.7 Atmospheric Description of Climates

The ground surface is a vital boundary for continuous thermal and moisture-vapour fluxes. As the soil gains water from atmospheric precipitation and loses it through evapotranspiration, the net water flux at the ground surface determines the degree of saturation of the subsoil and the pore-water pressure [21]. The average annual net water flux at the ground surface is used to classify the climate conditions of various places, which can be predominantly dry (arid, semi-arid) or wet (humid) [21]. In arid and semi-arid climates, where annual evaporation exceeds annual precipitation, there are thick unsaturated vadose zones with high negative pore-water pressures. In such regions, sand-rich soils are predominantly dry, while fine-grained soils, especially clay, shrink, crack, and desiccate. Therefore, soil resistivity and the resistance of earthing terminals in dry climates or weather conditions are relatively higher than in humid climates.

2.7.1 Parameters for Modelling Climatic Conditions

Climates are broadly classified as humid, semi-arid, or arid based on the frequency and quantity of precipitation and evaporation, and the variability of soil water is climate-dependent [69]. In semi-arid climates, the annual mean value of soil water content is proportional to annual precipitation and increases with depth. However, in arid climates, it depends on the day-night cycle of evaporation and precipitation. Evaporation, the major mechanism of subsoil water loss, occurs at different rates in wet and dry climates. In arid and semi-arid climates, the evaporation rate increases after rainfall and depends on wind velocity, atmospheric temperature, and the specific humidity of the air [69]. Under dry soil conditions, the evaporation rate strongly depends on soil water content and specific air humidity. Therefore, the evaporation rate is influenced by soil type, soil condition, and evaporation potential. The constant formation of vaporisation or condensation in the small pores of the soil establishes an

equilibrium state between the liquid and vapour phases in the soil [69]. Water movement in the soil occurs in both liquid and vapour phases, as expressed by Equation 2.24.

$$\frac{\partial \theta}{\partial t} = -\frac{1}{\rho_w}\frac{\partial}{\partial z}(Q_l + Q_v) \tag{2.24}$$

where Q_l and Q_v are water fluxes in the liquid and vapour phases, which are positive in the upward direction, θ is volumetric water content, t is time, ρ_w is the density of water, and z is the vertical direction, with zero at the ground surface.

2.7.2 Relative Humidity and Subsoil Suction

Conditions that significantly reduce the degree of soil saturation also affect soil resistivity [5]. These conditions alter the profile of soil suction and the magnitude of suction at the ground surface. Since water movement in the soil occurs in both liquid and vapour phases, a comprehensive description of evaporation can be developed using a model of transfer processes in the atmosphere, as well as the continuity of temperature, vapour pressure, water, and energy fluxes at the ground surface. By modelling the thermodynamic effects of these atmospheric parameters, the state of the ground surface can be determined [64].

The magnitude of ground surface suction depends on atmospheric pressure and humidity, which are temperature dependent. Relative humidity measures the amount of water vapour in the air relative to the saturation capacity of the air at a specific pressure and temperature. Equation 2.25 is the Magnus-Tetens equation, expressed in terms of atmospheric temperature (T) and dew point temperature (T_d), both in degrees Celsius (°C), used to determine relative humidity (H_R) as a percentage.

$$H_R = 100 \exp\left(\frac{17.625 T_d}{243.04 + T_d} - \frac{17.625\, T}{243.04 + T}\right) \tag{2.25}$$

The soil water potential (ψ) can be quantified in terms of relative humidity at the ground surface [21]. Equation 2.26 relates the water potential of the soil in megapascals (MPa) to the relative humidity (H_R) [70].

$$\psi = \psi_0 - (RT/M)\ \ln(0.01\, H_R) \tag{2.26}$$

where R is the universal gas constant (8.314 $J \cdot K^{-1} \cdot mol^{-1}$), T is the temperature in kelvin (K), M is the molecular weight of water (0.01802 kg/mol), and ψ_0 is the water potential of pure water under standard temperature and pressure (STP), which is 0 MPa.

For example, the atmospheric and dew point temperatures of a particular day were 7 ℃ and 0 ℃ for Johannesburg and 37 ℃ and 17 ℃ for Jeddah. Using Equation 2.25, the relative humidity is 61.05% for Johannesburg and 30.83% for Jeddah. Consequently, if the ground surface and air are at equilibrium, then using Equation 2.26, the magnitude of water potential at the ground surface in Johannesburg and Jeddah is -63.78 kPa (2.8132 pF) and -168.37 kPa (3.2347 pF), respectively. As atmospheric parameters, if temperature and relative humidity sustain soil desaturation for a long time, then the electrical resistivity of soil may be significantly impacted [13].

2.8 Water Flow in Porous Medium

Darcy's law, originally formulated to describe flow in saturated soils, can be adapted to describe water flow in unsaturated soils. This law states that the volumetric flow rate of water through a porous medium is proportional to the gradient of the hydraulic head. This relationship is mathematically expressed in Equation 2.27 [21]:

$$q = -K_s A \frac{\Delta H}{L} \tag{2.27}$$

where $q = Av$ [L^3/T] is the flux or flow rate of water through a cross-sectional area A [L^2], v [L/T] is the flow velocity, andK_s [L/T] is the saturated hydraulic conductivity. ΔH [L] is the difference in total hydraulic head between two points in the saturated porous medium separated by a distance L [L]. Given that $H = h_p + z$, where z [L] is the elevation head and h_p [L] is the pressure head, Darcy's law can be compactly expressed as:

$$v = q/A = -K_s \nabla H \tag{2.28}$$

In 1907, Buckingham extended Darcy's law to unsaturated porous media by substituting the constant K_s, which is characteristic of saturated conditions, with a function representing the hydraulic conductivity of the unsaturated medium. This function depends on the water content (θ) or capillary potential (ψ) of the soil and is known as the unsaturated hydraulic conductivity function, denoted as $K(\theta)$ or $K(h_p)$ [56]. Consequently, Darcy's law for unsaturated porous media is given by Equation 2.29:

$$v = -K(\theta)\nabla H = -K\big(h_p\big)\nabla H \tag{2.29}$$

The negative sign indicates that water flows in the direction of decreasing hydraulic head [21].

2.8.1 Coefficient of Permeability of the Soil

The coefficient of permeability describes the ability of a porous medium (such as soil, rock, or geological deposits) to transmit fluid, and therefore the rate at which the fluid flows through it [21]. For water flow, this coefficient reflects the ease with which water moves through the pore spaces of unsaturated soil. It is influenced by both the properties of the porous medium and the fluid. This parameter is crucial for analysing both steady and transient state flows of incompressible liquids through porous media. According to [71], the permeability of soil with respect to water is expressed by Equation 2.30:

$$k_w = \left(\frac{g\ \rho_l}{\mu}\right)\kappa \tag{2.30}$$

where μ (Pa.s) is the dynamic viscosity of the fluid, ρ_l (kg/m^3) is the density of the liquid, g (m/s^2) is the gravitational acceleration, and κ (m^2) is the intrinsic permeability, which depends on the porous medium.

Saturated soils typically have constant and relatively high values of the coefficient of permeability. In contrast, the coefficient of permeability in unsaturated soils varies widely with the degree of saturation and generally exhibits much lower values. When the flowing liquid is water, this coefficient is specifically referred to as the hydraulic conductivity of the porous medium. It depends on the properties of the flowing fluid (such as density, viscosity, and compressibility) and the characteristics of the porous medium, including the shape and geometric orientation of the pores.

2.8.2 Modelling Fluid Flow in Unsaturated Porous Medium

Richards' equation is a numerical model used to describe water flow in unsaturated porous media, accounting for both capillarity and gravity effects [72]. It combines Darcy-Buckingham's equation with the continuity equation for mass conservation. The three-dimensional form of the continuity equation in Cartesian coordinates is given by Equation 2.31:

$$\frac{\partial\theta}{\partial t} = -\nabla\cdot q = -\left(\frac{\partial q_x}{\partial x} + \frac{\partial q_y}{\partial y} + \frac{\partial q_z}{\partial z}\right) \tag{2.31}$$

in which θ [L^3L^{-3}] is volumetric water content, and t [T] is time, q_x, q_y and q_z are the components of flux in the x-, y- and z-axis respectively. The 3D form of Richards' equation is formed by substituting for q in the continuity equation, as derived from Equations 2.32 to 2.34, where θ [L^3L^{-3}] represents volumetric water content, and t [T] denotes time. The components of flux in the x-, y- and z-axes are q_x, q_y and q_z, respectively.

To derive Richards' equation, substitute q into the continuity equation, leading to Equations 2.32 to 2.34:

$$\frac{\partial \theta}{\partial t} = \nabla \cdot \left[K(h_p)\nabla(h_p + z)\right] \tag{2.32}$$

$$\frac{\partial \theta}{\partial t} = \nabla \cdot \left[K(h_p)\left(\frac{\partial h_p}{\partial x} + \frac{\partial h_p}{\partial y} + \frac{\partial h_p}{\partial z} + 1\right)\right] \tag{2.33}$$

$$\frac{\partial \theta}{\partial t} = \frac{\partial}{\partial x}\left(K(h_p)\frac{\partial h_p}{\partial x}\right) + \frac{\partial}{\partial y}\left(K(h_p)\frac{\partial h_p}{\partial y}\right) + \frac{\partial}{\partial z}\left[K(h_p)\left(\frac{\partial h_p}{\partial z} + 1\right)\right] \tag{2.34}$$

For vertical flow, such as infiltration, the one-dimensional form of Richards' equation in the vertical z-axis (negative downward) is given by Equation 2.35:

$$\frac{\partial \theta}{\partial t} = \frac{\partial}{\partial z}\left[K(h_p)\left(\frac{\partial h_p}{\partial z} + 1\right)\right] \tag{2.35}$$

Richards' equation can be expressed in different forms: the head form, the water content form, and the mixed form. Equation 2.35 represents the most common head form of Richards' equation. In this form, the first term represents capillarity effects, while the second term captures gravitational flux. Alternatively, Richards' equation can be expressed in terms of water content θ. This approach introduces another hydraulic property of soil, known as soil diffusivity, which describes the rate at which water diffuses within the soil. Diffusivity, also called the soil diffusion coefficient, is expressed in Equation 2.36 as:

$$D(\theta) = K(h_p)\left(\frac{d\theta}{dh_p}\right) = K(\theta)C(\theta) \tag{2.36}$$

where $C(\theta)$ [L^{-1}] is the specific water capacity of the soil $C(\theta) = d\theta/dh_p$. Using the chain rule and substituting $K(h_p)$ with $K(\theta)$, Equation 2.37 gives the water content form of Richards' equation.

$$\frac{\partial \theta}{\partial t} = \frac{\partial}{\partial z}\left(D(\theta)\frac{\partial \theta}{\partial z} + K(\theta)\right) \tag{2.37}$$

By applying the chain rule to the right-hand side, the time derivative of suction or pressure head can replace the time derivative of water content, resulting in Equations 2.38 and 2.39:

$$\frac{\partial \theta}{\partial h_p}\frac{\partial h_p}{\partial t} - \frac{\partial}{\partial z}\left[K(h_p)\left(\frac{\partial h_p}{\partial z} + \right)\right] = 0 \tag{2.38}$$

$$C(h_p)\frac{\partial h_p}{\partial t} - \frac{\partial}{\partial z}\left[K(h_p)\left(\frac{\partial h_p}{\partial z} + 1\right)\right] = 0 \tag{2.39}$$

The choice of Richards' equation form depends on the parameter to be solved and whether the subsoil is single-layered or multi-layered. In single-layered or homogeneous subsoils, water content is continuous across layers, making the water content form appropriate. For multi-layered soils, the pressure head is continuous across layer interfaces, making the head form more suitable for modelling water flow [56], [72]. To solve Richards' equation numerically, it is necessary to specify at least two hydraulic properties of the soil - $\theta(h_p)$, $K(h_p)$, and $D(\theta)$ - along with initial and boundary conditions, particularly at the ground surface.

Equation 2.39 can be rewritten as Equation 2.40, incorporating specific storage S_s [L^{-1}] and effective saturation $S_e(h_p)$ [-], commonly used in COMSOL Multiphysics® [73]:

$$[S_s S_e(h_p) + C(h_p)]\frac{\partial h_p}{\partial t} - \frac{\partial}{\partial z}\left[K(h_p)\left(\frac{\partial h_p}{\partial z} + 1\right)\right] = 0 \tag{2.40}$$

2.8.3 Soil Water Characteristics Curve

The soil water characteristics curve (SWCC) illustrates the relationship between soil water content and its energy status. This energy status can be represented either by the pressure head (energy per unit weight) or the matric potential (energy per unit volume). The SWCC is also known as the capillary pressure saturation curve or the pF curve, where pF denotes the negative logarithm (base 10) of the magnitude of the pressure head measured in centimetres [74]. Water content ranges from minimum (residual) to maximum (saturated) values and serves as curve-fitting parameters without direct physical significance to the soil. Water within the pores of unsaturated soil experiences capillarity and adsorption forces, resulting in a negative tension or pressure head known as the matric head.

The SWCC is used to describe the water retention and release attributes of the soil [21], [75], [76]. It graphically represents the relationship between soil volumetric water content (θ) (or degree of saturation) and soil water potential (ψ), which is indicated by matric suction or pressure head. Due to hysteresis in water retention and release, the SWCC consists of two distinct curves: one for the saturation process and one for the desaturation process.

Given that climatic conditions and seasonal variations affecting soil desaturation can lead to undesirably high soil resistivity, the soil water retention curve (SWRC) is preferred for studying or modelling the impact of seasonality on earthing resistance. Unlike the SWCC,

which includes both curves, the SWRC provides a single curve representing the relationship between soil suction and water content during the desaturation process. Figure 2.3 depicts a typical SWRC in a semi-logarithmic plot, showing volumetric water content (θ) against suction (ψ). This plot illustrates the transition of soil between saturated and desaturated states.

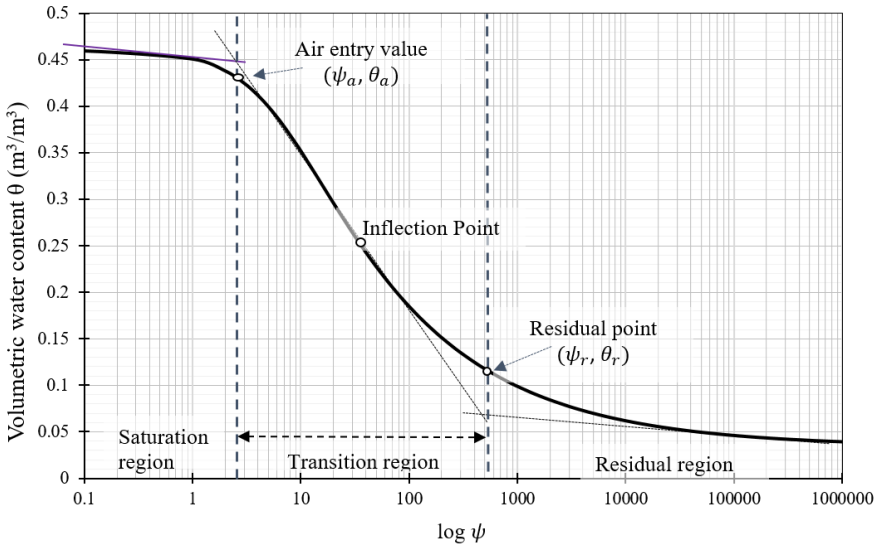


Figure 2.3: Soil water retention curve as a semi-logarithmic plot of volumetric water content (θ) versus suction (ψ) showing critical regions and points

Source: Author's conceptualisation. The figure presents a typical SWRC as a semi-logarithmic plot of volumetric water content (θ) versus suction (ψ). This figure illustrates the saturation, transition (or capillary), and residual regions of soil, as well as the key points of air entry, inflection, and residual.

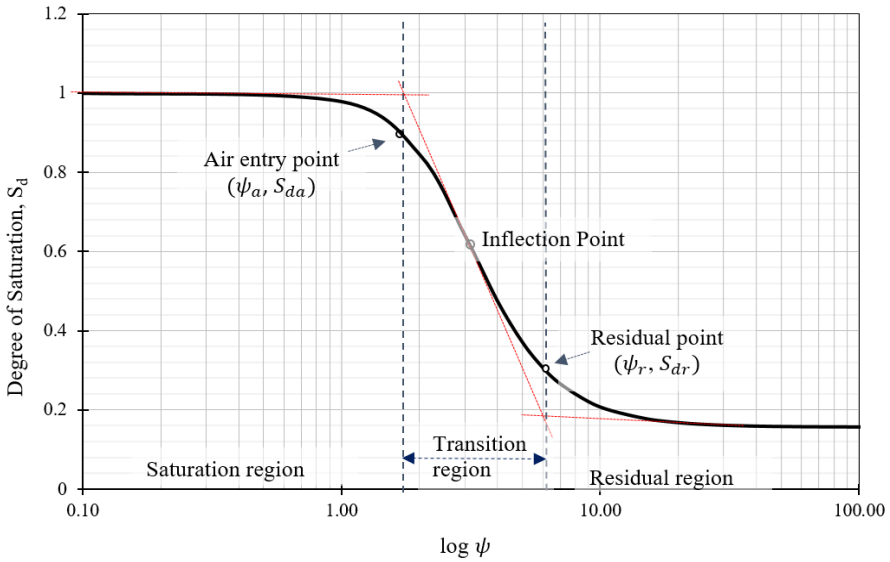


Figure 2.4: Soil water retention curve as a semi-logarithmic plot of soil suction (ψ) against the degree of saturation (Sd) showing critical regions and points

Source: Author's conceptualisation. The figure depicts a typical SWRC as a semi-logarithmic plot illustrating soil suction (ψ) against the degree of saturation (S_d). The figure delineates the different regions of soil behaviour, including the saturation, transition (or capillary), and residual zones. Additionally, it identifies critical points such as air entry, inflection, and residual, providing a comprehensive view of the soil's response to varying water content.

Figure 2.4 provides an alternative representation of the SWRC; this time using the degree of saturation instead of water content. Both plots reveal the soil's saturation, transition (or capillary), and residual regions. The residual and saturation regions correspond to the extreme conditions where soil pores are either fully occupied by air or fully saturated with water.

The capillary or transition region describes the state of the soil where water, held by capillary forces within the soil pores in the presence of air, exhibits significant changes in volumetric water content with small variations in soil suction. In soil science, geophysics, agriculture, and related fields, four critical water contents are commonly identified: saturated, field capacity, wilting point, and residual water contents.

1. Saturated volumetric water content (θ_s) indicates that the soil pores are filled with water.
2. Field capacity (θ_{fc}) is the amount of water remaining in the soil after gravitational drainage has occurred.
3. Permanent wilting point (θ_{pwp}) refers to the water content at which plants cannot extract water, leading to wilting.
4. Residual water content (θ_r) is the water remaining in the soil at high tension, where further changes in suction do not significantly alter the water content.

In addition to the air-entry, inflection, and residual points, the saturation and wilting points are critical for understanding soil transitions between saturated and unsaturated states [77]. Each of these points is defined by a coordinate pair (ψ, θ).

The saturation point is marked by (ψ_r, θ_s), indicating full pore saturation. As the soil transitions to an unsaturated state, air replaces the drained water, leading to the field capacity, with a suction value ψ_{fc} of -33 kPa. The inflection point is the point where the shape of the SWCC transitions between concave to convex. It represents the maximum slope, associated with the highest frequency of pore sizes and provides information about pore size distribution [78], [79]. Unlike others, the coordinates of the inflection point are not known a priori and are often determined with software [80]. The value of subsoil suction at permanent wilting point, ψ_{pwp} is -1500 kPa. Beyond this value, the water in the soil cannot be accessed by plants. The residual point marks the stage where an increase in suction results in no significant change of water content.

Understanding the influence of atmospheric and environmental conditions on soil water and suction allows for meaningful analysis of seasonal variations in soil resistivity and earthing system resistance. By computing soil resistivity values at critical points along the water retention curve (WRC), including the air-entry point (ψ_{ae}, θ_{ae}), field capacity (ψ_{fc}, θ_{fc}), inflection point (ψ_{ip}, θ_{ip}), wilting point (ψ_{wp}, θ_{wp}), and residual point (ψ_r, θ_r), one can gain insights into expected seasonal changes in earthing system resistance.

2.8.4 Hydraulic Conductivity of Porous Medium

As soil desaturates, the displacement of water by air in the soil pores disrupts the continuity of water flow, increasing the resistance between the solid and fluid phases. This interruption impedes the free movement of water through the soil, resulting in hydraulic conductivity being significantly higher at saturation compared to unsaturation. Soil texture also plays a critical role in determining hydraulic conductivity. Coarse-grained soils typically exhibit much higher hydraulic conductivity than fine-grained soils. However, due to their larger pores which facilitate rapid drainage, coarse soils often show lower hydraulic conductivity under unsaturated conditions compared to fine-textured soils.

Hydraulic conductivity at saturation remains constant and can be measured in the laboratory using the falling head and constant head tests for fine- and coarse-textured soils, respectively. An alternative to the time-consuming laboratory tests for estimating the saturated hydraulic conductivity (K_s) (m/day) is the empirical formula given in equation 2.41. This formula relates K_s to soil porosity (ϕ) and the inverse of suction at the air-entry point (α_h) (m^{-1}) [77], [81]:

$$K_s = 4.65 \times 10^{-2} \phi (\alpha_h)^2 \tag{2.41}$$

In contrast, the hydraulic conductivity of unsaturated soils depends on the soil water content or degree of saturation. As soil desaturates, the air-filled pores create additional non-conducting channels, reducing the effective cross-sectional area available for water flow [21]. This leads to increased tortuosity and irregularity in the flow pathways, making water movement more difficult. Hydraulic conductivity varies significantly with changes in suction beyond the air-entry suction ($\psi > \psi_{ae}$). There is a nonlinear relationship between changes in degree of saturation and hydraulic conductivity; a linear change in volumetric water content corresponds to a logarithmic change in hydraulic conductivity.

Several empirical models have been proposed to describe hydraulic conductivity functions [56], [74]. For example, in 1958 Gardner proposed the equation in Equation 2.42 [56]. It

expresses hydraulic conductivity as an exponential function of pressure head and a soil-specific parameter α_s:

$$K(h_p) = K_s e^{-\alpha_s h_p} \tag{2.42}$$

Equation 2.43 represents the hydraulic conductivity function (HCF) proposed by van Genuchten and describes hydraulic conductivity as a function of matric suction [74]:

$$K(h_p) = K_s \left\{ \frac{\left[1 - (\alpha_h h_p)^{n-1} \left(1 + (\alpha_h h_p)^n\right)^{-m}\right]^2}{\left[1 + (\alpha_h h_p)^n\right]^{\frac{m}{2}}} \right\} \tag{2.43}$$

Here, α_h is the inverse of the suction at the air-entry point, and n is a fitting parameter from the van Genuchten water retention model.

The model proposed by Mualem is expressed in equation 2.44. It is based on soil water content (θ) and represents the most widely used hydraulic conductivity function [82].

$$K(\theta) = K_s S_e^{0.5} \left\{ \left[\int_0^{\theta} \left(\frac{1}{h_p}\right) d\theta \right] / \left[\int_0^{\theta_s} \left(\frac{1}{h_p}\right) d\theta \right] \right\}^2 \tag{2.44}$$

In which α_h is the inverse of suction at the moment air enters the saturated soil, n a fitting parameter of the van Genuchten water retention model of the soil. However, the most popular HCF given as a function of θ, was proposed in 1976 by Mualem [82]. It is expressed in equation 2.44 as a function of the pressure head, effective saturation, and saturated hydraulic conductivity of the medium.

$$K(\theta) = K_s S_e^{0.5} \left\{ \left[\int_0^{\theta} \left(\frac{1}{h_p}\right) d\theta \right] / \left[\int_0^{\theta_s} \left(\frac{1}{h_p}\right) d\theta \right] \right\}^2 \tag{2.44}$$

2.8.5 Equations of Water Retention

Brooks and Corey [83], van Genuchten [84], and Fredlund and Xing [85] have developed constitutive equations that describe the relationship between soil water content and suction or pressure head. These models mathematically characterise the complex hydraulic properties of soil based on parameters obtained from regression analyses. While these equations estimate the water content (θ) of homogeneous soils for a given equilibrium and isotropic suction (ψ) or pressure head (h_p), the fitting parameters used may not always have a direct physical interpretation.

Amongst the various models, those proposed by Fredlund and Xing and van Genuchten are commonly used because they can effectively describe water retention in the regions that exhibit discontinuities, unlike the Brooks and Corey model. The Mualem-van Genuchten (MG) model, a modified version of the van Genuchten model with one fewer variable, is particularly popular. This model expresses S_e, θ, and κ_r in terms of h_p. The subsoil is considered saturated when the fluid pressure equals atmospheric pressure. That is $h_p = 0$. For $h_p > 0$, $S_e(h_p) = 1$. Under saturation conditions, $h_p \geq 0$: $S_e(h_p) = 1, \theta(h_p) = \theta_s$, and $\kappa_r = 1$. For unsaturated conditions $h_p < 0$, equations 2.45 – 2.47 applies.

$$S_e(h_p) = \left(\frac{1}{1 + (\alpha_h |h_p|)^n}\right)^m \tag{2.45}$$

$$\theta(h_p) = \theta_r + (\theta_s - \theta_r)\left(\frac{1}{1 + (\alpha_h |h_p|)^n}\right)^m \tag{2.46}$$

$$K(h_p) = K_s \cdot (S_e)^l \left[1 - \left(1 - (S_e)^{\frac{1}{m}}\right)^m\right]^2 \tag{2.47}$$

Equation 2.48 is the expression for diffusivity.

$$D(\theta) = \frac{(1-m)K_s}{\alpha_h m(\theta_s - \theta_r)} (S_e)^{l-1/m} \left[\left(1 - (S_e)^{\frac{1}{m}}\right)^m + \left(1 - (S_e)^{\frac{1}{m}}\right)^{-m} - 2\right] \tag{2.48}$$

Here, S_e denotes the effective saturation, and K_s represents the saturated hydraulic conductivity α_h is a fitting parameter, whose value is inversely proportional to the bubbling pressure or suction h_a at air entry. h_a represents the pressure where the largest pore begins to drain [81]. It has a unique value that can be determined from the SWRC. The relative permeability of the soil is denoted by κ_r, while κ_s is the permeability at saturation. The parameter l represents the connectivity-tortuosity coefficient, and n is a dimensionless fitting parameter related to the particle size distribution of the medium. For $n > 1$, the relationship between n and m is ($m = 1 - 1/n$) [74], [84].

2.9 Multiphysics Coupling of Fluid and Electric Current Flows in Subsoil

To achieve the research objectives, a coupled multiphysics differential equation (CMDE) is formulated based on the theoretical frameworks discussed. The CMDE integrates the differential equations governing fluid flow in unsaturated porous media and electric current flow in electrically conductive media using a version of Archie's equation [25], [86], [87]. To

simplify the model, the surface conductivity term (σ_s) from the complete Archie's law (Equation 2.17) can be neglected, resulting in Equation 2.49:

$$\sigma(S_d) = \sigma_w \phi^{\mathfrak{m}} (S_d)^{\beta} \tag{2.49}$$

Here, $\mathfrak{m}$ and β are the cementation factor and saturation index, respectively. Given that the electrical conductivity of the liquid phase σ_w is constant and $\phi = \theta_s$ at saturation, the term $\sigma_w \phi^{\mathfrak{m}}$ becomes a constant characteristic of the soil-fluid medium.

Denoting this constant by A_σ, Equation 2.49 simplifies to Equation 2.50:

$$\sigma(S_d) = A_\sigma (S_d)^{\beta} \tag{2.50}$$

In some cases, a normalised form of S_d, denoted S_e is used instead. In such instances, Equation 2.50 transforms Equation 2.51.

$$\sigma(S_e) = A_\sigma (S_e)^{\beta} \tag{2.51}$$

Equations 2.52 and 2.53 further express this relationship as functions of θ or h_p:

$$\sigma(\theta) = A_\sigma \left(\frac{\theta - \theta_r}{\theta_s - \theta_r}\right)^{\beta} \tag{2.52}$$

$$\sigma(h_p) = A_\sigma \left(\frac{1}{1 + (\alpha|h_p|)^n}\right)^{m\beta} \tag{2.53}$$

Thus, Archie's equation is expressed in terms of the S_d, θ, S_e, or h_p. Each form provides a basis for coupling the two partial differential equations that govern the flow of electric current and fluid in a variably saturated porous and electrically conductive medium. Substituting any of these forms into the CMDE (Equation 2.10) results in a CMDE, which describes the dispersion of electric current under the variable conditions of the porous medium. The CMDE can be expressed in terms ofS_e, θ and h_p in equation 2.54, 2.55 and 2.56 respectively:

$$\nabla \cdot J = -A_\sigma (S_e)^{\beta} \cdot (\nabla^2 V_p) \tag{2.54}$$

$$\nabla \cdot J = -A_\sigma \left(\frac{\theta - \theta_r}{\theta_s - \theta_r}\right)^{\beta} \cdot (\nabla^2 V_p) \tag{2.55}$$

$$\nabla \cdot J = -A_\sigma \left(\frac{1}{1 + (\alpha|h_p|)^n}\right)^{m\beta} \cdot (\nabla^2 V_p) \tag{2.55}$$

2.10 Definition of Terms

Water content (θ): This is the fraction of soil volume that is occupied by water, expressed either as a percentage or as a decimal fraction.

Porosity (ϕ): This refers to the fraction of soil volume that consists of void space or pores, expressed as a percentage or decimal fraction. It measures the soil's capacity to hold water and affects water flow through the soil.

Hydraulic conductivity (k): This represents the soil's ability to transmit water, which depends on the water content and pressure head of the soil.

Pressure head (h_p): This is a measure of the potential energy of soil water, indicating the height to which water will rise in a vertical column due to capillarity. Depending on the degree of saturation, it can be positive or negative.

Soil suction ψ): This represents the attraction of water to the particles or grains of unsaturated soil. It relates to capillary tension and influences water movement in unsaturated soils.

Matric suction: This is the capillary component of free energy, equivalent to the suction derived from measuring the partial pressure of water vapour in equilibrium with the soil water, relative to the partial pressure of water vapour in equilibrium with a solution identical in composition to the soil water.

Osmotic suction: This is the solute component of free energy, equivalent to the suction derived from measuring the partial pressure of water vapour in equilibrium with a solution identical in composition to the soil water, relative to the partial pressure of water vapour in equilibrium with pure water.

Total suction: This is the free energy of soil water, equivalent to the suction derived from measuring the partial pressure of water vapour in equilibrium with the soil water, relative to the partial pressure of water vapour in equilibrium with pure water.

Chapter 3 - Research Methodology and Simulation Modelling of Proposed Method

3.0 Introduction to Research Methodology

The research develops a novel hydro-geoelectric method for estimating the resistance and performance of earthing systems, the resistance reduction capacity of earthing enhancement materials under various subsoil conditions and climates. By leveraging the relationship between electrical conductivity, soil water content, and soil suction, the research utilises the simulation modelling of earthing systems with hydraulic properties of the subsoil alongside climate and subsoil condition indicators to achieve this goal.

This chapter outlines the creation of the geometric model of the earthing system in COMSOL Multiphysics® software, detailing the assignment of physics, specification of parameters, boundary and initial conditions, as well as geometric meshing. The finite element analysis (FEA) of the model is described, followed by a discussion on analytical equations used for post-processing analysis and model result validation.

3.1 Model Development

The development of the proposed hydro-geoelectric earthing model was conducted using COMSOL Multiphysics® software. The model integrates two independent physical phenomena: the dissipation of electric current and the flow and retention of water within the subsoil. These phenomena are governed by Laplace's equation for electric current and Richards' equation for water flow, respectively. Both equations are independently solved through finite element analysis (FEA) but are coupled using Archie's equation.

For a known boundary condition, specified as soil suction at the subsoil surface, the FEA of Richards' equation provides the volumetric water content or degree of saturation. The corresponding electrical conductivity of the subsoil is then determined through Archie's equation. When the value of electric current dissipated from the earth conductor into the subsoil is known, the electric potential at any point within the subsoil is calculated using the FEA of Laplace's equation, which governs the conservation of electric current within the conductive medium. The low-frequency resistance of the earthing system relative to the subsoil is determined from post-simulation analysis using an energetic formula, expressed as a function of electric field strength and electric potentials [88]. The simulation development process is illustrated in Figure 3.1.

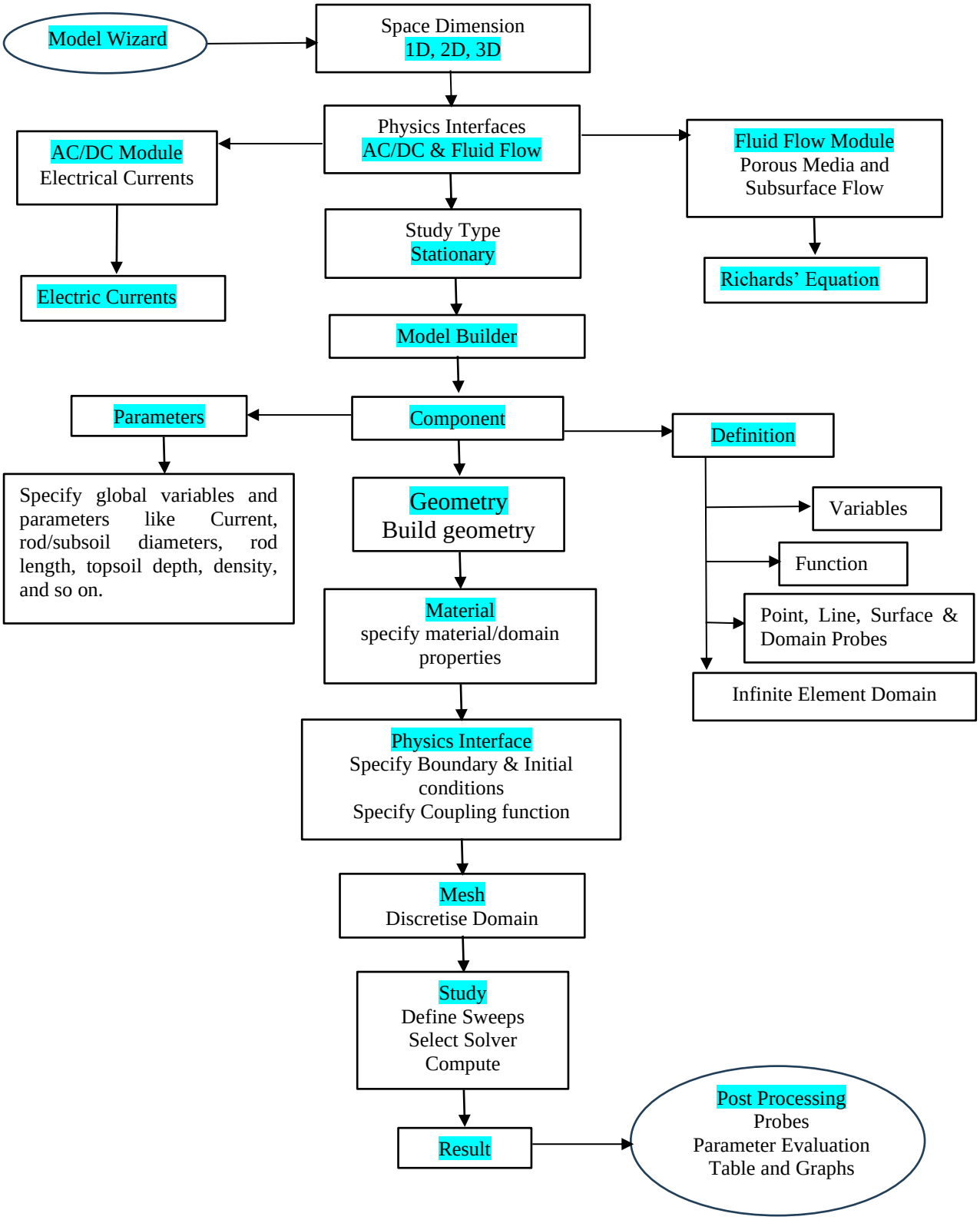


Figure 3.1: Flow diagram of Simulation Modelling and Evaluation Phases

Source: Author's conceptualisation

3.2 Hydro-Geoelectric Earthing Modelling in COMSOL Multiphysics®

In COMSOL Multiphysics® software as Figure 3.2 shows, the software provides six domain spaces within the Model Builder, of which the 2D axisymmetric and 3D domain spaces were utilised for the modelling process. A detailed description of the capabilities of the multiphysics software can be found in its documentation [89].

The governing equations for fluid flow in an unsaturated porous medium and for electric current dissipation in a conductive medium were analysed using the AC/DC and Fluid Flow modules of COMSOL Multiphysics®. The Laplace equation, formulated in terms of electrical conductivity, was used to determine the distribution of the electric field within the subsoil. The Fluid Flow module includes Richards' equation, which describes water content as a function of pressure head.

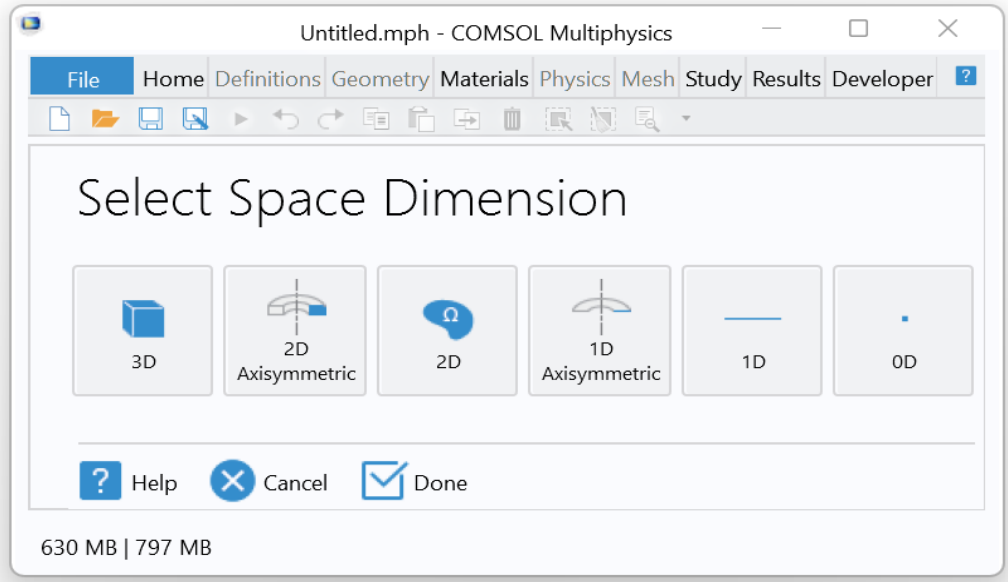


Figure 3.2: View for the space selection interface in COMSOL Multiphysics® software

Source: [89].

Since there is no inherent coupling between the Laplace and Richards' equations, the multiphysics solution was achieved by coupling these equations through Archie's law, which relates water content to resistivity. Water content at any given pressure head was determined using Richards' equation, allowing resistivity to be evaluated using Archie's law. Once the current or voltage at the earthing electrode is specified, the electric potential at any point within the soil domain can be calculated by solving the Laplace equation. The earthing resistance in the subsoil is determined by the ratio of the difference in electric potential between the

electrode surface and any horizontal point in the subsoil to the current dissipated from the electrode surface.

3.2.1 Geometric Modelling of Earthing Electrode in the Subsoil

The geometric model of the earth electrode was constructed within the *Component* node of the Model Builder. While various subsoil domain shapes can be utilised, cylindrical and hemispherical models were preferred due to their compatibility with the radial symmetry of the cylindrical earth rod, which is supported by the 2D axisymmetric and 3D space domains. For earth grids or meshes, the 3D domain space is recommended, as it allows for the use of radial symmetry fractions such as ½, ¼, ⅛, or 1⁄16 of the model. This approach reduces computational costs and mesh memory requirements. The subsoil domain was chosen to be significantly larger than the size of the earth rod to ensure that the electric potential at its outer boundary approaches zero or is sufficiently small to yield accurate results. The dimensions and parameters of the model were specified as variables with assigned numerical values.

The construction of the geometric model involved creating models for both the soil and the earthing electrode. One- and two-layer subsoil models were developed, with Figure 3.3 illustrating a sample of the subsoil models.

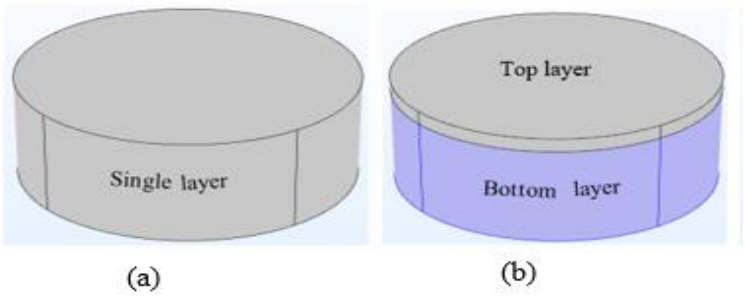


Figure 3.3: 3D representation of single- and two-layer subsoil models

Source: Author's conceptualisation

Several simulation models of earthing systems were developed to demonstrate the effectiveness of the proposed hydro-geoelectric method in estimating and predicting earthing resistance and performance in variably saturated soils. To assess the impact of soil texture on the resistance and performance of earthing systems, three soil textures - clay, silt, and sand - were used in the subsoil models. These textures were chosen because they are key components in soil textural classification, and their hydraulic and electrical properties were obtained from references [77], [90], [91]. The subsoil models, as outlined in Table 3.1, include the following configurations:

Table 3.1: Models of single-layer, double-layer, and triple-layer subsoils consisting of the combinations of clay, silty and sandy textured soils.

Subsoil model	Soil layer	
	Top	**Bottom**
Single	Clay	-
	Silty	-
	Sandy clay	-
Double	Sandy clay	Silty
	Sandy clay	Clay
	Silty	Clay

Source: Author's conceptualisation.

1. A single-layer subsoil model consisting of only clay, silty, or sandy soil.
2. A two-layer subsoil model with the following combinations:
   a. Top layer of silty soil and bottom layer of clay soil.
   b. Top layer of sandy soil and bottom layer of silty soil.
   c. Top layer of sandy soil and bottom layer of clay soil.

In this work, only vertical earth rod in single- and two-layer subsoils were modelled to demonstrate the proposed method, although the resistance of earthing with horizontal orientation, such as the horizontal strip and earth grid without rods are more susceptible to variation. However, since many subsoil layers respond differently under the same condition, the vertical rod was chosen because it can access more subsoil depth. Unlike the infinite subsoils that were modelled with approximate dimension, the geometric models of the earth electrodes were created with actual dimensions.

To demonstrate the resistance reduction capacity and efficiency of EEMs in high-resistivity, geometric models of EEMs around vertical rods were built for each of the three subsoil models. With respect to EEMs around vertical rods, two earthing models were developed, namely

1. Vertical earthing rod with earthing enhancement material, and
2. Earth grid with earthing enhancement material around the vertical rods.

Figure 3.4 shows a cross-sectional view of a vertical earth rod surrounded by a cylindrical EEM within the region of influence of the rod.

The efficiency of the EEM is determined by comparing the resistance of vertical earth rod system with EEM to the resistance of the rod without EEM at corresponding values of soil suction.

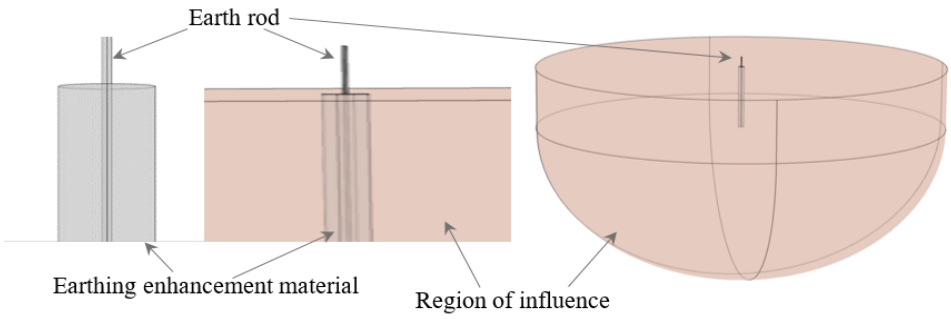


Figure 3.4: Cross-sectional view of vertical earth rod with earthing enhancement material within the region of influence of the rod

Source: Author's conceptualisation

3.2.2 Definition Branch of the Model Builder

Through the *Definition* branch, COMSOL Multiphysics® enables the definition of component parameters, functions, variables, geometric level (domain, boundary / surface / face, edge / line, or point) selection, probe, and integration for the simulation model. The *Definition* branch is accessed under the *Component* node, and it allows the user to define variables, parameters and functions in the Model Builder.

For instance, within the definition branch, Archie's equation or equation of electric conductivity $\sigma(h_p)$ or $\sigma(S_e)$, which is used as coupling between the differential equations for Richards' equation and Ohms' law, can be specified as an explicit function. The function is assigned a name, say *Econ* and is expressed as a function of the variable assigned to the average value of water content (W_{cs}), effective degree of saturation (S_{es}) within the subsoil. At any soil suction, the average value of water content or effective degree of saturation is determined by performing a domain probe for water content or degree of saturation for the subsoil. This domain probe is also defined within the *Definition* branch. If the variable assigned to water content domain probe is X_θ and X_{se} is assigned as the variable name for effective saturation domain probe, then the expression for electric conductivity is defined by either $Econ(X_\theta)$ or $Econ(X_{se})$.

The *Definition* branch also enables the assignment of the infinite element domain (IED) to space boundaries. The size of the finite geometric domain that represents the infinite (unbounded) subsoil may be inadequate to match the assigned boundary condition of 0V. An IED is required to numerically analyse the physical phenomena accurately at the virtual boundary. Assigned to the outer boundary of the geometric domain of the subsoil, the IED

converts the unbounded boundaries to bounded form that is suitable for finite element analysis. The pink-coloured portions of Figures 3.5 and 3.6 are examples of IED assigned to a subsoil model around vertical earth rod in 2D and a square earth grid in 3D spaces respectively.

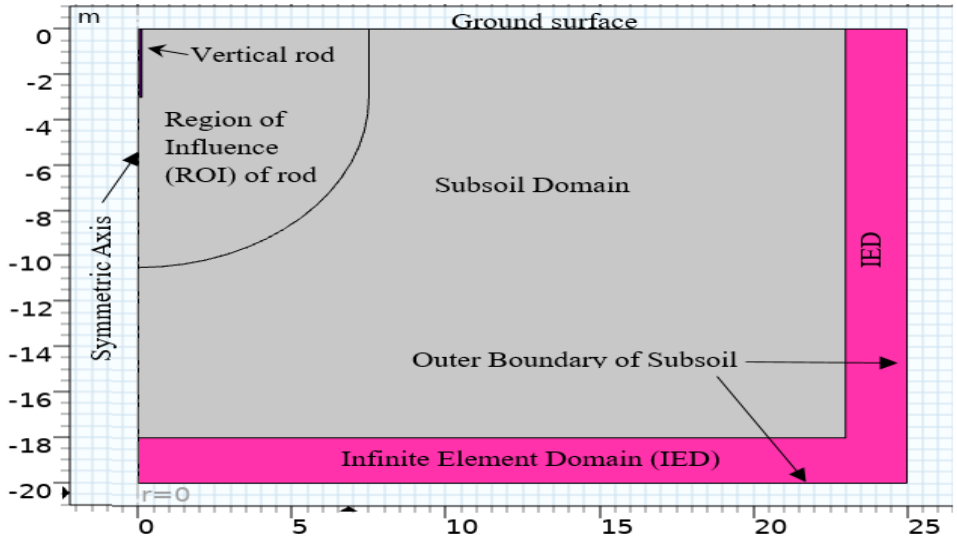


Figure 3.5: 2D axisymmetric view of vertical earth rod in single-layer subsoil model with infinite element domain (IED)

Source: Author's conceptualisation

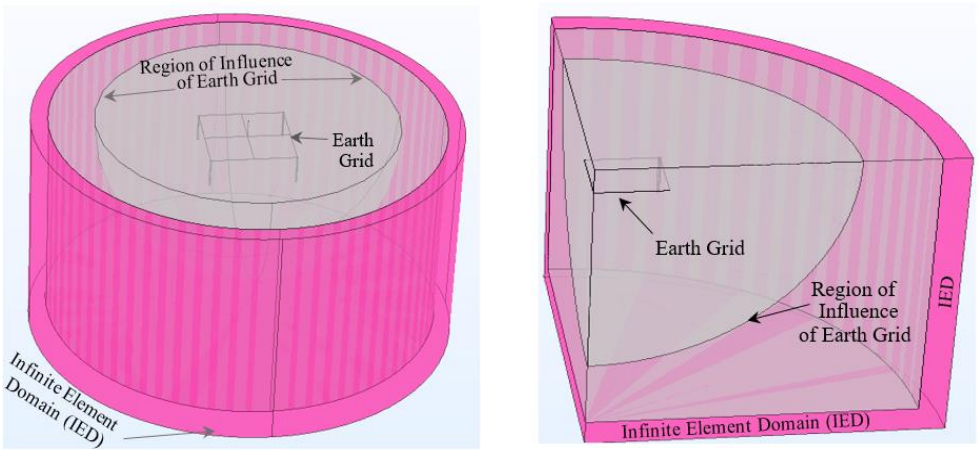


Figure 3.6: Whole and one-quarter 3D sections of earth grid in single-layer subsoil with infinite element domain (IED)

Source: Author's conceptualisation

3.2.3 Physics Interfaces

The differential equation governing the physics of fluid flow and electric current flow in conductive porous medium can be accessed within the Richards' equation (RE) interface and electric currents (EC) interface respectively. The RE interface is housed within the Porous Media and Subsurface Flow submodule under the Fluid Flow module, whereas the EC interface is found within the Electric Fields and Currents submodule under the Alternating Current and Direct Current (AC/DC) module.

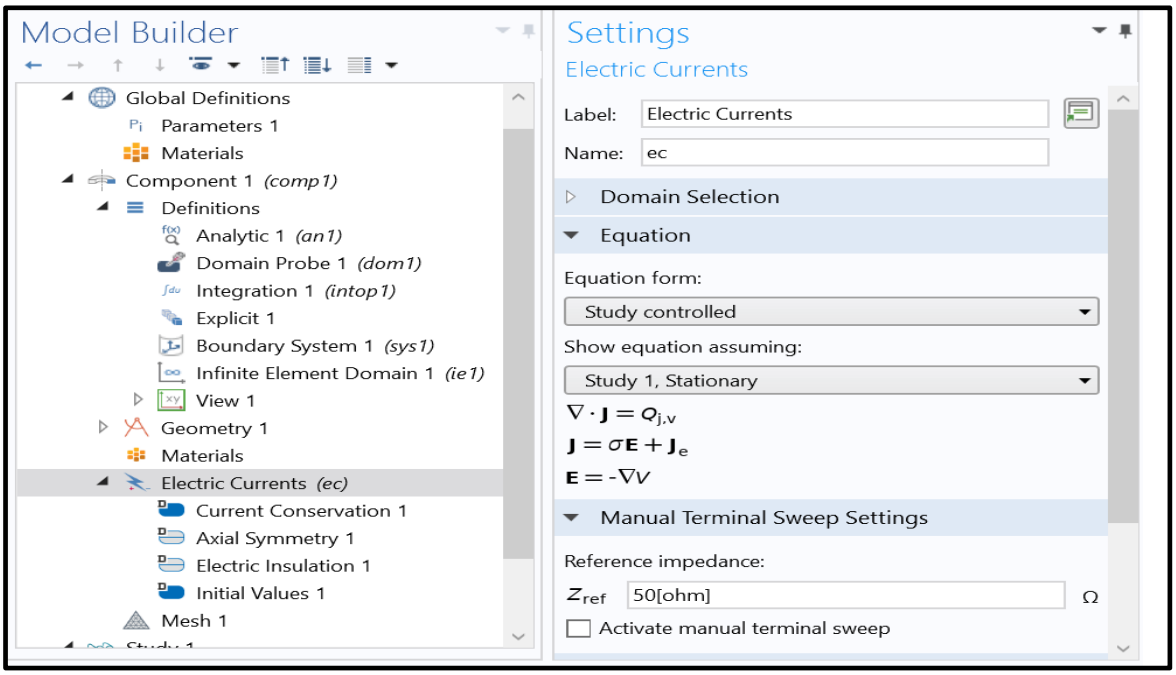


Figure 3.7: Model Builder interface in COMSOL Multiphysics®

Source: [89].

The EC interface solves the current conservation equation based on Ohm's law and determines electric field intensity, electric current density and distribution of electric potential within a conductive medium of negligible inductive effect using the scalar electric potential, V_p as the dependent variable.

As seen in Figure 3.7, three default and two user-assigned nodes are required to model the dispersion of electric current in 3D space. These nodes are the *Current Conservation* node, which is the main default node. Besides containing the governing differential form or Ohms' law, the main node provides the field for specifying the expression or value of electrical conductivity of the soil or porous media. If the geometric model contains many media of unique electrical conductivity, then additional *Current Conservation* nodes are assigned, one for each

medium. Other default nodes are the *Electric Insulation* node for specifying the boundaries inhibiting electric current flow, and the *Initial Value* node for assigning initial value of the dependent variable. The *Ground* node and any one of *Terminal* or *Floating Potential* nodes are the other nodes required for assigning other boundary conditions for electric current flow modelling. With the *Ground* node, the boundary where the electric potential is approximately zero can be assigned. The *Floating Potential* and *Terminal* nodes are mutually exclusively used to specify voltage or current at the surface of the earth electrode.

Similarly, the RE interface uses pressure as the dependent variable for solving fluid flow in variably saturated porous media. Interfaces in COMSOL Multiphysics® have predefined nodes that are added by default or the user to specify parameters and initial / boundary conditions of the simulation model. Four default nodes and one user-assigned node are required in the RE interface simulation modelling. The default and main node of RE interface is the *Richards' Equation* node. As the name implies, it contains Richards' equation which is the differential equation governing fluid flow in variably saturated soil. *Richards' Equation* node also provides fields for specifying the properties of fluid properties such as fluid viscosity μ, and density ρ_w, porous media properties such as hydraulic conductivity function or value, storage model, residual and saturated volumetric water contents, that is, θ_r and θ_s. The node also provides fields for specifying the parameters of a selected or user-defined water retention model of the porous medium. It is within this node that the fitting parameters of the van Genuchten water retention model, α_h, n and $l = 0.2$ (default value) are supplied.

If two or more porous medium or soil layers are involved, then as many *Richards' Equation* nodes are required. The *No Flow* node is another default node which is used for specifying the boundaries that are impermeable to fluid flow. To specify the initial value of dependent variable assigned to the porous medium in the form of pressure, hydraulic head or pressure head, the *Initial Value* node, a default node, is used. Since external influences are modelled as suction at the ground surface, any one of *Pressure*, *Hydraulic Head* or *Pressure Head* nodes can be used to specify the suction on the ground surface as a value or expression of pressure, hydraulic head or pressure head. If the geometric model is built in 1D or 2D axisymmetric space, then a default *Axial Symmetry* node is attached by default. This node marks the axis of vertical symmetry of the simulation model. Each interface has default nodes and allows additional nodes for specifying initial and boundary conditions.

3.2.4 Multiphysics Coupling Equation

The EC interface requires an expression for electric conductivity to couple the two physics interfaces. The setting window of the *Current Conservation* node of the EC interface permits the specification of the electric conductivity.

Expressed as function of θ or S_e from the formulation in the *Definition* branch, the electrical conductivity function is supplied in form of $Econ(X_\theta)$ or $Econ(X_{se})$ as a user-defined electrical conductivity under the constitutive *JC-E relation* field of the *Current Conservation* node. At any equilibrated value of suction, the $Econ(X_\theta)$ or $Econ(X_{se})$ evaluates the value of electric conductivity from the solution or dependent values (water content or effective saturation) of Richards's equation and provides the conductivity variable in Ohm's law. The variability of electrical conductivity because of changes in the degree of saturation or suction of the soil medium is responsible for the variability of electric field strength, current density or distribution of electric potential at any point within the soil domain as the magnitude of external influences (soil suction) changes.

3.2.5 Modelling Assumptions

In developing the hydro-geoelectric model that can estimate and predict the resistance and performance earthing systems under different climatic and environmental conditions, the fundamental assumption is that water content is the major determinant of the electrical conductivity of unsaturated soil, EEMs and any other porous media. Other assumptions are as follows.

1. Water in the soil, EEM or porous medium is incompressible.
2. Ground surface is initially at saturation.
3. The value of suction applied at the ground surface eventually equilibrates uniformly within the unsaturated portion of the subsoil.
4. At equilibrated suction, the water content of the subsoil, EEM or porous medium does not change.
5. Electrical conductivity of subsoil layers or homogeneous medium is isotropic and depends on its degree of saturation.
6. The component of surface conductivity of soil, EEM and porous medium is negligible.

3.2.6 Initial Condition

Initial condition refers to the value of the independent variables such as electric potential and pressure prior to the dispersion of electric current and equilibrated state of soil suction.

1. It is assumed a prior that the initial condition of the Vadose region of the ground is saturated. That is, $\theta(r,0) = \theta_s$. Then, the initial value of pressure head or suction (as function of pressure) within the saturated subsoil is zero. That is, $h_p(r,0) = 0$ or $\partial h_p/\partial z\big|_{z=0} = h_p$. The influence of the atmosphere which is exerted on the ground surface as pressure or suction is transmitted through the subsoil uniformly, resulting in de-saturation. This condition is specified at the *Initial Value node* of the RE interface.
2. Prior to the dissipation of electric current from the surface of the earth electrode, the initial value of electric potential at any point within the soil domain and the surface of the earth electrode is zero, that is, $V(0,z) = 0$. To specify this condition, the default *Initial Value* node of the EC interface is required.

3.2.7 Boundary Conditions

The simulation model has three unique boundaries which are shown in Figure 3.8. These boundaries are the soil-electrode interface, air-soil boundary or ground surface and the outer surface of the subsoil geometry which represents a boundary at or near infinity. Boundary conditions are described at boundaries marked at r horizontal distance from the surface of earthing electrode and at z depth from the ground surface. These boundaries are described as

1. Soil-electrode boundary (r_r, L_r)

At (r_r, L_r) representing the radius r_r, and length L_r, of the vertical rod, the soil-electrode interface defines the boundary where the total electric current density (J) normal to the surface of the buried electrode is equal to the current, I_f, dispersed from the electrode surface, S, to the soil domain. The governing equation at the soil-electrode surface is $\int(-\vec{\mathbf{n}} \cdot J)dS = I_f$: where $\vec{\mathbf{n}}$ is normal to the electrode surface. This boundary condition is specified as terminal current or current I_f in the *Terminal* node or by a constant voltage, $V(0,z) = V_E$ in the *Floating Potential* node of the EC. Since earthing resistance is independent of the current dispersed from the surface of the buried electrode, any value may be assigned to I_f. A value of $I_f = 1A$ has been used in this modelling analysis.

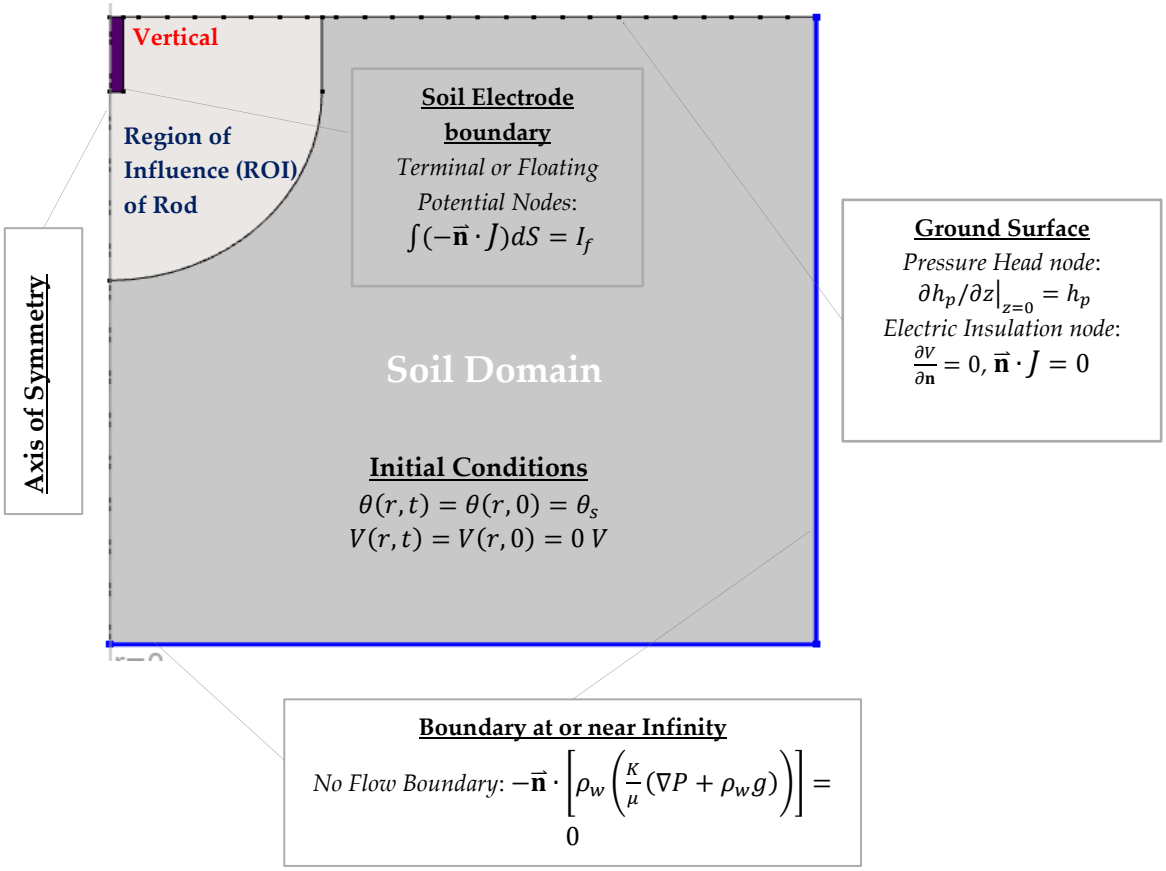


Figure 3.8: Annotated cross-sectional view of 2D axisymmetric model of vertical earth rod in single-layer subsoil with region of influence, initial and boundary conditions

Source: [92].

2. Ground Surface or Air-Soil boundary, $(0,0)$

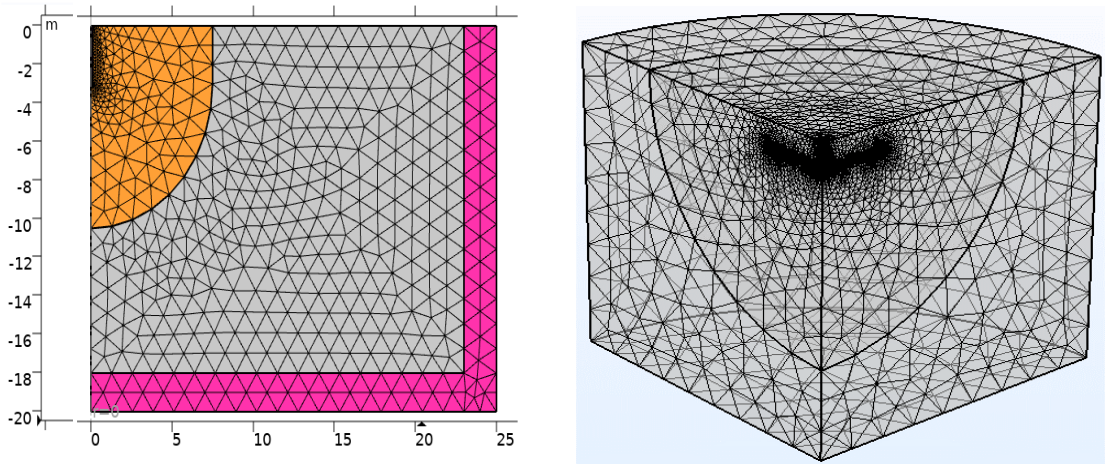
   The top boundary of Figure 3.8 is the ground surface interfacing with the ground soil and atmosphere. For electric current flow, the ground surface acts as an insulator impermeable to electric current flow. This means that the current density normal to this boundary is zero. That is, $\vec{\mathbf{n}}\cdot\boldsymbol{J} = 0$, where $\vec{\mathbf{n}}$ is the normal to ground surface. This boundary is assigned in the *Electric Insulation node* of the EC interface. The pressure exerted on the ground surface by the atmosphere produces a change in the energy potential of soil water that becomes constant within the unsaturated soil volume. The energy state of soil water at this boundary is specified using any of the following nodes in the RE interface, *Pressure*, *Hydraulic Head* or *Pressure Head nodes*. For time-dependent analysis, the value of pressure, and hydraulic / pressure head assigned must be consistent with the corresponding initial value assigned in the *Initial Value node* of the RE interface

3. Outer Domain Boundary, $(\infty, 0)$

Marked as the blue coloured lines at the right and bottom of Figure 3.8, these boundaries are characterised by the diminished effect of electric field from current dissipation, such that the electric potential there is assumed zero, that is, $V_p = 0V$. These boundaries are assigned in the EC interface using the *Ground* node. Boundaries whose water flux has minimal effect on water content within the ROI, are considered impermeable to water or no flow. These are boundaries considered to be at infinity whose governing equation is described as $-\vec{\mathbf{n}} \cdot \rho_w \boldsymbol{u} = 0$. They are assigned in the RE interface using the *No Flow* node.

3.2.8 Geometric Discretisation

COMSOL Multiphysics® permits user-defined or physics-controlled meshing, allowing the discretisation of the domain and solution of the continuous differential equations to be solved as discrete. For the 2D space domain, triangular-shaped mesh elements were used, while triangular or tetrahedrons elements were used in the 3D space discretisation as shown Figure 3.9 (a) and 3.9 (b) respectively. The radius of the soil domain and rod is 25 m and 9.525 mm, respectively; therefore, soil size is 2,624 times the rod size. Due to this dimensional difference, two discretisation levels are required for good numerical solution. Table 3.2 shows the input and output statistics for the 2D axisymmetric model (500 m^2 mesh area) and one-quarter section of the 3D model for earth grid with mesh volume 12,250 m^3.



(a) (b)

Figure 3.9: Mesh cross sections of 2D axisymmetric view of the vertical earth rod and one-quarter 3D earth grid in single-layer subsoil

Source: [89].

They were meshed by free triangles and tetrahedral / triangles respectively, with maximum and minimum mesh element size of 1.33/0.0075 m and 3/0.003175 m for the 2D and 3D models respectively.

Table 3.2: Input and output mesh statistics for 2D axisymmetric of vertical earth rod in homogeneous soil and 3D model of earthing grid in homogeneous soil

Meshing (input/output)	**Parameter**	**2D Model (Rod)**	**1/4 view of 3D Earth Grid**
	Mesh type	Free Triangles	Tetrahedrons/ Triangles
Meshing	Electrode maximum element size (m)	0.0096525	0.003175
Input	Electrode minimum element size (m)	0.003175	0.001905
	Max/Min soil domain element size (m)	1.33/0.0075	3/0.003175
	Mesh area (m^2)	500	-
	Mesh volume (m^3)	-	12,250
	Number of triangular elements	4,715	174,170
	Number of tetrahedral elements	-	30,74,774
	Edge element	585	28,535
	Vertex element	34	56
	Mesh vertices	2,531	534,568
Meshing	Min./Ave. skewness element quality (EQ)	0.5278/0.8257	0.1595/0.6479
Output	Min./Ave. max. angle element quality	0.6745/0.907	0.1980/0.7323
	Min./Ave. growth rate element quality	0.4807/0.8126	0.3011/0.3538
	Min./Ave. volume versus circumradius EQ	0.8396/0.9306	0.1037/0.6497
	Min./Ave. volume versus length element quality	0.7803/0.9531	0.1836/0.7513
	Min./Ave. condition number element quality	0.7803/0.9531	0.2680/0.8159

Source: Author's conceptualisation.

For the 2D model, this produced mesh 4,715 mesh elements (free triangles), 585 edge elements, 2,531 mesh vertices and 34 vertex elements. Whereas there were 174,170 triangles, 3,074,774 tetrahedrons, 28,535 edge elements, 534,568 mesh vertices, and 56 vertex elements. Good meshing requires that the minimum and average mesh element qualities be > 0.1 and all the criteria listed in the table, namely skewness, maximum angle, volume versus circumradius, volume versus length, and growth rate met this requirement. Figure 3.10 is the mesh plot for the 2D axisymmetric model showing good element quality in green colour with legend value close to 1.

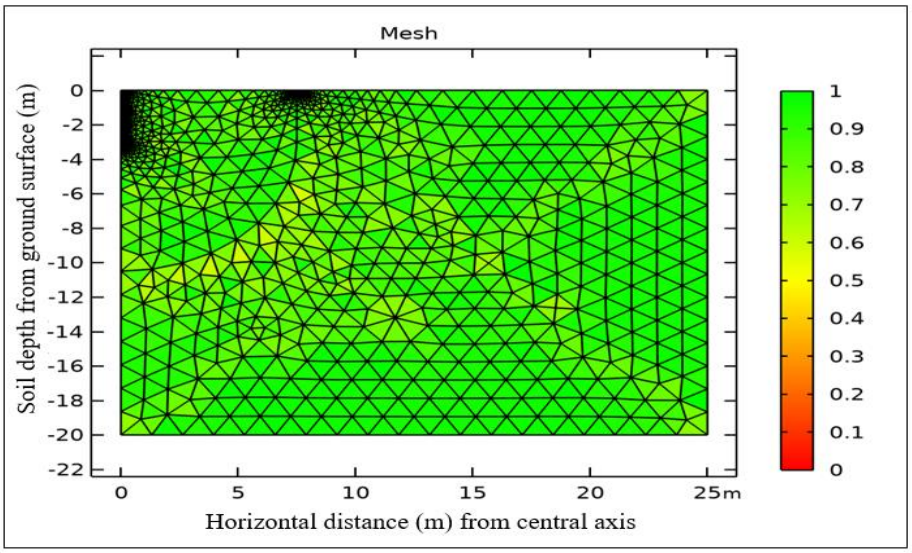


Figure 3.1: Mesh plot of 2D axisymmetric vertical earth rod in single-layer subsoil showing good quality mesh element in green colour

Source: [92].

3.2.9 Study Modes and Solvers

Based on the assumption of steady state, the stationary study mode was used in the model analysis. On the setting window of the study mode, parametric and auxiliary sweeps accessed and used to investigate the sensitivity and performance of the model to different values of variables, properties, dimensions and parameters. At the expense of longer convergence time, these sweeps enabled multiple model scenarios to be investigated without remodelling or changing the variables at the Model Builder level. These were extensively used to determine volumetric water content, soil resistivity, electric potentials. Parametric sweep was used to evaluate the response to geometric properties, parameters such as resistivity, diameter of earthing electrode (conductor), diameter of subsoil domain and EEM around the electrode. Auxiliary sweeps were used to access the sensitivity model to boundary conditions such as pressure at the air-ground interface.

Domain probes of volumetric water content and resistivity of the subsoil and point probes of electric potential were specified at the electrode surface, outer edge of EEM, at the ROI, and outer boundary of the subsoil, prior to the numerical solution of the model. The Parallel Sparse Direct Solver (PARDIS) solver was used as it was found to overcome the convergence problem that the default solver Multifrontal Massively Parallel Sparse (MUMPS) exhibited.

3.2.10 Modelling Hydraulic and Electrical Parameters

Three soil textures: clay soil, silty soil, and sandy clay soil were used in this study. The hydraulic parameters for silty and sandy clay soils, listed in rows one to five of Table 3.3, were sourced from [90], while those for clay soil were obtained from [91]. The expressions for electrical conductivity, presented in row six, were derived from [77], with the expression for sandy soil being applied to sandy clay soil.

Table 3.3: Hydraulic and electrical parameters of three soil textures for earthing subsoil modelling.

Soil parameters	Soil texture		
	Clay	Silty	Sandy clay
Saturation volumetric water content $\theta_s\ m^3/m^3$)	0.5100	0.4600	0.3800
Residual volumetric water content θ_r (m^3/m^3)	0.1020	0.0340	0.0900
van Genuchten fitting parameter n	1.0900	1.3700	1.2300
The inverse of air entry pressure head $\alpha_h(m^{-1})$	2.1000	1.6000	2.7100
Saturated hydraulic conductivity K_s $(m \cdot s^{-1})$	5.56 x 10^{-7}	6.94 x 10^{-7}	3.33 x 10^{-7}
Electrical conductivity expression σ (S/m)	$0.1456(S_e)^{1.753}$	$0.0648(S_e)^{1.132}$	$0.007386(S_e)^{2.247}$

Source: Author's conceptualisation.

Table 3.4 presents the hydraulic and electrical properties of the two EEMs. Using these parameters, the water retention curve can be generated, and the corresponding equation can be formulated. The equation for the electrical conductivity of EEM I was derived by curve fitting the resistivity-water content pairs obtained from the resistivity box and oven drying of the sample. The raw data is found in the appendix section in Table A1. The parameters of EEM II were taken from properties of other soil materials. For example, its electrical conductivity is the same as clay soil in Table 3.3.

Table 3.4: Hydraulic and electric parameters of earthing enhancement materials (EEM)

Soil parameters	EEM I	EEM II
Saturation volumetric water content $\theta_s\ m^3/m^3$)	0.6546	0.3800
Residual volumetric water content θ_r (m^3/m^3)	0.1169	0.068
van Genuchten fitting parameter n	1.3587	1.09
The inverse of air entry pressure head $\alpha_h(m^{-1})$	2.1000	1.6000
Saturated hydraulic conductivity K_s $(m \cdot s^{-1})$	3.90 x 10^{-6}	5.56 x 10^{-7}
Electrical conductivity expression σ (S/m)	$1.363(S_e)^{1.3527}$	$0.1456(S_e)^{1.4753}$

Source: Author's conceptualisation.

3.2.11 Post-Processing Analysis and Validation

Using the post-processing capabilities of COMSOL Multiphysics® software involves using formulas with variables determined from the simulation process to evaluate desired attributes. The post-processing and domain probes were used to evaluate earthing resistance, generate tables of water content, resistivity and resistance, and create plots. For earthing resistance, the energetic formula proposed in [88] and expressed in Equation 3.1 was used.

$$R_{ei} = (V_{Ei} - V_{r\,i})^2 \left(\sigma_i \int |E_{ir}|^2 dV\right)^{-1} \tag{3.1}$$

where R_{ei} is the resistance due to the earthing electrode in ith layer of the subsoil. V_{Ei} is the electric potential at the electrode surface in the ith layer, V_{ri} is the electric potential at a horizontal distance r from the electrode surface in the ith layer, σ_i is the electric conductivity of soil which is expressed as function of S_e or θ in the ith layer, and E_{ir} is the electric field strength at r horizontal distance from the electrode in the ith layer.

For homogeneous or single-layer soils, the layer index i is invariant. If each soil layer or EEM is assumed to be homogeneous and isotropic, then its electrical conductivity σ_i is uniform and a function of average volumetric water content θ, or degree of saturation S_e, then Equation 3.2 becomes,

$$R_{e1} = (V_E - V_r)^2 \left[\sigma(S_e) \int |E_r|^2 dV\right]^{-1} \tag{3.2}$$

If part of the earthing electrode or its ROI extends to n_l layers of the subsoil, then the general formula for the resulting resistance of the earthing system is expressed by Equation 3.3.

$$R_{e,1l_n} = \prod_{i=1}^{n_l} (V_{Ei} - V_{ri})^2 \left[\sum_{i=1}^{n_l} (V_{Ei} - V_{ri})^2\, \sigma_i(S_e) \int |E_{ri}|^2 dV\right]^{-1} \tag{3.3}$$

For $n_l = 2$, then the resistance of the earth electrode in two-layer subsoil, R_{e12} is defined by Equation 3.4.

$$R_{e12} = \frac{(V_{E1} - V_{r1})^2 (V_{E1} - V_{r1})^2}{(V_{E1} - V_{r1})^2\, \sigma_1(S_e) \int |E_{r1}|^2 dV + (V_{E2} - V_{r2})^2\, \sigma_2(S_e) \int |E_{r2}|^2 dV} \tag{3.4}$$

Where an EEM forms part of the earthing composition, then the equation for the earthing resistance in the single-layer subsoil model is expressed by Equation 3.5.

$$R_m = (V_E - V_m)^2 \left[\sigma_m(S_e) \int |E_m|^2 dV\right]^{-1} + (V_m - V_r)^2 \left[\sigma_r(S_e) \int |E_r|^2 dV\right]^{-1} \quad (3.5)$$

where V_E, V_m and V_r is the electric potential at the electrode-EEM interface, EEM-soil interface and at r horizontal distance within the soil, measured from the central axis within the soil, E_m and E_r electric field within the EEM and at r horizontal distance within the soil.

If part of the earthing electrode with EEM or its ROI extends to n_l layers of the subsoil, then the general formula for the resulting earthing resistance is expressed by Equation 3.6

$$R_{emi} \approx R_m + \sum_{i=1}^{n_l} R_i \quad (3.6)$$

- where R_m and R_i are expressed by Equations 3.7 and 3.8.

$$R_m = (V_{e1} - V_{m1})^2 \left[\sigma_m(S_e) \int |E_m|^2 dV\right]^{-1} \quad (3.7)$$

$$R_i = (V_{mi} - V_{ri})^2 \left[\sigma_{ri}(S_e) \int |E_{ri}|^2 dV\right]^{-1} \quad (3.8)$$

To validate the correctness of the modelling process, the resistance of vertical earth rod model with fixed subsoil resistivity (that is, suction independent resistivity earthing model) but built with the same modelling framework as the suction dependent resistivity earthing models (hydro-geoelectric earthing models) is compared to the resistance of the same configuration built evaluated from similar finite element method models in literature. Additionally, the model resistance values were compared to resistance from existing analytical formulas proposed [93]. In the case of the vertical earthing rod in homogeneous subsoil, its resistance was compared to the resistance evaluated using analytical formula in Equation 3.9.

$$R = \frac{\rho_s}{2\pi L_r}\left(\ln\frac{4r_r}{L_r} - 1\right) \quad (3.9)$$

Equation 3.9 is the Tagg-Sunde formula for determining the resistance of a vertical earthing rod in a single subsoil layer. It can be used to approximate the resistance in the multi-layer subsoil model, in which case an apparent resistivity (ρ_a) is required. Thug's apparent resistivity formula for multilayer subsoil model (Equation 3.10) was used.

$$\rho_a = \rho_1 \left\{1 + 4 \sum_{n_l=1}^{n_l} \frac{(k_c)^{n_l}}{\sqrt{1 + (2n_l h_1/d_s)^2}} - \frac{(k_c)^{n_l}}{\sqrt{4 + (2n_l h_1/d_s)^2}}\right\} \quad (3.10)$$

If the vertical rod is embedded in cylindrical EEM, the modified form of Equation 3.9, proposed by Fagan, which accounts for the new composition was used and expressed as Equation 3.11.

$$R_m = \frac{\rho_m}{2\pi L_m}\left(\ln\frac{4L_m}{r_r} - 1\right) + \frac{\rho_s - \rho_m}{2\pi L_r}\left(\ln\frac{4L_r}{r_{em}} - 1\right) \tag{3.11}$$

where r_r is the radius of the vertical earth rod, r_{em} is the radius of EEM, ρ_m is the resistivity of EEM, L_r is the length of vertical earth rod, L_m is the length of EEM, ρ_s is the resistivity of the homogeneous (single-layer) subsoil, ρ_a is the apparent resistivity of multi-layer subsoil model, d_s is depth of subsoil, h_1 is depth of upper subsoil layer, n_l is the number of subsoil layers. For two-layer subsoil model, $k_c = k_{12}$ such that $k_{12} = \frac{\rho_2 - \rho_1}{\rho_2 + \rho_1}$ is the reflection coefficient, ρ_1 is resistivity of upper subsoil layer, ρ_2 is lower layer resistivity.

3.2.12 Modelling Cases and Scenarios

Table 3.5 provides a summary of the modelling cases used in the research investigation.

Table 3.5: Summary of model cases for the proposed method of earthing design and resistance evaluation and prediction

Modelling	Section	Model constituents	Model Objectives
Hydro-geoelectric earthing modelling	4.1 4.2	Single-layer silty, clay and sandy clay subsoils	i. Demonstrate the method's capacity to model earthing system performance for different condition of subsoil and validate it result. ii. Investigate effect of suction and soil texture on water retention, soil resistivity, earthing resistance and ground electric potentials. iii. Investigate the effect and sensitivity of the proposed method to presence and width of infinite element domain (IED) on computed resistance, and distribution of ground electric potential. iv. Investigate the sensitivity of model to subsoil domain size.
Hydro-geoelectric earthing modelling with EEM in single-layer subsoil	4.3	Single-layer silty and sandy clay subsoils with two clay-based EEMs (EEM I and EEM II)	i. To investigate the effect of suction on the performance of EEMs. ii. Investigate the effect of volume and type of EEM on resistance reduction capacity iii. Investigate the effect of subsoil texture on EEEM. iv. The effect of size of EEM on resistance reduction capacity.
Hydro-geoelectric earthing modelling in two-layer subsoil with and without EEM	4.4	Six two-layer subsoil containing pairs of silty, clay and sandy clay soils with / without EEMs	i. To investigate the effect of topsoil depth and resistivity on the resistance and performance of vertical earth rod. ii. To investigate and compare the resistance reduction capacity of EEMs for suction conditions leading to high subsoil resistivity. iii. Identify soil-EEM pair with high resistance reduction performance.
Analytical estimation of water content in region of influence of earthing electrode	5.1 5.2	1- and two-layer subsoils	i. To numerically formulate water gradient function for estimating subsoil water content
Hydro-geoelectric earthing modelling in different climates	6.4	1- and two-layer subsoils in sub-humid, arid and semi-arid climates	i. To demonstrate the practical application of the new model in predicting seasonal values of subsoil resistivity and earthing resistance. ii. Investigate resistance reduction capacity of EEMs in different soils and climate. iii. Identify optimal soil-EEM pairs with high resistance reduction capacity for each climate.

Source: Author's conceptualisation.

Chapter 4 - Effect of Soil Texture and Hydraulic Properties on Resistance and Performance of Earthing Systems

4.0 Introduction

This chapter presents the application of the equations and methodologies for the simulation modelling and result of vertical earth rods in single and two-layer subsoil models. First, the variability of resistance and performance of earthing systems under variable conditions of soil is modelled and analysed for different soils. By comparing the simulation model with their analytical equivalent, the sensitivity of model size and features are analysed. This analysis involves investigating the effects of domain size, presence, and size of an infinite domain at subsoil boundary, and depth of subsoil. Analyses of resistance reduction capacity and efficiency of earthing enhancement materials in different subsoils and conditions are performed in the penultimate section, while the last section is devoted to modelling and analyses of earthing systems in two-layer subsoils.

4.1 Simulation of Hydro-Geophysical Earthing Modelling

External influences that affect the volume of water content and resistivity of the upper layers of the subsoil have been modelled as soil suction. The soil water retention curve (SWRC) provides the relationship between the negative pressure (suction) applied to the soil and the resulting volumetric water content, θ. Figure 4.1 shows the SWRC for the three subsoil textures, expressed as θ and the logarithm of soil suction ψ (kPa). The plots were generated with equation 2.47, where h_p (m) is converted to suction using the conversion, $1\ h_p(m) = 9.80681$ kPa and 1 pF $= Log_{10}(100h_p)$.

From Figure 4.1, soil water retention is progressively higher from sandy clay to clay soils under saturation conditions, a trend sustained in the transition or capillary region of the SWRC. In the residual region characterised by high values of suction, clay soils retain more water and have a wider transition region, unlike sandy soils with low water retention capacity. Sandy soils are predominantly coarse-textured with few but large-sized pores between the 0.05 to 2 mm grain size. As soil suction increases, the large pores of sandy soils make the conductivity of water high and the transition between saturation and unsaturation swift. Consequently, sandy soils have high hydraulic conductivity and a relatively shorter transition between saturation and residual states. Therefore, sandy soils transition from saturation to desaturation faster than silty and clay soils over a small increase in soil suction.

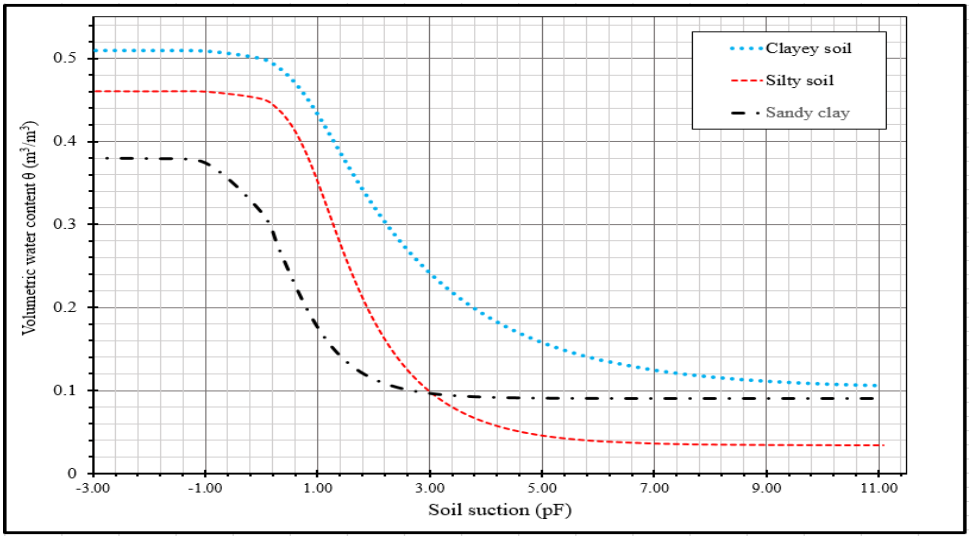


Figure 4.1: Soil water retention curves for sandy clay, silty and clay soils.

Source: Author's conceptualisation

Soils that are deficient in water retention capacity lose their electrical conductivity under drier climates and are susceptible to high-resistivity deviations, such subsoils pose a formidable challenge in maintaining reliable earthing performance.

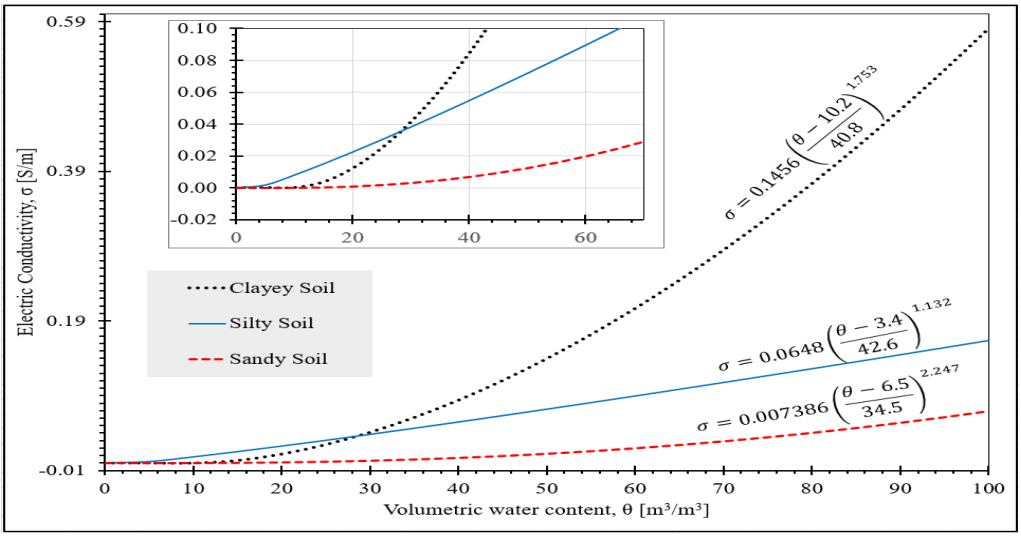


Figure 4.2: Graphical variation of electric conductivity of sandy clay, silty and clay soil with volumetric water content

Source: Author's conceptualisation.

Figure 4.2 shows the curves of electric conductivity which were generated using the hydraulic parameters and expressions in Table 4.1. The curves of the figure show the variation of electric conductivity over a complete range of volumetric water content, 0% to 100%. By comparing these curves, insights into how soil texture influences the hydraulic and electrical behaviour of

the subsoil are gained. For all degrees of saturation, sandy soil, and coarse-textured soil with poor water retention exhibit low electrical conductivity. As the degree of saturation increases, (water content less than 28%), the electric conductivity of silty becomes marginally higher than the other soil textures.

Relative to sandy soils, silty soils have smaller pore and particle (2 to 0.002 mm) sizes which are more compact than sandy soils. This allows more fluid transmission and retention than sandy soils and quicker saturation than the more compact clay soil, hence electric conductivity increases faster than other soils. However, as the degree of saturation increases with water content beyond 28%, the electrical conductivity of clay soil increases significantly compared to other soil textures. From the curves, the electrical conductivity of these soil textures over the complete range of volumetric water contents (0% to 100%) varies as 0.1456 to 0.5850 S/m for clay, 0.0648 to 0.1637 S/m for silty, and 0.007386 to 0.06939 S/m for sandy clay soils.

Using a range of soil suction representing the condition of the subsoil at and within saturation (>-33 kPa), field capacity (-33 kPa), permanent wilting point (-1500 kPa), and residual (≪ -1500 kPa) states, the performance of the vertical earth rod in each of the three subsoil textures are analysed. Table A8 is the simulation result over a range of soil suction between 0.98 kPa (0.1 m pressure head) and -98.1 MPa (10^4 m). It shows the volumetric water content and resistivity at each of the soil suctions and the corresponding post-processed resistance of vertical earth rods.

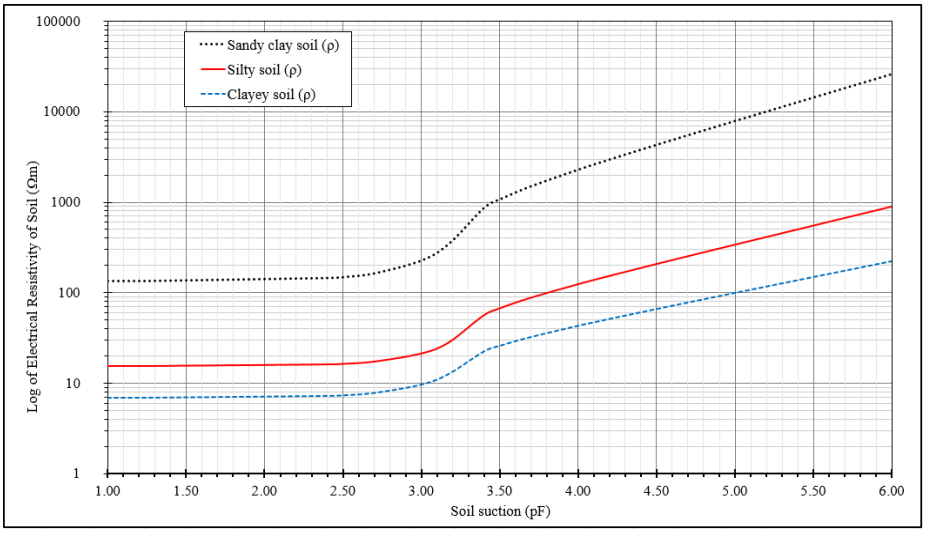


Figure 4.3: Soil suction resistivity curve of sandy clay, silty and clay soils

Source: Author's conceptualisation

Figure 4.3 is the soil suction resistivity curve (SSRC) which shows the variation of electric resistivity (inverse of electric conductivity) of soil due to changes in soil suction. It was plotted from the simulation data in Table A1. As the soil desaturates, sandy soil with the lowest electrical conductivity attains the highest resistivity and exhibits the largest change. As previously noted, the poor water retention and quick transition of sandy soils play a significant role in this behaviour. Consequently, the resistivity of sandy soils spikes quickly over a small range of suction, increasing to extreme values as suction increases.

Unlike their coarse counterparts, fine-textured clay soils retain more water and exhibit small variations of resistivity over large changes in soil suction. Silty soil exhibits intermediate magnitude and variation of resistivity for corresponding values of soil suction. Compared to sandy soil, the magnitude of change of resistivity is less in silty soil and less in clay soil. Given that earthing resistance is proportional to the actual or apparent resistivity of the subsoil, the resistance of the earthing system should follow the same trend as the resistivity of the subsoil their electrodes are buried in, such that earthing resistance in clay soil will exhibit marginal variation over the same change in suction that will produce significant change in resistance for the same earthing electrode in sandy soil.

4.1.1 Subsoil Resistivity

Table A2 shows the resistance of the vertical earthing rod in single subsoil models of clay, silty and sandy clay soil textures at different values of soil suction. Figure 4.4 is the logarithmic plot of the suction and resistance of vertical earth rods in the three subsoil textures. The curves exhibit the same trend as their corresponding resistivity curves.

Under low suction, earthing resistance in each of the soil textures remains relatively constant as the soil is considered relatively saturated. Beyond the field capacity (-33 kPa), the soil transitions towards desaturation, resulting in the increment in earthing resistance. Besides supporting high cation exchange capacity, the texture of clay soils also influences the least change in resistance. By associating suction change with the resulting change in resistance, the influence of soil texture on the resistance and performance of earthing systems can be estimated. The transition of suction at field capacity to permanent wilting point (-1500 kPa), accounts an increase of earthing resistance of 18.45%, 8.14%, and 5.98% for sandy clay, silty and clay soils respectively. With size $\leq 2\ \mu$m, the particles of clay soils are closely packed, inhibiting the flow of fluid.

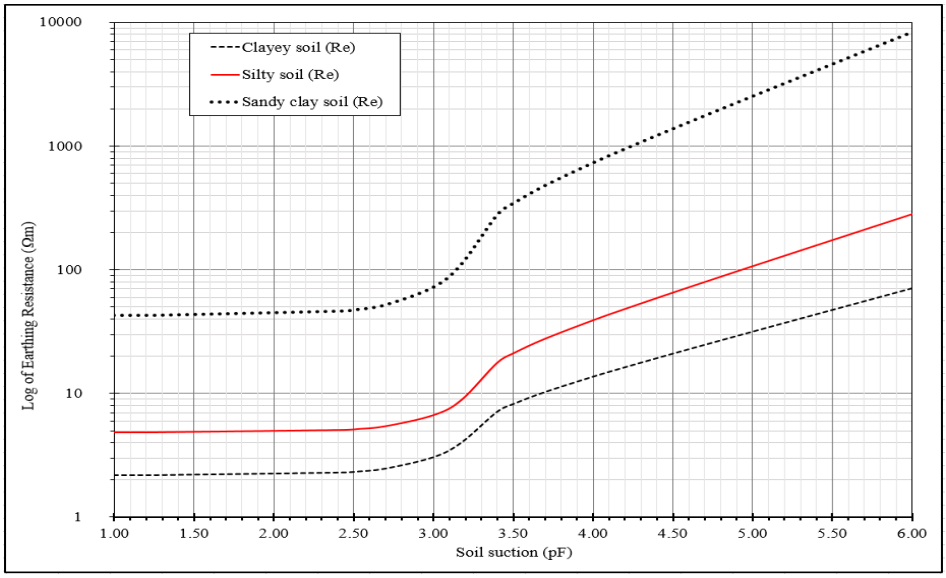


Figure 4.4: Resistance of vertical earth rod in single-layer clay, silty, and sandy clay subsoils

Source: Author's conceptualisation

Consequently, clay soils have low hydraulic conductivity, attain residual states slower and retain more water than other textures. High water retention characteristics of clay soil makes the resistance of earthing electrodes buried in them exhibit minimal changes over substantial environmental change. This property makes clay-based compounds the choice materials for earthing enhancements in sandy or rocky environments.

4.1.2 Model Validation

As a combination of two physics, the hydro-geophysical method consists of two independent models. The first model relates to suction and resistivity modelling, while the second models the relationship between resistivity of the subsoil and the earthing electrode. The first modelling process is to determine the volumetric resistivity of the subsoil from soil suction.

Table 4.1: Comparing the subsoil volumetric resistivity derived from the proposed model

Pressure head (m)	**θ(%)**		**ρ (Ωm)**		**% diff. resistivity**
	Model	**Piegari et al [31]**	**Model**	**Piegari et al [31]**	
-0.001	57	59	399	391	1.9
-5	57	67	400	357	10.7
-50	46	53	493	432	12.2
-100	38	39	589	574	2.5
-200	32	31	701	707	-0.9
-500	25	25	864	886	-2.6
-1000	22	21	996	1027	-3.1

Source: [31]. $\alpha = 0.046,\ n = 1.347, \theta_s = 0.57, \theta_r = 0.09, \sigma = 234(S_e)^{-0.95}\ (\Omega m)^{-1}$.

The result was found to be consistent with those in cited literature. Table 4.1 compares the result of the proposed model to the published result in [31]. For the pressure heads, the magnitudes of percentage difference varied between the resistivity varied between 0.866% to 12.214%. Higher differences were attained under high water content (low suction). But as suction increased (pressure head), the percentage difference reduces significantly.

The second model component determines the earthing system resistance from subsoil resistance when current is dispersed from the earthing conductor. Table 4.2 shows the resistance of a single vertical earth rod evaluated from the proposed model (denoted as M1) and compared to the resistance obtained from two other finite element method (FEM)-based models, denoted as M2 [94] and M3 [95]. The results of the M1, M2, and M3 were also compared to the resistance evaluated from the Tagg-Sunde equation for a vertical earth rod in homogeneous subsoil.

Table 4.2: Comparing the resistance of the proposed model to models in literature

parameters		**Resistance** (Ω)				**% diff. (ref Analy.)**		
Rod length (m)	**ρ (Ωm)**	Analytical	M1	M2	M3	M1	M2	M3
2	100	3.3	3.3	3.2	-	0.0	2.1	-
3	9.9	47.0	46.1	-	46.4	1.9	-	1.2

Source: Author's conceptualisation. Proposed model (M1) compared to M2 [94] and M3 [95], with all three compared to the analytical value of resistance obtained for cylindrical rod with 0.008 m radius.

For a rod length of 2 m and soil resistivity of 100 Ωm, the result of the proposed model was slightly higher than M2, however, M1 and the analytical resistance were the same. For rod length of 3 m and resistivity of 9.9 Ωm, M2 was less than the resistance of M3 and analytical formula. In both cases, M1 modelled the resistance within the 10% limit, indicating its efficacy and validating its results.

4.1.3 Distribution of Ground Electric Potential

Figures 4.5 to 4.7 are the plots of the ground surface distribution of electric potential due to current dissipation from a vertical earth rod in clay, silty, and sandy clay soils under saturation (-0.98 kPa), field capacity (-33 kPa) and permanent wilting point (-1500 kPa). Comparing the figures reveals that the desaturation of the subsoil results in higher magnitudes of surface potentials.

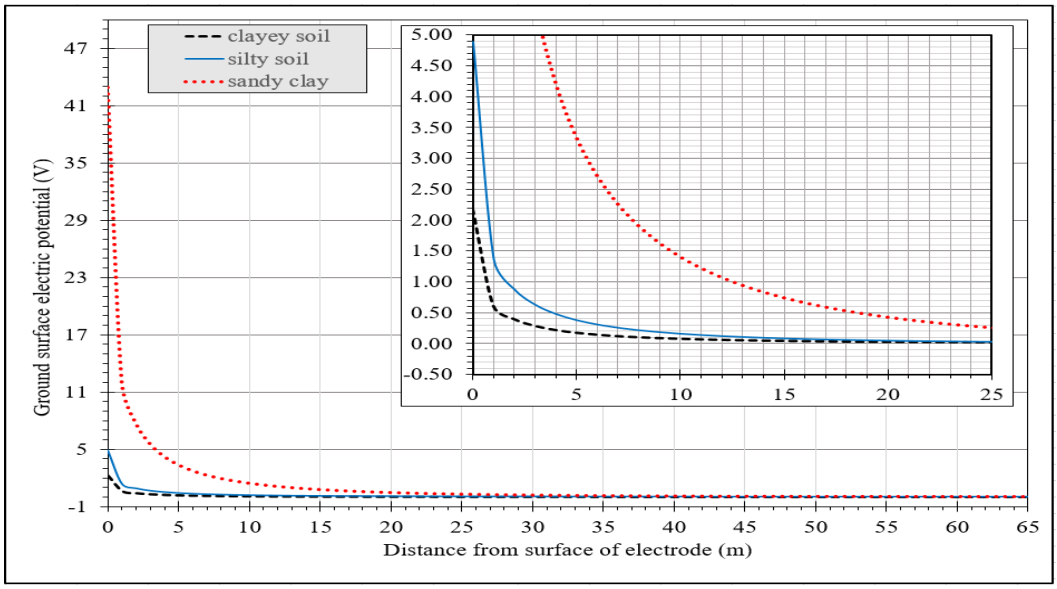


Figure 4.5: Distribution of ground surface electric potential on clay, silty, and sandy clay subsoils under saturation conditions

Source: Author's conceptualisation

The magnitude and distribution of electric potential are proportional to the resistivity as determined by the interaction between suction and water content. Regardless of soil condition, the profile of electric potential in sandy soil is significantly higher than in fine-textured soils.

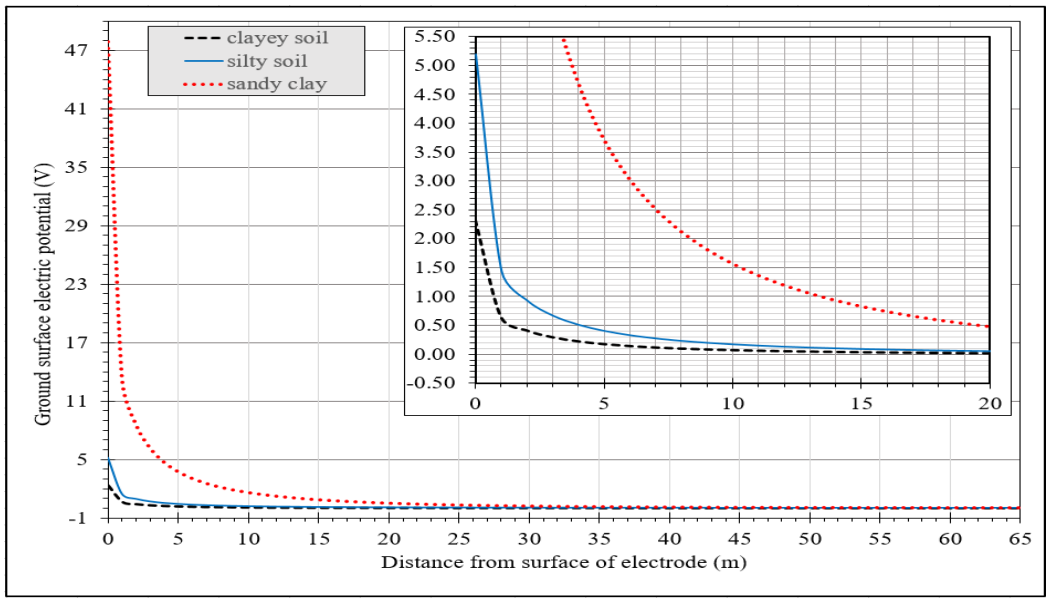


Figure 4.6: Ground surface distribution of electric potential on clay, silty, and sandy clay soils under field capacity (-33 kPa) conditions

Source: Author's conceptualisation

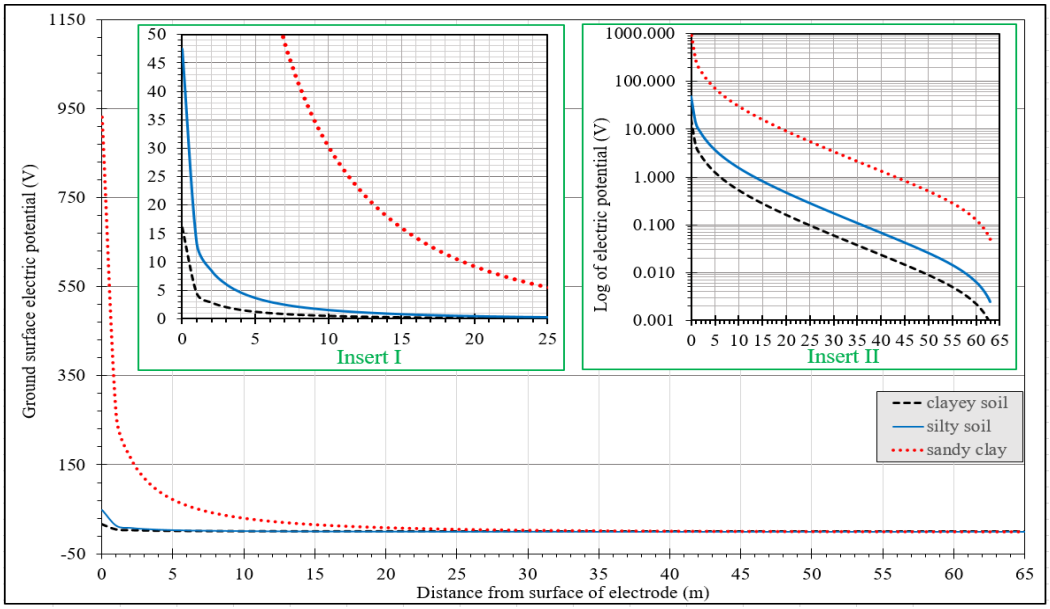


Figure 4.7: Ground surface distribution of electric potential on clay, silty, and sandy clay subsoils under permanent wilting point suction (-1500 kPa) condition

Source: Author's conceptualisation. Ground surface distribution of electric potential on clay, silty, and sandy clay soils under permanent wilting point suction condition (-1500 kPa). Inset I is the magnified portion of the plot showing the potential on clay and silty soil surfaces. Inset II is the semi-logarithmic equivalent plot of the ground surface electric potential distribution on the soils under -1500 kPa condition.

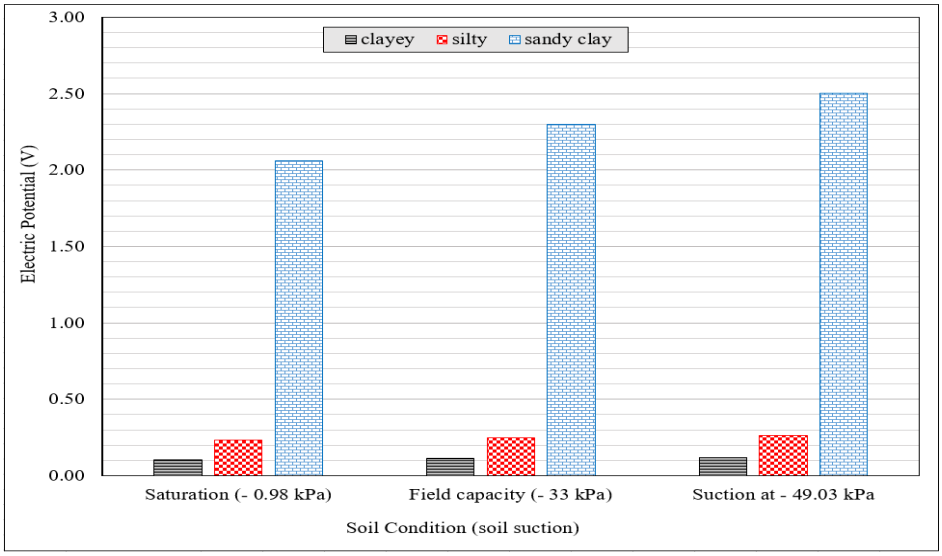


Figure 4.8: Comparison of ground surface electric potential at distance of 7.5 m from earth rod in clay, silty, and sandy clay subsoils at saturation and field capacity suctions

Source: Author's conceptualisation

Figures 4.8 and 4.9 show the excessively high profile of electric potential distributed on the ground surface of sandy soils relative to silty and clay subsoils at soil suction of -1500 kPa. Although the rate of decay or decline of electric potential at any point relative to the value at the surface of the electrode is equal regardless of subsoil, sandy soil maintains a higher profile

of electric potential than other soil textures. For example, under the condition of permanent wilting point, the electric potential at the radial distance of 7.5 m decayed from 16.07 to 0.77 V on clay and down from 47.54 to 2.29 V for silty soil but maintained a relatively high magnitude of 44.8 V, which is 58.2 and 19.6 times the potentials on clay and silty soils, respectively.

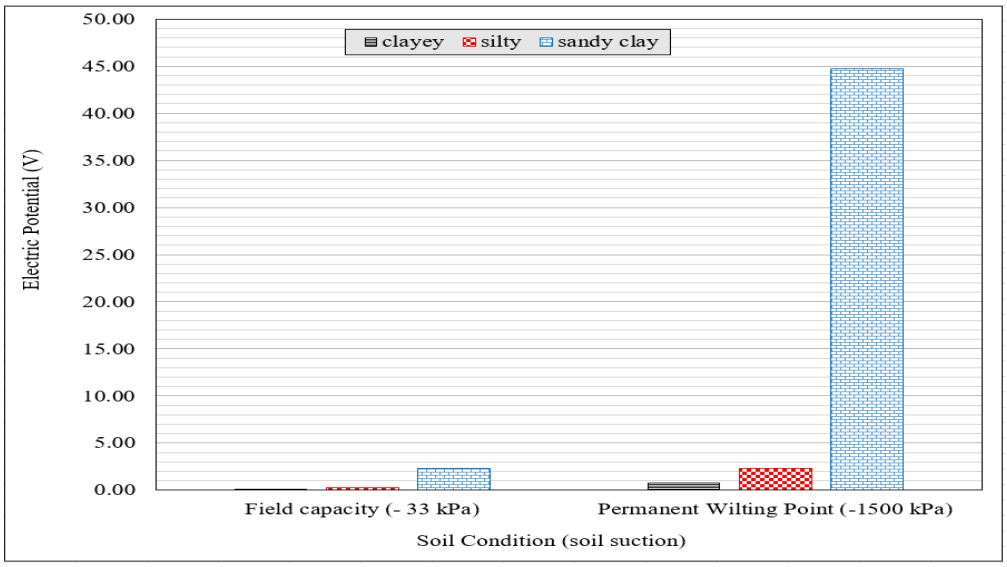


Figure 4.9: Comparison of ground surface electric potential of 7.5 m from earth rod in clay, silty, and sandy clay subsoils at field capacity and permanent wilting point suctions

Source: Author's conceptualisation

4.2 Model Sensitivity

The modelling of this multiphysics with the numerical solution of differential equations on discretised elements of the geometric model of the physical system sometimes requires a conscious compromise between the model complexity and computational cost, especially if the computation resources are restrictive, limited, or expensive. Higher complexity is likely to achieve a closer approximation of the physical system but at increased computational cost. Achieving a better approximation of the physical system and accurate result often requires increasing the complexity of the model at a high computational cost. The size of the geometric model, boundary definitions and conditions, and size of mesh elements are some of the modelling decisions and domain features that determine simulation complexity and computational cost.

The sensitivity of earthing resistance and electric potential to the parameters used for geometric modelling depends on the size of the subsoil as well as the presence and size of an infinite domain at the boundary of the subsoil. An appropriate subsoil dimension must be chosen for

efficient computational cost and accurate analysis and result. Large domain models yield many mesh elements with high computational cost and memory, while small domain models produce poor mesh element quality and affect the accuracy of post-processing analyses. Where computational cost is of negligible concern, a large domain model can be used; otherwise, an appropriately sized subsoil domain is required for efficient computational cost and analysis. Since the cylindrical model used in modelling the subsoil domain is formulated as a rectangular 2D axisymmetric space, its dimension is described by width and depth which is equivalent to the radius and height of the cylindrical domain.

Since the analytical formula for computing the earthing resistance of the vertical rod pertains to the infinitely sized homogeneous subsoil, the percentage difference between the reference analytically evaluated resistance and the resistance from post-processing the simulated earthing model provides an appropriate basis for analysing the efficiency of subsoil domain size.

4.2.1 Effect of Infinite Element Domain

In modelling the physical infinite earth, a bounded or finite geometry is used. An artificial infinite boundary or infinite element domain (IED) is sometimes assigned towards the outer boundary of the geometry to mimic the infinite extension of the earth [96], [97]. The choice for the use of IED and its size depends on the domain size of the subsoil geometry and the desired level of computational cost and accuracy. If the same mesh elements are used, large domains return more mesh elements. Domains with high mesh density produce accurate computational results at high computational costs (time and memory space). Computational efficiency is sometimes achieved by a trade-off between computational cost and accuracy.

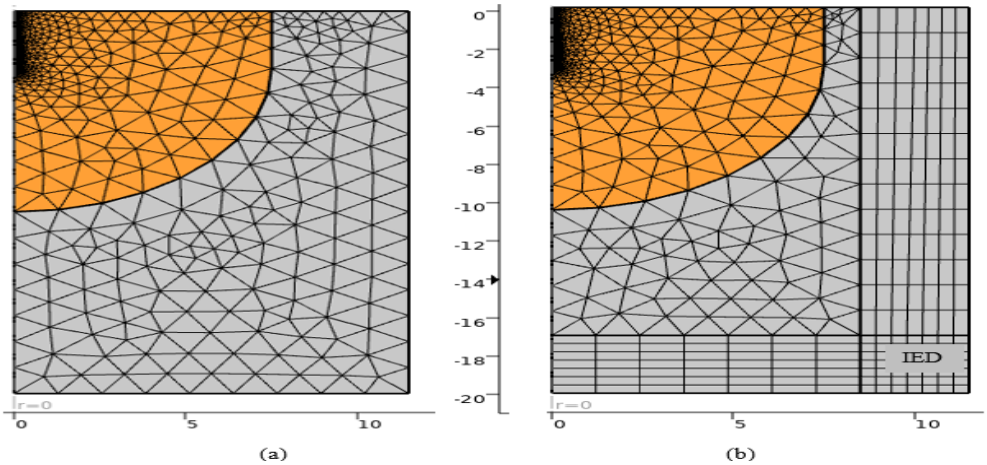


Figure 4.10: Distribution of mesh element of hydro-geophysical vertical earthing rod in different single-layer subsoil models

Source: Author's conceptualisation

Figure 4.10 shows the 2D axisymmetric mesh view of a single vertical earth rod in two homogeneous subsoil models: (a) domain without IED, and (b) domain with IED. The width (radius) and depth of the subsoil domain are 11.5 m and 20 m respectively. Domain dimensions must be chosen to exceed the area or volume bounded by the ROI of the earth electrode to ensure simulation convergence. Free quadrilaterals have been used to discretise the IED and free triangles for the remaining portion of the geometry, with 175 μm as the minimum edge of the mesh element.

Table A3 shows the mesh statistics of three subsoil domains of widths (radii), 11.5, 25.5, and 50.5 metres, each with a depth of 20 m. There are two subsoil models for each width: model with IED and without IED. The upper section of the table contains the quantity and type of mesh elements (triangle, quadrilateral) and parts of the mesh element (vertices, edge, vertex element). In all cases, the model with IED has more mesh elements than the model without the IED, which implies additional computational. From the discretisation, the quality of mesh elements is indicative of solution convergence and accuracy. For good meshing quality, the minimum and average values of each of the seven criteria that describe the quality of mesh elements must be ≥ 0.1.

4.2.2 Effect of the Width of Infinite Element Domain

Table A4 is the simulation result of three subsoil domains of width 13.5, 25.5, and 65.5 m each modelled with three widths of 1, 3 and 6 m of IED for four pressure heads (-0.1 m, -3.3734 m, -152.76 m and -200 m). Unlike the distribution of electric potential of the earthing model, the width of the IED does not affect the electrical and hydraulic properties of the subsoil. The analytical resistance computed using the corresponding resistivity of the subsoil for the pressure head is constant and independent of the IED. This feature of the analytically computed resistance makes it suitable as reference resistance for computing the effect of the presence and size of the IED in terms of resistance percentage difference.

Moving from left to right across the rows for the pressure head in Table A4 reveals that the magnitude of percentage difference reduces with subsoil domain size. For the 13.5 m subsoil, the value of the percentage difference reduces from the maximum value for subsoil without IED, to 1.44% at 1 m IED width to the minimum recorded value of 0.32% for 5 m IED width. To attain this relatively low percentage difference, the 5 m width IED suggests the effectiveness of the IED when modelling with small-size subsoil domains.

4.2.3 Effect of Infinite Element Domain on Ground Surface Electric Potential

Table A5 contains the electric potential at points on the ground surface of a 13.5 m subsoil domain under –0.98, –33, –1500, and –49034.03 kPa soil suctions. Comparing the electric potentials of corresponding points on the ground surface of the two subsoil models indicates that the model with infinite element domain (wIED) generally has marginally higher values than the model without IED. Figures 4.11, 4.12 and 4.13 are the plots of ground surface electric potentials for three subsoils (13.5, 25.5, and 65.5 m domain width) at –1500 kPa (–152.76 m) soil suction.

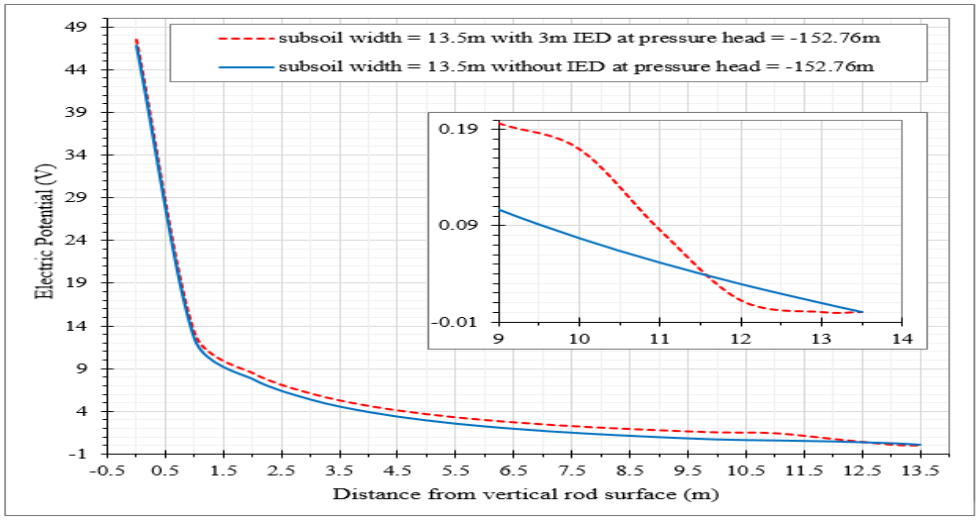


Figure 4.11: Plot of electric potential on the ground surface for subsoil model at field capacity suction

Source: Author's conceptualisation. Subsoil model radius 13.5 m with and without infinite element domain (IED) at field capacity (pressure head of -152.76 m).

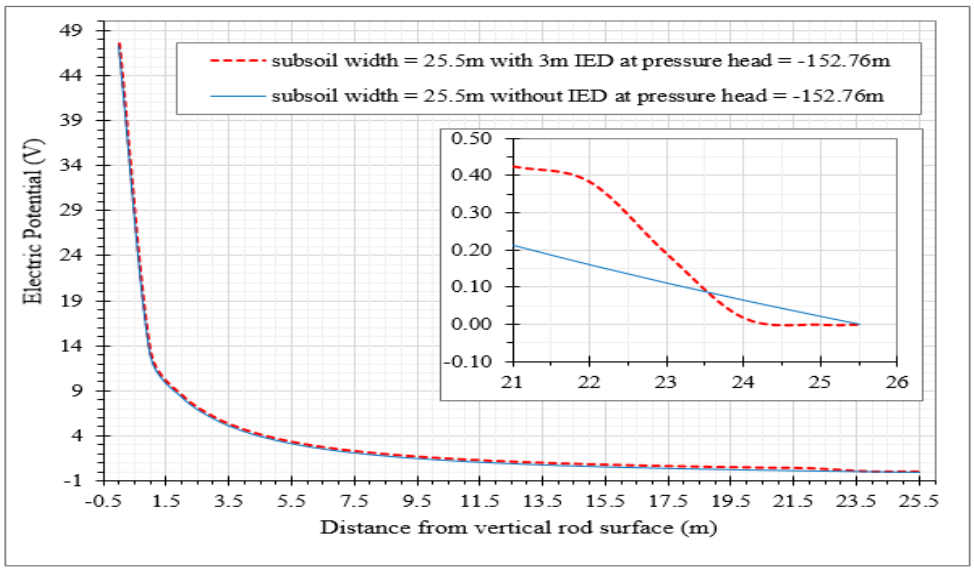


Figure 4.12: Plot of electric potential on the ground surface for subsoil model at permanent wilting point suction

Source: Author's conceptualisation. Subsoil model radius 25.5 m with and without infinite element domain (IED) at permanent wilting point (pressure head of -152.76 m).

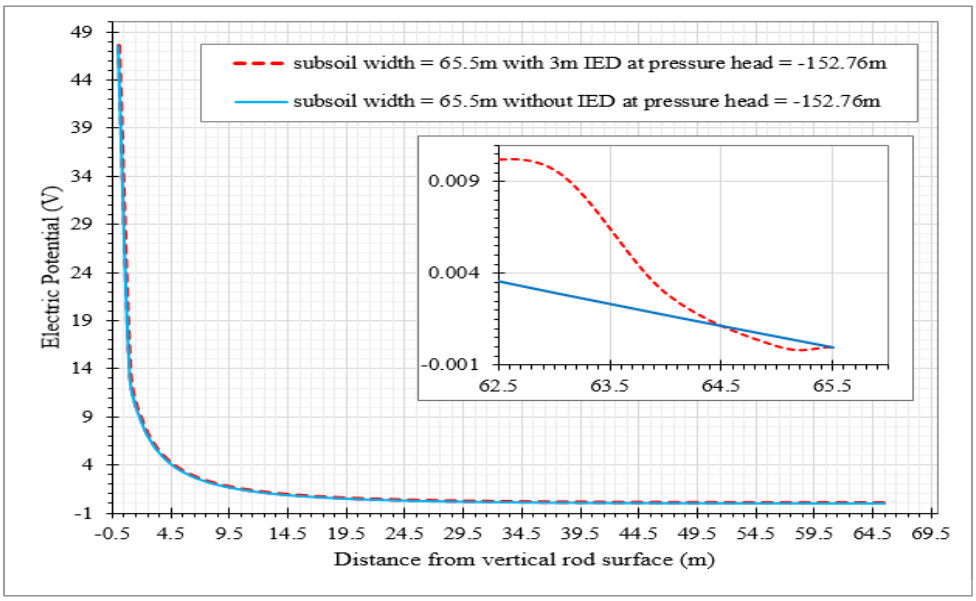


Figure 4.13: Plot of electric potential on the ground surface for subsoil model

Source: Author's conceptualisation. Subsoil model radius 65.5 m with and without infinite element domain (IED) at a pressure head of -152.76 m.

Each plot has two curves: the dashed red lines for subsoil with an IED of 3 m and the solid blue curve for subsoil without the IED. Each of the three red curves is above the blue curve except near the inner boundary of the IED, where it begins to slope downward. As the width of the subsoil domain increases, the magnitude of electric potentials for the two models becomes closely matched. The insets in each plot represent the magnification of the curves within the width of the IED. With a sharp slope, the gradient of the red dashed curve (with the same unit as electric field strength) is 0.076, 0.0154, and 0.0038 V/m for 13.5, 25.5, and 65.5 m subsoil domain diameters. Smaller gradients are attained as the width of the subsoil model increases infinitely, such that the effect of the IED becomes negligible.

4.2.4 Effect of Infinite Element Domain on Earthing Resistance

To evaluate the effect of the presence and width of IED, the percentage difference of resistance and distribution of ground surface electric potential are compared for subsoil models with and without IED. Since the analytical resistance is independent of domain size, it can be used as a reference. An IED of width 3 m is tested on three subsoil widths, 13.5, 25.5 and 65.5 m. Table A6 contains the simulation result and resistance analysis of two subsoil models (with and without IED) under six soil conditions (pressure head). Transitioning from saturation (-0.98 kPa) to a near residual state of -49034.03 kPa soil suction, the magnitude of earthing resistance increases in proportion to the resistivity of subsoil. At any soil suction, the percentage difference for the model without IED seems to be higher.

The magnitude of the percentage difference (% diff.) is smaller for the models with IED, especially for small subsoil domain widths. As the width of the subsoil increases, the effect of the IED diminishes. A similar trend is also observed for the 25.5 m subsoil domain. For the 65.5 m subsoil domain width, the range of IED width (1 to 5 m) has no effect. A similar trend is also observed for the 25.5 m subsoil domain. For the 65.5 m subsoil domain width, the range of IED width (1 to 5 m) has no effect.

The effect of IED in the subsoil seems to be negligible on the earthing resistance and the distribution of ground surface electric potential under saturated conditions but is significant under unsaturated conditions. For the soil domain under the same conditions, the higher the width of the IED, the smaller the value of the ground surface electric potential at corresponding points on the ground surface. Hence, if the computational resource is sufficiently available, then the earthing model can be modelled with a large domain size without the need for an IED. At 65.5 m, the effect of the 3 m width IED is substantially reduced as the resistance in the two subsoil models is equal.

Figure 4.14 is the histogram of resistance percentage difference for three subsoil domain widths under six soil conditions (pressure heads). For the smallest domain width, the magnitude of resistance percentage difference is significantly higher for the subsoil model with IED but reduces substantially as the width of the subsoil domain increases. At 65.5 m, the effect of the IED is insignificant, such that the percentage difference for the two subsoil models is 2.72% and equal. It implies that the effect of IED on large subsoil domains is negligible and results in approximately equal values of resistance for models with and without. Therefore, accurate earthing modelling with less computational cost can be achieved with subsoil models without the IED.

The ratio of IED width to subsoil width is approximately 0.2222, 0.1176 and 0.0458, respectively. As the ratio decreases, the percentage difference also decreases, suggesting a proportional relationship between them. This ratio may be significant in defining the influence of IEDs on simulation modelling. Since the influence of the 3 m IED depends on the size of the subsoil and reduces with subsoil domain width, it is imperative to determine the effective IED width relative to the width of the subsoil.

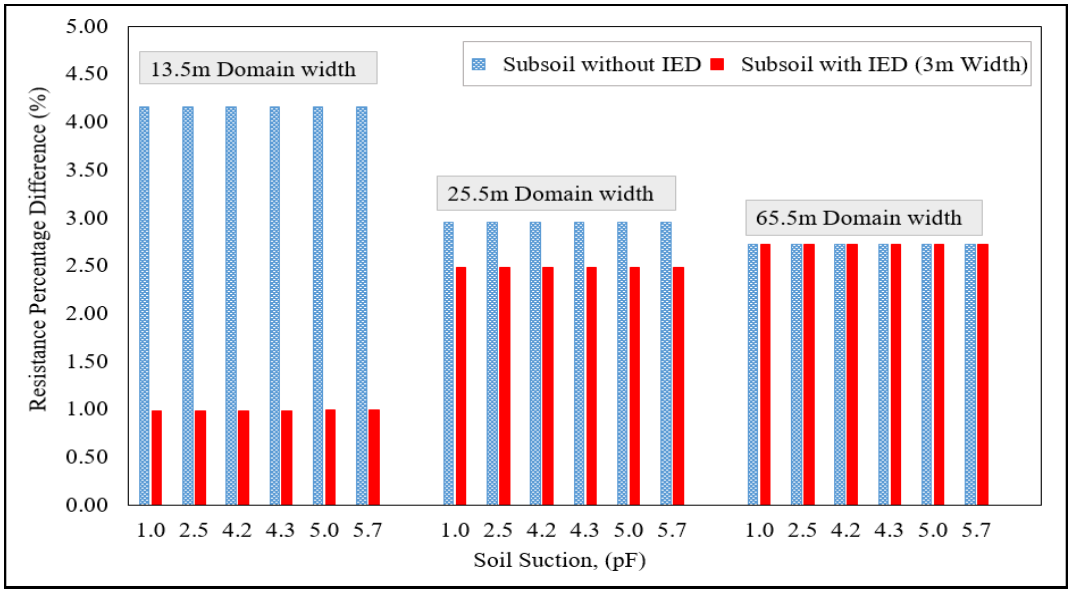


Figure 4.14: Percentage difference histogram of simulation and analytical earthing resistance of vertical rod in three subsoil domain widths

Source: Author's conceptualisation. Subsoil domain widths (13.5, 25.5, and 65.5 m) with and without infinite element domain (IED).

4.2.5 Effective Size of Subsoil Domain Width

The width of the subsoil domain determines the steepness of the decline of electric potential from the maximum $V_{e,i}$ at the rod surface to the 0 V at the outer edge of the subsoil model.

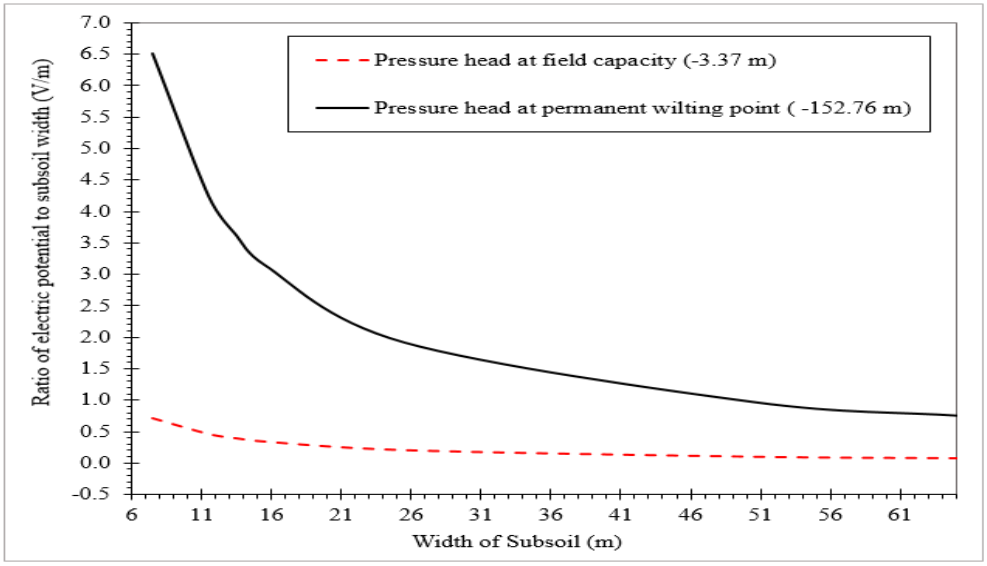


Figure 4.15: Plot of the ratio of electric potential to subsoil width against subsoil width for pressure head at field capacity and permanent wilting point

Source: Author's conceptualisation. Pressure head at field capacity (-3.37 m) and permanent wilting point (-152.76 m).

Figure 4.15 is the plot of this ratio to the subsoil width for -3.37 m and -152.76 m pressure heads, representing wet and dry soil conditions. The curves indicate that the magnitude of the ratio decreased as the subsoil width increased. A smaller ratio implies that the estimation of electric potential on the ground surface and simulation resistance is more accurate. Therefore, if computational resources are sufficiently available, the earthing model can be made using a large domain size without the need for an IED.

Figure 4.16 shows the graphical illustration of the distribution of electric potential on the ground surface for four domain radii, namely 7.5 ($2.5L_r$), 11.5, 25.5 and 65.5 m. The ratio of electric potential difference to subsoil width at permanent wilting point (-152.76 m) is 6.52, 4.25, 3.15, 1.92 and 0.75 V/m for 7.5, 11.5, 15.5, 25.5, and 65.5 m subsoil width.

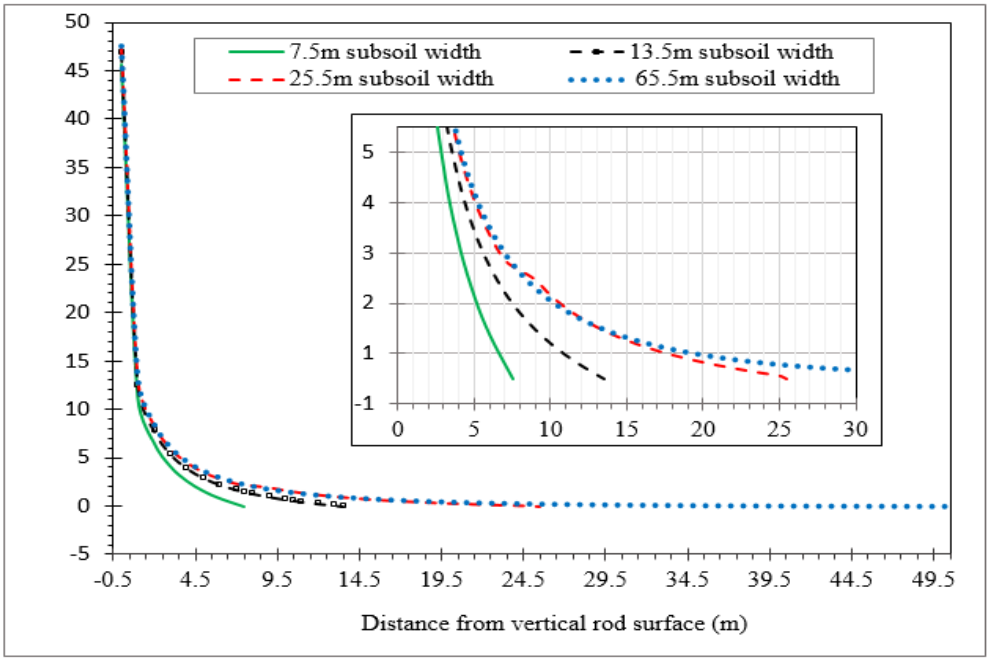


Figure 4.16: Distribution of ground surface electric potential for different width of subsoils under permanent wilting point suction

Source: Author's conceptualisation. Width of subsoil (7.5, 13.5, 25.5 and 65.5 m) under permanent wilting point (-152.76 m pressure head).

Table A7 contains the simulation post-processed and analytically computed resistance of a vertical earth rod in single-layer subsoil of different widths and domain depth of 20 m. From the table, the percentage difference between analytical and post-simulation computed resistances is independent of the condition of the soil but depends on the width of the subsoil. At 6.53%, the percentage difference for the minimum subsoil width 7.5 m, (that is, $2.5L$ or $L = 3$ m), is the maximum percentage difference for the set of subsoil width in Table A7. As the

width of the subsoil increases, the percentage difference reduces. The post post-simulation resistance formula (Equation 3.2) is proportional to $(V_E - V_r)^2$, where V_E and V_r are voltage at the electrode surface and outer boundary of the subsoil domain. Since the outer boundary condition is 0 V, the distribution of electric potential steeply declines from the maximum value at the electrode surface and outer boundary for small-sized domain width. Larger subsoil width permits the gradual decline from the maximum V_E to the subsoil boundary condition (0 V). This means that the accuracy of the distribution of electric potential on and within the subsoil increases as the width (radius) of the subsoil increases.

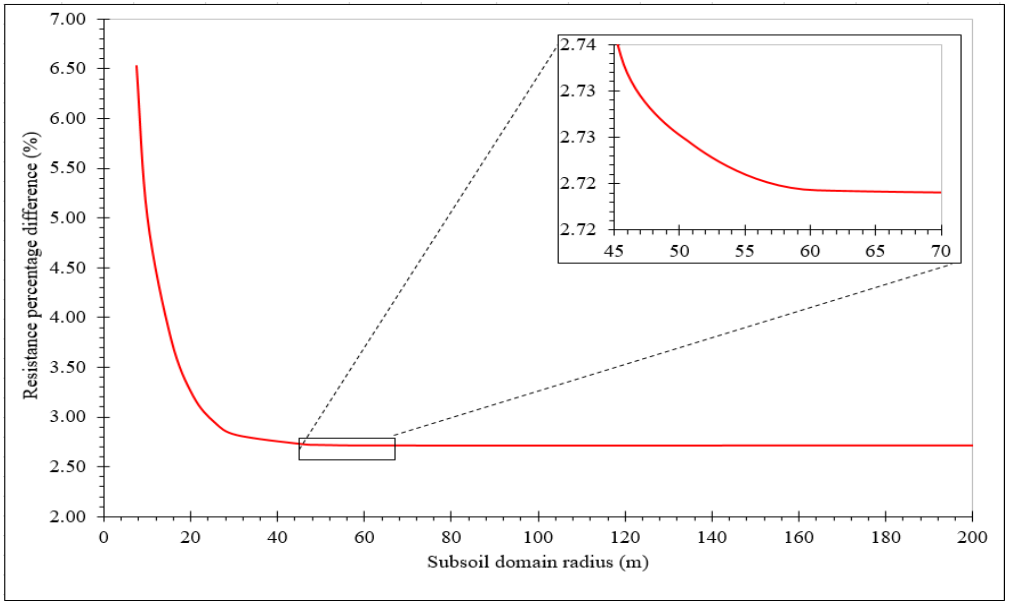


Figure 4.17: Percentage difference of simulation and analytical derived resistance for vertical earthing rod in single-layer soil without infinite element domain

Source: Author's conceptualisation

Consequently, the post-simulation resistance of the large subsoil model becomes equal to their analytically computed equivalent, such that the percentage difference reduces significantly. Figure 4.17 is a plot of the percentage difference against the width of the subsoil domain which is created using columns 2 and 7 of Table A7. The plot shows that the magnitude of the percentage difference decreases as the subsoil domain width increases and becomes constant as it approaches infinity.

The sensitivity of the depth of the subsoil domain is investigated by comparing the percentage difference for various depths of the subsoil domain. Table A8 provides a tabulated list of various combinations of domain width, depth, and soil conditions. The first two rows represent

earthing models with equal subsoil domain radius (7.5 m) and domain depth of 10.5 and 20 m respectively.

Under the -3.3734 m pressure head, the resulting percentage difference of earthing resistance is 6.60 and 6.53% respectively. If a large domain width, say 65 m (rows 10 and 17), is used with a relatively small domain depth (10.5 m), the magnitude of the percentage difference is comparatively high (4.31%), although less than 6.53%. For a range of large domain radius (50.5, 55.5, 60.5, and 65.5 m) and domain depth of 20 m, the percentage difference is approximately constant at 2.87% as represented by rows 7, 8, 9, 12, and 19. Therefore, it can be inferred that provided the domain width and depth exceed the radius and depth of the region of influence of the electrode ($3.5L$ for the rod of length L) substantially, then the resulting percentage difference decreases with an increase in domain depth. The sensitivity of the subsoil domain dimension on the simulation modelling depends more on the width or diameter than the depth, provided the depth is sufficiently greater than the depth bounded by the region of influence of the earthing system.

4.3 Hydro-Geophysical Earthing Modelling with Earthing Enhancement Materials in Single-Layer Subsoil

The performance of EEMs is defined by their ability to achieve resistance reduction in earthing sites with high resistivity values. As part of the fourth objective of the research (effectiveness of earthing enhancement materials in different subsoils, soil conditions and climatic zones), the resistance reduction capacity of different volumes of two EEMs (EEM I and EEM II) are evaluated in sandy clay and silty soils under saturated and unsaturated conditions of the soil. EEM I is bentonite clay, while EEM II is clay soil.

Figure 4.18 shows the water retention curves for the sandy clay and silty subsoils superimposed on the retention curve of the two EEMs (EEM I and EEM II). Note that soil suction has been expressed in pF: ($1\ \text{pF} = \ 0.98067$ kPa).

While the curves indicate the superior watered retention capacity of the EEMs at saturation, it is the suction transition width, ($\Delta\psi_{tr}$) and transition gradient ($\Delta\theta_{tr}/\Delta\psi_{tr}$) that are parameters of paramount importance needed for evaluating and analysing the performance of the earthing system. To specify these parameters, information about the transition suction (ψ_t) and residual coordinates are required. Transition suction, (ψ_t) is the suction at which the saturated porous material transitions to unsaturation states. Residual coordinates, (ψ_r, θ_r) are the pair of suction and volumetric water content at the point beyond which an increase in soil suction produces

marginal or no change in volumetric water content. Suction transition width, ($\Delta\psi_{tr}$) is determined from the difference between transition and residual suctions, that is, $\Delta\psi_{tr} = \psi_r - \psi_t$. Therefore, the transition gradient is evaluated as the ratio of the difference of water content, $\Delta\theta_{tr} = \theta_t - \theta_r$ to the suction transition width, $\Delta\psi_{tr}$.

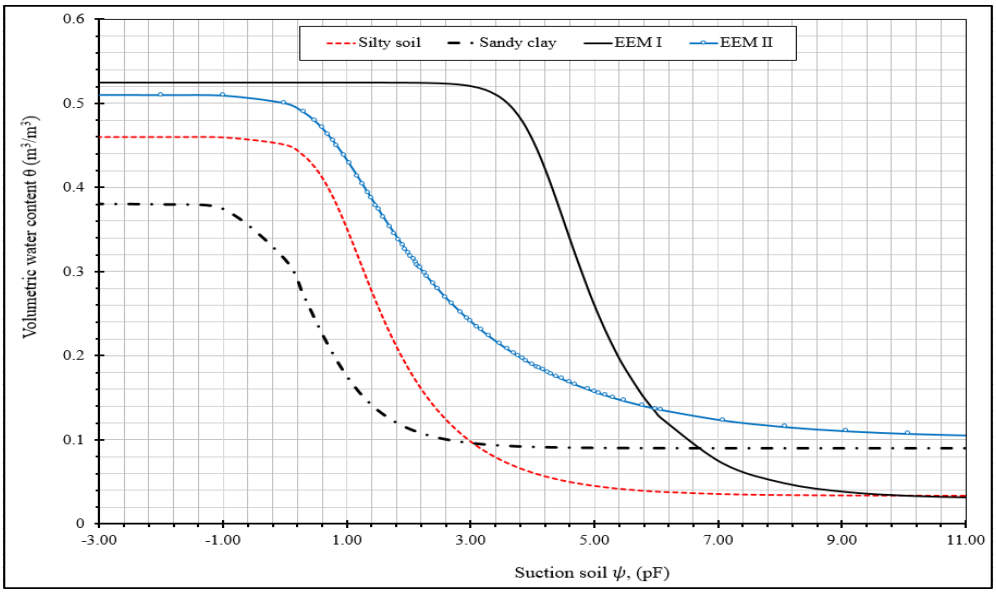


Figure 4.18: Water retention curves of silty and sandy clay subsoils with earthing enhancement materials

Source: Author's conceptualisation. EEM I (bentonite clay) and EEM II (clay soil).

Table 4.3 provides the coordinate values of transition and residual suction and volumetric water contents for the soils and EEMs. At relatively low suction (about 0.98 kPa), sandy clay begins to transition and attains a residual state around 4903.33 kPa.

The transition suction of silty soil is about 10 times the value for sandy clay and a suction transition of 1.1768×10^7 kPa, which is 2,400 times more than the suction transition width of sandy clay soil. While EEM I transition to unsaturated states at 12,747.37 kPa, EEM II transitions at about the value of suction as the silty soil with a transition width of order of 10^3 more than the silty soil. From the computation, the soils have smaller transition gradients of orders less than the EEMs. This means that the rate of water loss in the EEMs is less than in the soils, producing the desired consequence of earthing resistance reduction.

Table 4.3: Transition and residual suction values and corresponding volumetric water contents derived suction transition width and transition gradient

Soil/EEM	ψ_t (kPa)	ψ_r (kPa)	θ_t	θ_r	$\Delta\psi_{tr}$	$\Delta\theta_{tr}/\Delta\psi_{tr}$
Sandy clay	0.980665	4903.325	0.37439	0.09926	4.90236×10^{3}	-5.66×10^{-5}
Silty	9.80665	1.176×10^{7}	0.45090	0.03870	1.17686×10^{7}	-3.56×10^{-8}
EEM I	12747.37	1.186×10^{11}	0.51920	0.03354	1.17686×10^{11}	-4.16×10^{-12}
EEM II	9.80665	1.186×10^{11}	0.50020	0.10735	1.17686×10^{11}	-3.36×10^{-12}

Source: Author's conceptualisation. ψ_t *and* ψ_r *are the transition and residual suctions, and* θ_t *and* θ_r *are the transition and residual volumetric water content,* $\Delta\theta_{tr}/\Delta\psi_{tr}$ *is transition gradient,* $\Delta\psi_{tr}$ *is suction transition width.*

Figure 4.19 shows the curves of electric conductivity for soils (silty and sandy clay) and two earthing enhancement materials, denoted as EEM I (bentonite clay) and EEM II (clay soil). The curves show the minimum and maximum values of electric conductivity over the full volumetric water content range (0% to 100%).

While EEM II has the higher value of electric conductivity compared to EEM I, both EEMs exhibit relatively higher electrical conductivity than the soils, especially beyond 16% volumetric water content as their electrical conductivity equations and Figure 4.20 show. For example, at 13% and 16% volumetric water contents, the values of electric conductivity are 0.010591 and 0.016319 S/m for silty soil, 0.0001193 and 0.00040072 S/m for sandy clay soil, and 0.001278 and 0.044977 S/m for EEM I, and 0.00696 and 0.017117 S/m for EEM II.

Although the electrical conductivity of silty soil below the 16% volumetric water content threshold is higher than the EEM, the residual volumetric water contents of the EEMs at 11.69% for EEM I and 6.8% for EEM II which are greater than the 3.4% and 6.5% for silty and sandy clay soils respectively. With higher values of residual water and their proximity to the earthing electrodes, the EEMs offer significant earthing resistance reduction under high suction or dry conditions of soil.

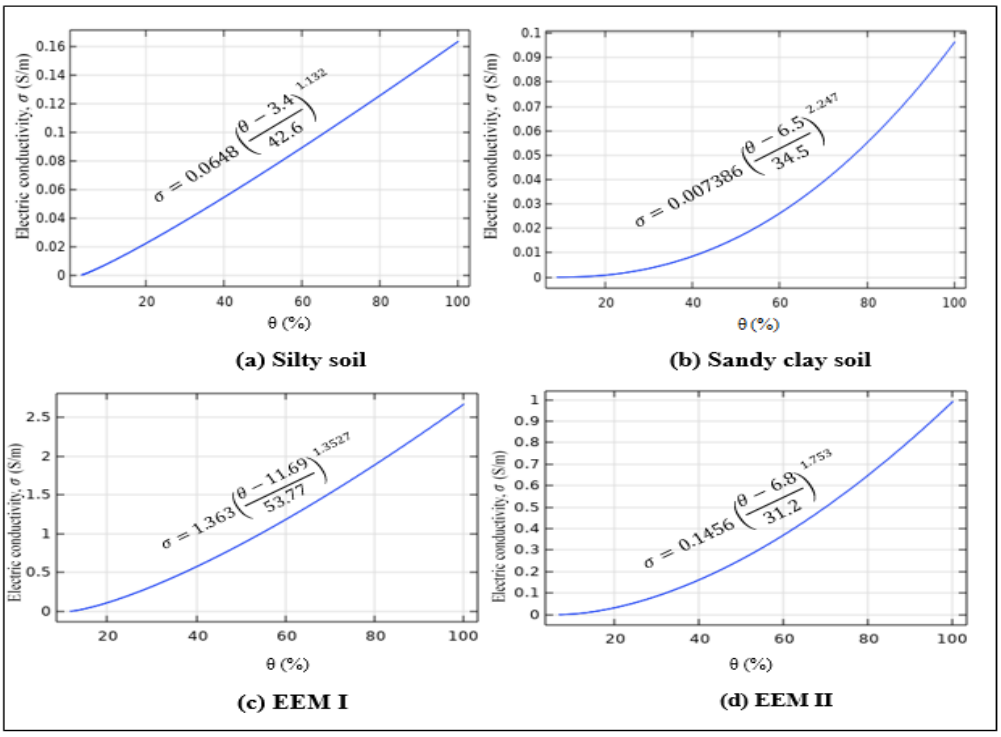


Figure 4.19: Plot of electric conductivity against volumetric water content for silty and sandy clay subsoils, and two earthing enhancement materials

Source: Author's conceptualisation

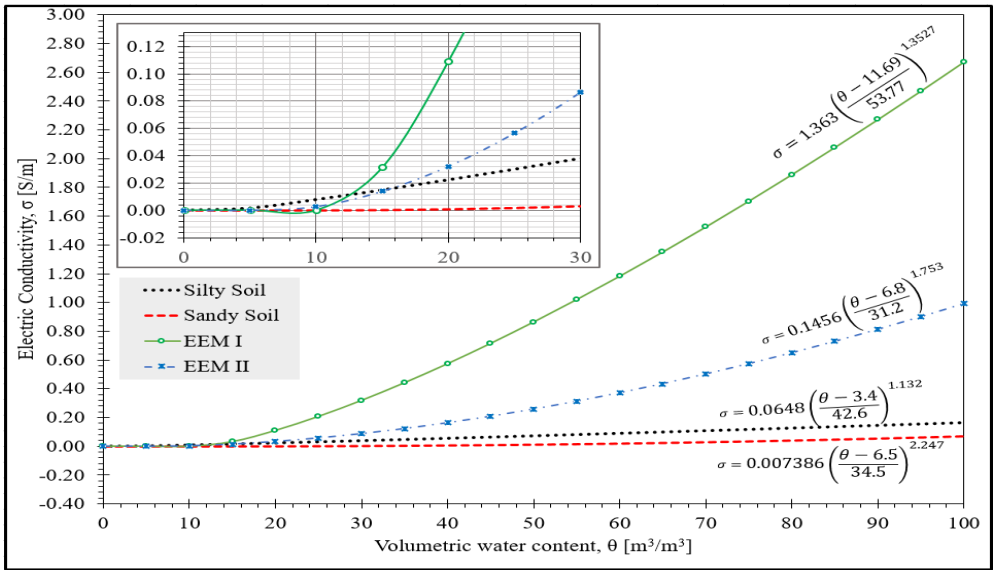


Figure 4.20: Plots showing the variation of electric conductivity of soil and earthing enhancement materials (EEMs) with volumetric water content

Source: Author's conceptualisation

Consequently, at high suction, the soils with low volumetric water contents attain high resistivity values. Table A9 shows the high-resistance values obtained by the vertical earth rod

(length 3 m, radius 95.62 mm) in silty and sandy clay soils which are reduced using EEM I and EEM II each of 0.1156 m radius. The percentage resistance reduction offered by EEM I and II in sandy clay is approximately equal without steep variation. However, in silty soil, the resistance reduction of the EEM I maintained a gradual increment from 39.12% at saturation to 42.1% at -98.0681 MPa suction. Of the two EEMs, EEM II offered the least percentage resistance reduction (32.19%) in silty soil. However, around the -147.10 kPa suction, the resistance reduction of EEM II in silty soil increased steeply to an approximately constant value of 41% for higher suction values.

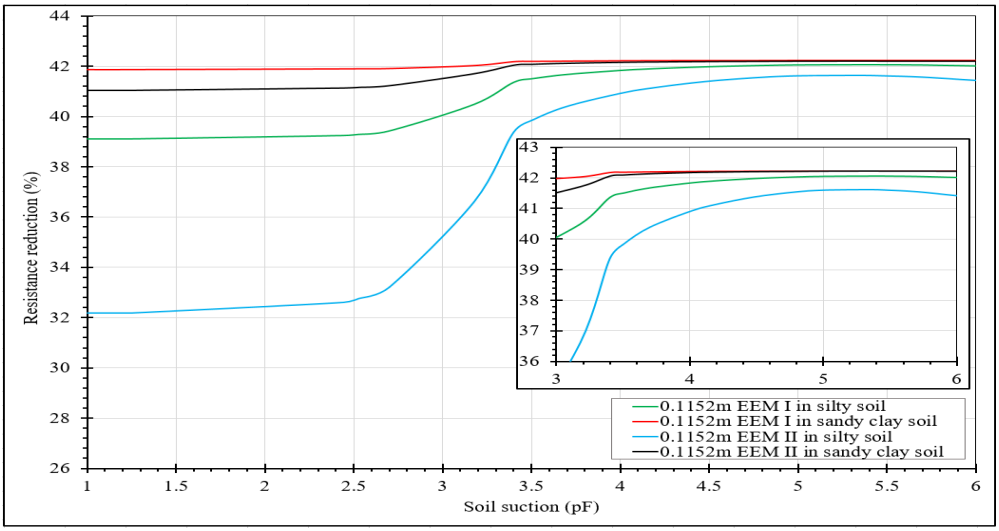


Figure 4.21: Variation of percentage resistance reduction of 0.1152 m radius of two earthing enhancement materials in sandy clay and silty subsoils

Source: Author's conceptualisation

Figures 4.21 and 4.22 are the percentage resistance reduction offered by 115.2- and 322.56-mm radius of EEM I and EEM II in silty and sandy clay soils. The shape of the resistance reduction curve is indicative of the performance of the EEM which is highly influenced by the water retention characteristics of the soil and EEM.

Both EEMs attained high and relatively constant resistant reductions in sandy clay soil unlike in silty soil where they exhibited significant performance variation. The insets in Figures 4.21 and 4.22 reveal details about the resistance reduction curve of EEM II in silty soil. It reveals a declining trend in resistance reduction after attaining the peak value around -9806.81 kPa (5 pF or –1000 m) and -29420.42 kPa (-3000 m) suction.

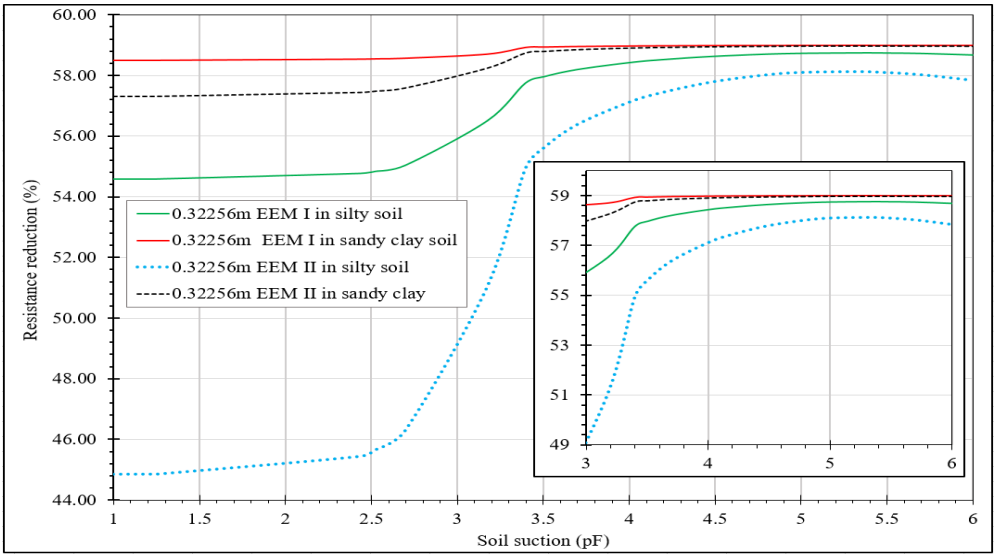


Figure 4.22: Variation of percentage resistance reduction of 0.32256 m radius of two earthing enhancement materials in sandy clay and silty soils

Source: Author's conceptualisation

4.3.1 Effect of Volume of Earthing Enhancement Material

The volume of EEM around the earthing electrode influences the magnitude of resistance reduction that it attains. Figures 4.23 and 4.24 contain the resistance reduction curves of different volumes (radius) of EEM I and EEM II around the vertical rod in sandy clay and silty soils respectively. The shape of the curves is independent of the diameter of the EEM. EEM I in sandy soil provide constant resistance reduction between saturation and unsaturated soil conditions, whereas EEM II offers a slight increase in resistance reduction

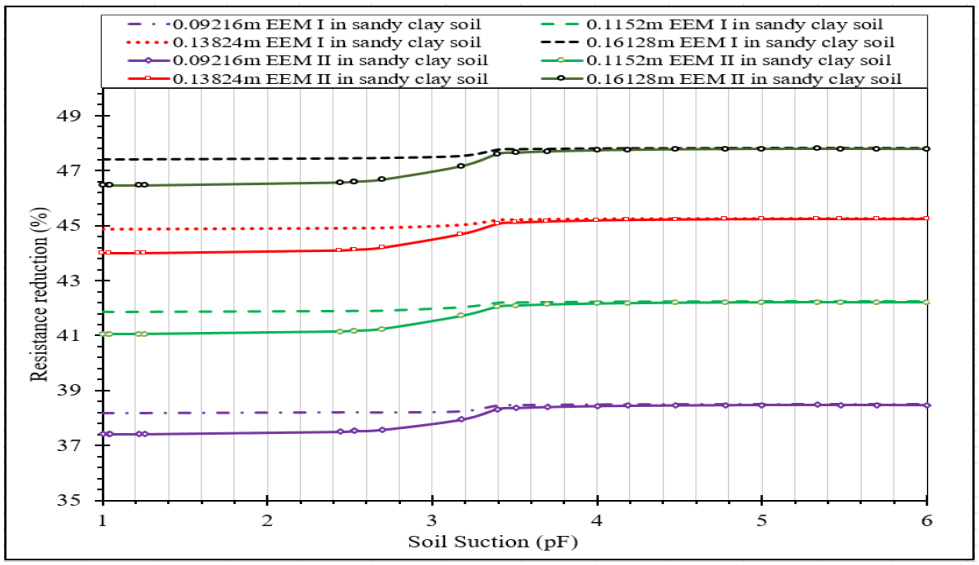


Figure 4.23: Percentage resistance reduction of different radii of two earthing enhancement materials in sandy clay subsoil under different soil suctions

Source: Author's conceptualisation

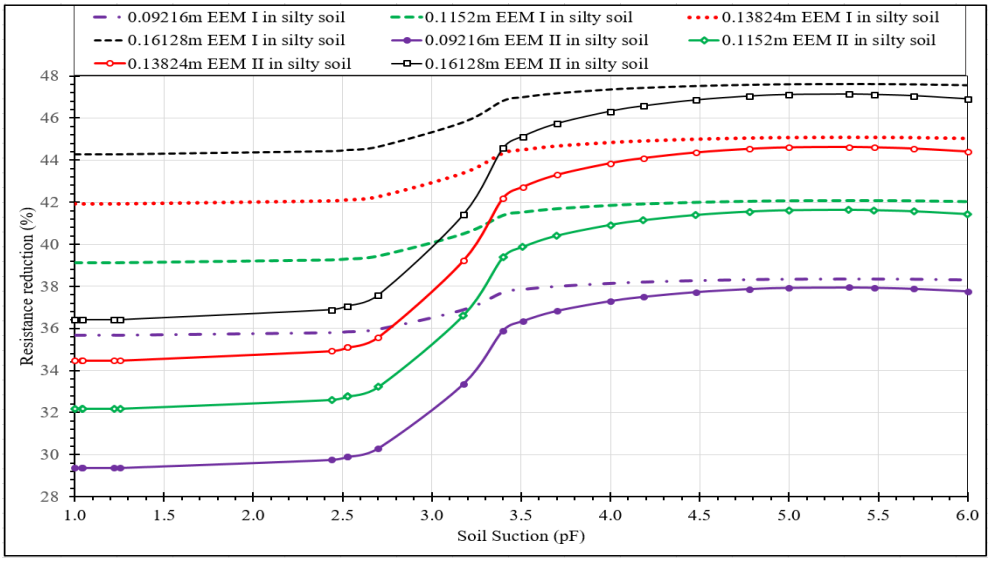


Figure 4.24: Percentage resistance reduction different radii of two earthing enhancement materials in silty subsoil under different soil suctions

Source: Author's conceptualisation

A similar resistance reduction pattern is exhibited by the EEMs in silty soil although with significant variation in performance over saturated and unsaturated suction values. Comparatively, EEM I offer more resistance reduction in both soils, while EEM II shows more resistance reduction variation. As the volume of the earthing enhancement material increases, the resistance reduction attained increases, as Figures 4.25 and 4.26 show. In each figure, there are two groups or clutter of resistance reduction curves with equal radius of EEM.

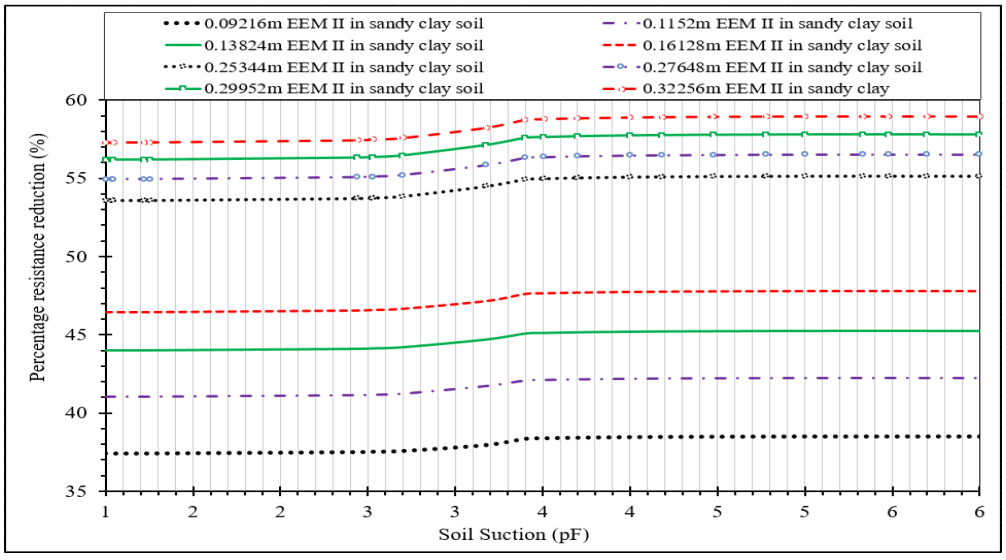


Figure 4.25: Effect of diameter of earthing enhancement materials on the percentage resistance reduction in sandy clay subsoil

Source: Author's conceptualisation

The curves in the lower group are for EEM with 0.09216, 0.1152, 0.13824, and 0.16128 m radius, while the upper group are for EEM of radius 0.25344, 0.27648, 0.299252, and 0.32256 m. Despite being equally spaced, curves in the lower group are not closely spaced, while those in the upper group are closely spaced. This indicates that there is a marginal increment in resistance reduction as the volume of the EEM increases, confirming findings in the literature [98].

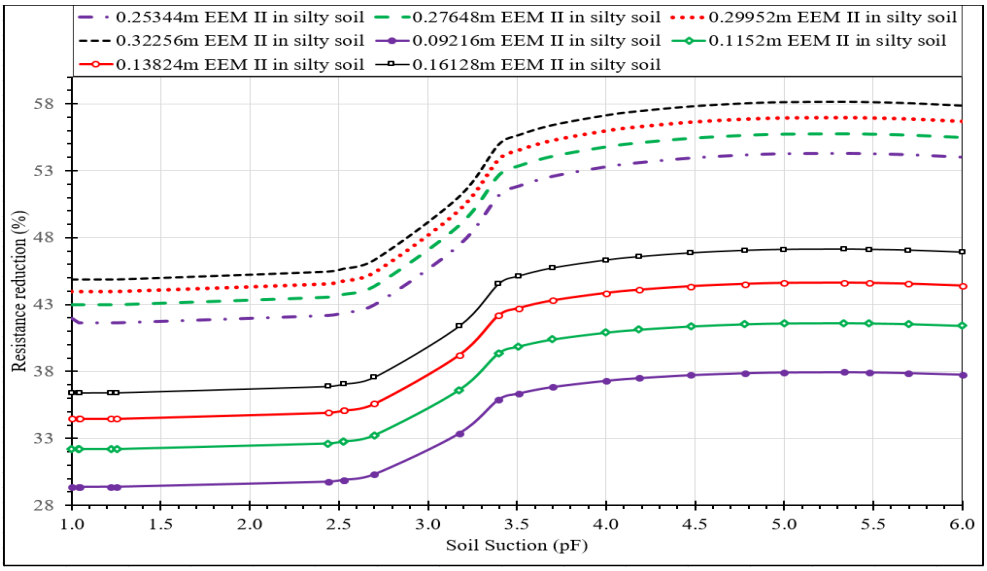


Figure 4.26: Effect of diameter of earthing enhancement materials on the percentage resistance reduction in silty subsoil

Source: Author's conceptualisation

4.3.2 Resistance Reduction of Earthing Enhancement Materials in Single-Layer Subsoils

The resistance reduction offered by EEMs around vertical rods in single-layer subsoil varies with the volume and water retention characteristics of the subsoil. Evaluating the mean percentage resistance reduction of different volumes of EEM over saturated and unsaturated soil conditions enables the formulation of the equation that predicts the resistance reduction capability of any volume of EEM using regression analysis. Figure 4.27 is the plot of the mean percentage resistance offered by EEM I and EEM II around a 3 m vertical earth rod in sandy clay and silty subsoils.

The equations were derived from regression analysis of the curves, each with a coefficient of determination, $R^2 = 1$ and valid for the radius of EEM, $r_{em} \geq 0.01$ m. For example, the defined r_{SCi} describes the resistance reduction of EEM I in sandy clay soil, while r_{STii} can be

used to predict the percentage resistance of EEM II in silty soil. Although high theoretical values of percentage resistance reduction can attain as $r_{em} \rightarrow \infty$, the practical restriction for attaining such values is imposed by the costs of EEM and installation.

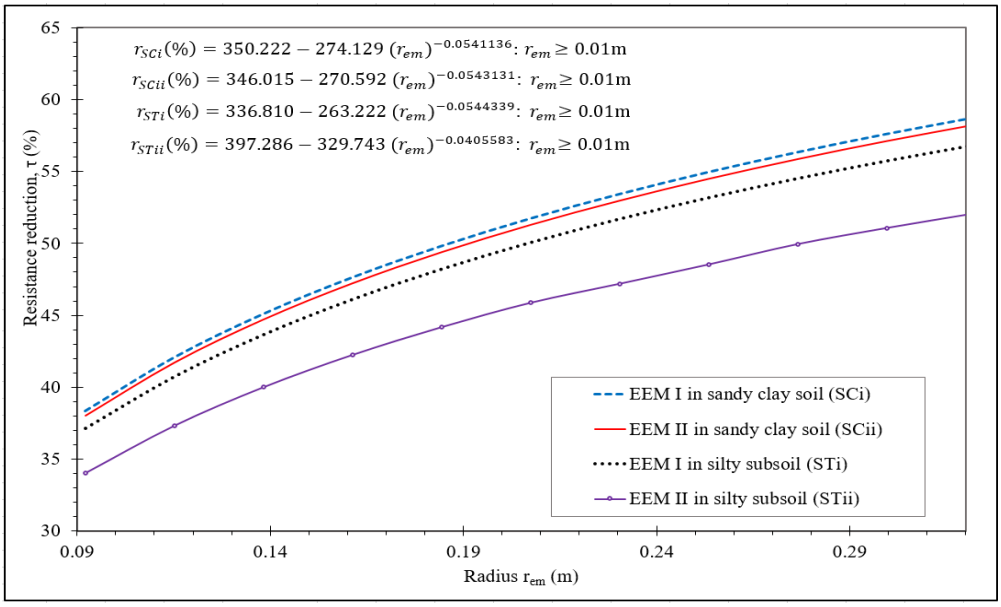


Figure 4.27: Plot of percentage resistance reduction against radius of earthing enhancement materials in single-layer sandy clay and silty subsoils

Source: Author's conceptualisation

4.4 Hydro-Geophysical Earthing Modelling of Two-Layer Subsoil

In the previous sections, the variability of resistivity and resistance of earthing electrodes in a single homogenous subsoil were extensively made. While the homogeneous model of the subsoil provides invaluable insights into earthing studies, it oversimplifies the earthing modelling and limits the reliability of the result. Earthing sites are typically multilayered but the two-layer model has been reported suitable for safe and reliable earthing design and implementation [99], [100].

Unlike the single-layer subsoil model, the two-layer model provides a more realistic representation of the multiphysics modelling of the actual earthing system. The geometric modelling of the subsoil requires details of each layer, specifically, the resistivity of the layers (ρ_1 and ρ_2), and the depth of the top layer, D_1. That is, (ρ_1, ρ_2, D_1). Since soil suction, unlike water content, is assumed to be continuous across adjacent layers, the volumetric water content dependent resistivity of each layer is derived independently.

4.4.1 Resistivity of Sublayers in Two-Layer Subsoil Model

Table A10 shows the resistance result of a 3 m-long cylindrical driven earth rod in two-layer subsoils (top layer depth, $D_1 = 1.4$ m) involving the layer permutations of clay, silty and sandy clay soil textures. The subsoil models are clay-sandy clay (CY-SC), clay-silty (CY-ST), silty-clay (ST-CY), silty-sandy clay (ST-SC), sandy clay-silty (SC-ST), and sandy clay-clay. The impact of soil suction on the variation of resistivity is influenced by the sublayer that the soil belongs to Table A10 also shows the values of resistivity for clay, silt and sandy clay soils when modelled in the top and bottom layers of the two-layer subsoil.

In all cases, the value of soil resistivity in the top and bottom layers varied significantly for a range of soil suction (1.5 to 4 pF) as seen in Figure 4.8. Within this suction range, the resistivity of soil in the top layer was always higher than the resistivity of the same soil in the bottom layer. One probable reason could be that the effect of suction on the bottom layer is reduced due to depth, which allows the same soil to retain more water in the bottom layer than in the top layer. Since suction affects water retention and release, a suction gradient exists along the depth of the subsoil. This implies that the layer position of a soil texture determines the impact of ground surface suction on the rate of water recharge, retention, or release.

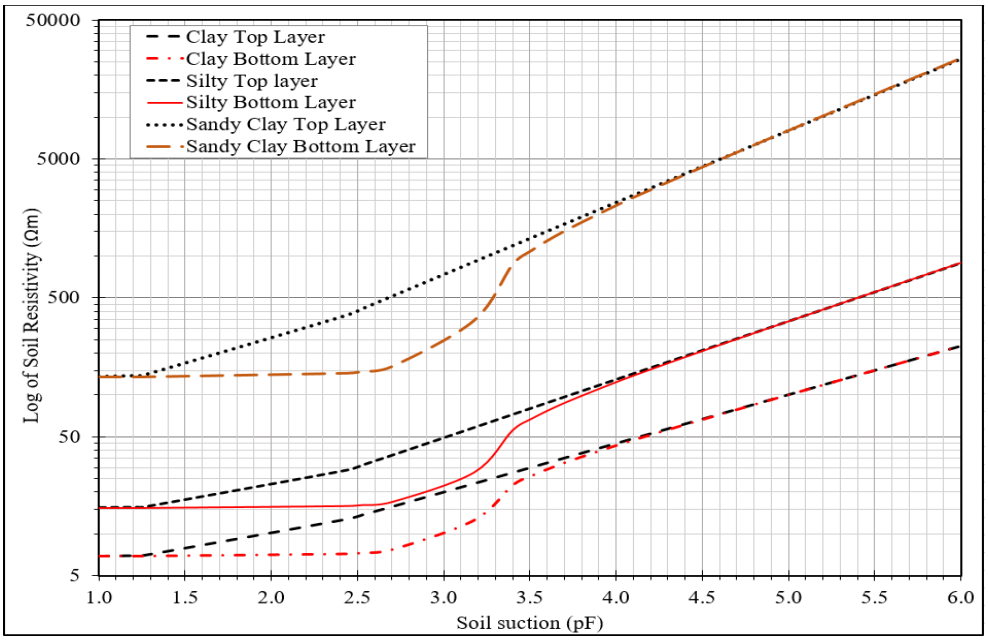


Figure 4.28: Suction-induced variability of soil resistivity in top and bottom layers of two-layer subsoil model

Source: Author's conceptualisation

For example, Table A11 shows the volumetric water contents (%) of three soils as single homogeneous layers, and above or below other soil layers. The rate and amount of water released from the sandy soil as a sublayer above and below the clay soil layer for a range of soil suction is not the same as with sandy soil in a single homogeneous layer. Placed below the clay layer, sandy soil exhibits a higher tendency of water loss by evaporation resulting in more water retention than when above the clay layer. At the top layer, soils experience unrestricted evaporation and less draining compared to the same soil at the bottom layer which has restricted evaporation and more draining.

Figure 4.29 shows volumetric water retention of sandy soil as a homogeneous single layer, above and below layers of clay soil. Within the 1.3 to 4 pF range of suction, the single homogenous soil layer retains the highest amount of water, followed by the bottom layer, while the sandy clay layer below the clay soil retains the least water content. Under steady-state conditions, this trend is typical of all soils for the stated range of soil suction, irrespective of their water retention characteristics. However, the depth of the top layer influences the magnitude of apparent resistivity and earthing resistance in multilayer subsoils.

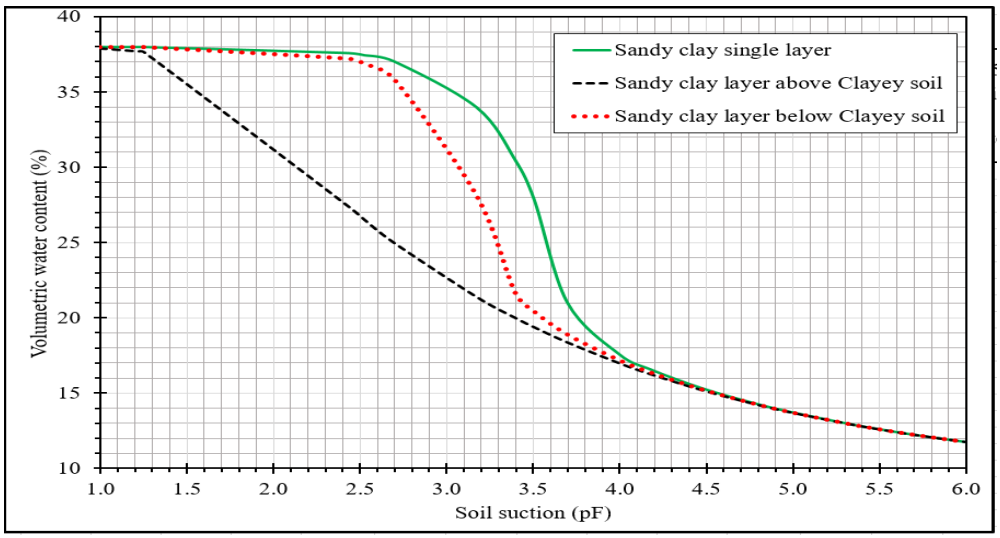


Figure 4.29: Comparison of volumetric water content in single layer, against sandy clay sublayer above and below clay subsoil layer

Source: Author's conceptualisation

4.4.2 Resistance of Earthing System in Two-Layer Subsoil Model

Table A12 provides the resistance of the 3 m-long cylindrical rod in single and two-layer subsoil models for the same range of soil suction (1 to 6 pF). The single soils are clay, silty and sandy clay soils, while the two-layer soils are layer permutation with clay, silty, and sandy clay

soils with the depth of the top layer 1.4 m. It had been previously discussed that under the same suction, single homogeneous soil layers retained more water than the same soil in the top or bottom layers, due to the relatively low value of resistivity, the corresponding resistance of the electrode in homogenous soil is lower. In Table A12, the pairs of columns 5, 6 and 7 and 8, 9 and 10, the earthing resistance in the two subsoils with the same pair of soil textures is always smaller in subsoils containing soil with higher water retention characteristics at the bottom layer. Figure 4.30 shows that two-layer subsoils with clay bottom soils exhibited the smallest magnitude of earthing resistance for the same electrode and soil suction, while subsoil with sandy soil produced the largest magnitudes of earthing resistance. The curves show that resistance increases with suction and is linear except during the transition suction.

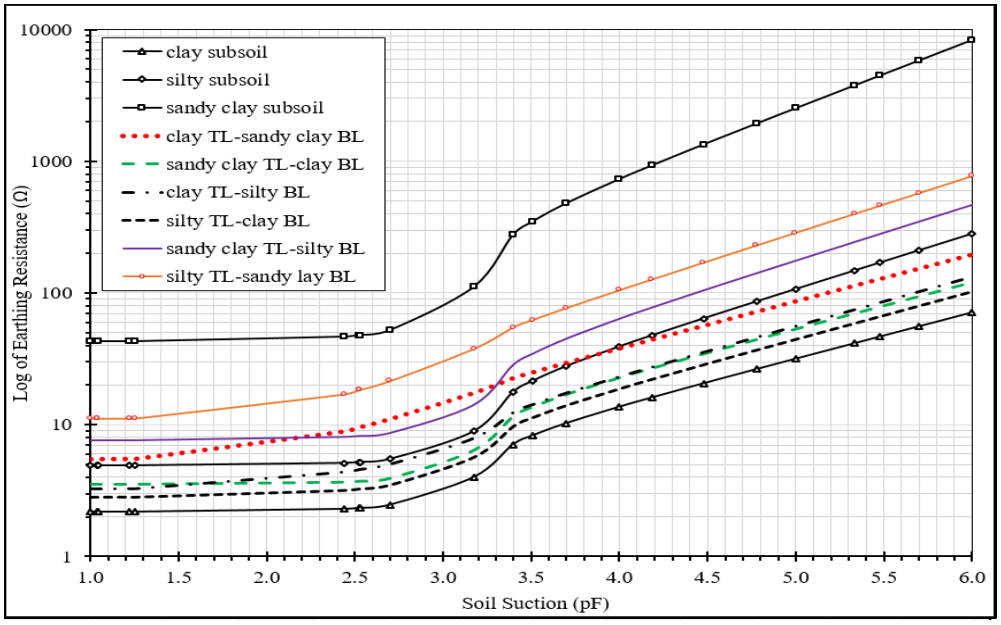


Figure 4.30: Variation of resistance of vertical earth rod in single and two-layer subsoils with top layer depth of 1.4 m

Source: Author's conceptualisation. Single-layer: (clay, silty and sandy clay) and two-layer subsoils: (clay-sandy clay, clay-silty, silty-clay, silty-sandy clay, sandy clay-silty, and sandy clay-clay) under variable soil suction.

The resistance of the earthing system in the two-layer subsoil model is influenced by the resistivity of the sublayers and the depth of the top layer [101], [102], [103]. Table A12 shows the resistance of a 3 m-long earthing rod in two-layer sandy clay-silty subsoil for a range of top layer depth of 0.5, 0.8, 1.4, 3, 3.5, and 4 m. The influence of the top layer increases with depth regardless of its resistivity relative to the resistivity of the bottom layer. Its influence on the apparent resistivity of the multi-layer subsoil increases with depth.

Figure 4.31 shows two clusters of plots for the resistance of a vertical rod in two-layer subsoil, consisting of silty soil at the bottom layer and sandy clay at the top layer. For the six top layer

depths, the two clusters correspond to resistance in top layer depth lesser and greater than the length of the vertical earth rod. The resistance of the vertical rod in subsoil with the top layer depth less than the rod length is significantly less than the corresponding resistance in subsoil with the top layer depth equal to or greater than the rod length.

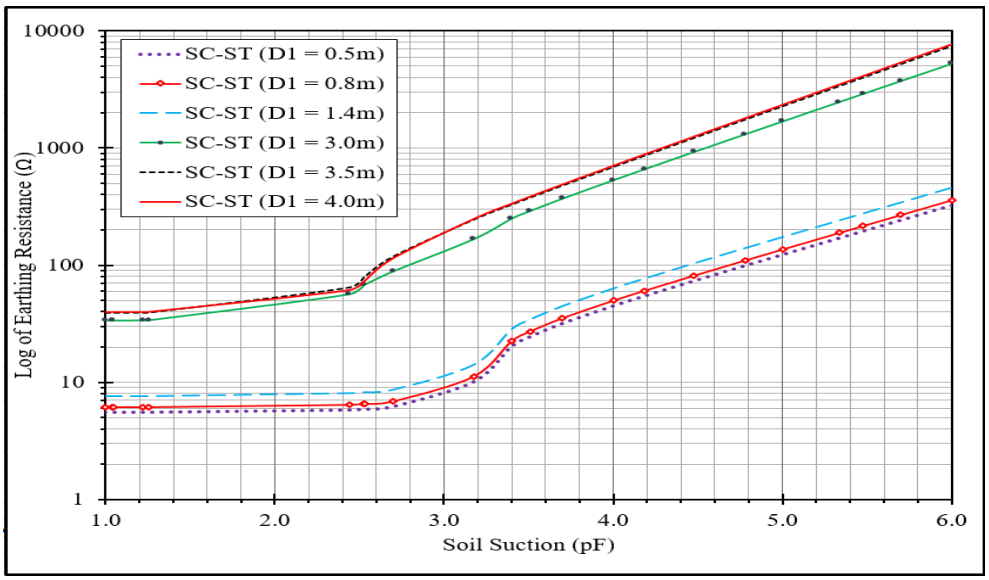


Figure 4.31: Effect of topsoil depth on the resistance of 3 m long vertically driven earth rod in two-layer (sandy clay-silty) subsoil

Source: Author's conceptualisation. Six topsoil layer depths: 0.5, 0.8, 1.4, 3, 3.5, and 4 m.

4.4.3 Resistance Reduction of Earthing Enhancement Materials in Two-Layer Subsoils

As demonstrated in single subsoil models, earthing enhancement materials can also be used to achieve reduced earthing for soil conditions with high resistivity. To achieve reduced earthing resistance, the material must have higher water retention capability and maintain low resistivity under high soil suction. The inset of Figure 4.32 is the magnified semi-logarithmic plot of the variation of resistivity with suction for sandy clay and silty soils as well as two earthing enhancement materials: EEM I and EEM II. Having higher water retention characteristics (Figure 4.18) and lower resistivity, the two EEMs are suitable for achieving a significant reduction in earthing resistance under high soil suction.

The earthing system has been modelled as 0.1152 m radius and 3 m-long EEM around the earth rod in two two-layer subsoils. A variety of subsoil models with EEMs have been developed to analyse their effective resistance reduction for different subsoil conditions. These models aim to evaluate the resistance reduction of the two EEMs in two-layer subsoils for different (i) soil

texture pairs, (ii) depth of the top layer, and (iii) volume of EEM around the earth rod. In terms of sublayer resistivity: ρ_1 and ρ_2 as resistivity of top and bottom layers, silty-sandy clay subsoil can be described as $\rho_1 \ll \rho_2$, whereas sandy clay-silty can be described with $\rho_1 \gg \rho_2$.

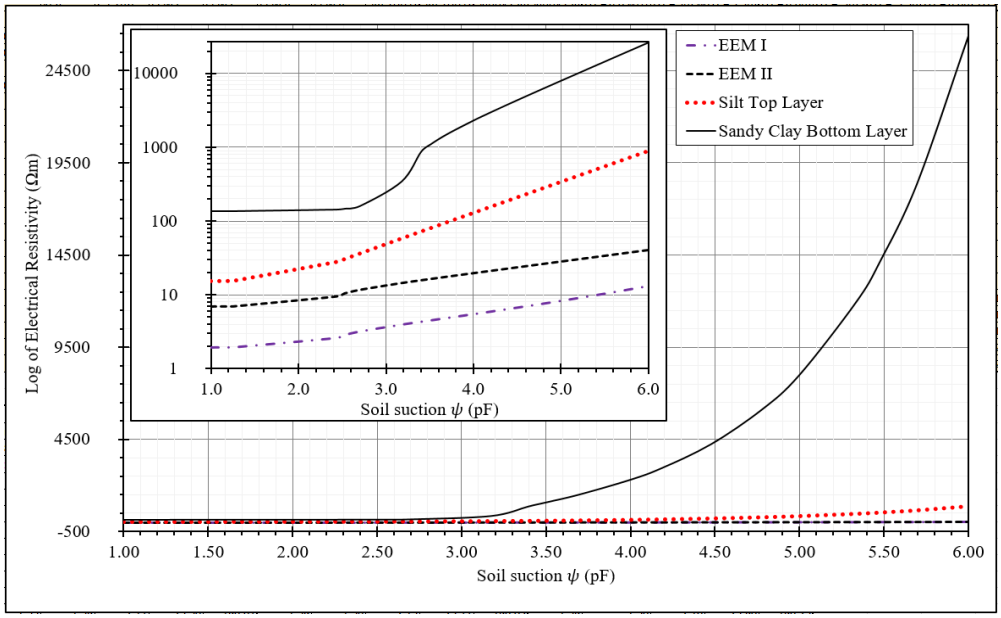


Figure 4.32: Suction resistivity curve of sandy clay and silty subsoils and two earthing enhancement materials (EEM I and EEM II)

Source: Author's conceptualisation

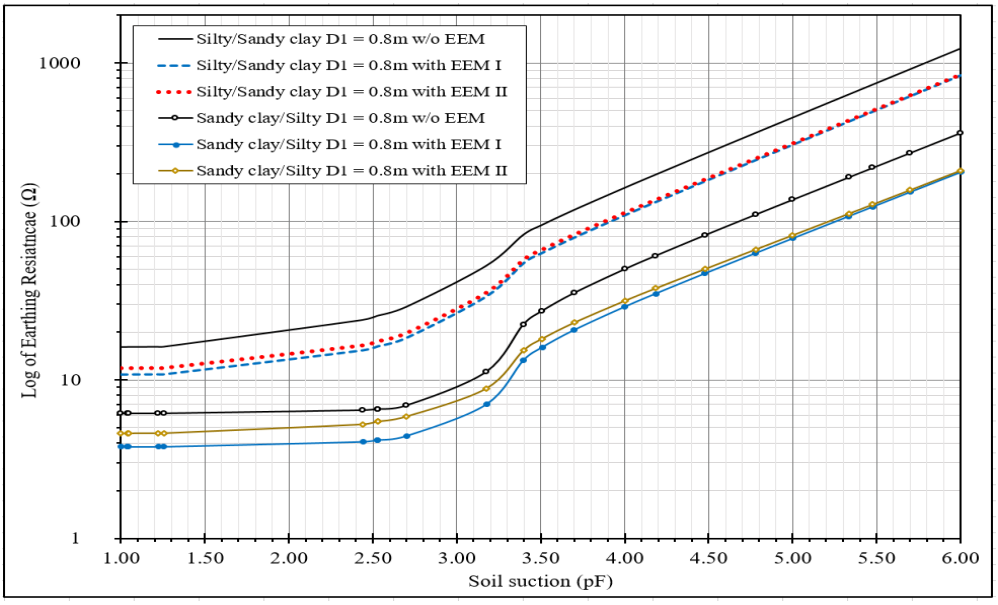


Figure 4.33: Comparison of resistance reduction performance of two 0.1152 m radius earthing enhancement materials (EEM I and EEM II) around a vertical earth rod relative to the resistance of earth rod without earthing enhancement

Source: Author's conceptualisation. Variation of resistance of vertical earth rod in two-layer soil (silty-sandy clay, and sandy clay-silty soils) of top layer depth D1 = 0.8 m without (w/o) and with 0.1152 m radius earthing enhancement materials under variable suction.

Figure 4.33 contains the plot of resistance for the vertical rod in the two-layer subsoil model with and without the EEMs. It shows that relative to earthing models without EEM, the EEMs achieved resistance reduction in all the two-layer subsoils but with unequal magnitude. For suction less than permanent wilting point suction (-1500 kPa), EEM I attained a relatively lower resistance than EEM II in both silty-sandy clays but reduced the resistance more significantly in sandy clay-silty subsoils. As suction increased, earthing resistance due to the two EEMs in the two subsoils converged towards similar values.

The descriptive statistics for percentage resistance reduction of 0.1152 m radius of the EEMs (EEM I and EEM II) in two-layer subsoils (sandy clay-silty and silty-sandy clay) for three top layer depths (0.8, 3, and 3.5 m) are provided in Table 4.4. The minimum, maximum and mean values of percentage resistance reduction that EEM I attained are higher than the corresponding values for EEM II in both two-layer subsoils. The superior water retention characteristics and smaller resistivity profile give EEM I the comparative edge in performance.

Table 4.4: Descriptive statistics for percentage resistance reduction of two-layer subsoil models for three top layer depths

Topsoil	Bottom soil	Topsoil depth (m)	EEM	Resistance Reduction (%)			
				Min	Max	Mean	Std. dev.
Sandy clay	Silt	0.8	I	35.68	43.48	40.16	2.69
			II	14.63	42.02	30.50	9.26
Silt	Sandy clay	0.8	I	32.43	36.61	33.84	1.36
			II	26.30	32.07	29.89	2.01
Sandy clay	Silt	3.0	I	61.37	77.03	70.23	5.12
			II	46.35	55.80	52.25	2.15
Sandy clay	Silt	3.5	I	46.30	47.82	47.24	0.56
			II	44.41	47.76	46.40	1.27
Silt	Sandy clay	3.5	I	30.65	33.87	31.88	0.82
			II	19.02	31.15	25.24	4.80

Source: Author's conceptualisation. Percentage resistance reduction showing the minimum (Min), maximum (Max) and standard deviation (STDEV) due to 0.1152 m radius of two enhancement materials (EEM I and EEM II) in three top layer depths (0.8, 3, and 3.5 m) of two-layer subsoil models (sandy clay –silty, and silty-sandy clay).

Figure 4.34 is the plot of percentage resistance reduction of EEM I and EEM II in sandy clay-silty and silty-sandy clay two-layer subsoils of 0.8 m top layer depth. The figure provides insight into the performance of the EEMs under variable conditions. As suction increased from saturation to 2.6pF, percentage resistance reduction increased in silty-sandy clay subsoil but decreased in sandy clay-silty subsoil attaining maximum and minimum values respectively. Between 2.6 and 3.4 pF, resistance reduction increased steadily and steeply due to EEM I and

EEM II respectively in sandy clay-silty subsoil, whereas resistance reduction due to these EEMs decreased steeply in silty-sandy clay subsoil.

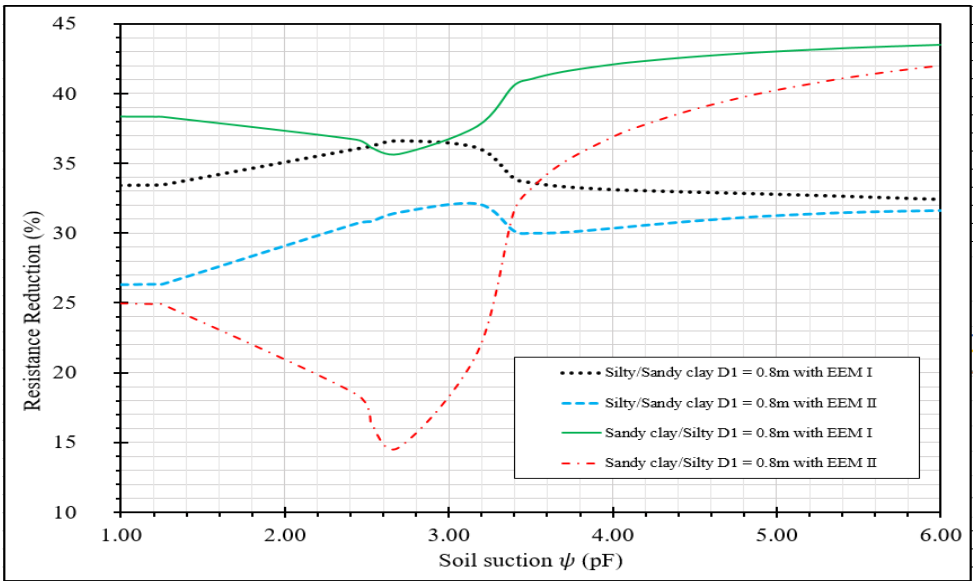


Figure 4.34: Soil suction induced percentage resistance reduction variation of two earthing enhancement materials

Source: Author's conceptualisation. Earthing enhancement materials (EEM I and EEM II), each of 0.1152 m radius around a vertical earth rod in two double-layer subsoils of 0.8 m depth of top subsoil layer depth (D1).

Beyond 3.4 pF, resistance reduction increased at a constant rate with EEM I and almost linearly with EEM II in the sandy clay-silty subsoil and converged steadily to a constant value. Although the percentage resistance reduction of the EEMs differs in the two two-layer subsoils, the trend of variation is determined by the resistivity of the sublayers. The interaction of the resistivity of the EEM and top layer soil influences the value of earthing resistance and the resistance reduction capacity of the EEM.

Besides its resistivity, the depth of the top layer of soil plays a significant role in the performance of the EEM. Figure 4.35 shows the resistance reduction capacity of EEM I in three top layer depths (0.8, 3, and 3.5 m) of two two-layer subsoils. Between saturation and field capacity suction, the performance of the EEM is inversely proportional to the depth of the top layer for subsoil with $\rho_1 \ll \rho_2$. In other words, more resistance reduction is achieved as the depth of the high-resistivity bottom layer reduces. After marginal fall and rise from 2.4 to 3.5 pF, resistance reduction continues to decrease and increase steadily for D1 $\leq L_r$ and D1 $> L_r$ beyond the 3.5 pF suction. For $\rho_1 \gg \rho_2$, the influence of top layer depth on the performance of the EEM is significant but without trend. Relative to the other top layer depths, D1 $< L_r$ and D1 $> L_r$, D1 $= L_r$ offers the highest resistance reduction for $\rho_1 \gg \rho_2$ subsoil.

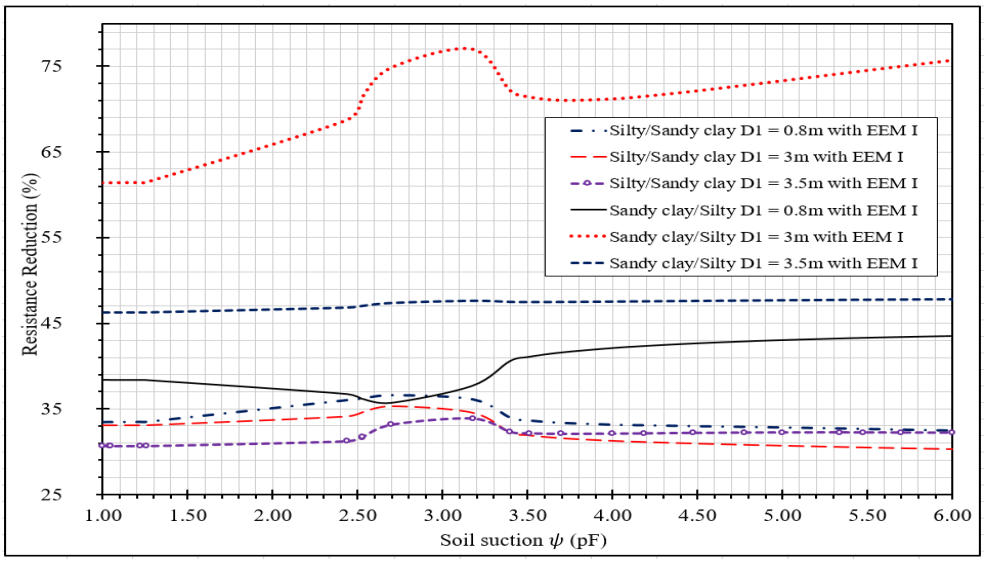


Figure 4.35: Soil suction induced percentage resistance reduction variation of an earthing enhancement materials (EEM I) around a vertical earth rod in two double-layer subsoils

Source: Author's conceptualisation. Radius of rod = 0.1152 m. Two-layer (sandy clay-silty and silty-sandy clay) subsoils for three top layer depths (D1 = 0.8, 3, and 3.5 m).

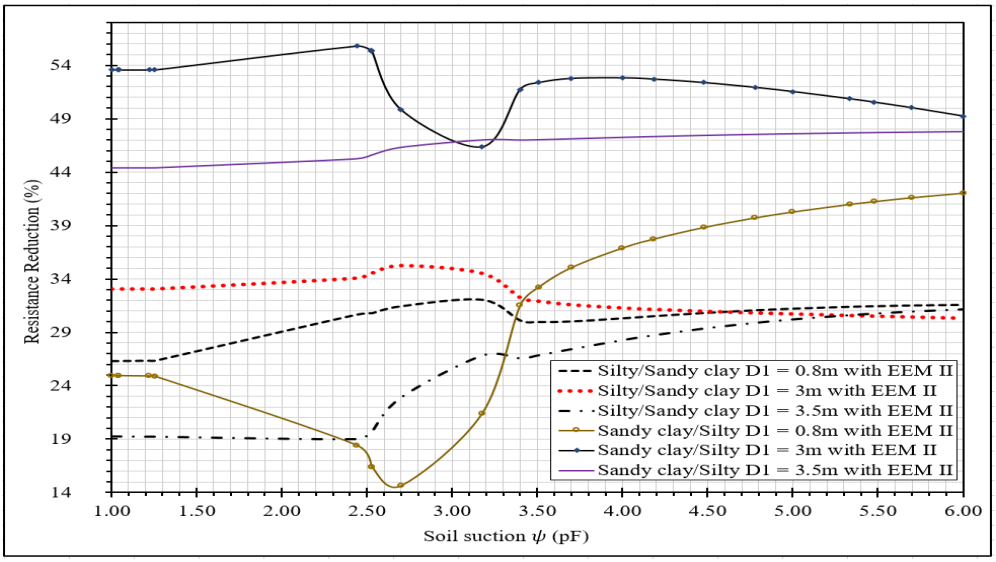


Figure 4.36: Soil suction induced percentage resistance reduction variation of two separate earthing enhancement materials (EEM II) around a vertical earth rod in two double-layer subsoils

Source: Author's conceptualisation. Radius of rod = 0.1152 m. Two-layer (sandy clay-silty and silty-sandy clay) subsoils for two top-layer depths (D1 = 0.8, 3, and 3.5 m).

Figure 4.36 is the equivalent of Figure 4.35 for EEM II. It contains the plots of percentage resistance reduction of EEM II in three top layer depths of the two two-layer subsoils. Whereas the resistance reduction of the two EEMs is unequal, EEM II exhibits a similar performance trend as EEM I in the $\rho_1 \ll \rho_2$ subsoil. Like EEM I in $\rho_1 \gg \rho_2$, resistance reduction offered by EEM II is significantly influenced by the depth of the top layer. Despite offering maximum

resistance reduction in the D1 = L_r, $\rho_1 \gg \rho_2$ subsoil model, the performance of EEM II in D1 = L_r exhibits a similar trend as in D1< L_r subsoil.

Figure 4.37 shows the resistance reduction of EEM I and EEM II in different top layer depths of $\rho_1 \ll \rho_2$ and $\rho_1 \gg \rho_2$ subsoil models. Table A15 and Figure 4.37 show the comparative performance edge EEM I have over EEM II; however, the EEMs reveal no instructive performance trend in the different top layer depth of the $\rho_1 \ll \rho_2$ subsoil. The last aspect of resistance reduction capacity of the EEMs is the analysis of the impact of the volume (width or radius) of EEM in the $\rho_1 \ll \rho_2$ subsoil. The $\rho_1 \ll \rho_2$ subsoil is the most suitable subsoil model where the use of EEM is required to improve earthing conditions due to an earth rod. Unlike $\rho_1 \gg \rho_2$ where single or multiple driven rods may be adequate to achieve good earthing.

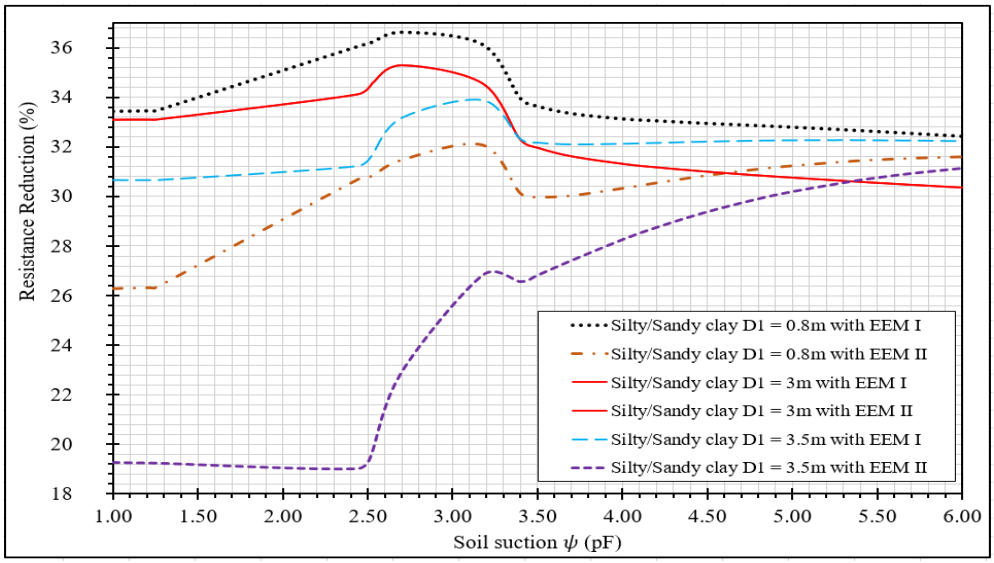


Figure 4.37: Soil suction induced percentage resistance reduction variation of two earthing enhancement materials around a vertical earth rod in a double-layer (silty-sandy clay) subsoil

Source: Author's conceptualisation. Radius of rod = 0.1152 m. Double-layer (silty-sandy clay) subsoil for two top-layer depths (D1 = 0.8, 3, and 3.5 m).

Table 4.5 shows the descriptive statistics of percentage resistance reduction of various radii of EEM I and EEM II in silty-sandy clay subsoil for a range of soil suction. The performance of EEM I is generally superior to EEM II in the $\rho_1 \ll \rho_2$ (silty-sandy clay two-layer) subsoil. However, beyond 3 pF (permanent wilting point), the performance of EEM I declined, while that of EEM II improved. EEM II has a high prospect of maintaining constant resistance in the subsoil at high suction conditions. As with single-layered homogeneous subsoils, an increase in the volume of the EEM produced more resistance reduction by both EEMs. This trend is

evident in Figure 4.38; a plot of the variability of resistance reduction with suction for different radii of EEM I and EEM II in silty-sandy clay soil.

Table 4.5: Descriptive statistics of percentage resistance reduction of EEM I and EEM II in two-layer silty-sandy clay subsoil

EEM	Resistance reduction (%)				
	Radius (m)	**Minimum**	**Maximum**	**Mean**	**Standard deviation**
EEM I	0.11520	32.43	36.61	33.88	7.50
	0.13824	34.81	39.31	36.39	8.04
	0.16128	36.83	41.60	38.51	8.51
	0.18432	38.58	43.57	40.36	8.91
	0.20736	40.12	45.31	41.99	9.26
	0.23040	41.51	46.87	43.45	1.85
	0.25344	42.76	48.28	44.77	1.90
	0.27648	43.90	49.56	45.98	1.95
	0.29952	44.95	50.74	47.10	2.00
	0.32256	45.93	51.83	48.13	2.04
EEM II	0.11520	26.30	32.07	30.25	6.78
	0.13824	28.51	34.54	32.59	7.28
	0.16128	30.43	36.64	34.58	7.70
	0.18432	32.13	38.48	36.33	8.07
	0.20736	33.67	40.11	37.89	8.39
	0.23040	35.06	41.59	39.30	1.64
	0.25344	36.34	42.92	40.58	1.64
	0.27648	37.53	44.15	41.76	1.63
	0.29952	38.64	45.39	42.85	1.64
	0.32256	39.67	46.39	43.87	1.63

Source: Author's conceptualisation.

Figure 4.38 illustrates how an increase in EEM radius achieves more resistance reduction but also shows that the space between adjacent curves decreases with an increase in the radius of EEM. This space decrease indicates that marginal resistance reduction is achieved as the radius of EEM increases infinitely. Although the curves may be extrapolated for higher theoretical values of resistance reduction, the costs of the EEM and their installation impose practical restrictions on the implementable volume of EEM.

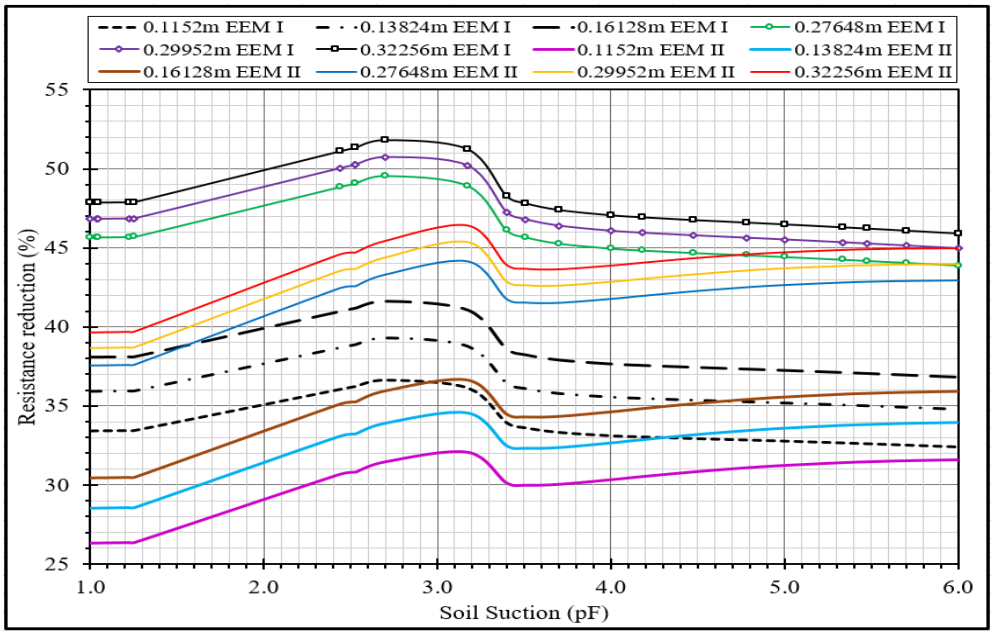


Figure 4.38: Soil suction induced percentage resistance reduction variation of two earthing enhancement materials (EEM I and EEM II) of different radius around a vertical earth rod in a double-layer (silty-sandy clay) subsoil of 0.8 m depth of top subsoil layer.

Source: Author's conceptualisation.

Chapter 5 - Equation Formulation Water Content Variation Within the Region of Influence of Vertical Earth Electrodes

5.0 Sphere of Influence of Earth Electrode

In the previous chapter, the evaluation of resistance and performance analyses of earthing electrodes were based on the resistivity and volumetric water content of the entire subsoil. Although finite models of subsoil were used, they are dimensional approximations of the actual earth, which is infinite. Because the electric connection between infinite earth and earth electrodes is conductor-to-area based [104], it is the volume of the earth around the electrode that provides the electrical conduction and its resistivity that influences earthing resistance.

This assumption is consistent with simulation results and field measurements of earthing resistance in homogeneous subsoils. These measurements indicate that the resistance of the earthing electrode decreases exponentially from the electrode. Consequently, the earth is modelled as concentric shells around the electrode, such that the resulting resistance is inversely proportional to their cross-section and diminishes asymptotically to zero. The region of subsoil accounting for approximately 95% of the earthing resistance is called the critical resistance area or sphere of influence of the electrode [42], [104]. It implies that the variation of water content and resistivity within this region regulates changes in earthing resistance.

5.1 Volume of the Sphere of Influence of Earth Electrode

The volume of the sphere of influence depends on the configuration and orientation of the earthing terminal or electrode. For example, the sphere of influence of a vertical-driven rod of length L is described as the region within a $2.5L_r$ radius from the surface of the rod [2].

Mapping the surface inscribed by the radius, as shown in Figure 5.1, the volume of the sphere of influence consists of a cylindrical volume above a hemispherical bottom. Given that the volume may not necessarily be spherical, it is subsequently referred to as the region of influence (ROI) of the earth electrode.

Relative to a cylindrical volume modelling an infinite subsoil, Figure 5.1 (a) shows a vertical earth rod and its ROI. Figure 5.1 (b) is the annotated description of the dimensions of the ROI. According to the IEEE ROI model for driven rod [2], if the length of the buried rod is L_r, then the ROI consists of a cylindrical top of radius $2.5L_r$ and height L_r above a hemispherical volume of $2.5L_r$ radius. Therefore, the depth of the ROI measured from the ground surface is $3.5L_r$. Depending on the size of the electrode, the ROI can extend into several layers of subsoil,

implying that changes in the constituent layers control the variation of resistance and performance of the earthing system.

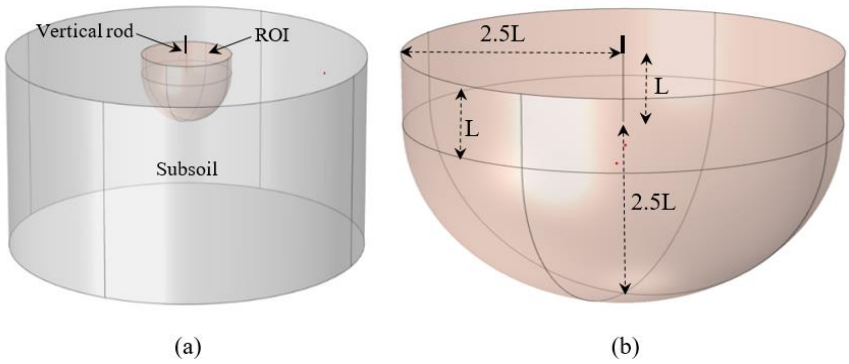


Figure 5.1: Annotated 3D view of earthing model showing the region of influence of vertical earth rod

Source: Author's conceptualisation. $L = L_r$, the length of earth rod [105].

5.1.1 Effects of the Region of Influence and Soil Domain on Earthing Modelling in Single-Layer Subsoil

Table A13 shows the result of volumetric water content within the ROI and infinite subsoil domain for sandy clay, clay, and silty soils over a range of saturated and residual conditions of the soil. Comparing values in the infinite subsoil domain and ROI, values in the former are characteristically higher and become equal as the degree of saturation of soil decreases. The effect is that soil resistivity within the ROI is slightly higher, resulting in marginally higher values of earth resistance, as Table A14 shows. Under the isotropic conditions, soil resistivity in both the soil domain and ROI should be constant. However, the difference exists due to the impact of the variation of the degree of saturation of soil along the soil column. Due to the positioning of the ROI relative to the soil domain, desaturation influences impact the ROI significantly more than the soil domain.

The variation of the percentage difference between the magnitude of volumetric water content and earthing resistance of soil domain and ROI depends on the subsoil condition and type. As Figure 5.2 shows, these variations for the three soil types are significantly less at the extreme ends of saturation and residual conditions. However, during the transition or capillary states, silty soil exhibits the most evident variation, clay soil the least, while sandy clay soil shows intermediate characteristics. Since the boundary condition (electric potential) at the outer boundary of the ROI ($2.5L_r$) was not modelled with infinite domain property, its electric

potential is not 0 V. The ratio of electric potential at the rod surface and outer boundary of the ROI is 20.79:1.

The ratio of electric potential at the rod surface and outer boundary of the ROI is 20.79:1. Representing 95.19% of the electric potential at the electrode surface, this ratio implies that the ROI accounts for 95.19% of the magnitude of earthing resistance of the full subsoil domain, which is consistent with the accepted definition of the ROI in the literature *[2], [88], [104]*.

Any meaningful determination of water content that affects earthing resistance, involves either destructive soil sampling or non-destructive insertion of the moisture probe within the ROI of the earth electrode. Since the electric potential ratio is constant regardless of soil type and condition, it is a suitable correction factor for estimating the actual value of soil resistivity or earthing resistance, especially when soil resistivity has been estimated from the parameters of soil within the ROI.

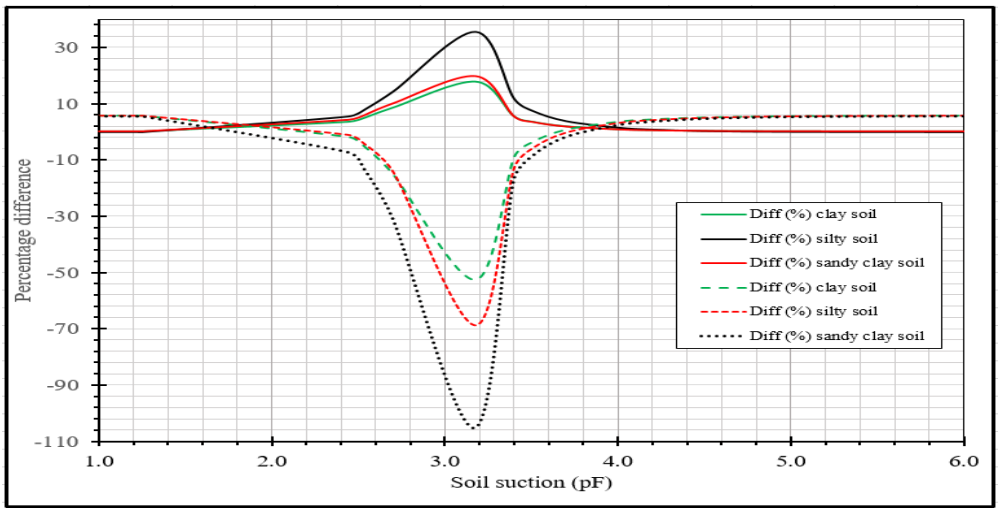


Figure 5.2: Percentage difference of volumetric water contents in entire domain and region of influence of subsoil on the vertical earth rod and the corresponding earthing resistances for single-layer subsoil

Source: Author's conceptualisation.

5.1.2 Effects of the Region of Influence and Soil Domain on Earthing Modelling in the Two-Layer Subsoil

Although the volume mapped by the region of influence of earthing electrode in the multi-layered subsoil model and single-layer model are equal, the distinction is that the ROI in the multilayer model contains many sublayers that depend on the depth of superficial layers and the size of the electrode. Unlike the single-layer model, the resistivity of the ROI with multilayers is impacted by the volumetric water contents of constituting sublayers. Consequently, the resistance of the earthing system depends on the depth, hydraulic and electric properties of the sublayers within the ROI. For a two-layer model described by (ρ_1, ρ_2, h_1), earthing resistance depends on the depth of the top layer, h_1 and the coefficient of reflection, k_c expressed in terms of layer resistivity, ρ_1 and ρ_2, as $k_c = (\rho_2 - \rho_1)/(\rho_2 + \rho_1)$. The soil texture profile and degree of saturation of sublayers determines the value of k_c, as $k_c < 0$, $k_c = 0$ or $k_c > 0$. Two two-layer subsoil profiles, silty top-sandy clay bottom (ST-SC) and sandy clay top-silty bottom (SC-ST) are used to demonstrate the effects of soil texture and layer depth on the resistance of a vertical electrode within the ROI of rod and infinite subdomain model.

Table A15 is the post-processed resistance of the vertical rod within the ROI and infinite model of two two-layer subsoils with values of h_1. The effect of suction on the degree of saturation of homogeneous soil is characteristic of the soil texture but shows with marginal difference that depends on the layer that the soil texture appeared in Figure 5.3 plots the percentage difference of resistance of vertical rod for five subsoil conditions against different depths of the top layer in two-layer ROI and infinite model of silty top, sandy clay bottom subsoil. Like Table A15, the trend of the plots shows the influence of the depth of the top layer in the resistance of the vertical electrode in the silty top-sandy clay bottom. The variation of the percentage difference between resistance due to ROI and infinite domain (SD) model of silty top-sandy clay bottom subsoil follows a similar trend for a range of suction where resistance due to ROI is always less than resistance due to infinite domain model, except around field capacity, -33 kPa (2.527 pF). As Figure 5.3 shows, resistance in ROI and SD is approximately equal for $L_r/3 \leq h_1 \leq L_r$ for FC but varies with higher values with an increase in desaturation. At $L_r \leq h_1 \leq 7L_r/6$, the percentage difference rises and subsequently drops all soil suction.

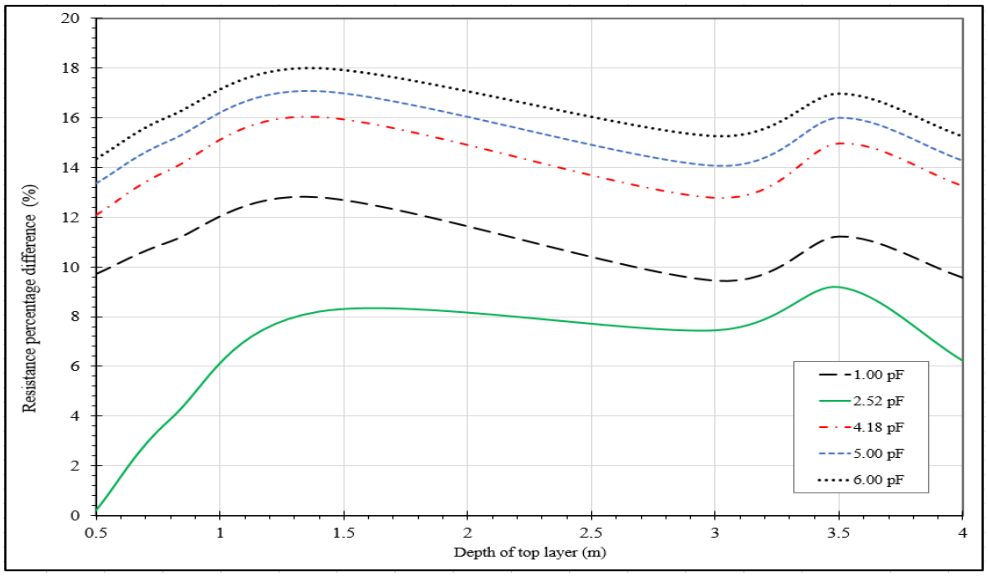


Figure 5.3: Percentage difference of volumetric water contents in entire subsoil domain and region of influence of the vertical earth rod and the corresponding earthing resistances for different depths of topsoil of a double-layer subsoil

Source: Author's conceptualisation.

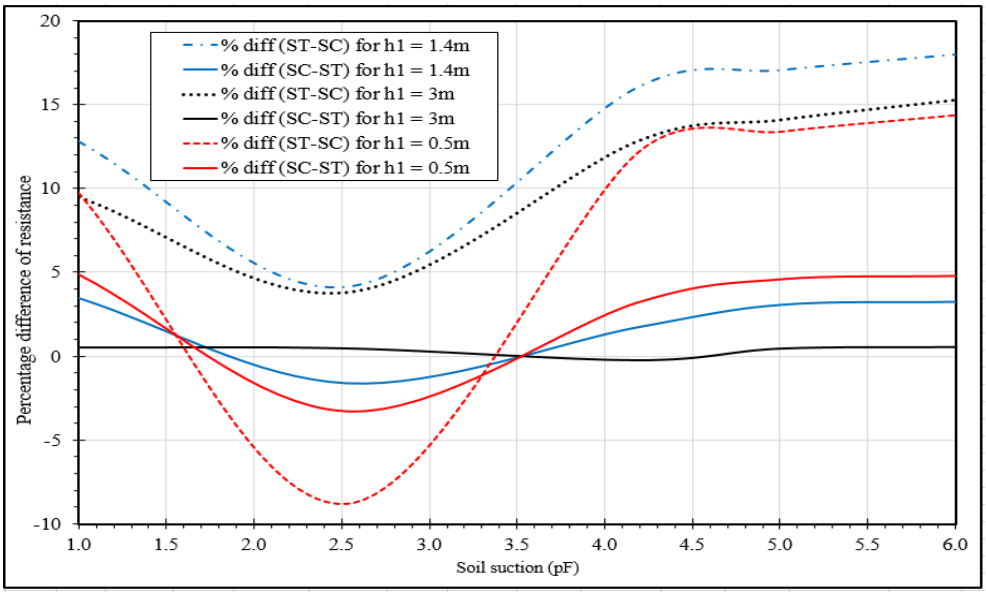


Figure 5.4: Percentage difference of volumetric water contents in entire subsoil domain and region of influence of the vertical earth rod and the corresponding earthing resistances for two different depths of topsoil of two double-layer subsoil

Source: Author's conceptualisation.

Figure 5.4 compares the variation of resistance percentage difference of a vertical rod in ROI and SD of two two-layer subsoils with three top layer depths (0.5, 1.4, and 3 m). Figure 5.4 shows the post-processing evaluations of vertical rods in two two-layer subsoils: sandy clay top-silty bottom (SC-ST) and silty top-sandy clay bottom (ST-SC) soils. The resistance of the vertical rod was evaluated concerning the rod in ROI and SD with different top-layer depths, h_1. As suction ψ varied, $k_c > 0$ for ST-SC and $k_c < 0$ for SC-ST for all h_1. The resistance

percentage difference between the resistance of the rod due to ROI and SD varied significantly for $k_c > 0$ with minimal variation for $k_c < 0$. For $k_c > 0$, the magnitude of variation reduced as h_1 increased unlike for $k_c < 0$ where the effect of h_1 does not produce a significant difference between the resistance due to ROI and SD.

From these discussions, it could be inferred that, unlike the single-layer subsoil model, the effects of h_1 and k_c of the two-layer subsoil model restrict the formulation of factors to correct resistance evaluated due to ROI to their actual value.

5.2 Formulation of Gradient Function of Water Content

The interaction of suction, capillarity, and gravity governs the water content gradient within the soil, providing valuable insights into soil behaviour. Under equilibrium conditions, this gradient develops along the subsoil column. Accurately determining water content at various depths is crucial for calculating the volumetric resistivity of the subsoil, which involves integrating the gradient over the soil depth. While this can be addressed analytically, a more rigorous approach involves inversion and regression analysis of multiple numerical solutions of Richards' equation at different pressure heads to determine $d\theta/dz$. This section outlines both methods.

5.2.1 Profile of Soil Water Under Suction

Water content at any depth of homogeneous soil can be evaluated from the numerical or simulation analysis flow equations (Richards' equation) and water retention models. Water content at depth z along the soil column corresponds to the equilibrated energy or suction applied to the soil. The application of pressure on the free surface of the wet soil column induces a water content gradient along the soil column. Under certain conditions, suction applied to the ground surface creates an actual or apparent depth, above which a variably saturated region of soil exists, below which a continuous body of water exists. The depth is called, depth of saturation or saturation depth z_s, because the water content of soil below it equals the saturated value, θ_s. This subsoil region above z_s, also known as the Vadose zone is bounded by maximum suction at $z = 0$, and minimum suction at $z = z_s$. In other words, a water content gradient exists along the depth of subsoil with maximum and minimum values at saturation depth and ground surface respectively.

The interaction of suction, capillarity and gravity controls the movement of the continuous mass of underground water and determines the degree of saturation of the subsoil. Suction

applied at the ground surface desaturates the soil so that the depth of saturation varies. As z_s vary, water content within the region of subsoil above it also changes. The size of the unsaturated region and its water content depends on the magnitude of suction applied at $z = 0$ and the water retention characteristics of the soil. The magnitude of z_s corresponds to the applied soil suction expressed in the pressure head (h_p). This means that the gradient function of water content $\theta_z(z)$ can be expressed in terms of z_s. If the SWRC or equation is known, the volumetric water content or degree of saturation corresponding to a suction value can be estimated. Alternatively, the effective volumetric water content can be determined from the volume integral of the gradient function of volumetric water content for the interval $0 \leq z \leq z_s$.

Assuming ground interflow (lateral movement of water) is negligible or constant, the gradient function of volumetric water content, $\partial\theta/\partial z$ is the rate of change of volumetric water content with depth. Due to relational complexity, the theoretical evaluation of $\partial\theta/\partial z$ is tedious. As expressed in Equation 5.1, $\partial\theta/\partial z$ is expressed as

$$\frac{\partial\theta}{\partial z} = \frac{\partial\theta}{\partial h_p} \times \frac{\partial h_p}{\partial z} \tag{5.2}$$

where $\partial\theta/\partial h_p$ is determined from partial derivatives of SWRC as expressed in Equation 5.2,

$$\frac{\partial\theta}{\partial h_p} = \frac{n^2\alpha_h\left(\alpha_h|h_p|\right)^{n-1}}{(1-n)\left(1+\left(\alpha_h|h_p|\right)^n\right)^{\frac{1-2n}{n}}}(\theta_s - \theta_r) \tag{5.2}$$

Suction applied at the ground surface distributes along the subsoil column, from the maximum at $z = 0$ to zero at $z = z_s$, $\partial h_p/\partial z$ is determined from the partial derivative of Richards' (fluid flow) equation; Equation 2.41, whose steady-state form is expressed in Equation 5.3.

$$\frac{\partial}{\partial z}\left[K(\theta)\left(\frac{\partial h_p}{\partial z} + 1\right)\right] = 0 \tag{5.3}$$

$\partial\theta/\partial z$ can be determined for a range of pressure heads, h_p: $h_{ps} \leq h_p \leq h_{pr}$. where h_{ps} and h_{pr} (which can be estimated from the SWRC) are saturation and residual pressure heads.

Empirical formulation from the post-numerical solution of fluid flow and water retention equations provides an alternative form of formulating the gradient function of water content.

Formulating a gradient function equation requires performing a numerical solution of Richards' equation and curve fitting the corresponding plot of water content against soil depth. The curve fitting requires the plot of water content, θ against soil depth, z. For each h_p, the coordinate pair (θ, z) for a range of regular or random depth, $0 \leq z \leq z_s$ is determined and plotted. To limit the infinite number of coordinate pairs (θ, z) within $0 \leq z \leq z_s$, the coordinates are taken at regular d. Given the depth $[0,\ z_s]$, the $2 + z_s/d_s$ data point pairs (θ, z) are plotted and curve fitted to formulate expression for gradient function, $\theta_z(z)$ in terms of subsoil depth z: $0 \leq z \leq z_s$ expressed in Equation 5.4.

$$\theta_z(z) = a_z \mathrm{e}^{zb_z} + c_z \tag{5.4}$$

Alternatively, as in Equation 5.5, $\theta_z(z)$ can also be expressed in terms of minimum water content θ_{min}, at or near $z = 0$ corresponding to the h_p.

$$\theta_z(z) = a_z(\mathrm{e}^{zb_z} - 1) + \theta_{min} \tag{5.5}$$

For every negative pressure applied to the group surface, the soil water pressure head represents the level or depth of the meniscus of the continuous water column within the soil measured from the soil top. For partially or fully unsaturated soil conditions, the topsoil surface retains the minimum water content along the depth of the soil volume. The regression models for the minimum water content at the topsoil θ_{min} at (z = 0) can be expressed as functions of the saturation depth (z_s). Without soil disturbance, the topsoil water content θ_{min} within 0 -10 cm soil depth can be measured easily with a moisture meter. The saturation depth z_s: $0 \leq z_s \leq 11$ corresponding to the measured θ_{min} for any homogeneous soil texture can be determined using Equation 5.6.

$$z_s \approx \frac{1}{b_z} \ln\left(\frac{a_z}{\theta_{min} - c_z}\right) \tag{5.6}$$

Each h_p generates a unique gradient function that can determine water content at any depth z: $0 \leq z \leq\ z_s$. The number of h_p between h_s and h_{pr} is infinite, which implies an infinite number of gradient functions. However, gradient functions for the critical suction at saturation h_s, air entry point h_a, field capacity h_{fc}, permanent wilting point h_{pwp}, and residual point h_r may be determined. Alternatively, a curve fitting the individual plots of similar coefficients of gradient functions, a_z, b_z, and c_z against their h_p, a general expression can be formed for the coefficients of 5.4 or 5.5 in terms of h_p. For example, each of a_z, b_z, and c_z, forms a coordinate

pair with its h_p as in $(a_z,\ h_p)$, $(b_z,\ h_p)$ and $(c_z,\ h_p)$. Similar pairs corresponding to the number of gradient functions are plotted and curve fitted to formulate regression models as h_p for $a_z, b_z,$ and c_z as in Equations 5.7 to 5.9.

$$a_z(h_p) = f(h_p) = A_a \ln\left(B_a + \frac{C_a}{h_p}\right) \tag{5.7}$$

$$b_z(h_p) = f(h_p) = A_b \ln\left(B_b + \frac{C_b}{h_p}\right) \tag{5.8}$$

$$c_z(h_p) = f(h_p) = A_c \ln\left(B_c + \frac{C_c}{h_p}\right) \tag{5.9}$$

For homogeneous subsoil, the magnitude of pressure head, $|h_p|$ is coincides with the depth of capillary rise in the subsoil column and approximated as saturation depth, z_s.

5.2.2 Predicting Volumetric Water Content in Variably Saturated Region of Influence of Rod in Single-Layer Subsoil

Volumetric water content is defined as the ratio of the volume of water in the soil volume to the volume of soil, expressed as a percentage. While the volume of subsoil or ROI is fixed, the volume of water within the subsoil or ROI can change with suction. External influences induce soil suctions that produce variation in the water content of the subsoil by the rise and fall of water in the subsoil column. High soil suction produces unsaturated conditions while low suction happens at saturated soil conditions.

Depending on soil suction, the water content in the ROI can be

i. Saturated (soil pores filled with water)
ii. Unsaturated (soil pores filled with air)
iii. Partially saturated (soil pores mixed with air and water)

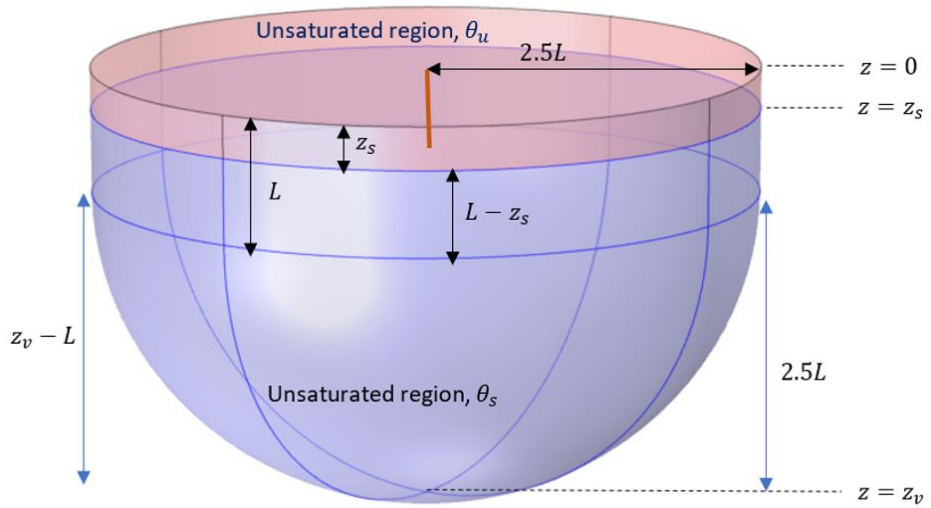


Figure 5.5: Region of influence of vertical earth rod showing saturated and unsaturated zones of the subsoil

Source: [105].

Whereas the volumetric water content of the saturated volume, θ_s is often known and unique to soils, determining the volumetric water content of the unsaturated volume, θ_u is not straightforward. It requires a numerical solution or the integral of the gradient of water content, $\theta_u(z)$ for the unsaturated volume. The formulation of the gradient function, $\theta_u(z)$ requires extensive numerical computation and curve fitting. The integration of $\theta_u(z)$ over the depth of the unsaturated volume yields the required volumetric water content.

Figure 5.5 shows a partially saturated ROI. If z_v represents the depth of ROI in the soil domain measured from the topsoil, then the unsaturated soil is defined between the soil top $z = 0$ and $z = z_s$, while the saturated portion is bounded between $z = z_s \; and \; z = z_v$.

The resistivity of soil within the ROI is determined by its average water content θ_a. That is, the resistivity of variably saturated ROI ρ_{roi} is expressed as $\rho_{roi}(\theta_a)$. θ_a is the ratio of the volume integral of the gradient function to the volume of subsoil. Mathematically, θ_a is expressed in Equation 5.10 as:

$$\theta_a = \frac{\text{volume integral of water content ROI } (\text{m}^3)}{\text{volume of ROI } (\text{m}^3)} = \frac{1}{V_{roi}} \int \theta_{roi} \, dz \tag{5.10}$$

The volume integral of water content in any homogeneous isotropic subsoil is the sum of the volume integrals of saturated and unsaturated portions of ROI. Equation 5.11 is the expression of the volume integral water content of the ROI of the rod.

$$\int \theta_{roi}\, dz = \left(\frac{V_u}{d_u}\int_0^{d_u} \theta_u(z)\, dz\right) + \left(\frac{V_{sat}}{z_s - d_u}\int_{d_u}^{z_s} \theta_s\, dz\right) \tag{5.11}$$

where d_u is the depth of the unsaturated soil portion, $\theta_u(z)$ is the gradient function of water content in the unsaturated portion of soil volume, V_u, and θ_s is the water content of the saturated volume, V_{sat} of the soil. The sum of V_u and V_{sat} gives the volume of ROI, $V_{roi} = \frac{8}{3}\pi(2.5L)^2 L$.

As the soil becomes increasingly unsaturated, the position of z_s progresses downward and the $|z_s|$ magnitude of saturation depth increases. Relative to the fixed depth of ROI z_v, the position of the depth of saturation z_s along the depth of the ROI determines the degree of saturation of the ROI as saturated, partially saturated, or unsaturated. In other words, the position of the saturation depth determines the presence and volume of the unsaturated portion of the ROI.

Given that the ground surface is the line of reference with $z = 0$, depth measurements are taken in the negative sense. For a partially saturated soil column, the saturation depth marks the boundary between the saturated and unsaturated regions of the soil column. Saturation depth, z_s varies with suction and is a vital reference line for describing the variable volumetric water content that affects the resistivity of the ROI. Unlike the z_s, the depth (volume) of the ROI, $3.5L_r$ and depth (length) of the rod, L, is fixed. Consequently, the positions of the saturation depth relative to the fixed parameters can be described concisely as follows:

i. At a depth above or equal to rod length, $0 \leq |z_s| \leq L_r$
ii. At a depth greater than rod length but less than the depth of ROI, $L < |z_s| < 3.5L_r$
iii. At a depth equal to or greater than the depth of ROI, $|z_s| \geq 3.5L_r$

Expanding these positions yields five positions for the depth of saturation, each describing a unique composition of the variable state of saturation of the ROI. The positions are as follows.

1. $|z_s| = 0$

This position describes a state of full saturation of the ROI. In this condition, the water content of homogeneous ROI is the saturated volumetric water content of the soil, θ_s. It is a unique quantity of soil that is easily determined or given.

2. For $0 < |z_s| \leq L_r$

At this position, the ROI consists of an upper unsaturated cylindrical volume bounded by $0 \leq z \leq z_s$ and a bottom saturated portion bounded by $z_s \leq z \leq L_r$. The bottom volume consists

of a thin cylindrical volume, of height $L_r - z_s$, above a hemispherical volume of radius $2.5L_r$. Under this condition, the average volumetric water content is expressed in Equation 5.12 and reduced to compact form in Equation 5.13.

$$\int \theta_{roi}\, dz = (2.5L_r)^2\pi \int_0^{z_s} \theta_u\, dz + (2.5L_r)^2\pi \int_{z_s}^{L_r} \theta_s\, dz + \frac{2(2.5L_r)^3\pi}{3}\left(\frac{1}{3.5L_r - L_r}\right)\int_{L_r}^{3.5L_r} \theta_s\, dz \qquad (5.12)$$

If $\theta_u = a_0 e^{(a_1 z_s)} + a_2$, then

$$\int \theta_{roi}\, dz = (2.5L_r)^2\pi \left\{3\left(\frac{a_0}{a_1}e^{(a_1 z_s)} + a_2 z_s\right) + \frac{(8L_r - 3z_s)}{3}\theta_s\right\} \qquad (5.13)$$

For $0 < |z_s| \leq L_r$, θ_{ave} of ROI is expressed in equation 5.14 as

$$\theta_{ave} = \frac{1}{8L_r}\left\{3\left(\frac{a_0}{a_1}e^{(a_1 z_s)} + a_2 z_s\right) + (8L_r - 3z_s)\theta_s\right\} \qquad (5.14)$$

3. For $L_r < z_s < 3.5L_r$

At this position, z_s divides the ROI into an unsaturated top of two regular volumes and a saturated volume at the bottom of the ROI. The top part of the unsaturated region is a cylindrical volume bounded by $0 \leq z \leq L_r$. The bottom part of the unsaturated region is a hemispherical segment bounded by $L_r \leq z \leq z_s$. Finally, the saturated bottom spherical segment or cap is bounded by $z_s \leq z \leq 3.5L_r$. The volume of the spherical cap, V_{sc} is expressed in Equation 5.18 as

$$V_{sc} = \pi(h_{sc})^2(3r - h_{sc})/3 \qquad (5.18)$$

where the height of the spherical cap, is $h_{sc} = 3.5L_r - z_s$ and the radius of the sphere the cap is part of, $r = 2.5L_r$. The volume of the hemispherical segment is derived by subtracting the volume of the spherical segment from the volume of the hemisphere, V_{hs} as in Equation 5.19.

$$V_{hs} - V_{sc} = \frac{\pi}{3}\left(2(2.5L_r)^3 - (3.5L_r - z_s)^2(4L_r + z_s)\right) \qquad (5.19)$$

Then, the ROI volume integral of water content is the summation expressed in Equation 5.20 as:

$$\int \theta_{roi}\, dz = (2.5L_r)^2 \pi L_r \left(\frac{1}{L_r}\right) \int_0^{L_r} \theta_u\, dz + \left(\frac{\pi\left(2(2.5L_r)^3 - (3.5L_r - z_s)^2(4L_r + z_s)\right)}{3}\right)\left(\frac{1}{z_s - L_r}\right) \int_{L_r}^{z_s} \theta_u\, dz + \left(\frac{\pi(3.5L_r - z_s)^2(4L_r + z_s)}{3}\right)\left(\frac{1}{3.5L_r - z_s}\right) \int_{z_s}^{3.5L_r} \theta_s\, dz \quad (5.20)$$

Consequently, θ_{ave} for ROI for $L_r \leq z_s < 3.5L_r$ is given by Equation 5.21, as

$$\theta_{ave} = \frac{3}{8L_r} \int_0^{L_r} \theta_u\, dz + \left(\frac{2(2.5L_r)^3 - (3.5L_r - z_s)^2(4L_r + z_s)}{8(2.5L)^2(z_s - L)L}\right) \int_{L_r}^{z_s} \theta_u\, dz + \left(\frac{(3.5L_r - z_s)^2(4L_r + z_s)}{8(2.5L_r)^2 L_r}\right) \theta_s \quad (5.21)$$

4. For $z_s \geq 3.5L_r$

With $z_s \geq 3.5L_r$, the entire ROI is unsaturated. The corresponding volume integral water content is expressed in Equation 5.22.

$$\int \theta_{roi}\, dz = \frac{8}{3} \pi (2.5L_r)^2 L_r \left(\frac{1}{3.5L_r}\right) \int_0^{3.5L_r} \theta_u\, dz \quad (5.22)$$

Therefore, the average water content in the ROI is Equation 5.23, which is simplified in Equation 5.24.

$$\theta_{ave} = \frac{\frac{8}{3} \pi (2.5L_r)^2 L_r \left(\frac{1}{3.5L_r}\right) \int_0^{3.5L_r} \theta_u\, dz}{\frac{8}{3} \pi (2.5L_r)^2 L_r} \quad (5.23)$$

$$\theta_{ave} = \frac{1}{3.5L_r} \int_0^{3.5L_r} \theta_u\, dz \quad (5.24)$$

The values of θ_{ave} can be used in place θ in the resistivity function, $\rho(\theta)$ to determine the resistance of the driven-rod earth electrode, $R(\theta)$ in terms of soil water content.

5.2.3 Predicting Volumetric Water Content in Variably Saturated Region of Influence of Rod in Two-Layer Subsoil

The depth of saturation is indicative of the degree of saturation: saturated, partially saturated or unsaturated. For a partially saturated subsoil column, the top portion is likely to be unsaturated, while the bottom region is likely to be saturated with the continuous body of water. Unlike homogeneous ROI, the effective volumetric water content of ROI with multiple sublayers is individually determined for each layer of the ROI. For example, in a two-layer

subsoil, two average volumetric water content (one for each layer) are required to determine the resistivity of each layer.

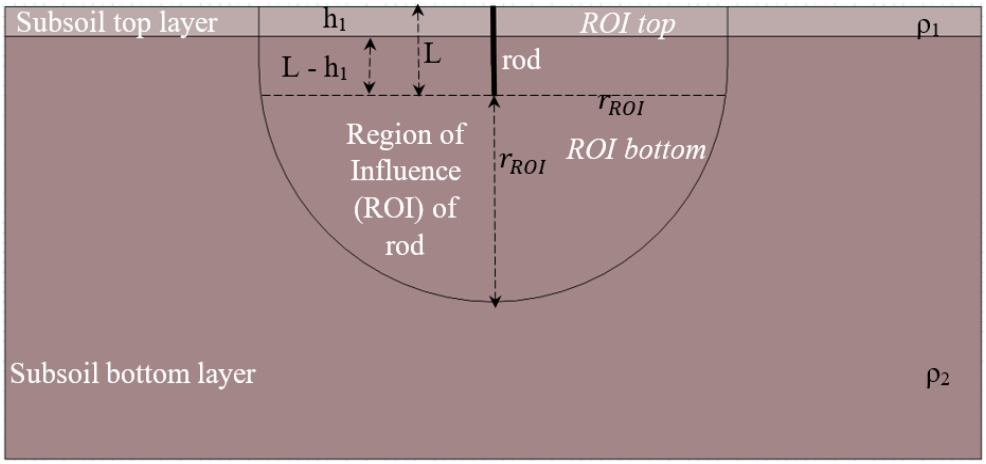


Figure 5.6: 2D cross-sectional view of the region of influence of vertical earth rod in two-layer subsoil model

Source: Author's conceptualisation.

Depending on the saturation depth, the saturated and unsaturated regions of the two-layer ROI can be composed of two layers. Under such conditions, the saturation depth partitions the ith layer (i is the index of the sublayer) into saturated and unsaturated regions. Effective volumetric water content, θ_{ai} of such a layer is the ratio of volume integral of volumetric water content, $\int \theta_i(z)\, dz$ to volume, V_i of the ith layer. θ_{ai} is mathematically expressed in Equation 5.25 as:

$$\theta_{ai} = \frac{1}{V_i} \int \theta_i(z)\, dz \tag{5.25}$$

where V_i is the sum of unsaturated, V_{ui} and saturated, V_{si} volume of the partially saturated ith layer of ROI and $\theta_i(z)$ is the gradient function of the volumetric water content of the ith layer of ROI.

Given that h_1 and z_s are the depth of the top layer and saturation depth respectively, and $\theta_i(z)$ is the gradient function of the volumetric water content of the ith layer, then the volumetric integral of water content is determined as follows.

If $|z_s| \ll |h_1|$, $V_{u2} = 0$, then for $i = 1$, $\int \theta_i(z)\, dz$ is expressed in Equation 5.26 as

$$\int \theta_1\,(z) dz = \left(\frac{V_{u1}}{z_s} \int_0^{z_s} \theta_{u1}(z)\, dz\right) + \left(\frac{V_{s1}}{h_1 - z_s} \int_{z_s}^{h_1} \theta_{s1}\, dz\right) \tag{5.26}$$

If $|z_s| \gg |h_1|$, $V_{s1} = 0$, and then $\int \theta_i(z)\, dz$ for $i = 1{,}2$ is expressed in (5.27) and (5.28) as

$$\int \theta_1(z)dz = \left(\frac{V_{u1}}{h_1}\int_0^{h_1}\theta_{u1}(z)\,dz\right) \tag{5.27}$$

$$\int \theta_2(z)dz = \left(\frac{V_{u2}}{z_s - h_1}\int_{z_s}^{h_1}\theta_{u2}(z)\,dz\right) + \left(\frac{V_{s2}}{3.5L - z_s}\int_{z_s}^{3.5L}\theta_{s1}\,dz\right) \tag{5.28}$$

Saturation depth may be described in terms of three fixed depths: depth of top layer (h_1), depth of earth rod (L), and depth of ROI ($3.5L$). Using these fixed reference depths, the description of the saturation depth may be any of the following

i. Equal to the ground surface, $|z_s| = 0$
ii. Within the top layer, $0 < |z_s| < h_1$
iii. At a depth equal to the depth of the top layer, $|z_s| = h_1$
iv. Below the top layer depth but less than the depth of the rod, $D1 < |z_s| < L_r$
v. Equal to the depth of the buried rod end, $|z_s| = L_r$
vi. Below the depth of the buried rod end but less than the depth of the region of influence, $L_r < |z_s| < 3.5L_r$
vii. Equal or greater to the depth of region of influence, $|z_s| \geq 3.5L_r$

The equations for the effective volumetric water content are described as follows.

1. $0 \leq |z_s| \leq h_1$

At $z_s = 0$, the entire two-layer ROI is saturated. This means that the effective volumetric water content of the two layers is their saturated volumetric water contents, θ_{s1} and θ_{s2}. For $0 < \mathrm{z} \leq \mathrm{z_s}$, average water content is required.

Figure 5.4 illustrates the position of $\mathrm{z_s}$ relative to other depths. At this position, the bottom layer is saturated, but the top layer is partitioned into unsaturated and saturated regions. This implies that the ROI is divided into three volumes. In descending order, the topmost is an unsaturated region within the top layer bounded by $0 \leq \mathrm{z} \leq \mathrm{z_s}$.

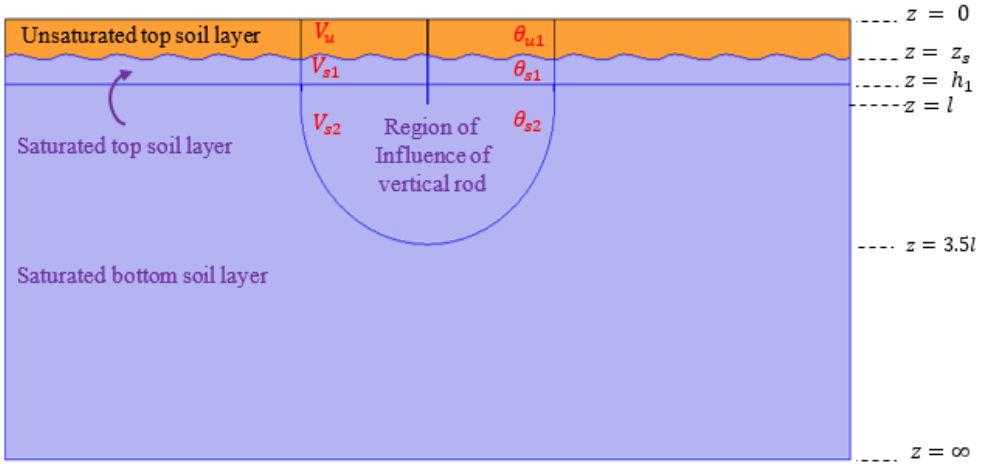


Figure 5.7: 2D cross-sectional view the region of influence of vertical earth rod in a two-layer showing the saturation depth

Source: Author's conceptualisation. Depth ($0 \leq z_s \leq h_1$), where l is the length of the earth rod.

The cylindrical volume and gradient function of volumetric water content are $V_{u1} = \pi(2.5L_r)^2 z_s$ and θ_{u1}/z_s respectively. Below it is a saturated segment bounded by $z_s \leq z \leq h_1$ within the top layer. θ_{s1} denotes the volumetric water content, while its volume $V_{s1} = \pi(2.5L_r)^2(h_1 - z_s)$. The third volume is a saturated segment in the bottom layer segment of the ROI bounded by $h_1 \leq z \leq 3.5L_r$ with θ_{s2} as volumetric water content. This bottom segment consists of a cylindrical top and a hemispherical bottom with combined volume, $V_{s2} = \frac{\pi}{3}(2.5L_r)^2(8L_r - 3h_1)$.

By substituting the corresponding variable of Equation 5.26, the volume of the integral water content of the top layer of ROI for $|z_s| < |h_1|$ is expressed in Equation 5.29 as.

$$\int \theta_1(z)dz = \left(\frac{\pi(2.5L_r)^2 z_s}{z_s}\int_0^{z_s} \theta_{u1}(z)\,dz\right) + \left(\frac{\pi(2.5L_r)^2(h_1 - z_s)}{h_1 - z_s}\int_{z_s}^{h_1} \theta_{s1}\,dz\right) \tag{5.29}$$

Upon simplification and substituting in Equation 5.25, the effective volumetric water content of the partially saturated top layer (of $\pi(2.5L)^2 h_1$ volume) is expressed in Equation 5.30 as:

$$\theta_{a1} = \frac{z_s\theta_{u1}(z) + (h_1 - z_s)\theta_{s1}}{h_1} \tag{5.30}$$

Equation 5.30 is also suitable for when $|z_s| = h_1$.

2. $h_1 < z_s \leq 3.5L_r$ and $z_s > 3.5L_r$

Figure 5.8 shows the position of saturation depth z_s which partitions the bottom layer within the ROI into an unsaturated top region and a saturated bottom region. The unsaturated and saturated regions of the bottom layer are bounded within $h_1 < z \leq z_s$ and $z_s < z \leq 3.5L_r$ respectively.

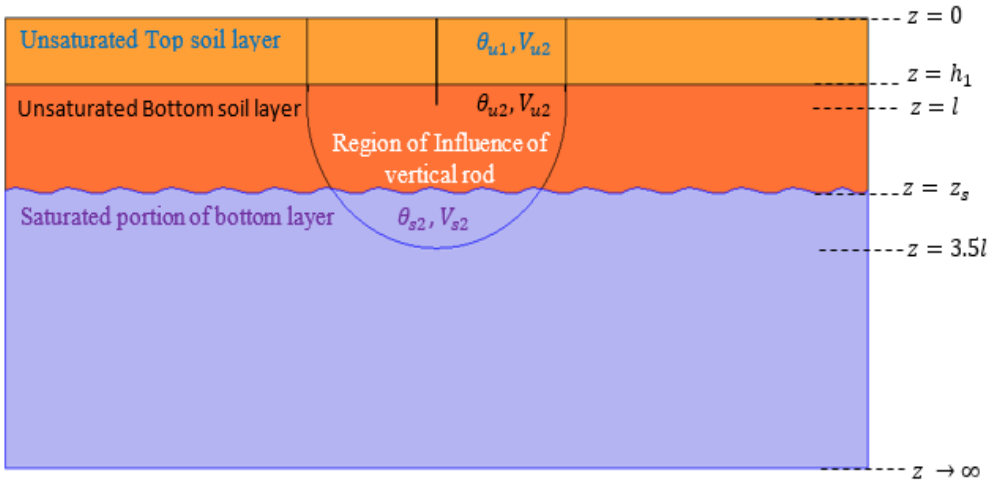


Figure 5.8: 2D cross-sectional view the region of influence of vertical earth rod in a two-layer showing the saturation depth

Source: Author's conceptualisation. Depth ($h_1 \leq z_s \leq 3.5L_r$), with l as the length of the earth rod.

Unlike the cylindrical volume of the unsaturated layer of the topsoil $\pi(2.5L_r)^2 h_1$, the volume of the unsaturated region in the bottom layer of ROI, V_{u2} depends on z_s and may be irregular. If V_{hem} and V_{seg} represent the volumes of the variably saturated hemispherical bottom layer and the saturated spherical segment or cap of height h_{seg}, then the volume of the unsaturated bottom layer with the ROI equals $V_{hem} - V_{seg}$. With $V_{hem} = \left(\frac{125}{12}\right)\pi(L_r)^3$, $h_{seg} = 3.5L_r - z_s$, and $V_{seg} = \left(\frac{1}{3}\right)\pi(4L_r + z_s)(3.5L_r - z_s)^2$, then V_{u2} is expressed in Equation 5.31 as:

$$V_{u2} = \frac{\pi}{12}\{-71(L_r)^3 + 63(L_r)^2 z_s + 12L_r(z_s)^2 - 4(z_s)^2\} \tag{5.31}$$

Given that θ_{u1}/h_1 and $\theta_{u2}/(z_s - h_1)$ are the gradient functions of the top and bottom layer soils, then by substituting the corresponding variables into Equation 5.26, the volume integral water content of the top $\int \theta_1(z)dz$ is expressed in Equation 5.32 as;

$$\int \theta_1(z)dz = \left(\frac{\pi(2.5L_r)^2 h_1}{h_1}\int_0^{h_1} \theta_{u1}(z)\,dz\right) \tag{5.32}$$

Upon simplifying,

$$\theta_{a1} = \int_0^{h_1} \theta_{u1}(z)\, dz \tag{5.33}$$

Similarly, the average volumetric water content of the ROI bottom layer is formulated as follows: ROI bottom layer volume integral of water content $\int \theta_1\,(z)dz$ is,

$$\int \theta_2\,(z)dz = \left(\frac{V_{u2}}{z_s - h_1}\int_{h_1}^{z_s} \theta_{u2}(z)\, dz\right) + \left(\frac{V_{seg}}{3.5L_r - z_s}\int_{z_s}^{3.5L_r} \theta_{s1}\, dz\right) \tag{5.34}$$

Upon substituting, $\int \theta_2\,(z)dz$ and simplifying gives

$$\int \theta_2\,(z)dz = \left[\frac{\pi}{12}(-71(L_r)^3 + 63(L_r)^2 z_s + 12L_r(z_s)^2 - 4(z_s)^2)\right]\theta_{u2}(z) + \left[\left(\frac{\pi}{3}\right)(4L_r + z_s)(3.5L_r - z_s)^2\theta_{s1}\right] \tag{5.35}$$

Upon simplification and substituting in Equation 5.25, the effective volumetric water content of the partially saturated top layer (of $\pi(2.5L_r)^2 h_1$ volume) is expressed in Equation 5.36 as.

$$\theta_{a2} = \frac{12}{125\pi(L_r)^3}\left\{\begin{array}{c}\left[\frac{\pi}{12}(-71(L_r)^3 + 63(L_r)^2 z_s + 12L_r(z_s)^2 - 4(z_s)^2)\right]\theta_{u2}(z) + \\ \left[\left(\frac{\pi}{3}\right)(4L_r + z_s)(3.5L_r - z_s)^2\theta_{s1}\right]\end{array}\right\} \tag{5.36}$$

5.3 Application in Single-Layer Subsoil Model

The formulations described above are applied to estimate the average water content, and soil resistivity of ROI of a vertical rod in single-layer silty soil. Noting the minimum water content at the ground surface, water content from the ground surface to an arbitrary depth (10.5 m) at regular intervals is determined for a range of soil suction, spanning saturated and unsaturated conditions. For each suction, gradient functions of water content in the form of Equations 5.4 or 5.5 are formulated by regression analysis. Subsections 5.3.1 to 5.3.3 illustrate the applications of Sections 5.1 and 5.2. Resistance evaluated from the analytical formulation is compared for validation with post-simulation evaluations for the infinite subsoil model.

5.3.1 Estimating Gradient Function

From simulation analysis, the values of the coefficients a, b and c, and the minimum water content, θ_{min} corresponding to a range of soil suctions for homogeneous silty soil are given Table A16. For instance, if $\theta_{min} = 0.2350$, then by inspecting Table A16, this value of θ_{min} falls between 0.24401 and 0.22852 which corresponds to the soil suction depth range of 4 to

4.99 m. Using θ_{min} and the corresponding values of $a = 0.196125, b = 0.280965, c = 0.180260$ corresponding to the range of saturation depth from Table A16, $z_s \approx 4.54$ m.

The depth-wise regression models $\theta(z)$ for determining the water content at any soil depth (z) between the topsoil $(z = 0)$ and the saturation depth $(z = z_s)$, is expressed in the form of $ae^{bz} + c$ or $a(e^{bz} - 1) + \theta_{min}$ in Equation 5.37.

$$\theta(z) = 0.014736(e^{0.560604\,z} - 1) + 0.22839 \tag{5.37}$$

The corresponding coefficients and terms of this equation (for some saturation depths) are given in Table A17. For instance, if $h_p = 5$ m. then $\theta(z) = 0.014736e^{0.560604\,z} + 0.21777: 0 \leq z \leq 5$ m. Alternatively, $\theta(z)$ can be written in terms of θ_{min} as $\theta(z) = 0.014736(e^{0.560604\,z} - 1) + 0.22839$.

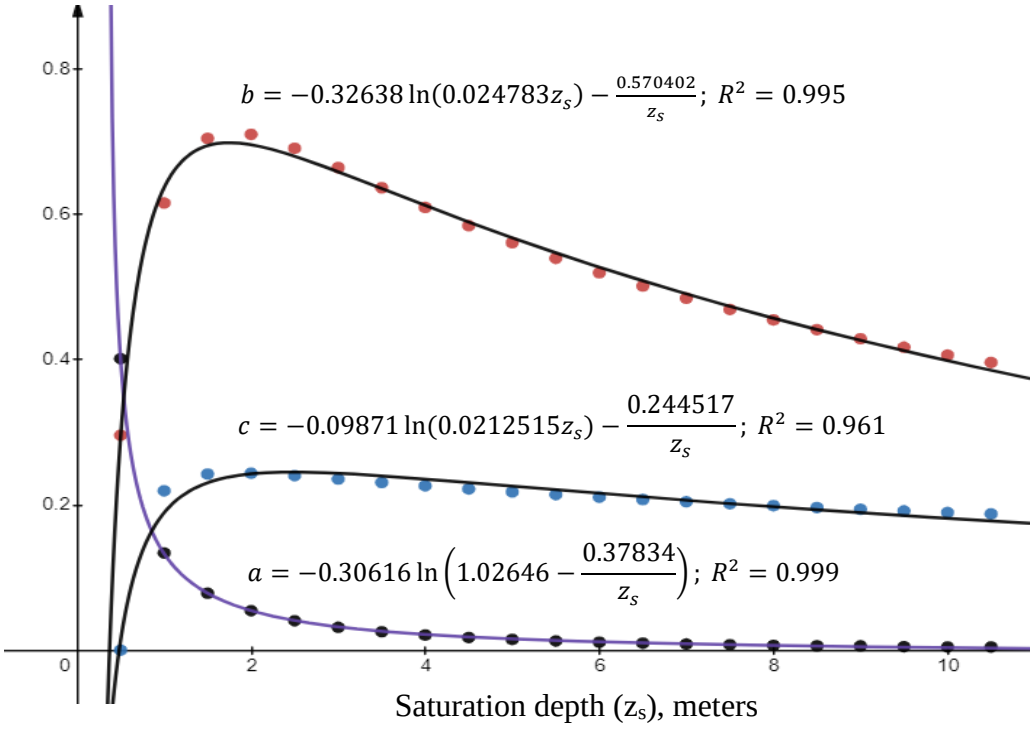


Figure 5.9: Regression plot determining the coefficients of the water content gradient function $\theta s(z)$ at soil depth (z) due to pressure head at $z = z_s$.

Source: Author's conceptualisation.

If the saturation depth and water content of the topsoil are known, then the coefficients a, b and c of the expression $\theta(z) = ae^{bz} + c$ or $\theta(z) = a(e^{bz} - 1) + \theta_{min}$ that approximates the water content in homogeneous silty soil for a saturation depth between $0.5 \leq z_s \leq 10.5$ m are found

by fitting curves to the respective plot of a, b and c against z_s from Table A17. Then a, b and c are expressed in Equations 5.38 to 5.40.

$$\mathrm{a} = -0.30616 \ln\left(1.02646 - \frac{0.37834}{z_s}\right) \tag{5.38}$$

$$\mathrm{b} = -0.32638 \ln(0.024783 z_s) - \frac{0.570402}{z_s} \tag{5.39}$$

$$\mathrm{c} = -0.09871 \ln(0.0212515 z_s) - \frac{0.244517}{z_s} \tag{5.40}$$

Alternatively, if rather than the ground surface (where $z = 0$), water content at depth $z = 0.1$ m, $\theta_{(z=0.1\,m)}$ is known, then the corresponding saturation depth $z_s: 0.1 \leq z_s \leq 11$ can be determined with $\theta_{(z=0.1\,m)} = ae^{-bz_s} + c$ using Equation 5.41.

$$z_s = \frac{1}{b} \ln\left(\frac{a}{\theta_{(z=0.1\,m)} - c}\right) \tag{5.41}$$

The values of the coefficients a, b and c for the gradient function have been evaluated and shown in Table A18. Consequently, water content $\theta(z)$ at any depth $z: 0.1 \leq z \leq z_s$ can be expressed in the form of $ae^{bz} + c$ or as $a(e^{bz} - 1) + \theta_{(z=0.1)}$. Table A19 contains the coefficients for the regression model $\theta(z)$ for some pressure heads or saturation depths with $\theta_{(z=0.1)}$ known.

5.3.2 Prediction of Volumetric Water Content Within Region of Influence of Vertical Earth Rod in Single-Layer Subsoil

If the water content measured at a depth of 0.1 m of a uniform silty soil is $0.2314\ m^3/m^3$, the average water content in the region of influence defined by a vertical rod of length 3 m can be found as follows.

1. From the information provided, the length of the rod $L_r = 3$ m and the water content measured at soil depth $z = 0.1$ m, $\theta_{(z=o.1m)} = 0.2314$.

2. From Table A20, the value of $\theta_{(z=o.1m)}$ is within the water content range of 0.24584 to 0.22990, which corresponds to the range of saturation depth of 4 to 4.99 m with coefficients $a = 0.202861, \mathrm{b} = 0.286681$ and $c = 0.181388$. The approximate saturation depth can be found using Equation 5.41, in which case $z_s \approx 4.88$ m

3. The saturation depth at 4.88 m divides the region of influence into an unsaturated volume within $0 \leq z < 4.88$ m and a saturated volume $of\ 4.88 \leq z < 10.5$ m. The coefficients of the variables of $ae^{bz} + c$, that describes water content $\theta(z)$ within the unsaturated volume is at $z_s = 5$ m in Table A19. That is, $\theta(z) = 0.014355e^{0.565472\,z} + 0.218589$ or in terms of $\theta_{(z=0.1m)}$ as Equation 5.42.

$$\theta(z) = 0.014355(e^{0.565472\,z} - 1) + 0.2314 \tag{5.42}$$

4. For the region of influence, the saturation depth lies within $L_r \leq z_s < 3.5L$. At this depth, z_s divides the region of influence into three portions. First is an unsaturated cylindrical top portion between $0 \leq z \leq 3$ m. The second portion is also an unsaturated volume positioned at $0\ 3 \leq z \leq 4.88$ m and finally a saturated bottom spherical cap within $4.88 \leq z \leq 10.5$ m. The average water content within the region of influence of the vertical earth electrode is evaluated using Equation 5.28, where $L_r = 3$ m, $z_s = 4.54$ m, $\theta_u(z) = 0.014736(e^{0.560604\,z} - 1) + 0.2350$ and $\theta_s = 0.46$, then $\theta_{ave} = 0.36017$.

Therefore, knowing θ_{min} the water content at the surface or $\theta_{(\mathrm{z=0.1m})}$ the water content at 10 cm depth (below the surface) of uniform soil, the saturation depth z_s and the average water content within the region of influence θ_{ave} can be determined from the deductions in the sections above. Table A20 compares the average water content for the region of influence computed analytically using $\theta_u(z) = a(e^{b\,z} - 1) + \theta_{(z=0.1m)}$ and evaluated by the simulator.

Chapter 6 - Performance of Earthing Systems in Different Soils and Climates

6.0 Introduction

Previous discussions have been focused on the arbitral variation of soil suction and its influence on the resistance and performance of earthing systems in single- and double-layered subsoils. The resistance and performance variations were not associated with the seasonal changes of any climatic zone. Using vertical rods in single- and double-layered subsoils, this chapter is devoted to modelling and analysis of seasonal variability of earthing system resistance and performance in different climatic zones.

6.1 Spatial and Temporal Changes of Subsoil Suction

Under field conditions, climate change induces seasonal soil moisture fluxes through infiltration and evapotranspiration [24]. Infiltration and evapotranspiration are the two mechanisms of water flux exchanges between the atmosphere and the subsoil. While the former wets the subsoil, the latter dries it. These fluxes develop a suction profile with the largest value at the topsoil air - soil interface decreasing towards a zero value at the water table through a depth of equilibrium suction. As seasons change, suction at any soil depth changes. A region of significant seasonal suction changes called the active zone depth or penetration depth, z_{es} exists within the subsoil. At this depth, a constant suction U_e is established. The active zone depth is bounded by the ground surface and the depth of equilibrium suction. The magnitude and depth of seasonal suction change will depend on the climatic cycle, vegetation cover, topography, drainage, profile, and type of soil of the location [21], [70], [106]. For predominantly wet climates, the penetration depth is negligible but significant in places with distinctive and sufficiently spaced wet and dry climates [70].

Depending on the frequency of the dry-wet cycle, a climate–appropriate surface suction value or function will vary from the topsoil to the depth of equilibrium or constant suction. This variation can affect the resistivity of the ROI and produce significant changes to the resistance of the buried earth electrode.

If the vegetation cover, drainage, and climate of an earthing site induce periodic changes in suction as a function of time, then by solving the diffusion equation under certain boundary conditions, the suction at any depth, z of the subsoil column can be determined at any time, t [65]. Peter Mitchell formulated a periodic function of suction using the one-dimensional diffusion equation on the assumption that the surface suction changes sinusoidal [70]. The

resulting formula is expressed in terms of depth z, time t and climatic frequency n_f, and diffusion coefficient α as in Equation 6.1.

$$U(z,t) = U_e + U_a \exp\left(-\sqrt{n_f \frac{\pi}{\alpha}} z\right) \cos\left\{2n_f \pi t - \left(\sqrt{n_f \frac{\pi}{\alpha}} z\right)\right\} \quad (6.1)$$

where n_f is the seasonal frequency (cycle/year) representing the number of cycles of seasons in a year, α is diffusion coefficient, [L^2/T], t is time [T], U_e equilibrium suction (pF), and U_a amplitude of surface suction (pF). Therefore, at the ground surface $(z = 0)$, surface suction reduces to the form in Equation 6.2.

$$U(0,t) = U_e + U_a \cos 2n_f \pi t \quad (6.2)$$

This implies that suction at the ground surface (z = 0) leads the suction at depth z by a time of $\sqrt{z^2/4\pi\alpha n_f}$ and that the amplitude of soil suction at any depth z decreases exponentially.

The influence of surface suction on the subsoil suction profile and the existence of the constant suction at the depth of equilibrium suction makes it suitable for describing the impact of climate on the soil [107]. Therefore, the subsoil water content due to surface suction changes can be estimated using the suction–water content relationship of the subsoil.

6.1.1 Estimating Diffusion Coefficient, α

The diffusion coefficient plays a vital role in modelling and describing the transport of constituent masses (gas, water, or solute) and heat due to the concentration gradient in porous media. It is highly influenced by the structure, texture, porosity, compaction, and water content of the porous medium as well as environmental factors. The diffusion coefficient is a site–soil parameter influenced by the water retention characteristics and mineralogy of the soil profile and used for estimating the periodic suction changes of earthing sites [106]. Generally, the diffusion coefficient of an earthing site can be determined from field measurements if the values of suctions at depths $z = 0$ and $z > 0$ are known. It can be estimated using parameters like the suction compression index (SCI), the inverse of the slope of the water characteristic curve, $(d\psi/d\theta)$ or Thornthwaite moisture index (TMI), which indicates the response of the subsoil to suction changes [106]. Alternatively, it can be determined using the rate of change of suction with time on the boundary of a specimen; where the soil sample at initial suction ψ_0 is made to gain or lose moisture from one end under an environment of suction ψ_1. The procedural details are available in [70].

6.1.2 Estimating Climate Frequency, n_f

If an earthing site experiences multiple wet–dry cycles over a period of $2p$ months, then the climate frequency n_f is the inverse of the period, that is $(2p)^{-1}$ in the unit of cycle per year [70], [106]. For instance, if one dry–wet cycle is completed within 8, 9.6, 12, 18, 24, 32, or 36 months, then n_f is 1.49, 1.25, 1, 0.67, 0.5, 0.37, and 0.33 cycles per year respectively. The values of n_f are equivalent to the inverse of these periods in years, i.e. 0.67, 0.8, 1.0, 1.5, 2.0, 2.26, and 3 yr. n_f is a site soil-climate dependent parameter whose value varies annually between 0.5 and 1.5 cycles per year [106]. Its value indicates the magnitude of suction change and depth of the active zone. Places where $1.25 \leq \mathrm{n}_f \leq 1.50$ are classified as unstable, with very shallow active zones and marginal surface suction changes. Sites with $\mathrm{n}_f \leq 0.5$ have deeper active zones with very significant surface suction changes as it takes at least two years for a complete cycle of dry–wet climate. The wet and dry season may have unequal spread as it may be predominantly dry or wet.

6.2 Modelling Climate-Based Variation of Soil Suction

The Fourier series expansion of the sinusoidal function of suction proposed by Mitchell for the spatial and temporal variation of suction at any depth and time, $U(z,t)$, that is, Equation 6.1 and ground surface suction is Equation 6.2 can be expressed as a summation of the partial wave functions. These are expressed in Equations 6.3 and 6.4 respectively.

$$U(z,t) = \frac{1}{2}U_0 + U_1 \exp\left(-z\sqrt{n_f \frac{\pi}{\alpha}}\right)\cos\left\{2\pi\mathrm{t}(n_f) - z\sqrt{n_f \frac{\pi}{\alpha}}\right\} + U_2 \exp\left(-z\sqrt{(2n_f)\frac{\pi}{\alpha}}\right)\cos\left\{2\pi\mathrm{t}(2n_f) - z\sqrt{(2n_f)\frac{\pi}{\alpha}}\right\} + \cdots \quad (6.3)$$

$$U(0,t) = \frac{1}{2}U_0 + U_1 \cos 2\pi\,(n_f)t + U_2 \cos 2\pi\,(2n_f)t + U_3 \cos 2\pi\,(3n_f)t \cdots \quad (6.4)$$

where $U_0, U_2, U_2, \cdots$ are Fourier coefficients which are derived from Equation 6.5.

$$U_{m_c} = \frac{2}{P}\int_0^P U(0,t)cos\frac{m_c}{P}\pi t\, dt \qquad m_c = 0,\ 1,\ 2,\ 3,\ 4,\ \ldots \quad (6.5)$$

6.2.1. Depth of Equilibrium Suction

At the depth of equilibrium, suction z_{es}, suction change is zero. Therefore, the value of z_{es} can be evaluated by solving the homogeneous equation of the first derivative of $U(z,t)$ or Equation 6.1 with respect to z.

That is,

$$\frac{d}{dz}U(z,t) = \frac{d}{dz}\left[U_e + U_a \exp\left(-\sqrt{\mathrm{n}_f \frac{\pi}{\alpha}}z\right)\cos\left\{2\mathrm{n}_f \pi \mathrm{t} - \left(\sqrt{\mathrm{n}_f \frac{\pi}{\alpha}}z\right)\right\}\right] = 0 \tag{6.6}$$

$$\begin{aligned}\frac{d}{dz}U(z,t) = {} & U_a\sqrt{n_f \frac{\pi}{\alpha}}\exp\left(-z\sqrt{n_f \frac{\pi}{\alpha}}\right)\cos\left(2n_f \pi t - z\sqrt{n_f \frac{\pi}{\alpha}}\right) \\ & + U_a\sqrt{n_f \frac{\pi}{\alpha}}\exp\left(-z\sqrt{n_f \frac{\pi}{\alpha}}\right)\sin\left(2n_f \pi t - z\sqrt{n_f \frac{\pi}{\alpha}}\right)\end{aligned} \tag{6.7}$$

This simplifies to

$$\cos\left(2n_f \pi t - z\sqrt{n_f \frac{\pi}{\alpha}}\right) + \sin\left(2n_f \pi t - z\sqrt{n_f \frac{\pi}{\alpha}}\right) = 0$$

$$\sin\left(2n_f \pi t - z\sqrt{n_f \frac{\pi}{\alpha}}\right) = -\cos\left(2n_f \pi t - z\sqrt{n_f \frac{\pi}{\alpha}}\right)$$

$$\tan\left(2n_f \pi t - z\sqrt{n_f \frac{\pi}{\alpha}}\right) = -1 \tag{6.8}$$

Therefore,

$$\left(2n_f \pi t - z\sqrt{n_f \frac{\pi}{\alpha}}\right) = \frac{7\pi}{4} \tag{6.9}$$

$$z = \left(\frac{8\pi t}{4}n_f - \frac{7\pi}{4}\right)\sqrt{\frac{\alpha}{\pi n_f}} \tag{6.10}$$

at any time including $t = 0$, $z = z_{es}$ and therefore the depth of equilibrium suction becomes

$$z_{es} = \left|\frac{-7\pi}{4}\sqrt{\frac{\alpha}{\pi n_f}}\right| \tag{6.11}$$

6.2.1 Limits of Suction at Soil Depth

The solution of the homogeneous equation of the first derivative of $U(z,t)$ with respect to t provides the respective limits of suction at any depth z.

$$\frac{d}{dt}U(z,t) = \frac{d}{dt}\left\{U_e - U_a \exp\left(-\sqrt{n_f \frac{\pi}{\alpha}}z\right)\cos\left(2n_f \pi \mathrm{t} - \left(\sqrt{n_f \frac{\pi}{\alpha}}z\right)\right)\right\} = 0 \tag{6.12}$$

$$\frac{d}{dt}U(z,t) = 2U_a \pi n_f \exp\left(-z\sqrt{n_f \frac{\pi}{\alpha}}\right)\sin\left(2n_f \pi t - z\sqrt{n_f \frac{\pi}{\alpha}}\right) \tag{6.13}$$

This simplifies to

$$2U_a \pi n_f \exp\left(-z\sqrt{n_f \frac{\pi}{\alpha}}\right)\sin\left(2n_f \pi t - z\sqrt{n_f \frac{\pi}{\alpha}}\right) = 0 \tag{6.14}$$

Since $2U_a \pi n_f \exp\left(-z\sqrt{n_f \frac{\pi}{\alpha}}\right) \neq 0$, then the solution of $\sin\left(2n_f \pi t - z\sqrt{n_f \frac{\pi}{\alpha}}\right) = 0$ gives

$$t = \begin{cases} \dfrac{z}{2\pi n_f}\sqrt{n_f \dfrac{\pi}{\alpha}} \\ \dfrac{1}{2\pi n_f}\left(\pi + z\sqrt{n_f \dfrac{\pi}{\alpha}}\right) \end{cases} \tag{6.15}$$

Substituting the values of t from Equation 6.15 into Equation 6.1 derives the expression for the minimum and maximum values of suction at any depth, as expressed in Equations 6.16 and 6.17 respectively.

At $t = \frac{z}{2\pi n_f}\sqrt{n_f \frac{\pi}{\alpha}}$

$$U(z)_{\min} = U_e - U_a \exp\left(-\sqrt{n_f \frac{\pi}{\alpha}}z\right) \tag{6.16}$$

At $t = \frac{1}{2\pi n_f}\left(\pi + z\sqrt{n_f \frac{\pi}{\alpha}}\right)$

$$U(z)_{\max} = U_e + U_a \exp\left(-\sqrt{n_f \frac{\pi}{\alpha}}z\right) \tag{6.17}$$

6.2.2 Maximum Change of Soil Suction

The maximum suction change at any depth, especially at the surface, is important. This value is defined by the difference between the maximum and minimum suction values. It is denoted $\Delta U(z)_{\max}$ and is expressed in Equation 6.18 as

$$\Delta U(z)_{\max} = 2U_a \exp\left(-\sqrt{n_f \frac{\pi}{\alpha}} z\right) \tag{6.18}$$

At the depth of equilibrium or constant suction z_{es}, the maximum change of soil suction $\Delta U_{es_{\max}}$ is expressed in Equation 6.19.

$$\Delta U_{es_{\max}} = 2U_a \exp\left(-\sqrt{n_f \frac{\pi}{\alpha}} z_{es}\right) \tag{6.19}$$

At $z = 0$, the maximum change of soil suction $\Delta U_{s_{\max}}$ becomes

$$\Delta U_{s_{\max}} = 2U_a \tag{6.20}$$

6.2.3 Critical Coefficients of Periodic Suction Expression

The limit of minimum and maximum at the subsoil surface $U_{s_{\min}}$ and $U_{s_{\max}}$ are derived by solving Equations 6.16 and 6.17 for $z = 0$. These are expressed in Equations 6.21 and 6.22 respectively.

$$U_{s_{\min}} = U_e - U_a \tag{6.21}$$

$$U_{s_{\max}} = U_e + U_a \tag{6.22}$$

Therefore, the maximum suction change, $\Delta U_{s_{\max}}$ which occurs at the ground surface becomes

$$\Delta U_{s_{\max}} = U_{s_{max}} - U_{s_{min}} \tag{6.23}$$

Then the coefficients of Equation 2.30, U_e and U_a, which represent equilibrium suction and amplitude of surface suction are determined in terms of $U_{s_{max}}$ and $U_{s_{min}}$ as expressed in Equations 6.24 and 6.25.

$$U_e = \frac{U_{s_{\max}} + U_{s_{min}}}{2} \tag{6.24}$$

$$U_a = \frac{U_{s_{max}} - U_{s_{min}}}{2} \tag{6.25}$$

6.2.4 Equations of Subsoil Suction Profile of Climates With Two Seasons

Consider an earthing site (site A), under the influence of two distinctive dry and wet seasons that alternate over a period, P, as shown in Figure 6.1.

If at time P_1, the dry season commenced (with rising surface suction), and at time P_2 the wet season (with falling surface suction) commenced afterwards, and $U(0,t)_{min}$ and $U(0,t)_{max}$ correspond to the minimum and maximum values of surface suction over the full period, then the analytical description of surface suction-time plot over the complete period P at this site is expressed by Equation 6.26.

$$U(0,\ t) = \begin{cases} U(0,t)_{max} & P_1 < t < P_2 \\ U(0,t)_{min} & P_2 < t < P_1 \end{cases} \tag{6.26}$$

Using an initial reference time $t = 0$, the equivalent analytical surface suction description is expressed as Equation 6.27.

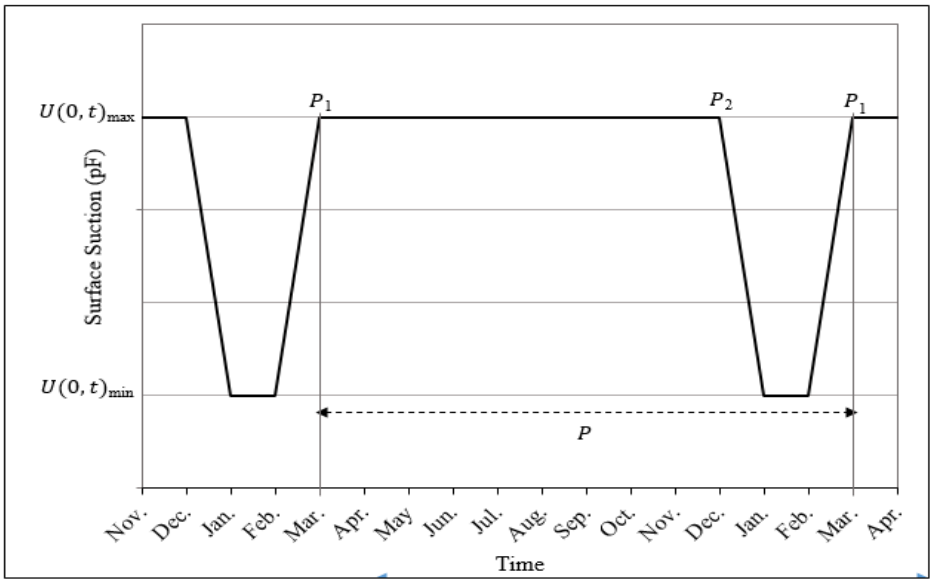


Figure 6.1: Time plot of surface suction for predominantly arid climate.

Source: Author's conceptualisation.

$$U(0,\ t) = \begin{cases} U(0,t)_{min} & 0 < t < P_1 \\ U(0,t)_{max} & P_1 < t < P_2 \\ U(0,t)_{min} & P_2 < t < P \end{cases} \tag{6.27}$$

If the total duration of falling and rising surface suction over the full period are denoted by P_{min} and P_{max}, then as shown in Figure 6.1, the relationship between the seasonal commencement time, (P_1 and P_2), seasonal duration (P_{min} and P_{max}) and period P for this site is expressed in Equations 6.28 and 6.29.

$$P_{max} = P_2 - P_1 \tag{6.28}$$

$$P_{min} = P + P_1 - P_2 \tag{6.29}$$

The corresponding Fourier coefficients for the sinusoidal surface suction function of the sites can be determined by substituting the numerical values of m_c in Equation 6.5.

For $m_c = 0$, U_0 is expressed in Equation 6.30 as

$$U_0 = \left(\frac{2}{P}\right)[(P + P_1 - P_2)U(0,t)_{min} + (P_2 - P_1)U(0,t)_{max}] \tag{6.30}$$

Substituting Equations 6.28 and 6.29, U_0 takes the form of Equation 6.31.

$$U_0 = \frac{2}{P}[P_{min}U(0,t)_{min} + P_{max}U(0,t)_{max}] \tag{6.31}$$

The general expression for $m_c = 1,\ 2,\ 3,\ \cdots$, is given in Equation 6.32.

$$U_m = \frac{2}{\pi m_c}[U(0,t)_{max} - U(0,t)_{min}]\left(\sin\frac{P_2}{P}\pi m_c - \sin\frac{P_1}{P}\pi m_c\right) \tag{6.32}$$

Similarly, if in another site (site B), the wet season commenced at P_1, before the commencement of the dry season at P_2, as illustrated in Figure 6.2, then the analytical description of surface suction-time plot over the complete period P at this site is expressed in Equation 6.33 as,

$$U(0,t) = \begin{cases} U(0,t)_{min} & P_1 < t < P_2 \\ U(0,t)_{max} & P_2 < t < P_1 \end{cases} \tag{6.33}$$

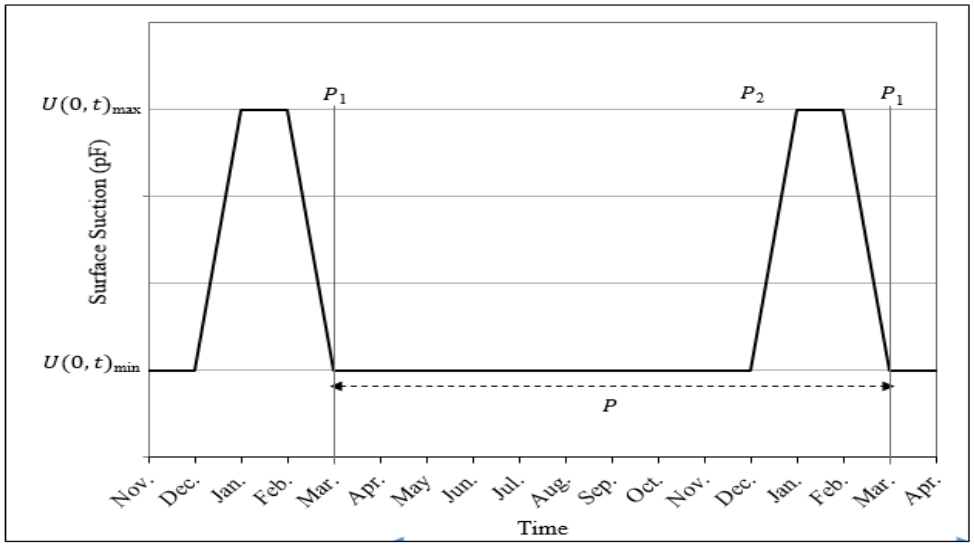


Figure 6.2: Illustrative surface suction-time plot of a predominantly humid climate.

Source: Author's conceptualisation.

If $t = 0$ is the initial reference time, then the expanded equivalent analytical description of the surface suction for site B is,

$$U(0,t) = \begin{cases} U(0,t)_{max} & 0 < t < P_1 \\ U(0,t)_{min} & P_1 < t < P_2 \\ U(0,t)_{max} & P_2 < t < P \end{cases} \tag{6.34}$$

The resulting relationship between the period and seasonal commencement time and duration is expressed in Equations 6.35 and 6.36.

$$P_{min} = P_2 - P_1 \tag{6.35}$$

$$P_{max} = P + P_1 - P_2 \tag{6.36}$$

By substituting the numerical values of m in Equation 6.5, the corresponding Fourier coefficients for the sinusoidal surface suction function of the sites are determined.

At $m_c = 0$, U_0 is expressed in Equation 6.37 as

$$U_0 = \frac{2}{P}[(P + P_1 - P_2)U(0,t)_{max} + (P_2 - P_1)U(0,t)_{min}] \tag{6.37}$$

Substituting Equations 6.35 and 6.36 transforms Equation 6.37 to Equation 6.31.

So, for $m_c = 1,2,3,\cdots$ the Fourier coefficients are determined using Equation 6.38.

$$U_m = \frac{2}{\pi m_c}[U(0,t)_{max} - U(0,t)_{min}]\left(\sin\frac{P_1}{P}\pi m_c - \sin\frac{P_2}{P}\pi m_c\right) \qquad (6.38)$$

6.3 Application: Formulations of Temporal Variation of Suction in Different Climates

Consider the states of surface suction for three climatic zones; sub-humid, arid and semi-arid climates, which were described in [70].

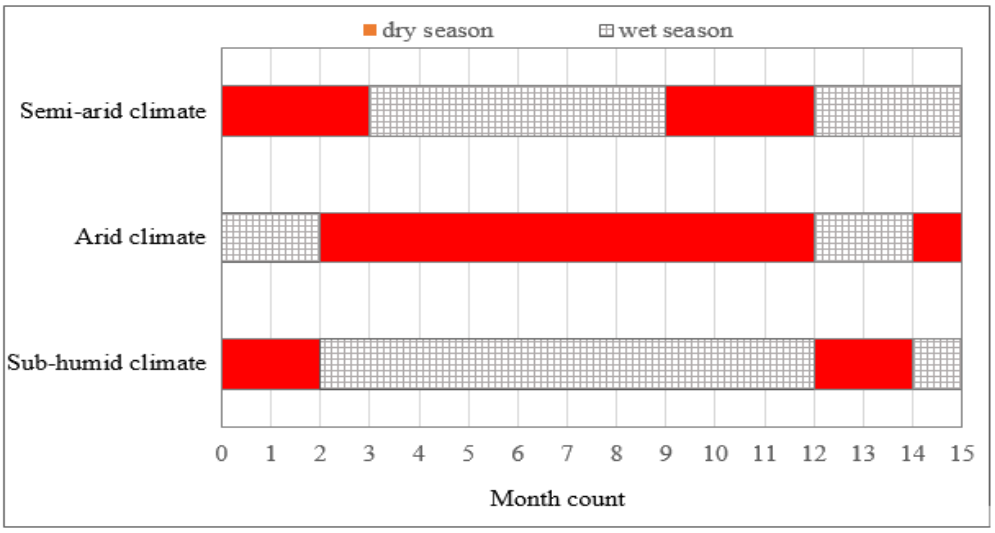


Figure 6.3: Typical wet and dry seasonal cycle in sub-humid, arid and semi-arid climates.

Source: Author's conceptualisation.

If the duration of the wet season is ten months (March to December) for the sub-humid climate, two months (January to February) for the arid climate and six months (April to September) in a semi-arid climate, and the remaining months of the year in each climatic zone is the dry season. The monthly distribution of the wet and dry seasons for these climatic zones is described diagrammatically in Figure 6.3.

If the minimum and maximum suction recorded during the wet and dry seasons are assumed to be $U_{s_{min}} = 3.10$ pF and $U_{s_{max}} = 5.60$ pF respectively, then by comparison, the arid climate is similar to site A, while the sub-humid and semi-arid climates are described analytically by site B. Table 6.1 shows the result of the analytical description of seasonal periods for the three climatic zones. The application of the analytical formulation of sites A and B to these climates produces the sinusoidal function of suction at any subsoil depth.

Table 6.1: Analytical description of surface suction during wet and dry seasons in sub-humid, arid and semi-arid climatic zones.

Climate	Seasonal duration	Surface suction	Period
Sub-humid	January – February: Dry March – December: Wet	$\begin{cases}5.6 & 0 < t < 1\\ 3.1 & 1 < t < 11\\ 5.6 & 11 < t < 12\end{cases}$	$P_1 = 1, P_2 = 11, P = 12,$ $P_{min} = P_2 - P_1 = 10,$ $P_{max} = P + P_1 - P_2 = 2$
Arid	January – February: Wet March – December: Dry	$\begin{cases}3.1 & 0 < t < 1\\ 5.6 & 1 < t < 11\\ 3.1 & 11 < t < 12\end{cases}$	$P_1 = 1, P_2 = 11, P = 12,$ $P_{min} = P + P_1 - P_2 = 2,$ $P_{max} = P_2 - P_1 = 10$
Semi-arid	April – September: Dry October – March: Wet	$\begin{cases}5.6 & 0 < t < 3\\ 3.1 & 3 < t < 9\\ 5.6 & 9 < t < 12\end{cases}$	$P_1 = 3, P_2 = 9, P = 12,$ $P_{min} = P_2 - P_1 = 6$ $P_{max} = P + P_1 - P_2 = 6$

Source: Author's conceptualisation.

To formulate the expression equivalent to Equations 6.3 or 6.4 for each of the climatic zones, the numerical values of $m = 0,1,2,3,\cdots$, are substituted into Equation 6.5 to the non-zero coefficients, $U_0, U_1, U_2, \cdots$. Table A21 contains the evaluations of some of the first ten non-zero Fourier coefficients for the three climates. Substituting the coefficients, the sinusoidal functions for suction at any depth, $U(z,t)$ and at the surface of the subsoil, $U(0,t)$ are expressed in Equations 6.39 to 6.44.

For sub-humid climate

$$U(z,t) = 3.515 + 0.7958\exp\left(-z\sqrt{n_f\frac{\pi}{\alpha}}\right)\cos\left\{2\pi t\left(n_f\right) - z\sqrt{nn_f}\right\} + 0.6892\exp\left(-z\sqrt{2n_f\frac{\pi}{\alpha}}\right)\cos\left\{2\pi t(2n_f) - z\sqrt{2n_f\frac{\pi}{\alpha}}\right\} + \cdots \quad (6.39)$$

$$U(0,t) = 3.515 + 0.7958\cos n_f\,(2\pi t) + 0.6892\cos 2n_f\,(2\pi t) + \cdots \quad (6.40)$$

For arid climate

$$U(z,t) = 5.1850 - 0.7958\exp\left(-z\sqrt{n_f\frac{\pi}{\alpha}}\right)\cos\left\{2\pi t\left(n_f\right) - z\sqrt{n_f\frac{\pi}{\alpha}}\right\} - 0.6892\exp\left(-z\sqrt{2n_f\frac{\pi}{\alpha}}\right)\cos\left\{2\pi t\left(2n_f\right) - z\sqrt{2n_f\frac{\pi}{\alpha}}\right\} - \cdots \quad (6.41)$$

$$U(0,t) = 5.1850 - 0.7958\cos n_f\,(2\pi t) - 0.6892\cos 2n_f\,(2\pi t) + \cdots \quad (6.42)$$

For semi-arid climate

$$U(z,t) = 4.3500 + 1.5915\exp\left(-z\sqrt{n_f\frac{\pi}{\alpha}}\right)\cos\left\{2\pi t(n_f) - z\sqrt{n_f\frac{\pi}{\alpha}}\right\} - 0.5305\exp\left(-z\sqrt{2n_f\frac{\pi}{\alpha}}\right)\cos\left\{2\pi t(2n_f) - z\sqrt{2n_f\frac{\pi}{\alpha}}\right\} + \cdots \quad (6.43)$$

$$U(0,t) = 4.3500 + 1.5915\cos n_f(2\pi t) - 0.5305\cos 2n_f(2\pi t) + \cdots \quad (6.44)$$

To describe suction at any depth and time using these equations requires values for climate frequency, n_f and soil diffusion coefficient, α. If $\alpha = 2.5 \times 10^{-4}$ cm^2/s is assumed for the three soil textures, and $n_f = 1$ cycle/yr, implying that one seasonal wet-dry cycle is completed in twelve months, then the variation of suction at any depth, $|z| \geq 0$ can be described for any time scale using appropriate equivalent values shown in Table A22.

Figure 6.4 is the plot showing the daily variation of ground surface suction for sub-humid, arid, and semi-arid climates. From the curves, the maximum suction in an arid climate and minimum suction in a semi-arid climate exceeds the specified values, $U_{s_{max}} = 5.60$ pF and $U_{s_{min}} = 3.10$ pF respectively. This is an approximation error that exists due to the finite number of Fourier coefficients used in evaluating the sinusoidal functions. However, the trend of the daily suction curves follows the same pattern for the wet and dry seasons. As described analytically, sub-humid and arid climates experience opposite seasons at any time.

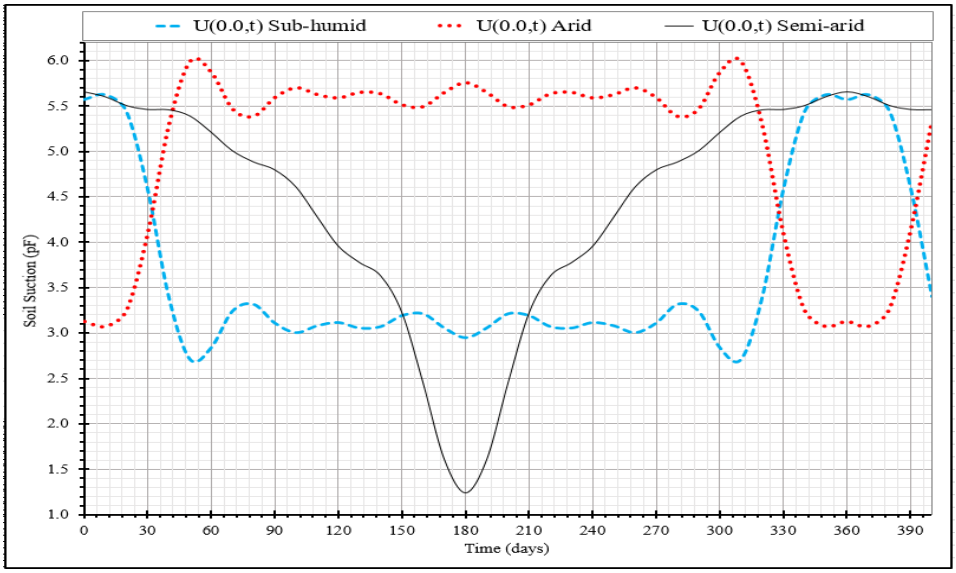


Figure 6.4: Typical daily variation of ground surface suction in sub-humid, arid and semi-arid climates

Source: Author's conceptualisation.

The magnitude and variation of the ground surface determine the profile of suction along the depth of the subsoil. Figure 6.5 shows the daily variation of suction at a selected depth of subsoil within a sub-humid climate.

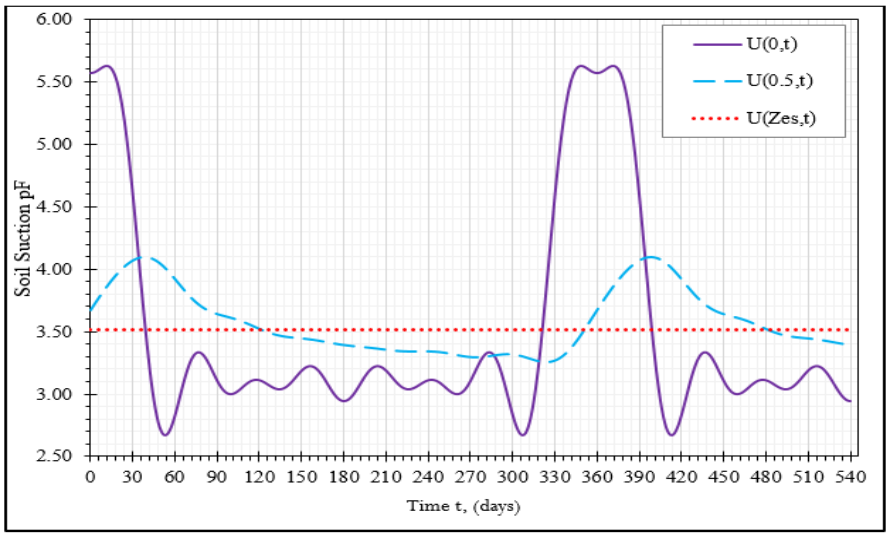


Figure 6.5: Daily variation of suction from ground surface to depth of constant suction in sub-humid climate

Source: Author's conceptualisation. $z = 0$, $z = 0.5$ m, and depth of constant suction, $z = z_{es}$

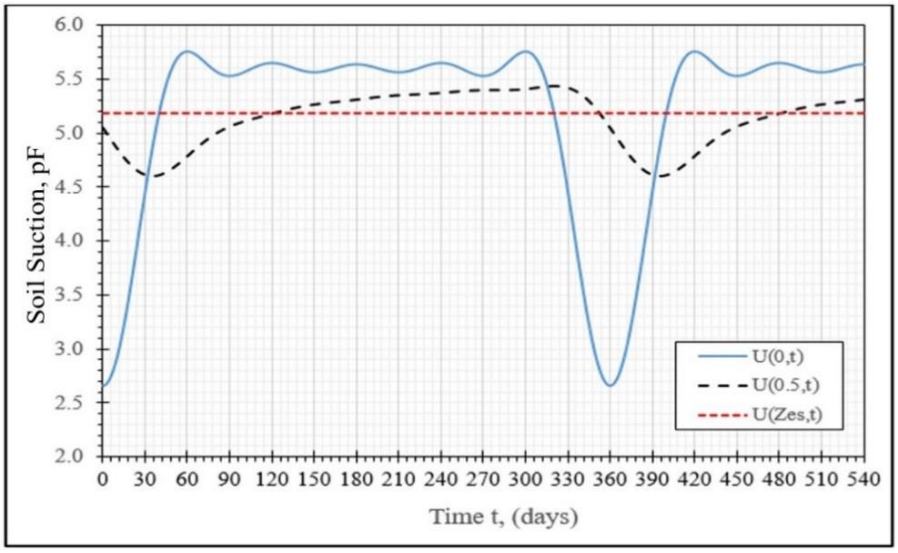


Figure 6.6: Daily variation of suction from ground surface to depth of constant suction in arid climate.

Source: Author's conceptualisation. $z = 0$ m, $z = 0.5$ m, and depth of constant suction, $z = z_{es}$.

Figures 6.6 and 6.7 are the equivalent plots for arid and semi-arid climates. In all cases, suction at the surface is often out of phase and unequal in magnitude with subsurface suction. There is a lead-lag relationship between the ground surface and subsurface suctions. In the dry season, the magnitude of subsurface suction is smaller than the ground surface suction for the three

climatic zones. For example, whereas the ground surface suction during the dry season in a sub-humid climate is 5.63 pF (day 10), suction is 3.84 and 3.47 pF at 0.5 m and 1.5 m depth of subsoil respectively. Conversely, in the wet season, subsurface suction is predominantly higher than ground surface suction.

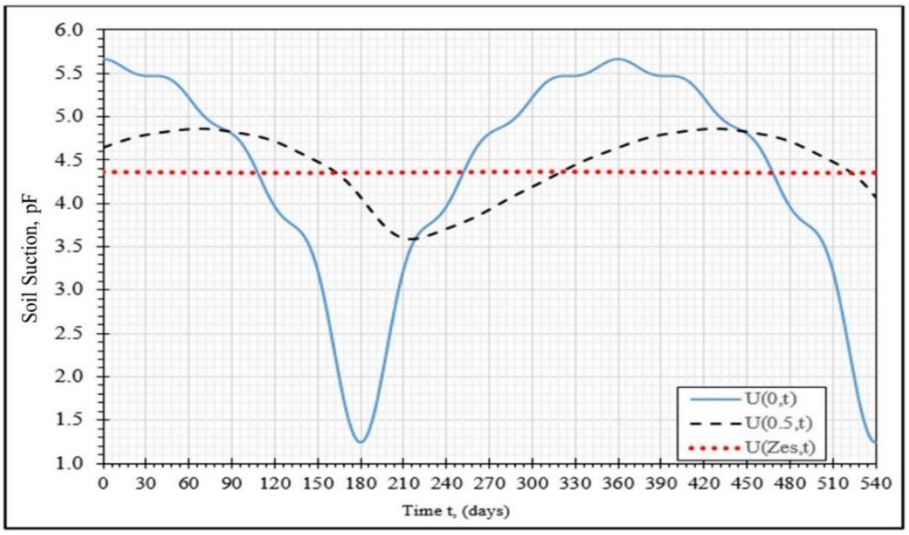


Figure 6.7: Daily variation of suction from ground surface to depth of constant suction in semi-arid climate

Source: Author's conceptualisation. $z = 0$ m, $z = 0.5$ m, and depth of constant suction, $z = z_{es}$.

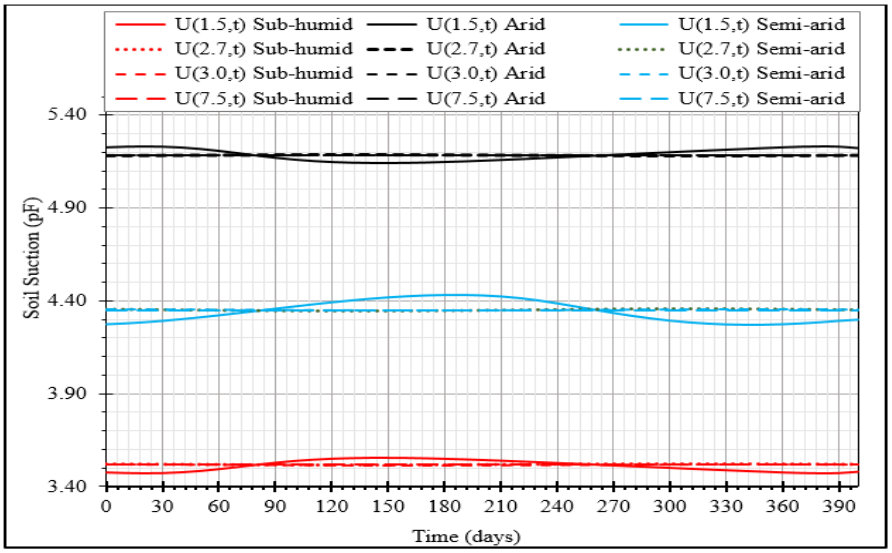


Figure 6.8: Daily variation of suction at depth exhibiting constant suction in sub-humid, arid, and semi-arid climates

Source: Author's conceptualisation.

Figure 6.8 shows the profile of subsurface suction at 1.5, 2.7, 3, and 7.5 m depths in sub-humid, arid, and semi-arid climates. As the subsoil depth increases, the suction curve converges

towards a constant value for each climate. Equation 6.11 predicts the depth of equilibrium or constant suction, which is 3.86 m using the specified parameters. Soils in different climatic zones do not necessarily have equal depths of constant suction, whose value differs with location and depends on climatic, n_f and earthing site α, parameters.

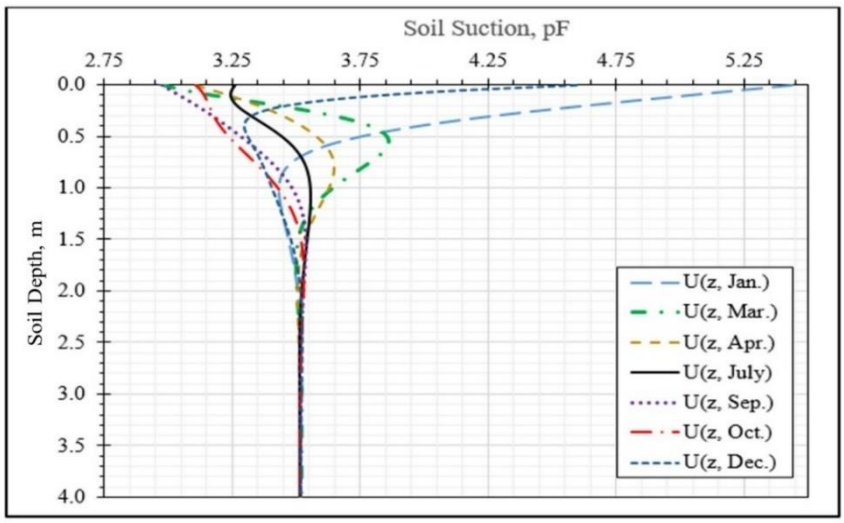


Figure 6.9: Profile of monthly ground surface and subsurface suctions in a sub-humid climate

Source: Author's conceptualisation.

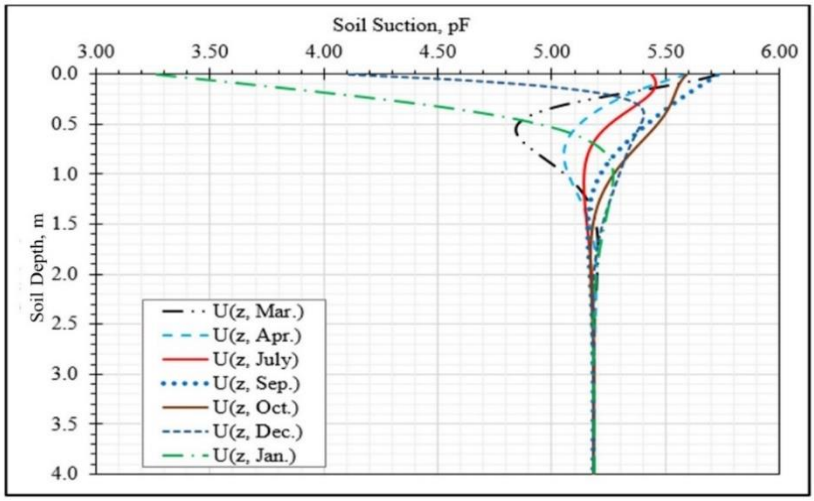


Figure 6.10: Profile of monthly ground surface and subsurface suctions in arid climate

Source: Author's conceptualisation.

Subsurface suction is constantly in a dynamic state of change due to changes in environmental and climatic conditions. Figures 6.9 to 6.11 are the monthly variation of subsurface suction for sub-humid, arid and semi-arid climates. These curves illustrate how suction induced at the ground surface is transmitted and changes along the depth of the subsoil. Subsurface suction is

significantly influenced by the previous state or suction, such that certain depths can transition to suction of magnitude higher or lower than the ground surface suction at that time. For example, in continuance with suction rise from the previous month, the sub-humid ground surface suction is approximately 3.25 pF for the month of July. However, at 1 m depth, suction is slightly higher and approximately 3.55 pF in the same month. These curves also show that the profile of suction changes periodically above the depth of constant suction.

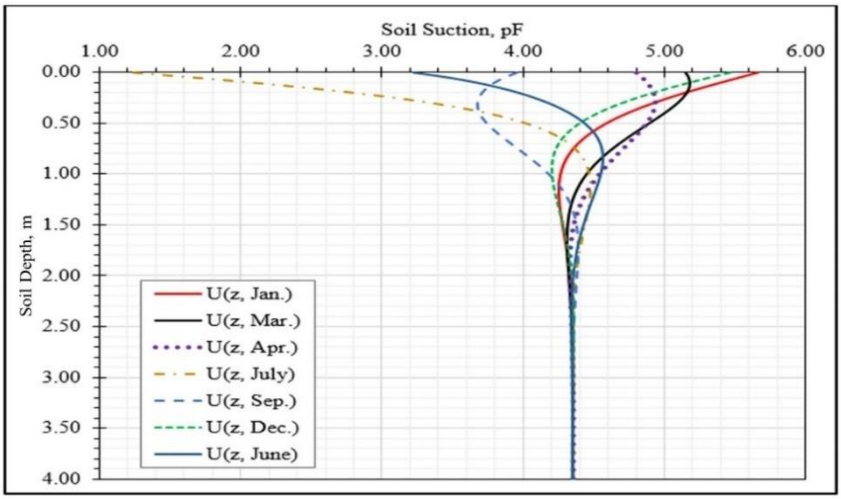


Figure 6.11: Profile of monthly ground surface and subsurface suctions in a semi-arid climate

Source: Author's conceptualisation.

Whereas the depth of equilibrium suction is equal given that the same climate-site parameters were used, the magnitude of equilibrium suction shown in Figures 6.9, 6.10 and 6.11 is unequal. The magnitudes of equilibrium suction are 3.52 pF (-324.73 kPa), 5.18 pF (-14842.97 kPa), 4.36 pF (-2246.57 kPa) for sub-humid, arid and semi-arid climates respectively. These values are consistent with actual field measurements. The difference is explained theoretically by the difference in Fourier coefficients of the sinusoidal suction functions of the climate zones.

6.4 Application: Earthing System Performance in Different Climatic Zones

To avoid unacceptable values of earthing resistance because of seasonal changes, earthing systems are often designed using estimates of likely variation. Since seasonal cycles are climate-driven, the impact of different climates and wet-dry cycles on different soil textures is investigated in this section.

Table A23 is the daily variation of ground surface suction and volumetric water content of sandy clay, silty and clay soils in sub-humid, arid and semi-arid climates for 380 days at intervals of 10 days. As weather condition drives the daily change of suction on the ground

surface of these soils, their water content and resistivity also change. The highest values of suction were attained increasingly in sub-humid climates (5.63 pF), semi-arid (5.66 pF) and then arid climates (5.99 pF). However, semi-arid climates experience the smallest magnitude of ground surface suction, approximately 1.24 pF, followed by 2.71 pF in sub-humid climates while arid climates experience 3.07 pF. During these variations of suction, water retention and release from the soils are controlled by their hydraulic characteristics.

Figure 6.13 and 6.14 show a typical daily variation of ground surface suction and volumetric water content of sandy clay, silty and clay soils in sub-humid, arid and semi-arid climates respectively.

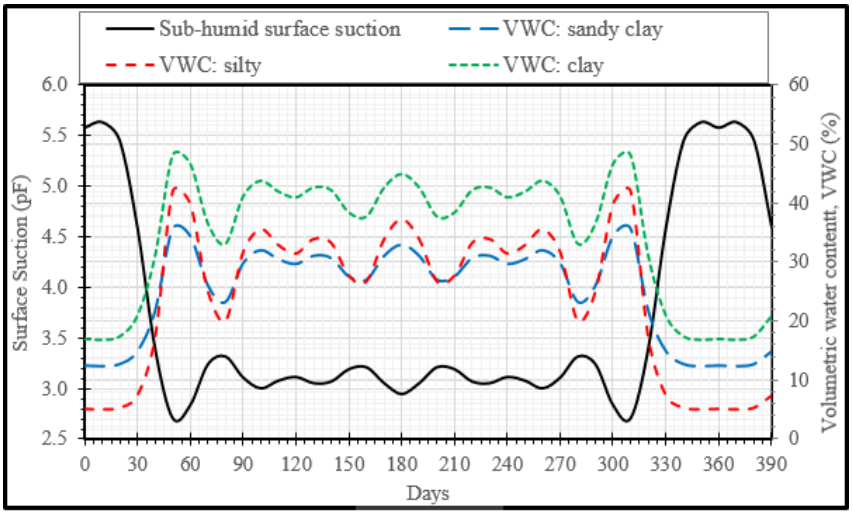


Figure 6.12: Daily variation of surface suction and volumetric water content of clay, silty and sandy clay subsoils in sub-humid climate

Source: Author's conceptualisation.

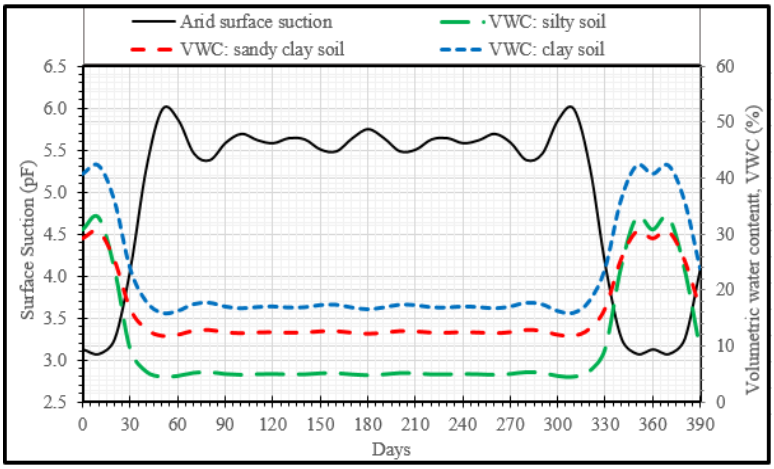


Figure 6.13: Daily variation of surface suction and volumetric water contents of clay, silty and sandy clay subsoils in arid climate

Source: Author's conceptualisation.

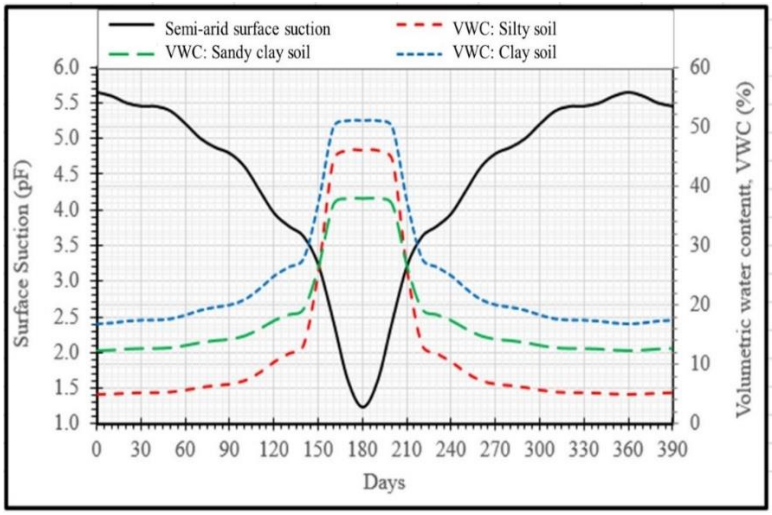


Figure 6.14: Daily variation of surface suction and volumetric water contents of clay, silty and sandy clay subsoils in semi-arid climate

Source: Author's conceptualisation.

As expected, water content reduces as suction increases; clay soil retains more volumetric water than the other two soils. In some instances, the composition of clay in sandy clay soil improves the water retention capacity of sand in sandy clay and makes it retain more water than silty soil.

Archie's law describes the effect of volumetric water content change on the resistivity of soils. Table A24: Resistivity of silty, sandy clay, and clayey subsoils in sub-humid, arid, and semi-arid climates.Table A24 shows the corresponding values of resistivity of silty, clay and sandy clay soils in sub-humid, arid, and semi-arid climates. In sub-humid climates, the minimum resistivity of sandy clay, silty, and clay soils are 17.33, 165.42, and 7.79 Ωm respectively. As suction increased, the highest suction attained approximately 20.4, 35, and 96 times their minimum resistivity values.

In arid climates, the highest values of resistivity are approximately 38, 99, and 21 times the minimum resistivity of silty, sandy clay, and clay soils during low suction values. Under semi-arid conditions, the highest resistivity of the soils attained at 5.66 pF (day 360) is 41.34, 129.43, and 24.8 times the minimum value of resistivity of silty, sandy clay and clay soils respectively.

Table 6.2 is the descriptive statistics of the resistivity of clay, silty and sandy clay soils in sub-humid, arid, and semi-arid climates. Table 6.2 was generated with data samples for half of the period, that is, 0 to 180 days, as in Table A23. By comparing the mean and standard deviation of resistivity of the three soils in the three climates, the effect of climate on resistivity changes

can be better understood. Despite having the same resistivity - water content relationship, the resistivity of all three soils (clay, silty, and sandy clay) varied differently in the three climates.

Table 6.2: Descriptive statistics of resistivity of clay, silty, and sandy clay soils in sub-humid, arid, and semi-arid climates.

Soil	Climate	Minimum (Ωm)	Maximum (Ωm)	Mean (Ωm)	Standard deviation (Ωm)
Silty	Sub-humid	17.33	620.44	124.65	206.97
	Arid	23.31	881.83	500.98	256.21
	Semi-arid	15.44	638.31	286.86	221.85
Sandy clay	Sub-humid	165.42	16926.00	2971.37	5686.31
	Arid	264.78	26119.00	13594.13	7497.27
	Semi-arid	135.47	17530.00	7112.28	6166.10
Clay	Sub-humid	7.79	166.40	38.00	54.65
	Arid	10.54	223.33	135.46	64.70
	Semi-arid	6.87	170.40	83.02	58.17

Source: Author's conceptualisation.

Arid climates produce significantly high values of mean resistivity, which is approximately 3.6 and 4.57 times that of the sub-humid climate for clay and sandy clay soils respectively. Like the mean resistivity, a higher standard deviation is induced in arid climates. The effect of equally dry and wet seasons also makes the standard deviation in semi-arid climates more significant than in sub-humid climates. This implies that the extent of variation of earthing resistance is both soil and climate dependent.

6.4.1 Earthing System Without EEM in Single and Double-Layer Subsoils

This section discusses changes to the resistance of earthing rods corresponding to the variations of water content and resistivity of soil due to changes in climate-induced suction. Figure 6.15 shows the variation resistance of earthing rods in (a) silty, (b) clay, and (c) sandy clay soils under sub-humid, arid, and semi-arid climates. It is assumed that suction at the ground surface is transmitted evenly to the entire depth of the subsoil. Like the resistivity curve, earthing resistance curves follow the same trend as the suction curve of that climate.

However, earthing resistance attained in sandy clay soils has a higher magnitude and a wider range of variation in all climates. Figure 6.16 shows the graphical difference in the magnitude and variation of resistance of earth rods' inhomogeneous layers of clay, silty, and sandy clay subsoils under an arid climate. In all instances, an arid climate induces high resistance values and wider variation than in other climates.

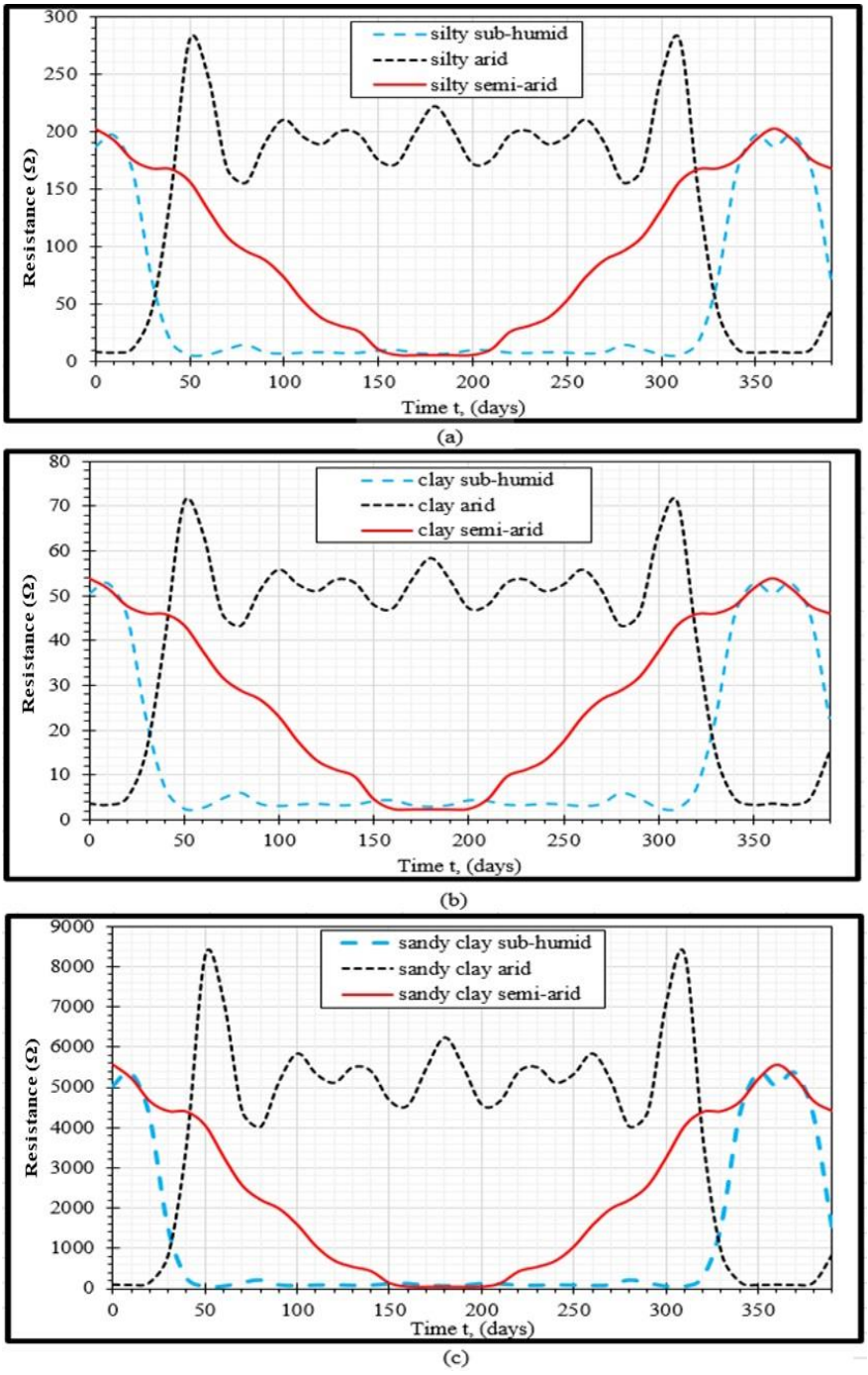


Figure 6.15: Daily variation of resistance of vertical rod in silty, clay, and sandy clay subsoils under (a) sub-humid, ((b) arid, and (c) semi-arid climates

Source: Author's conceptualisation.

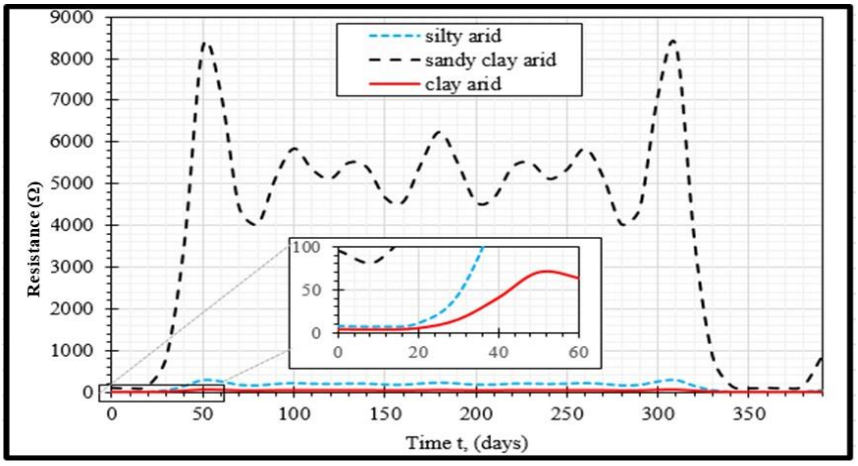


Figure 6.16: Daily variation of resistance of vertical rod of silty, clay, and sandy clay single-layer subsoils under arid climate

Source: Author's conceptualisation.

Table 6.3 shows the descriptive statistics of earthing resistance corresponding to Table 6.2. As indicated by the ratios of means, and maximum to minimum values of resistance and resistivity, the magnitude and variation of earthing resistance in any soil-climate pair is proportional to their corresponding resistivity. Under arid climates, the resistance attained in all the soils is not only higher but as the large value of standard deviation indicates, arid climates also induce the widest range of variation. For example, the maximum resistance attained by a 3 m length, 9,562 mm radius earth rod buried vertically in sandy clay soil in sub-humid, semi-arid and arid climates is 5,362.4, 5,553.6, and 8,274.9 Ω respectively. These resistances were attained when sandy clay resistivity in sub-humid (5.63 pF), arid (5.99 pF), and semi-arid (5.66 pF) climates is 16,926, 26,119, and 17,530 Ωm respectively

Table 6.3: Descriptive statistics of resistance of earthing rod in clay, silty, and sandy clay soils under sub-humid, arid, and semi-arid climates.

Soil	Climate	Minimum (Ω)	Maximum (Ω)	Mean (Ω)	Standard deviation (Ω)
	Sub-humid	5.49	196.56	39.49	65.57
	Arid	7.39	279.37	158.72	81.17
Silty	Semi-arid	4.89	202.22	90.88	70.28
	Sub-humid	52.41	5362.40	941.36	1801.47
	Arid	83.89	8274.90	4306.79	2375.24
Sandy clay	Semi-arid	42.92	5553.60	2253.24	1953.47
	Sub-humid	2.47	52.72	12.04	17.31
	Arid	3.34	70.75	42.91	20.50
Clay	Semi-arid	2.18	53.98	26.30	18.43

Source: Author's conceptualisation.

This implies that given the possibility that such suction and resistivity can be attained, the resistance of a fault or surge current senses must remain within acceptable limits for maximum safety. Given the wide deviation from the mean value (large standard deviation), earthing terminals in sandy or rocky sites must be designed in consideration of the worst possible resistivity the earthing site can attain over the seasonal cycle. Depending on the most feasible, either/or combination of the earthing terminal size, configuration, orientation and composition can be adjusted to achieve and ensure low earthing resistance under high suction conditions. However, cost and space could dictate which single or combined strategies are implementable for each case

6.4.2 Earthing System With EEM in Single- and Double-Layer Subsoils

The use of earthing enhancement materials around the earthing terminal is a typical example of achieving low resistance by adjusting the composition of the earthing terminal. Like the native soil, these EEMs are porous mediums with hydraulic and electrical properties that are affected by changes in the degree of saturation. Using the same materials (EEM I and EEM II) and soils used in Chapter Four, this section investigates and analyses the effectiveness of EEM for resistance reduction in different soils and climates. It is assumed that the entire depth of the subsoil is at equilibrium with equal distribution of ground surface suction throughout the soil depth.

Table A25 shows the daily variation (at intervals of 10 days) of the resistivity of earthing enhancement materials, EEM I and EEM II for three (sub-humid, arid and semi-arid) climate zones. Unlike the resistivity of soils shown in Table A24, which varies rapidly, the resistivity of EEMs is more consistent with a smaller variation range for a large range of suction change.

This low varying characteristic of the resistivity of EEM and their proximity to the bare metallic terminal of earthing systems ensures lower resistance than the earthing composition without EEM.

Table A26 compares the daily resistance of the vertical rod in native soils; silty and sandy clay soils (without EEM) to the resistance with EEMs (EEM I and EEM II) of radius 115.2 mm around the rod under sub-humid and arid climate conditions. The result indicates that the EEMs achieved significant resistance reduction for all conditions. Although lower resistances are attained during the period of low suction, EEM still provides resistance reduction. However, the reduction provided during high suction periods ensures the safe operation of the earthing system.

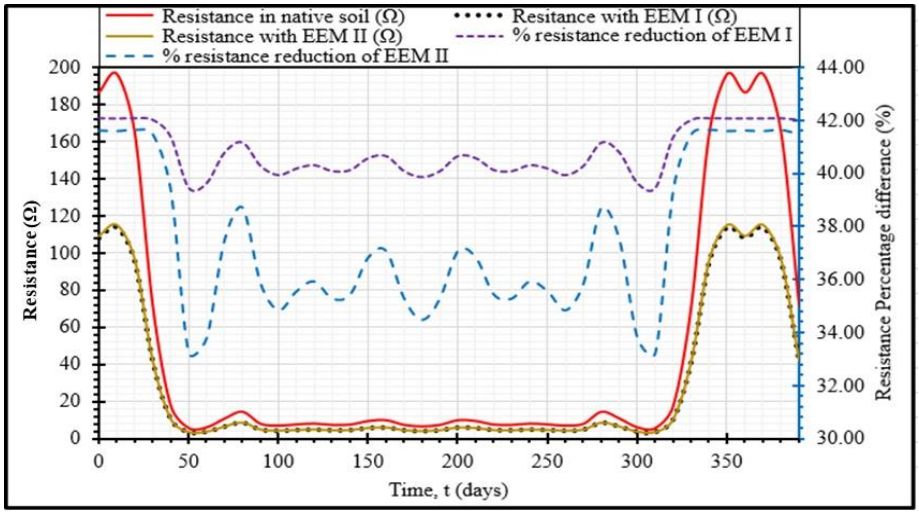


Figure 6.17: Daily variation of resistance of vertical rod without and with earthing enhancement materials (EEM I and EEM II) each of radius 115.2 mm in single-layer silty subsoil under sub-humid climate

Source: Author's conceptualisation.

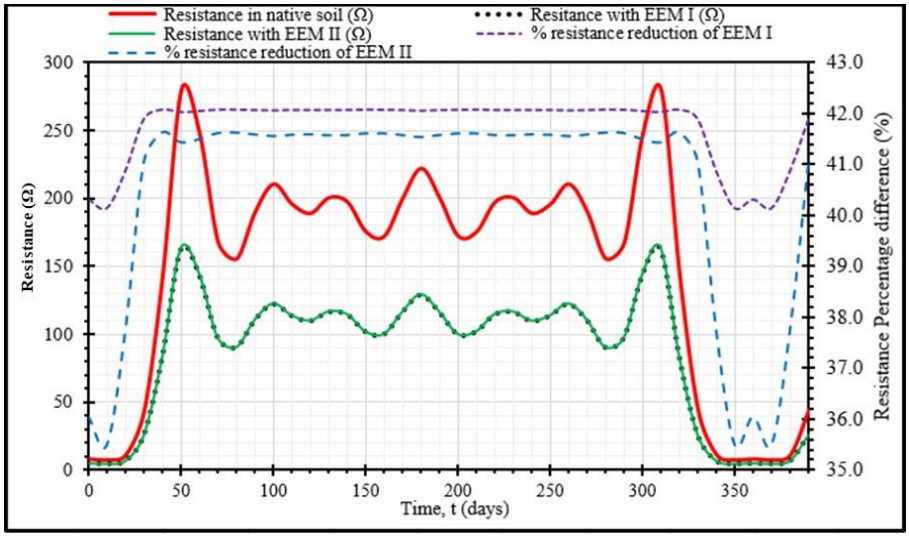


Figure 6.18: Daily variation of resistance of vertical rod without and with earthing enhancement materials (EEM I and EEM II) each of radius 115.2 mm in single-layer silty subsoil under arid climate

Source: Author's conceptualisation.

Figures 6.17 and 6.18 show the plot of resistance of the reference earthing (without EEM) compared with the resistance of two earthing systems with EEMs in silty soil and their percentage resistance reductions under sub-humid and arid climates. During the dry high suction seasons, there is significant resistance reduction that the EEMs provide for earth rods in silty soil under both climates. Although both EEMs achieve similar resistance reduction, EEM I performed better.

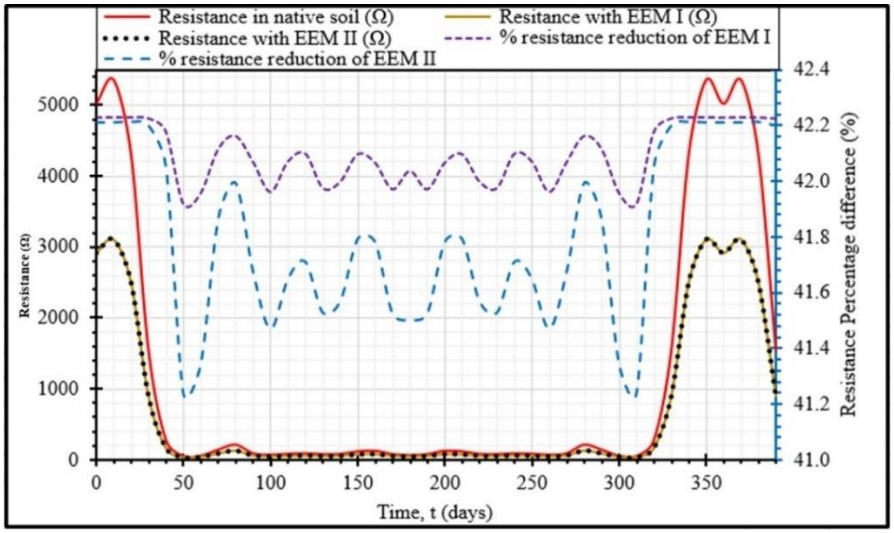


Figure 6.19: Daily variation of resistance of vertical rod without and with earthing enhancement materials (EEM I and EEM II) each of radius 115.2 mm in single-layer sandy clay soil under sub-humid climate

Source: Author's conceptualisation.

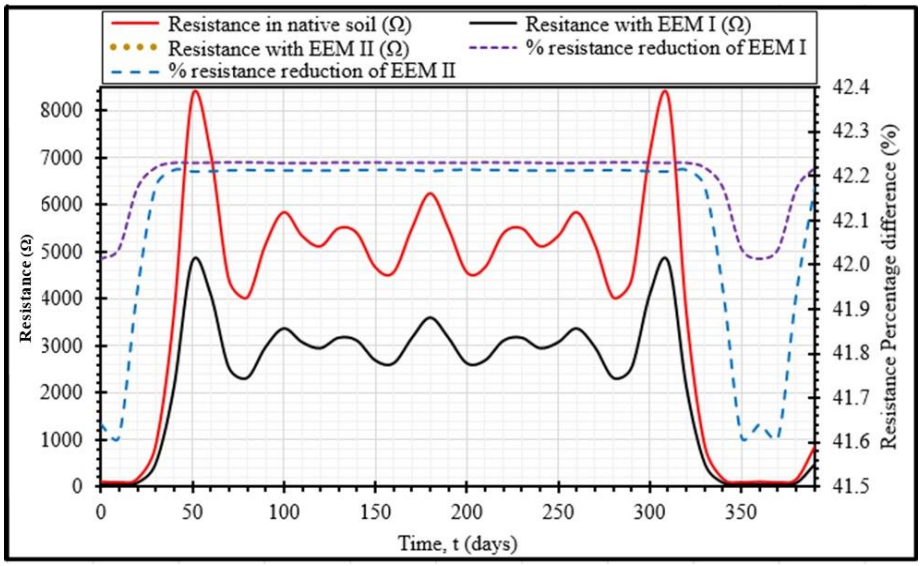


Figure 6.20: Daily variation of resistance of vertical rod without and with earthing enhancement materials (EEM I and EEM II) each of radius 115.2 mm in single-layer sandy clay soil under arid climate

Source: Author's conceptualisation.

As seen in Figures 6.19 and 6.20, the resistance reduction capability of EEM I and EEM II in sandy clay was relatively the same in both arid and sub-humid climates.

Table 6.4 shows the descriptive statistics of the percentage resistance reduction offered by EEM I and EEM II in silty and sandy clay soils under sub-humid and arid climates. In both climates and soils, EEM I outperform EEM II and maintains less performance variation, as indicated by the smaller standard deviation.

Table 6.4: Descriptive statistics of resistance reduction of earthing enhancement materials (EEM I and EEM II) in silty and sandy clay soils under sub-humid and arid climates.

			Resistance reduction (%)			
Climate	Soil	EEM	Minimum	Maximum	Mean	Standard deviation
Sub-humid	Silty	I	39.45	42.06	40.66	0.87
		II	33.25	41.62	37.13	2.79
	Sandy clay	I	41.92	42.23	42.08	0.10
		II	41.24	42.21	41.77	0.31
Arid	Silty	I	40.14	42.07	41.79	0.62
		II	35.49	41.63	40.73	1.96
	Sandy clay	I	42.01	42.23	42.21	0.06
		II	41.61	42.22	42.13	0.19

Source: Author's conceptualisation.

EEM II experienced more performance variation in silty soil than in sandy clay soil. A likely reason for this better performance is that besides having higher water retention capacity, EEM I have more electrical conductivity than EEM II under the same condition. So, as suction changes, the resistivity of EEM I remains relatively low, whereas the same suction fluctuation produces a significant change in water content and resistivity of EEM II.

The difference in the resistance reduction of EEM in different soils, seasons and climates indicates that the selection of EEM should not only be based on the four criteria recommended by IEC standard 62561-7, but also that hydraulic properties of native soil and prospective EEM, and the effect of climate be additional selection criteria. Water retention capacity, variation of water content and resistivity under changing suction of prospective EEM and the native soil should be determined. A model of each EEM in the native soil should be simulated and their resistance reduction evaluated. The optimal soil-EEM pair that should be selected for earthing implementation is likely the EEM which achieves the highest resistance reduction capacity with minimal variation over changing periodic seasons.

Chapter 7 - Conclusion and Recommendations

7.0 Conclusion

Although the seasonal variations in earthing resistance are linked to external climatic and environmental factors, the precise relationship between these changes has not been quantified using climatic parameters, soil properties, and soil conditions. Existing techniques rely on climate records and historical measurements of earthing resistance or soil resistivity for predictions. This research proposes a novel method for modelling and evaluating the resistance and performance of earthing systems across different soil types by focusing on hydraulic properties. By exploring the relationship between soil suction, water retention, and soil resistivity, this method models the soil-electrode system to assess earthing resistance under the influence of external factors affecting the hydraulic and electrical properties of soil. If the degree of soil saturation or water content directly influences resistivity, the variability of hydraulic properties - such as water retention characteristics and hydraulic conductivity under changing suction - regulates soil resistivity, thereby determining the earthing system's resistance. External climatic and environmental influences, which control soil water content, are modelled as soil suction, ranging from low to high values representing saturated and unsaturated soil conditions. The simulation results and subsequent analysis demonstrate that earthing resistance and performance are influenced by soil type (resistivity), while variations are governed by the soil's water retention characteristics, hydraulic conductivity, and water diffusion coefficient. Water retention characteristics dictate how water is retained within the soil matrix under desaturation conditions, while hydraulic conductivity and water diffusion coefficient govern water movement within the soil matrix.

The study also examined the impact of soil texture on the resistance and performance of earthing electrodes under fault or surge current dissipation conditions, focusing on three soil textures: clayey, silty, and sandy soils. The findings revealed that earthing resistance and electric potential at the ground surface are dependent on both soil type and condition. Fine-grained soils, such as clay and silt, exhibit smaller changes in volumetric water content under high suction due to their smaller particle sizes and higher compaction between adjacent grains, resulting in numerous small pores within the soil matrix. In contrast, coarse-grained soils, like sandy soils, have loosely held grains that lead to higher hydraulic conductivity. Consequently, fine-grained soils possess high water retention and low hydraulic conductivity, while sandy soils exhibit high hydraulic conductivity and relatively low water retention. Under high soil

suction, clayey and silty soils retain more water and transmit less, whereas sandy soils transmit water more quickly with relatively less retention.

This method offers a significant advantage over existing techniques by predicting the seasonal variability of earthing resistance. It allows for the modelling of earthing sites by incorporating the unique properties and features of each site. This approach can help power utility companies predict the likely resistance and performance of earthing systems at problematic sites, thereby reducing the need for actual measurements. Additionally, it provides a framework for comparing the performance and effectiveness of earthing enhancement materials (EEMs) across different soils and conditions, enabling stakeholders to make more informed decisions regarding the selection and use of EEMs in varying environments.

7.1 Research Contributions

The research has provided significant advancements in the design and resistance evaluation and prediction of earthing systems.

Firstly, it offers engineers a robust alternative to predicting seasonal changes in earthing resistance with prospect of higher accuracy. Current methods rely on broad rainfall data and historical measurement of soil resistivity and earthing resistance, but often overlook critical *in situ* factors of the subsoil like vegetation, topography, and texture. By incorporating these factors, the actual water retained in the subsoil and not rainfall on its surface provides more reliable evaluation and prediction of soil resistivity and earthing resistance.

Secondly, the incorporation of water retention characteristics enables the quantification, evaluation and prediction of resistance reduction capacity of earthing enhancement materials and comparison of performance of different EEMs in different soils and condition. This provides insight on impact of environment, land use and climate on earthing resistance and performance, addressing a significant gap in the existing knowledge base.

Thirdly, the research provides a practical and effectiveness method for selecting and implementing earthing enhancement materials in different soil types and climatic conditions. This ensures efficient and cost-effective earthing system designs, enhancing safety and operational reliability of the power system.

Lastly, by keeping data of soil resistivity at earthing sites and access to meteorological data, power utility companies can conveniently estimate the variation of earthing resistance and

performance for any transmission or distribution tower. This provides improved and convenient reliability assessment for the earthing system.

7.2 Research Limitation

The proposed method effectively models soil texture, condition, seasons, and climate, and estimates their impact on the resistance and performance of earthing systems. The accuracy of the model was assessed by comparing the resistance estimated using the energetic approach (Joule's law) of the finite element method (FEM) with that calculated using existing analytical formulas, which served as references. For a vertical rod in homogeneous isotropic soil, the percentage error between the energetic and reference resistance, as shown in Table A6, ranges from approximately 2.72% to 6.53%. This suggests that the proposed model meets the satisfactory criteria established for FEMs, where simulation errors of less than 10% compared to actual measurements are considered acceptable [88], [94], [108]. However, despite the apparent accuracy of the model, it requires validation with actual earthing measurements to fully determine its scope, limitations, and potential for predicting earthing system performance. This validation would help eliminate any doubt regarding the proposed method's effectiveness.

7.3 Recommendation for Future Research

Based on the success and potential of this new earthing modelling method, the following recommendations are proposed for future research:

1. The model currently assumes an even distribution of ground surface suction across the entire subsoil depth, ignoring the effect of constant suction depth. Future research should incorporate this depth to explore the extent of resistance and performance variations of earthing systems in different soils and climates.

2. Given that earth grids are typically buried within or above the constant suction depth, further studies should compare the variations in different configurations and orientations of earthing systems across various climatic conditions.

3. The current research models resistivity as solely dependent on water content. Future studies could develop more complex models that account for additional factors affecting resistivity, such as soil compaction, surface conductance, and cation exchange capacity.

4. This research focused on the variation of low (power) frequency resistance. Future work could explore the variation of high frequencies under transient conditions.

References

[1] IEEE Std. 1410-, *IEEE Guide for Improving the Lightning Performance of Electric Power Overhead Distribution Lines*, Jan. 2011. doi: 10.1109/IEEESTD.2011.5706451.

[2] IEEE Std. 81-2012, *IEEE Guide for Measuring Earth Resistivity, Ground Impedance, and Earth Surface Potentials of a Grounding System*, New York, USA., 2012. doi: DOI: 10.1109/IEEESTD.2012.6392181.

[3] IEC 62561-7, "Lightning protection system components (LPSC) – Part 7: Requirements for earthing enhancing compounds," 2018.

[4] N. A. F. Mohamad Nasir *et al.*, "Impact of earthing system designs and soil characteristics on tower footing impedance and ground potential rise: a modelling approach for sustainable power operation," *Sustainability*, vol. 13, no. 15, p. 8370, Jul. 2021, doi: 10.3390/su13158370.

[5] V. P. Androvitsaneas, G. J. Tsekouras, I. F. Gonos, and I. A. Stathopulos, "Seasonal Variation and Timeless Evolution of Ground Resistance," in *2018 IEEE International Conference on High Voltage Engineering and Application (ICHVE)*, Athens, Greece: IEEE, Sep. 2018, pp. 1–4. doi: 10.1109/ICHVE.2018.8641909.

[6] M. Kizhlo, A. Kanbergs, and M. Kizhlo, "Correlation Analysis between Grounding Resistance and Seasonal Variations of Upper Soil Resistivity of Two-Year Period in Balozhi, Latvia," in *International Symposium on Power Electronics, Electrical Drives, Automation and Motion*, Sorrento, Italy: IEEE, Jun. 2012, pp. 890–893. doi: 10.1109/SPEEDAM.2012.6264517.

[7] F. E. Asimakopoulou, G. J. Tsekouras, I. F. Gonos, and I. A. Stathopulos, "Estimation of Seasonal Variation of Ground Resistance using Artificial Neural Networks," *Electric Power Systems Research*, vol. 94, pp. 113–121, Jan. 2013, doi: 10.1016/j.epsr.2012.07.018.

[8] C. Thomas and Eskom, "Seasonal Variation of Soil Resistivity and the Correction Factor," presented at the 8th Southern African Regional Conference, Cape Town, South Africa: CIGRE, Nov. 2017.

[9] A. Madikizela, M. Kabeya, and I. E. Davidson, "Seasonal Variation of Soil Resistivity and Corrective Factor for Optimal Substation Earth Grid Design in Eastern Cape," in *2022 30th Southern African Universities Power Engineering Conference (SAUPEC)*, Durban, South Africa: IEEE, Jan. 2022, pp. 1–6. doi: 10.1109/SAUPEC55179.2022.9730743.

[10] C. Wang, X. Liang, E. P. Adajar, and P. Loewen, “Investigation of Seasonal Variations of Tower Footing Impedance in Transmission Line Grounding Systems,” *IEEE Trans. on Ind. Applicat.*, vol. 57, no. 3, pp. 2274–2284, May 2021, doi: 10.1109/TIA.2021.3057349.

[11] A. Samouëlian, I. Cousin, A. Tabbagh, A. Bruand, and G. Richard, “Electrical Resistivity Survey in Soil Science: A Review,” *Soil and Tillage Research*, vol. 83, no. 2, pp. 173–193, Sep. 2005, doi: 10.1016/j.still.2004.10.004.

[12] W. Bai, L. Kong, and A. Guo, “Effects of physical properties on electrical conductivity of compacted lateritic soil,” *Journal of Rock Mechanics and Geotechnical Engineering*, vol. 5, no. 5, pp. 406–411, Oct. 2013, doi: 10.1016/j.jrmge.2013.07.003.

[13] R. Andolfato, D. Cuccarollo, and D. Lewis, “Soil Model Seasonal Analysis for Grounding Systems,” Jan. 2021.

[14] J. D. Rhoades, P. a. C. Raats, and R. J. Prather, “Effects of Liquid-phase Electrical Conductivity, Water Content, and Surface Conductivity on Bulk Soil Electrical Conductivity,” *Soil Science Society of America Journal*, vol. 40, no. 5, pp. 651–655, 1976, doi: 10.2136/sssaj1976.03615995004000050017x.

[15] M. A. Mojid and H. Cho, “Estimating the fully developed diffuse double layer thickness from the bulk electrical conductivity in clay,” *Applied Clay Science*, vol. 33, no. 3, pp. 278–286, Aug. 2006, doi: 10.1016/j.clay.2006.06.002.

[16] L.-W. Kong, W. Bai, and A.-G. Guo, “Effects of Cracks on the Electrical Conductivity of a Fissured Laterite: A Combined Experimental and Statistical Study,” *Geotech. Test. J.*, vol. 35, no. 6, p. 20120070, Nov. 2012, doi: 10.1520/GTJ20120070.

[17] J. Hong-jing, L. Shun-qun, and L. Lin, “The Relationship between the Electrical Resistivity and Saturation of Unsaturated Soil,” *Geology*, vol. 19, 2014.

[18] L. Fang, S. Shulin, and Z. Deheng, “Correlation between Electrical Resistivity and Suction for Unsaturated Coastal Saline Soil,” *IOP Conf. Ser.: Earth Environ. Sci.*, vol. 362, no. 1, p. 012143, Nov. 2019, doi: 10.1088/1755-1315/362/1/012143.

[19] P. J. Higgs, “An investigation of earthing resistances,” *Journal of the Institution of Electrical Engineers*, vol. 68, no. 402, pp. 736–750, Jun. 1930, doi: 10.1049/jiee-1.1930.0078.

[20] L. Kong, H. Md. Sayem, X. Zhang, and S. Yin, “Relationship between Electrical Resistivity and Matric Suction of Compacted Granite Residual Soil,” in *PanAm Unsaturated Soils 2017*, Dallas, Texas: American Society of Civil Engineers, Jun. 2018, pp. 430–439. doi: 10.1061/9780784481707.043.

[21] D. G. Fredlund, H. Rahardjo, and M. D. Fredlund, *Unsaturated soil mechanics in engineering practice*, 1st ed. Hoboken, N.J: John Wiley & Sons, 2012. Accessed: Oct. 30, 2022. [Electronic resource]. Available: http://catalogimages.wiley.com/images/db/jimages/9781118133590.jpg

[22] V. L. Coelho, A. Piantini, H. A. D. Almaguer, R. A. Coelho, W. do C. Boaventura, and J. O. S. Paulino, "The influence of Seasonal Soil Moisture on the Behavior of Soil Resistivity and Power Distribution Grounding Systems," *Electric Power Systems Research*, vol. 118, pp. 76–82, Jan. 2015, doi: 10.1016/j.epsr.2014.07.027.

[23] R. J. Gustafson, R. Pursley, and V. D. Albertson, "Seasonal grounding resistance variations on distribution systems," *IEEE Trans. Power Delivery*, vol. 5, no. 2, pp. 1013–1018, Apr. 1990, doi: 10.1109/61.53115.

[24] Jinliang He *et al.*, "Seasonal Influences on Safety of Substation Grounding System," *IEEE Trans. Power Delivery*, vol. 18, no. 3, pp. 788–795, Jul. 2003, doi: 10.1109/TPWRD.2003.813895.

[25] G. E. Archie, "The Electrical Resistivity Log as an Aid in Determining Some Reservoir Characteristics," *Transactions of the AIME*, vol. 146, no. 01, pp. 54–62, Dec. 1942, doi: 10.2118/942054-G.

[26] M. H. Waxman and L. J. M. Smits, "Electrical Conductivities in Oil-Bearing Shaly Sands," *Society of Petroleum Engineers Journal*, vol. 8, no. 02, pp. 107–122, Jun. 1968, doi: 10.2118/1863-A.

[27] D. Kazmi, S. Qasim, F. I. Siddiqui, and S. B. Azhar, "Exploring the Relationship between Moisture Content and Electrical Resistivity for Sandy and Silty Soils," vol. 5, no. 7, Jul. 2016.

[28] H. Sun *et al.*, "Assessing the value of electrical resistivity derived soil water content: Insights from a case study in the Critical Zone of the Chinese Loess Plateau," *Journal of Hydrology*, vol. 589, p. 125132, Oct. 2020, doi: 10.1016/j.jhydrol.2020.125132.

[29] Y. Guan, K. Grote, J. Schott, and K. Leverett, "Prediction of Soil Water Content and Electrical Conductivity Using Random Forest Methods with UAV Multispectral and Ground-Coupled Geophysical Data," *Remote Sensing*, vol. 14, p. 1023, Feb. 2022, doi: 10.3390/rs14041023.

[30] P. De Vita, R. Di Maio, and E. Piegari, "A study of the correlation between electrical resistivity and matric suction for unsaturated ash-fall pyroclastic soils in the Campania region (southern Italy)," *Environmental Earth Sciences*, vol. 67, no. 3, pp. 787–798, Oct. 2012, doi: 10.1007/s12665-012-1531-4.

[31] E. Piegari and R. Di Maio, “Estimating soil suction from electrical resistivity,” *Nat. Hazards Earth Syst. Sci.*, vol. 13, no. 9, pp. 2369–2379, Sep. 2013, doi: 10.5194/nhess-13-2369-2013.

[32] R. M. Azoor, R. N. Deo, N. Birbilis, and J. Kodikara, “On the optimum soil moisture for underground corrosion in different soil types,” *Corrosion Science*, vol. 159, p. 108116, Oct. 2019, doi: 10.1016/j.corsci.2019.108116.

[33] R. Azoor, R. Deo, B. Shannon, and J. Kodikara, *Using soil moisture retention curves and corrosimetry to characterise the role of soil moisture in underground corrosion*. 2019.

[34] V. P. Androvitsaneas, I. F. Gonos, and I. A. Stathopulos, “Performance of Ground Enhancing Compounds during the Year,” in *2012 International Conference on Lightning Protection (ICLP)*, Vienna, Austria: IEEE, Sep. 2012, pp. 1–5. doi: 10.1109/ICLP.2012.6344356.

[35] A. Galvan D., G. Pretelin G., and E. Gaona E., “Practical evaluation of ground enhancing compounds for high soil resistivities,” in *2010 30th International Conference on Lightning Protection (ICLP)*, Cagliari: IEEE, Sep. 2010, pp. 1–4. doi: 10.1109/ICLP.2010.7845889.

[36] J. A. Laver and H. Griffiths, “The Variability of Soils in Earthing Measurements and Earthing System Performance,” *Rev. Energ. Ren. : Power Engineering*, pp. 57–61, 2001.

[37] J. He, Y. Gao, R. Zeng, W. Sun, J. Zou, and Z. Guan, “Optimal Design of Grounding System Considering the Influence of Seasonal Frozen Soil Layer,” *IEEE Trans. Power Delivery*, vol. 20, no. 1, pp. 107–115, Jan. 2005, doi: 10.1109/TPWRD.2004.835434.

[38] N. Abdullah, A. M. A. Marican, M. Osman, and N. A. A. Rahman, “Case study on impact of seasonal variations of soil resistivities on substation grounding systems safety in tropical country,” in *2011 7th Asia-Pacific International Conference on Lightning*, Nov. 2011, pp. 150–154. doi: 10.1109/APL.2011.6111092.

[39] B. E. Kushare and M. G. Unde, “Impact of seasonal variation of soil resistivity on safety of substation grounding system,” in *Fifth International Conference on Advances in Recent Technologies in Communication and Computing (ARTCom 2013)*, Bangalore, India: Institution of Engineering and Technology, 2013, pp. 173–182. doi: 10.1049/cp.2013.2199.

[40] H. Kutter and W. Lange, “Earthing improvement by using Bentonite,” *Elecktrie*, vol. 21, pp. 421–424, 1967.

[41] Okyere Philip and Eduful George, “Reducing Earth Electrode Resistance by Replacing Soil in Critical Resistance Area,” *Journal of Modern Engineering*, vol. 6, 2006.

[42] G. Eduful, J. E. Cole, and P. Y. Okyere, “Optimum mix of ground electrodes and conductive backfills to achieve a low ground resistance,” in *2009 2nd International Conference on Adaptive Science & Technology (ICAST)*, Accra, Ghana: IEEE, Dec. 2009, pp. 140–145. doi: 10.1109/ICASTECH.2009.5409734.

[43] L.-H. Chen, J.-F. Chen, T.-J. Liang, and W.-I. Wang, “A research on used quantity of ground resistance reduction agent for ground systems,” *Euro. Trans. Electr. Power*, p. n/a-n/a, 2009, doi: 10.1002/etep.322.

[44] A. A. Al-Arainy, Y. Khan, M. I. Qureshi, N. H. Malik, and F. R. Pazheri, “Optimized pit configuration for efficient grounding of the power system in high resistivity soils using low resistivity materials,” in *2011 Fourth International Conference on Modeling, Simulation and Applied Optimization*, Kuala Lumpur, Malaysia: IEEE, Apr. 2011, pp. 1–5. doi: 10.1109/ICMSAO.2011.5775486.

[45] Y. Khan, F. R. Pazheri, N. H. Malik, A. A. Al-Arainy, and M. I. Qureshi, “Novel approach of estimating grounding pit optimum dimensions in high resistivity soils,” *Electric Power Systems Research*, vol. 92, pp. 145–154, Nov. 2012, doi: 10.1016/j.epsr.2012.06.003.

[46] J. Trifunovic, “A Mathematical Method for Determining Optimal Quantity of Backfill Materials Used for Grounding Resistance Reduction,” *Mathematical Problems in Engineering*, vol. 2018, pp. 1–9, 2018, doi: 10.1155/2018/4863702.

[47] Z. I. Rahman Noor, B. Anggoro Soedjarno P, and P. O. Hadi, “Analysis of Bentonite AC and DC Performance Under Water Content and Chemical Content Variation for Grounding Applications,” in *2021 3rd International Conference on High Voltage Engineering and Power Systems (ICHVEPS)*, Bandung, Indonesia: IEEE, Oct. 2021, pp. 247–252. doi: 10.1109/ICHVEPS53178.2021.9600940.

[48] V. P. Androvitsaneas, G. J. Tsekouras, I. F. Gonos, and I. A. Stathopulos, “Design of an Artificial Neural Network for Ground Resistance Forecasting,” in *Power Generation, Transmission, Distribution and Energy Conversion*, Athens Greece, Nov. 2014. doi: http://dx.doi.org/10.13140/RG.2.1.2509.6807.

[49] F. E. Asimakopoulou, G. J. Tsekouras, I. F. Gonos, and I. A. Stathopulos, “Artificial neural network approach on the seasonal variation of soil resistance,” in *2011 7th Asia-Pacific International Conference on Lightning*, Chengdu, China: IEEE, Nov. 2011, pp. 794–799. doi: 10.1109/APL.2011.6110235.

[50] M. U. A. Khan, S. K. Shukla, and M. N. A. Raja, “Soil–conduit interaction: an artificial intelligence application for reinforced concrete and corrugated steel conduits,” *Neural Comput & Applic*, vol. 33, no. 21, pp. 14861–14885, Nov. 2021, doi: 10.1007/s00521-021-06125-0.

[51] Z. Duan, X. Yan, Q. Sun, X. Tan, and X. Chen, “New models for calculating the electrical resistivity of loess affected by moisture content and NaCl concentration,” *Environ Sci Pollut Res*, vol. 29, no. 12, pp. 17280–17294, Mar. 2022, doi: 10.1007/s11356-021-16971-z.

[52] S. Anbazhagan, “Athens seasonal variation of ground resistance prediction using Neural Networks,” *IJSC*, vol. 06, no. 01, pp. 1113–1116, Oct. 2015, doi: 10.21917/ijsc.2015.0154.

[53] Z. G. Datsios and P. N. Mikropoulos, “Characterization of the frequency dependence of the electrical properties of sandy soil with variable grain size and water content,” *IEEE Transactions on Dielectrics and Electrical Insulation*, vol. 26, no. 3, pp. 904–912, Jun. 2019, doi: 10.1109/TDEI.2018.007864.

[54] Z. G. Datsios, P. N. Mikropoulos, and I. Karakousis, “Laboratory characterization and modeling of DC electrical resistivity of sandy soil with variable water resistivity and content,” *IEEE Transactions on Dielectrics and Electrical Insulation*, vol. 24, no. 5, pp. 3063–3072, Oct. 2017, doi: 10.1109/TDEI.2017.006583.

[55] Woessner, William W and Eileen P. Poeter, *Hydrogeologic Properties of Earth Materials and Principles of Groundwater Flow.*, 1st ed. Ontario, Canada: The Groundwater Project, Guelph, 2020. [Online]. Available: https://gw-project.org/books/hydrogeologic-properties-of-earth-materials-and-principles-of-groundwater-flow/

[56] S. Assouline, “Infiltration into soils: Conceptual approaches and solutions: review: Infiltration into soils,” *Water Resour. Res.*, vol. 49, no. 4, pp. 1755–1772, Apr. 2013, doi: 10.1002/wrcr.20155.

[57] IUSS Working Group WRB., *International soil classification system for naming soils and creating legends for soil maps*, Vienna, Austria., 2022. [Online]. Available: https://wrb.isric.org/files/WRB_fourth_edition_2022-12-18.pdf

[58] W. M. Alley, T.E. Reilly, and O.L. Franke, “Sustainability of Ground-Water Resources,” Denver, Colorado, 1999. [Online]. Available: https://pubs.usgs.gov/circ/circ1186/pdf/circ1186.pdf

[59] M. Widomski, D. Kowalski, M. Iwanek, and G. Lagod, *Modeling of water flow and pollutants transport in porous media: with exemplary calculations in FEFLOW*, 1st ed., vol. 1. Lublin, Poland: Lublin University of Technology, 2013.

[60] V. V. Sai and T. Hemalatha, "Computational methods for simulating soil parameters using electrical resistivity technique," in *2017 8th International Conference on Computing, Communication and Networking Technologies (ICCCNT)*, Delhi: IEEE, Jul. 2017, pp. 1–7. doi: 10.1109/ICCCNT.2017.8204145.

[61] A. A. Khafizov, R. S. Akhmetshin, R. T. Nasibullin, and L. R. Sarimov, "Method Increasing the Reliability of the Soil Measured Specific Electrical Resistance in the Field," in *2019 International Multi-Conference on Industrial Engineering and Modern Technologies (FarEastCon)*, Vladivostok, Russia: IEEE, Oct. 2019, pp. 01–04. doi: 10.1109/FarEastCon.2019.8934055.

[62] F. I. Siddiqui and S. B. A. B. S. Osman, "Simple and multiple regression models for relationship between electrical resistivity and various soil properties for soil characterization," *Environ Earth Sci*, vol. 70, no. 1, pp. 259–267, Sep. 2013, doi: 10.1007/s12665-012-2122-0.

[63] K. Wang, Z. Xia, and X. Li, "Matrix Suction Evaluation of Soil-Rock Mixture Based on Electrical Resistivity," *Water*, vol. 13, no. 20, p. 2937, Oct. 2021, doi: 10.3390/w13202937.

[64] J. R. Philip, "Evaporation and moisture and heat fields in the soil," *Journal of the Atmospheric Sciences*, vol. 14, no. 4, 1957, Accessed: Jul. 12, 2023. [Online]. Available: https://journals.ametsoc.org/view/journals/atsc/14/4/1520-0469_1957_014_0354_eamahf_2_0_co_2.xml

[65] P. W. Mitchell, "Footing design for residential type structures in arid climates," *Australian Geomechanics Journal*, vol. 43, pp. 51–68, Dec. 2008.

[66] Krahn, J and Fredlund, D. G, "On total Matric suction and osmotic suction," *Soil Science*, vol. 114, no. 5, pp. 339–348, Nov. 1972.

[67] J. Selker and D. Or, *Fundamentals of Soil Hydrology and Bio-Physics*, 1st ed., vol. 1. Corvallis Oregon: Oregon State University, 2019. Accessed: May 01, 2023. [Online]. Available: https://open.oregonstate.education/soilhydrologyandbiophysics/chapter/fundamentals-of-soil-hydrology-and-bio-physics/

[68] ASTM D5298 – 16, *Standard Test Method for Measurement of Soil Potential (Suction) Using Filter Paper*, 2016.

[69] J. Kondo and J. Xu, “Seasonal Variations in the Heat and Water Balances for Nonvegetated Surfaces,” *Journal of Applied Meteorology and Climatology*, vol. 36, no. 12, pp. 1676–1695, Dec. 1997, doi: 10.1175/1520-0450(1997)036<1676:SVITHA>2.0.CO;2.

[70] Peter W. Mitchell, *The Structural Analysis of Footings on Expansive Soils*, 2nd ed. Newtown, South Australia: Kenneth W. G. Smith & Associates Pty. Ltd., 1980.

[71] R. Wallach, “Physical Characteristics of Soilless Media,” in *Soilless Culture (Second edition)*, 2nd ed., Michael Raviv, J. Heinrich Lieth, and Asher Bar-Tal, Eds., Elsevier, 2019, pp. 33–112. Accessed: Feb. 25, 2023. [Online]. Available: https://linkinghub.elsevier.com/retrieve/pii/B9780444529756500058

[72] M. W. Farthing and F. L. Ogden, “Numerical Solution of Richards’ Equation: A Review of Advances and Challenges,” *Soil Sci. Soc. Am. j.*, vol. 81, no. 6, pp. 1257–1269, Nov. 2017, doi: 10.2136/sssaj2017.02.0058.

[73] R. R. Hayes, “Integration of EIT, Soil Structure and Plant Physiology Models for 3D Imaging of Crop Root Function Phnotype,” M.Phil, University of Manchester, Manchester, 2015.

[74] M. Th. Van Genuchten and Y. A. Pachepsky, “Hydraulic Properties of Unsaturated Soils,” in *Encyclopedia of Agrophysics*, J. Gliński, J. Horabik, and J. Lipiec, Eds., in Encyclopedia of Earth Sciences Series. , Dordrecht: Springer Netherlands, 2014, pp. 368–376. doi: 10.1007/978-90-481-3585-1_69.

[75] C. Chen, K. Hu, T. Ren, Y. Liang, and E. Arthur, “A Simple Method for Determining the Critical Point of the Soil Water Retention Curve,” *Soil Science Society of America Journal*, vol. 81, no. 2, pp. 250–258, Mar. 2017, doi: 10.2136/sssaj2016.06.0187.

[76] V. K. Too, C. T. Omuto, E. K. Biamah, and J. P. O. Obiero, “Suitability of Soil Water Retention Characteristic Models (SWRC) in Regions and Soil Depth,” *JWARP*, vol. 11, no. 06, pp. 740–747, 2019, doi: 10.4236/jwarp.2019.116044.

[77] Rukshan Maliq Azoor, “Evaluation of soil aeration as applicable to underground metal corrosion,” Doctor of Philosophy, Monash University, Australia, 2019.

[78] Q. Zhai, H. Rahardjo, and A. Satyanaga, “Effects of residual suction and residual water content on the estimation of permeability function,” *Geoderma*, vol. 303, pp. 165–177, Oct. 2017, doi: 10.1016/j.geoderma.2017.05.019.

[79] J. Zhou, J. Ren, and Z. Li, “An Improved Prediction Method of Soil-Water Characteristic Curve by Geometrical Derivation and Empirical Equation,” *Mathematical Problems in Engineering*, vol. 2021, pp. 1–22, Jun. 2021, doi: 10.1155/2021/9956824.

[80] A. M. Almeida, E. F. Fraga Junior, R. D. Coelho, T. H. S. Barros, and A. J. Farias, “Field capacity estimation from the inflection point of the soil moisture retention curve,” in *IV Inovagri International Meeting*, Fortaleza, Ceará, Brasil: Inovagri/esalq-usp/abid/ufr8/inct-elEI/INCTSal/INSTITUTO FUTURE, 2017. doi: 10.7127/iv-inovagri-meeting-2017-res0250268.

[81] L. Guarracino, “Estimation of saturated hydraulic conductivity Ks from the van Genuchten shape parameter α,” *Water Resources Research*, vol. 43, no. 11, 2007, doi: 10.1029/2006WR005766.

[82] Y. Mualem, “A new model for predicting the hydraulic conductivity of unsaturated porous media,” *Water Resour. Res.*, vol. 12, no. 3, pp. 513–522, Jun. 1976, doi: 10.1029/WR012i003p00513.

[83] R. H. Brooks and A. T. Corey, “Hydraulic properties of porous media,” *Hydrology Paper, Colorado State University*, vol. 27, no. 3, 1963.

[84] M. Van Genuchten, “A Closed-form Equation for Predicting the Hydraulic Conductivity of Unsaturated Soils1,” *Soil Science Society of America Journal*, vol. 44, Sep. 1980, doi: 10.2136/sssaj1980.03615995004400050002x.

[85] D. G. Fredlund and A. Xing, “Equations for the soil-water characteristic curve,” *Can. Geotech. J.*, vol. 31, no. 4, pp. 521–532, Aug. 1994, doi: 10.1139/t94-061.

[86] P. Glover, “A new theoretical interpretation of Archie’s saturation exponent,” *Solid Earth*, vol. 8, pp. 805–816, Jul. 2017, doi: 10.5194/se-8-805-2017.

[87] Y. Fu, R. Horton, T. Ren, and J. L. Heitman, “A general form of Archie’s model for estimating bulk soil electrical conductivity,” *Journal of Hydrology*, vol. 597, p. 126160, Jun. 2021, doi: 10.1016/j.jhydrol.2021.126160.

[88] A. Martins, S. Mariano, and M. D. Rosario Calado, “The IEEE Model for a Ground Rod in a Two Layer Soil – A FEM Approach,” in *Finite Element Analysis - New Trends and Developments*, 1st ed., vol. 1, 1 vols., F. Ebrahimi, Ed., in 1, no. 1, vol. 1. , Rijeka, Croatia: InTech, 2012, pp. 143–160. doi: 10.5772/48252.

[89] F. J. Leij, W. J. Alves, M. T. Van Genuchten, and J. R. Williams, “UNSODA Unsaturated Soil Hydraulic Database User’s Manual Version 1.0. EPA/600/R-96/095 (NTIS 97-149496), 1996.”

[90] R. F. Carsel and R. S. Parrish, “Developing joint probability distributions of soil water retention characteristics,” *Water Resour. Res.*, vol. 24, no. 5, pp. 755–769, May 1988, doi: 10.1029/WR024i005p00755.

[91] COMSOL Multiphysics® v. 5.3, “User’ Guide.” COMSOL Inc., 2017.

[92] O. S. Nnamdi and G. Chandima, “New Method for Modelling Seasonal Variation in Resistance and Performance of Earthing Systems,” *Energies*, vol. 16, no. 19, p. 7002, Oct. 2023, doi: 10.3390/en16197002.

[93] George Frank Tagg, *Earth Resistance*. New York, USA: Pitman Publishers, 1964.

[94] Sajad Samadinasab, Farhad Namdari, and Mohammad Bakhshipour, “A Novel Approach for Earthing System Design Using Finite Element Method,” *Journal of Intelligent Procedures in Electrical Technology*, vol. 8, no. 29, pp. 54–63, 2017.

[95] B. Abdelkader, Z. Boubakeur, S. Tahar, and S. Yahia, “Implentation and Design of Grounding Systems Using COMSOL multiphysics,” in *020 1st International Conference on Communications, Control Systems and Signal Processing (CCSSP)*, EL OUED, Algeria: IEEE, May 2020, pp. 513–517. doi: 10.1109/CCSSP49278.2020.9151798.

[96] M. Saleh Asheghabadi and Z. Ali, “Infinite element boundary conditions for dynamic models under seismic loading,” *Indian J Phys*, vol. 94, no. 6, pp. 907–917, Jun. 2020, doi: 10.1007/s12648-019-01533-4.

[97] G. S. Schajer and L. To, “Simulation of Infinite Boundaries for Axisymmetric Finite Element Models,” *Exp Mech*, vol. 63, no. 5, pp. 965–971, Jun. 2023, doi: 10.1007/s11340-023-00963-w.

[98] W. Jones, “Bentonite Rods Assure Ground Rod Installation In Problem Soils,” *IEEE Trans. on Power Apparatus and Syst.*, vol. PAS-99, no. 4, pp. 1343–1346, Jul. 1980, doi: 10.1109/TPAS.1980.319556.

[99] C.-N. Chang and C.-H. Lee, “Computation of ground resistances and assessment of ground grid safety at 161/23.9-kV indoor-type substation,” *IEEE Transactions on Power Delivery*, vol. 21, no. 3, pp. 1250–1260, Jul. 2006, doi: 10.1109/TPWRD.2005.860245.

[100] H. G. Zaini and S. S. Ghoneim, “Earth surface potential and grounding resistance for grounding grid in two-layer model soil,” in *2012 IEEE International Conference on Power System Technology (POWERCON)*, Oct. 2012, pp. 1–5. doi: 10.1109/PowerCon.2012.6401396.

[101] C. J. Blattner, “Study of Driven Ground Rods and Four Point Soil Resistivity Tests,” *IEEE Transactions on Power Apparatus and Systems*, vol. PAS-101, no. 8, pp. 2837–2850, Aug. 1982, doi: 10.1109/TPAS.1982.317563.

[102] J. A. Sullivan, “Earthing calculations using a commercial program,” in *IEE Seminar on Substation Earthing - Shedding Light on the Black Art (Ref. No. 2000/033)*, Mar. 2000, p. 1/1-111. doi: 10.1049/ic:20000191.

[103] J. A. Sullivan, “Alternative earthing calculations for grids and rods,” *IEE Proc., Gener. Transm. Distrib.*, vol. 145, no. 3, p. 271, 1998, doi: 10.1049/ip-gtd:19981696.

[104] R. B. Carpenter and J. A. Lanzoni, “Designing for A Low Resistance Earth Interface (Grounding).” Lightning Eliminators & Consultants Inc, Oct. 2007.

[105] S. N. Onyedikachi, C. Gomes, and J. Van Coller, “Equations for Predicting the Volumetric Water Content affecting the Resistivity of Soil in the Vicinity of a Driven Earth Electrode in Variably Saturated Homogeneous Soil,” in *2022 36th International Conference on Lightning Protection (ICLP)*, Cape Town, South Africa: IEEE, Oct. 2022, pp. 1–6. doi: 10.1109/ICLP56858.2022.9942536.

[106] R. G. McKeen and L. D. Johnson, “Climate-Controlled Soil Design Parameters for Mat Foundations,” *J. Geotech. Engrg.*, vol. 116, no. 7, pp. 1073–1094, Jul. 1990, doi: 10.1061/(ASCE)0733-9410(1990)116:7(1073).

[107] R. M. Azoor, R. N. Deo, N. Birbilis, and J. K. Kodikara, “Coupled Electro-Chemical-Soil Model to Evaluate the Influence of Soil Aeration on Underground Metal Pipe Corrosion,” *Corrosion*, vol. 74, no. 11, pp. 1177–1191, Nov. 2018, doi: 10.5006/2860.

[108] B. Abdelkader, B. Zegnini, and S. Tahar, “Determination of the resistance of a grounding system with application of finite element method,” *Przeglad Elektrotechniczny*, vol. 2021, pp. 5–11, May 2021, doi: 10.15199/48.2021.05.02.

Appendices

Appendix A: Tables A1 to A26

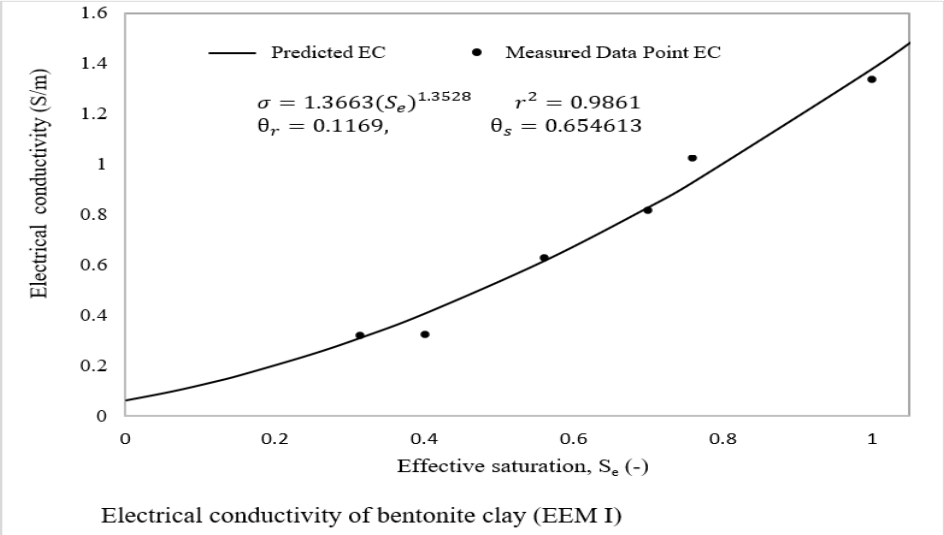
Table A1: Measured values of water content and resistivity for EEM I

θ	Saturation		electric conductivity $(\Omega m)^{-1}$	
	S_e (effective)	S_d (degree)	$\sigma_{measured}$	$\sigma_{predicted}$
0.11720	0.00056	0.17904	-	0.06237
0.15000	0.06156	0.22914	-	0.09723
0.18000	0.11735	0.27497	-	0.13500
0.20000	0.15454	0.30552	-	0.16319
0.25000	0.24753	0.38190	-	0.24384
0.28609	0.31465	0.43704	0.31949	0.31082
0.33257	0.40109	0.50804	0.32468	0.40756
0.41882	0.56149	0.63980	0.62893	0.61721
0.49346	0.70029	0.75381	0.81766	0.82911
0.52513	0.75919	0.80219	1.02564	0.92733
0.65461	1.00000	1.00000	1.33690	1.37884

Water Content and resistivity measurement for Bentonite (EEM I)

Dry Density of Bentonite Powder (g/cm^3)	2.26
Gravimetric WC of Bentonite Powder (%)	11.27
Mass of Resistivity Box w/Electrodes (g)	109.89
Area of current Electrode (cm^2)	9.00
Potential Electrode gap (cm)	9.00
Current Electrode Gap (cm)	13.80
Volume of Resistivity Box (cm^3)	124.20
Volumetric water content = Gravimetric water content / Bulk density	
Volumetric water content = 100(Wet mass – Dry Mass) / Wet Volume	
Bulk density = Dry Mass / Wet Volume	
Gravimetric Water Content = Oven Wet mass – Oven Dry mass) / Oven Dry Mass	

Source: Author's conceptualisation.



Electrical conductivity of bentonite clay (EEM I)

Source: Author's conceptualisation.

Table A2: Post-simulation computed resistance Re (Ω) of earthing rod in a single layer and corresponding volumetric water content, subsoil resistivity and soil suction

Soil condition		**Clayey soil**			**Silty soil**			**Sandy clay soil**		
h_p **(m)**	ψ **(kPa)**	θ**(%)**	ρ**(Ωm)**	R_e **(Ω)**	θ**(%)**	ρ**(Ωm)**	R_e **(Ω)**	θ**(%)**	ρ**(Ωm)**	R_e **(Ω)**
-0.1000	-0.98	51.00	6.87	2.18	46.00	15.43	4.89	38.00	135.40	42.90
-0.1095	-1.07	51.00	6.87	2.18	46.00	15.43	4.89	38.00	135.41	42.90
-0.1107	-1.09	51.00	6.87	2.18	46.00	15.43	4.89	38.00	135.41	42.90
-0.1667	-1.63	50.99	6.87	2.18	45.99	15.44	4.89	37.99	135.47	42.92
-0.1798	-1.76	50.99	6.87	2.18	45.99	15.44	4.89	37.99	135.48	42.92
-2.7510	-26.98	49.86	7.22	2.29	44.37	16.13	5.11	36.98	146.79	46.50
-3.3650	-33.00	49.46	7.35	2.33	43.77	16.40	5.20	36.63	150.99	47.84
-3.3734	-33.08	49.46	7.35	2.33	43.76	16.41	5.20	36.62	151.05	47.86
-5.00	-49.03	48.26	7.76	2.46	41.98	17.26	5.47	35.60	164.35	52.07
-10.00	-98.07	43.92	9.59	3.04	35.569	21.208	6.72	31.97	228.53	72.40
-15.00	-147.10	39.04	12.62	4.00	28.47	28.13	8.91	27.97	351.41	111.33
-25.00	-245.17	31.03	22.32	7.07	17.09	55.81	17.68	21.66	871.91	276.23
-32.22	-315.98	29.25	26.11	8.27	14.95	67.62	21.42	20.41	1101.10	348.85
-50.00	-490.34	27.05	32.37	10.26	12.59	87.65	27.77	18.90	1514.10	479.67
-100.00	-980.68	24.50	43.14	13.67	10.18	123.61	39.16	17.20	2312.80	732.73
-152.76	-1498.09	23.24	50.72	16.07	9.11	150.05	47.54	16.37	2937.20	930.56
-300.00	-2942.04	21.52	65.04	20.60	7.79	201.95	63.98	15.26	4237.50	1342.50
-600.00	-5884.08	20.02	83.42	26.43	6.78	271.93	86.15	14.32	6117.00	1937.90
-1000	-9806.81	19.05	100.02	31.69	6.19	337.76	107.01	13.72	7992.90	2532.30
-2161	-21192.51	17.78	131.29	41.60	5.49	467.48	148.10	12.95	11936.00	3781.60
-3000	-29420.42	17.30	147.36	46.69	5.25	536.62	170.01	12.66	14151.00	4483.20
-5000	-49034.03	16.61	176.35	55.87	4.93	665.02	210.69	12.26	18439.00	5841.70
-10000	-98068.06	15.78	224.94	71.26	4.59	889.40	281.77	11.78	26396.00	8362.60

Source: Author's conceptualisation. Post-simulation computed resistance Re (Ω) of earthing rod in a single homogeneous layer of clayey, silty, and sandy clay soils and their corresponding volumetric water content θ (%) and resistivity ρ (Ωm) at different values of soil suction.

Table A3: Mesh statistics for soil domain showing infinite element domain (IED)

		Subsoil domain radius					
		11.5 m		25.5 m		65.5 m	
Mesh element geometry		**w/o IED**	**w IED**	**w/o IED**	**w IED**	**w/o IED**	**w IED**
Width of IED		-	3 m	-	3 m	-	3 m
Mesh Area		230 m^2	230 m^2	510 m^2	510 m^2	1310 m^2	1310 m^2
Number of elements		4141	4171	4425	4531	4537	4635
Free Triangles		4141	3982	4425	4314	4537	4453
Free Quadrilaterals		-	189	-	217	-	182
Mesh vertices		2232	2350	2382	2554	2452	2603
Edge elements		561	612	575	634	601	656
Vertex element		20	25	34	39	74	79
Element Area Ratio		2.7E-05	2.7E-05	4.6E-06	1.8E-05	4.65E-06	5.22E-06
		11.5 m		**25.5 m**		**65.5 m**	
Mesh element quality		**w/o IED**	**wIED**	**w/o IED**	**wIED**	**w/o IED**	**wIED**
Skewness	Minimum	0.5510	0.4285	0.5382	0.4328	0.4773	0.3243
	Average	0.8150	0.8211	0.8225	0.8264	0.8171	0.8223
Maximum Angle	Minimum	0.6978	0.5799	0.6887	0.5969	0.6385	0.4316
	Average	0.8992	0.9025	0.9056	0.9074	0.9046	0.9077
Volume versus Circumradius	Minimum	0.6755	0.4477	0.6625	0.4190	0.5647	0.1768
	Average	0.9243	0.9125	0.9298	0.9116	0.9293	0.9080
Volume versus length	Minimum	0.8086	0.5296	0.8013	0.4211	0.7394	0.1772
	Average	0.9490	0.9367	0.9526	0.9340	0.9517	0.9299
Condition number	Minimum	0.8086	0.5270	0.8013	0.4182	0.7394	0.1740
	Average	0.9490	0.9367	0.9526	0.9340	0.9517	0.9299
Growth rate	Minimum	0.4680	0.4402	0.4473	0.2629	0.4759	0.3309
	Average	0.7961	0.8043	0.8062	0.8100	0.7932	0.3309
Curved skewness	Minimum	0.5510	0.4285	0.5382	0.4328	0.4773	0.3243
	Average	0.8149	0.8210	0.8224	0.8263	0.8169	0.8222

Source: Author's conceptualisation. Mesh statistics for soil domain radii (11.5, 25.5 and 60.5 m) with (w) and without (w/o) infinite element domain (IED) at the boundary of the soil domain.

Table A4: Effect of width of infinite element domain on earthing resistance

Model Parameters (m)		Resistance: 13.5 m subsoil width			Resistance: 25.5 m subsoil width			Resistance: 65.5 m subsoil width		
hp	**IED**	**Sim**	**Analy.**	**% diff.**	**Sim**	**Analy.**	**% diff.**	**Sim**	**Analy.**	**% diff.**
-0.1	0	4.82	5.03	4.15	4.88	5.03	2.95	4.89	5.03	2.72
	1	4.95	5.03	1.44	4.90	5.03	2.54	4.89	5.03	2.72
	2	4.96	5.03	1.24	4.90	5.03	2.51	4.89	5.03	2.72
	3	4.98	5.03	0.99	4.90	5.03	2.48	4.89	5.03	2.72
	5	5.01	5.03	0.32	4.91	5.03	2.41	4.89	5.03	2.72
-3.3734	0	5.12	5.34	4.16	5.18	5.34	2.95	5.20	5.34	2.72
	1	5.27	5.34	1.44	5.21	5.34	2.54	5.20	5.34	2.72
	2	5.28	5.34	1.24	5.21	5.34	2.51	5.20	5.34	2.72
	3	5.29	5.34	0.99	5.21	5.34	2.48	5.20	5.34	2.72
	5	5.33	5.34	0.32	5.21	5.34	2.41	5.20	5.34	2.72
-152.76	0	46.84	48.87	4.15	47.42	48.87	2.95	47.54	48.87	2.73
	1	48.16	48.87	1.44	47.63	48.87	2.54	47.54	48.87	2.72
	2	48.26	48.87	1.24	47.64	48.87	2.51	47.54	48.87	2.72
	3	48.38	48.87	0.99	47.65	48.87	2.48	47.54	48.87	2.72
	5	48.71	48.87	0.32	47.69	48.87	2.40	47.54	48.87	2.72
-200	0	52.80	55.09	4.16	53.46	55.09	2.95	53.59	55.09	2.72
	1	54.29	55.09	1.44	53.69	55.09	2.54	53.59	55.09	2.72
	2	54.41	55.09	1.23	53.71	55.09	2.51	53.59	55.09	2.72
	3	54.55	55.09	0.99	53.72	55.09	2.48	53.59	55.09	2.72
	5	54.91	55.09	0.32	53.76	55.09	2.41	53.59	55.09	2.72

Source: Author's conceptualisation. Percentage difference (% diff.) analysis between analytical (Analy.) and simulation (Sim) resistance of the effect of infinite element domain (IED) width (0, 1, 2, 3, 5 m) in different subsoil domain width (13.5, 25.5, 65.5 m) over a range of soil conditions (pressure head, h_p).

Table A5: Effect of infinite element domain on ground surface electric potential

	h_p = – 0.98 kPa		h_p = – 33 kPa		h_p = – 1500 kPa		h_p = – 49034.03 kPa	
Distance (m)	**wIED**	**w/o IED**	**wIED**	**w/o IED**	**wIED**	**w/o IED**	**wIED**	**w/o IED**
0	4.82	4.97	5.12	5.29	46.84	47.54	207.58	210.70
1	1.28	1.44	1.36	1.53	12.48	13.19	55.29	58.45
2	0.80	0.96	0.85	1.02	7.78	8.50	34.50	37.68
3	0.55	0.71	0.59	0.75	5.38	6.10	23.84	27.05
4	0.40	0.56	0.43	0.60	3.91	4.65	17.34	20.59
5	0.30	0.46	0.32	0.49	2.93	3.68	13.00	16.30
6	0.23	0.39	0.24	0.41	2.24	2.99	9.91	13.27
7	0.18	0.34	0.19	0.36	1.71	2.49	7.59	11.03
7.5	0.15	0.32	0.16	0.34	1.50	2.29	6.65	10.13
8	0.13	0.30	0.14	0.32	1.30	2.10	5.78	9.31
9	0.10	0.26	0.11	0.28	0.98	1.80	4.32	7.96
10	0.07	0.24	0.08	0.25	0.70	1.55	3.11	6.87
10.5	0.06	0.23	0.06	0.24	0.59	1.45	2.60	6.42
11	0.05	0.16	0.05	0.17	0.47	0.78	2.08	3.46
12	0.03	0.07	0.03	0.07	0.27	0.11	1.18	0.49
13	0.01	0.02	0.01	0.02	0.09	0.00	0.38	0.00
13.5	0.00	0.00	0.00	0.00	0.00	0.00	0.00	0.00

Source: Author's conceptualisation. Ground surface electric potential of 13.5 m width subsoil domain models with infinite element domain (wIED) and without (w/o) IED under –0.98, –33, –1500, and –49034.03 kPa soil suctions.

Table A6: Effect of subsoil size with infinite element size on subsoil water content and resistivity).

Parameters			Soil domain		Resistance (Ω)				
Subsoil width (m)	Soil suction					Simulation		% difference	
	kPa	pF	θ (%)	ρ (Ωm)	Analytical	w/o IED	with IED	w/o IED	with IED
	-0.98	1.00	46.00	15.43	5.03	4.82	4.98	4.15	0.99
	-33	2.53	43.76	16.41	5.34	5.12	5.29	4.16	0.99
	-1500	4.18	9.11	150.05	48.87	46.84	48.38	4.15	0.99
	-1961.36	4.30	8.54	169.16	55.09	52.80	54.55	4.16	0.99
	-9806.8	5.00	6.19	337.76	110.00	105.43	108.91	4.15	0.99
13.5	-49034.03	5.70	4.93	665.02	216.58	207.58	214.44	4.16	0.99
	-0.98	1.00	46.00	15.43	5.03	4.88	4.90	2.95	2.48
	-33	2.53	43.76	16.41	5.34	5.18	5.21	2.95	2.48
	-1500	4.18	9.11	150.05	48.87	47.42	47.65	2.95	2.48
	-1961.36	4.30	8.54	169.16	55.09	53.46	53.72	2.95	2.48
	-9806.8	5.00	6.19	337.76	110.00	106.75	107.27	2.95	2.48
25.5	-49034.03	5.70	4.93	665.02	216.58	210.19	211.20	2.95	2.48
	-0.98	1.00	46.00	15.43	5.03	4.89	4.89	2.72	2.72
	-33	2.53	43.76	16.41	5.34	5.20	5.20	2.72	2.72
	-1500	4.18	9.11	150.05	48.87	47.54	47.54	2.72	2.72
	-1961.36	4.30	8.54	169.16	55.09	53.59	53.59	2.72	2.72
	-9806.8	5.00	6.19	337.76	110.00	107.01	107.01	2.72	2.72
65.5	-49034.03	5.70	4.93	665.02	216.58	210.68	210.69	2.72	2.72

Source: Author's conceptualisation. Simulation result showing subsoil water content (θ) and resistivity (ρ) and earthing resistance analysis of a vertical rod in three subsoil domain widths (13.5, 25.5, and 65.6 m) with (3 m diameter) infinite element radius (wIED) and without IED (w/o IED

Table A7: Effect of size of subsoil domain on hydro-geophysical earthing modelling

Pressure head (m)	Subsoil domain			Resistance (Ω)		
	Radius (m)	θ (%)	ρ (Ωm)	Simulation	Analytical	% Diff.
-0.10	7.5	46.00	15.43	4.70	5.03	6.53
-0.10	10.5	46.00	15.43	4.77	5.03	5.01
-0.10	15.5	46.00	15.43	4.84	5.03	3.78
-0.10	25.5	46.00	15.43	4.88	5.03	2.95
-0.10	30.5	46.00	15.43	4.88	5.03	2.83
-0.10	50.5	46.00	15.43	4.89	5.03	2.73
-0.10	60.5	46.00	15.43	4.89	5.03	2.72
-0.10	200.5	46.00	15.43	4.89	5.03	2.72
-3.3734	10.5	43.76	16.41	4.99	5.34	6.53
-3.3734	15.5	43.76	16.41	5.07	5.34	5.01
-3.3734	25.5	43.76	16.41	5.14	5.34	3.78
-3.3734	30.5	43.76	16.41	5.19	5.34	2.95
-3.3734	50.5	43.76	16.41	5.19	5.34	2.83
-3.3734	60.5	43.76	16.40	5.20	5.34	2.73
-3.3734	200.5	43.76	16.41	5.20	5.34	2.72
-3.3734	10.5	43.76	16.41	5.20	5.34	2.72
-152.76	15.5	9.11	150.05	45.68	48.87	6.53
-152.76	25.5	9.11	150.05	46.42	48.87	5.01
-152.76	30.5	9.11	150.05	47.02	48.87	3.78
-152.76	50.5	9.11	150.05	47.42	48.87	2.95
-152.76	60.5	9.11	150.05	47.49	48.87	2.82
-152.76	200.5	9.11	150.05	47.53	48.87	2.73
-152.76	10.5	9.11	150.05	47.54	48.87	2.72
-152.76	15.5	9.11	150.05	47.54	48.87	2.72
-200	25.5	8.54	169.16	51.49	55.09	6.53
-200	30.5	8.54	169.16	52.33	55.09	5.01
-200	50.5	8.54	169.16	53.01	55.09	3.78
-200	60.5	8.54	169.16	53.46	55.09	2.95
-200	200.5	8.54	169.16	53.53	55.09	2.82
-200	10.5	8.54	169.16	53.59	55.09	2.72
-200	15.5	8.54	169.16	53.59	55.09	2.72
-200	25.5	8.54	169.16	53.59	55.09	2.72

Source: Author's conceptualisation. Effect of size of subsoil domain on multiphysics modelling of earthing rod in single-layer soil.

Table A8: Sensitivity of subsoil depth on the simulation earthing modelling

Pressure head (m)	Subsoil domain					Resistance (Ω)		
	radius (m)	depth (m)	Area (m^2)	θ (%)	ρ (Ωm)	Simulation	Analytical	% Diff.
-3.3734	7.50	10.5	78.75	46.00	15.43	4.69	5.03	6.60
-3.3734	7.50	20	150.00	43.76	16.41	4.99	5.34	6.53
-3.3734	15.5	20	300.00	43.76	16.41	5.14	5.34	3.78
-3.3734	15.5	60	900.00	45.25	15.74	4.94	5.13	3.74
-3.3734	25.5	25	625.00	44.21	16.20	5.13	5.28	2.78
-3.3734	25.5	60	1500.00	45.25	15.74	4.99	5.13	2.68
-3.3734	50.5	20	1010.00	43.76	16.40	5.19	5.34	2.87
-3.3734	55.5	20	1110.00	43.76	16.41	5.19	5.34	2.87
-3.3734	60.5	20	1210.00	43.76	16.41	5.19	5.34	2.86
-3.3734	65.5	10.5	687.75	41.73	17.39	5.42	5.66	4.31
-3.3734	65.5	15.5	1015.25	43.11	16.71	5.26	5.44	3.29
-3.3734	65.5	20	1310.00	43.76	16.41	5.19	5.34	2.86
-3.3734	65.5	35	2292.50	44.72	15.97	5.08	5.20	2.34
-3.3734	60.5	50	3025.00	45.10	15.81	5.03	5.15	2.22
-3.3734	65.5	131	8580.50	45.66	15.57	4.96	5.07	2.17
-3.3734	80.5	35	2817.50	44.72	15.98	5.08	5.20	2.33
-152.76	65.5	10.5	687.75	9.04	152.17	47.42	49.56	4.31
-152.76	65.5	15.5	1015.25	9.08	151.06	47.58	49.20	3.29
-152.76	65.5	20	1310.00	9.11	150.05	47.47	48.87	2.86
-152.76	65.5	35	2292.50	9.23	146.53	46.60	47.72	2.34
-152.76	65.5	50	3275.00	9.37	142.77	45.47	46.50	2.21
-152.76	65.5	131	8580.50	10.69	113.94	36.30	37.11	2.17
-152.76	80.5	35	2817.50	9.23	146.53	46.61	47.72	2.33

Source: Author's conceptualisation.

Table A9: Resistance reduction different earthing enhancement materials in single layer silty and sandy clay subsoils for varying degrees of saturation

	Sandy clay soil					Silty soil				
		0.1165 m EEM I		0.1165 m EEM II			0.1165 m EEM I		0.1165 m EEM II	
suction soil (kPa)	R_e **(Ω)**	R_{em} **(Ω)**	**RR (%)**	R_{em} **(Ω)**	**RR (%)**	R_e **(Ω)**	R_{em} **(Ω)**	**RR (%)**	R_{em} **(Ω)**	**RR (%)**
0.98	42.90	24.93	41.88	25.29	41.05	4.89	2.98	39.12	3.32	32.19
1.07	42.90	24.93	41.88	25.29	41.05	4.89	2.98	39.12	3.32	32.19
1.09	42.90	24.94	41.87	25.29	41.05	4.89	2.98	39.12	3.32	32.19
1.63	42.92	24.95	41.88	25.30	41.05	4.89	2.98	39.12	3.32	32.19
1.76	42.92	24.95	41.88	25.30	41.05	4.89	2.98	39.12	3.32	32.19
26.98	46.50	27.02	41.90	27.37	41.14	5.11	3.10	39.25	3.44	32.61
33.00	47.84	27.79	41.91	28.14	41.17	5.20	3.15	39.30	3.49	32.77
33.08	47.86	27.80	41.91	28.16	41.17	5.20	3.15	39.30	3.49	32.77
49.03	52.07	30.24	41.92	30.60	41.23	5.47	3.31	39.44	3.65	33.22
147.10	111.33	64.54	42.03	64.89	41.71	8.91	5.30	40.49	5.65	36.61
245.17	276.23	159.71	42.18	160.07	42.05	17.68	10.37	41.36	10.72	39.37
315.98	348.85	201.66	42.19	202.02	42.09	21.42	12.53	41.51	12.88	39.87
490.34	479.67	277.23	42.20	277.59	42.13	27.77	16.20	41.68	16.55	40.40
980.68	732.73	423.40	42.22	423.76	42.17	39.16	22.78	41.84	23.14	40.91
1498.09	930.56	537.67	42.22	538.04	42.18	47.54	27.62	41.90	27.98	41.13
2942.04	1342.50	775.62	42.23	776.01	42.20	63.98	37.12	41.98	37.50	41.38
5884.08	1937.90	1119.60	42.23	1120.00	42.21	86.15	49.94	42.03	50.36	41.55
9806.81	2532.30	1462.90	42.23	1463.40	42.21	107.01	62.01	42.05	62.48	41.61
21192.51	3781.60	2184.60	42.23	2185.20	42.21	148.10	85.80	42.06	86.45	41.63
29420.42	4483.20	2589.90	42.23	2590.70	42.21	170.01	98.50	42.06	99.27	41.61
49034.03	5841.70	3374.70	42.23	3375.80	42.21	210.69	122.09	42.05	123.13	41.56
98068.06	8362.60	4831.10	42.23	4832.70	42.21	281.77	163.38	42.02	165.04	41.43

Source: Author's conceptualisation. Resistance reduction of 0.1165 m radius of earthing enhancement materials (EEM I and EEM II) in a single layer of silty and sandy clay soils for varying degrees of saturation.

Table A10: Suction-induced variability of soil layer resistivity for clayey, silty and sandy clay as top and bottom layer subsoils

Suction (pF)	Clay soil		Silty soil		Sandy clay	
	Clay Top Layer	Clay Bottom Layer	Silty Top layer	Silty Bottom Layer	Sandy Clay Top Layer	Sandy Clay Bottom Layer
1.000	6.90	6.87	15.47	15.43	136.43	135.39
1.039	6.90	6.87	15.48	15.43	136.69	135.39
1.044	6.91	6.87	15.48	15.43	136.73	135.39
1.222	6.95	6.87	15.55	15.43	138.48	135.39
1.255	6.97	6.87	15.56	15.43	138.91	135.39
2.439	12.75	7.13	28.77	15.94	377.16	143.92
2.527	13.66	7.25	31.21	16.20	418.92	147.86
2.528	13.67	7.25	31.25	16.20	419.46	147.92
2.699	15.66	7.64	36.75	17.02	515.08	160.65
3.176	22.99	12.47	58.23	27.78	913.08	344.92
3.398	27.51	22.21	72.19	55.48	1190.6	865.44
3.508	30.07	26.02	80.31	67.34	1358.1	1095.5
3.699	35.09	32.31	96.59	87.44	1705.6	1509.6
4.000	44.75	43.09	129.20	123.48	2442.1	2309.6
4.184	51.93	50.69	154.33	149.94	3040.8	2934.7
4.477	65.80	65.02	204.79	201.88	4311.1	4235.7
4.778	83.91	83.41	273.81	271.88	6169.2	6115.6
5.000	100.37	100.01	339.16	337.73	8033.6	7991.9
5.335	131.50	131.29	468.37	467.46	11964	11936
5.477	147.53	147.36	537.36	536.60	14175	14150
5.699	176.47	176.34	665.56	665.00	18458	18439
6.000	225.01	224.93	889.76	889.39	26409	26396

Source: Author's conceptualisation.

Table A11: Volumetric water contents of soil textures as top and bottom layer soils

Suction (pF)	Sandy clay single layer	Sandy clay layer above Clayey soil	Clayey below Sandy clay soil	Clayey layer alone	Clayey layer above Sandy clay soil	Sandy clay layer below Clayey soil	Sandy clay layer below Silty soil	Sandy clay layer above Silty soil
1.000	38.00	37.90	51.00	51.00	50.90	38.00	38.00	37.90
1.039	38.00	37.88	51.00	51.00	50.88	38.00	38.00	37.88
1.044	38.00	37.87	51.00	51.00	50.87	38.00	38.00	37.87
1.222	38.00	37.71	51.00	51.00	50.71	38.00	38.00	37.71
1.255	38.00	37.67	51.00	51.00	50.67	38.00	38.00	37.67
2.439	37.59	27.38	50.15	50.55	38.87	37.22	37.22	27.38
2.527	37.45	26.54	49.76	50.39	37.77	36.89	36.89	26.54
2.528	37.45	26.53	49.76	50.38	37.75	36.88	36.88	26.53
2.699	37.04	25.00	48.59	49.91	35.70	35.88	35.88	25.00
3.176	33.98	21.40	39.24	46.21	30.68	28.13	28.14	21.40
3.398	30.50	20.02	31.09	41.92	28.69	21.70	21.70	20.02
3.508	27.86	19.39	29.29	38.62	27.77	20.44	20.44	19.39
3.699	21.04	18.39	27.07	30.07	26.29	18.92	18.92	18.39
4.000	17.59	17.01	24.51	25.10	24.21	17.21	17.21	17.01
4.184	16.58	16.26	23.25	23.55	23.07	16.38	16.38	16.26
4.477	15.34	15.22	21.52	21.64	21.44	15.27	15.27	15.22
4.778	14.35	14.30	20.02	20.07	19.99	14.32	14.32	14.30
5.000	13.74	13.71	19.05	19.08	19.04	13.72	13.72	13.71
5.335	12.96	12.95	17.78	17.79	17.77	12.95	12.95	12.95
5.477	12.67	12.66	17.30	17.30	17.29	12.66	12.66	12.66
5.699	12.26	12.25	16.61	16.61	16.60	12.26	12.26	12.25
6.000	11.78	11.78	15.78	15.78	15.78	11.78	11.78	11.78

Source: Author's conceptualisation.

Table A12: Resistance vertical earth rod in single- and two-layer subsoils

Suction (pF)	Single-layer subsoil			Two-layer subsoil					
	Clay	Silt	Sandy clay	CY-SC	SC-CY	CY-ST	ST-CY	SC-ST	ST-SC
1.000	2.18	4.89	42.90	5.48	3.54	3.28	2.80	7.63	11.17
1.039	2.18	4.89	42.90	5.48	3.54	3.28	2.80	7.63	11.17
1.044	2.18	4.89	42.90	5.48	3.54	3.28	2.80	7.63	11.17
1.222	2.18	4.89	42.92	5.49	3.54	3.29	2.80	7.63	11.19
1.255	2.18	4.89	42.92	5.50	3.54	3.29	2.80	7.63	11.19
2.439	2.29	5.11	46.50	8.90	3.68	4.40	3.15	8.10	17.06
2.527	2.33	5.20	47.84	9.58	3.74	4.60	3.24	8.23	18.42
2.528	2.33	5.20	47.86	9.59	3.74	4.61	3.24	8.23	18.44
2.699	2.46	5.47	52.07	11.05	3.93	5.05	3.46	8.66	21.48
3.176	4.00	8.91	111.33	17.51	6.44	7.96	5.65	14.17	37.78
3.398	7.07	17.68	276.23	22.64	11.60	12.44	9.68	28.38	54.86
3.508	8.27	21.42	348.85	25.04	13.63	14.26	11.26	34.49	62.48
3.699	10.26	27.77	479.67	29.55	16.97	17.42	13.94	44.87	76.92
4.000	13.67	39.16	732.73	38.09	22.70	23.16	18.64	63.55	105.09
4.184	16.07	47.54	930.56	44.40	26.74	27.35	22.00	77.29	126.66
4.477	20.60	63.98	1342.50	56.58	34.35	35.44	28.41	104.31	170.03
4.778	26.43	86.15	1937.90	72.49	44.13	46.08	36.73	140.79	229.60
5.000	31.69	107.01	2532.30	86.96	52.96	55.84	44.29	175.16	286.26
5.335	41.60	148.10	3781.60	114.38	69.59	74.51	58.64	242.97	398.96
5.477	46.69	170.01	4483.20	128.51	78.15	84.22	66.05	279.15	459.43
5.699	55.87	210.69	5841.70	154.05	93.58	101.88	79.48	346.39	572.24
6.000	71.26	281.77	8362.60	196.94	119.45	131.86	102.11	464.04	770.61

Source: Author's conceptualisation. Resistance (Ω) of 3 m long cylindrical driven earth rod in single (clayey, silty and sandy clay) and two-layer subsoils with 1.4 m top layer depth: clay-sandy clay (CY-SC), clay-silty (CY-ST), silty-clay (ST-CY), silty-sandy clay (ST-SC), sandy clay-silty (SC-ST), and sandy clay-clay.

Table A13: Volumetric water contents within the subsoil domain and region of influence of vertical rod of three single-layer subsoils

soil	Clay soil		Silty soil		Sandy clay soil	
suction (pF)	ROI	SD	ROI	SD	ROI	SD
1.0000	50.99	51.00	46.00	46.00	37.99	38.00
1.0393	50.99	51.00	45.99	46.00	37.99	38.00
1.0442	50.99	51.00	45.99	46.00	37.99	38.00
1.2219	50.98	50.99	45.98	45.99	37.98	37.99
1.2549	50.98	50.99	45.98	45.99	37.98	37.99
2.4395	48.16	49.86	41.93	44.37	35.44	36.98
2.5270	47.15	49.46	40.42	43.77	34.57	36.63
2.5281	47.14	49.46	40.40	43.76	34.55	36.62
2.6990	44.18	48.26	35.99	41.98	32.03	35.60
3.1761	32.13	39.04	18.40	28.47	22.43	27.97
3.3979	29.37	31.03	15.07	17.09	20.49	21.66
3.5081	28.26	29.25	13.84	14.95	19.73	20.41
3.6990	26.56	27.05	12.10	12.59	18.58	18.90
4.0000	24.32	24.50	10.02	10.18	17.08	17.20
4.1840	23.14	23.24	9.03	9.11	16.31	16.37
4.4771	21.47	21.52	7.76	7.79	15.24	15.26
4.7782	20.00	20.02	6.77	6.78	14.31	14.32
5.0000	19.04	19.05	6.18	6.19	13.72	13.72
5.3347	17.78	17.78	5.49	5.49	12.95	12.95
5.4771	17.29	17.30	5.25	5.25	12.66	12.66
5.6990	16.61	16.61	4.93	4.93	12.26	12.26
6.000	15.78	15.78	4.59	4.59	11.78	11.78

Source: Author’s conceptualisation.

Table A14: Resistance of vertical earth rod relative to the subsoil domain and region of influence of vertical rod of three single-layer subsoils

soil	Clay soil		Silty soil		Sandy clay soil	
suction (pF)	ROI	SD	ROI	SD	ROI	SD
1.0000	2.05	2.18	4.62	4.89	40.52	42.90
1.0393	2.06	2.18	4.62	4.89	40.52	42.90
1.0442	2.06	2.18	4.62	4.89	40.52	42.90
1.2219	2.06	2.18	4.62	4.89	40.56	42.92
1.2549	2.06	2.18	4.62	4.89	40.56	42.92
2.4395	2.33	2.29	5.17	5.11	49.85	46.50
2.5270	2.44	2.33	5.41	5.20	53.76	47.84
2.5281	2.45	2.33	5.41	5.20	53.82	47.86
2.6990	2.83	2.46	6.25	5.47	67.98	52.07
3.1761	6.10	4.00	15.05	8.91	228.41	111.33
3.3979	7.72	7.07	20.00	17.68	324.11	276.23
3.5081	8.58	8.27	22.68	21.42	378.59	348.85
3.6990	10.19	10.26	27.89	27.77	488.42	479.67
4.0000	13.20	13.67	37.99	39.16	715.27	732.73
4.1840	15.39	16.07	45.66	47.54	897.25	930.56
4.4771	19.59	20.60	60.92	63.98	1280.70	1342.50
4.7782	25.04	26.43	81.68	86.15	1839.10	1937.90
5.0000	29.98	31.69	101.28	107.01	2398.10	2532.30
5.3347	39.31	41.60	139.99	148.10	3575.40	3781.60
5.4771	44.11	46.69	160.65	170.01	4237.20	4483.20
5.6990	52.77	55.87	199.02	210.69	5518.90	5841.70
6.0000	67.30	71.26	266.10	281.77	7898.10	8362.60

Source: Author's conceptualisation. Resistance of vertical earth rod concerning soil domain (SD) and region of influence (ROI) single-layer subsoil models of clayey, silty, and sandy clay soils

Table A15: Resistance of vertical earth rod relative to the region of influence and presence of infinite element domain for two two-layer subsoil models

Top layer depth (m)	**model**	**Soil suction (pF)**									
		1		**2.527**		**4.184**		**5**		**6**	
		ST-SC	**SC-ST**	**ST-SC**	**SC-ST**	**ST-SC**	**SC-ST**	**SC-ST**	**ST-SC**	**SC-ST**	**ST-SC**
	ROI	18.92	5.32	30.89	6.14	243.40	53.19	558.87	118.22	1531.50	311.11
0.5 m	SD	20.96	5.59	30.95	5.94	276.88	54.93	645.06	123.86	1788.10	326.65
	ROI	14.38	5.86	24.42	6.71	170.12	59.06	384.68	131.48	1037.60	346.43
0.8 m	SD	16.17	6.13	25.40	6.53	197.64	60.69	453.02	137.05	1236.40	361.85
	ROI	9.74	7.37	16.91	8.38	106.36	76.06	237.41	169.99	631.87	449.48
1.4 m	SD	11.17	7.64	18.42	8.24	126.66	77.39	286.26	175.37	770.61	464.60
	ROI	4.41	24.45	8.86	41.71	47.28	408.53	105.73	994.56	282.12	2899.10
3.0 m	SD	4.88	24.58	9.21	41.90	54.21	407.45	123.04	999.02	332.91	2914.90
	ROI	4.79	36.93	7.03	75.68	49.09	833.44	108.80	2214.20	287.08	7297.50
3.5 m	SD	5.40	37.04	7.75	75.90	57.73	838.30	129.52	2228.90	345.77	7350.40
	ROI	4.71	38.05	8.87	70.21	47.93	855.47	106.20	2273.50	280.01	7489.50
4.0 m	SD	5.21	38.31	9.45	70.68	55.25	864.45	123.88	2299.10	330.37	7579.00

Source: Author's conceptualisation. Earthing resistance due to vertical rod in the region of influence (ROI) of vertical rod and infinite subdomain (SD) model for two two-layer subsoils (silty top-sandy clay (ST-SC) bottom and sandy clay top-silty (SC-ST) bottom subsoils).

Table A16: Coefficients of regression and corresponding coefficient of determination for minimum water content for silty subsoil

Range of Saturation depth (m)	a	b	c	R^2	Range of θ_{min}
0.0 – 0.09	-0.0067448	-8.674070	0.466894	0.999	0.46000 – 0.45225
0.1 – 0.19	-0.0911931	-1.153970	0.553469	1	0.45111 – 0.43993
0.2 – 0.49	0.338883	0.432219	0.127896	1	0.43863 – 0.42022
0.5 – 0.99	0.214901	0.803747	0.257231	1	0.40101 – 0.35420
1.0 – 1.99	0.223115	0.654377	0.237348	1	0.35343 – 0.29792
2.0 – 2.99	0.218021	0.462351	0.211001	1	0.29752 – 0.26568
3.0 – 3.99	0.207004	0.350632	0.193110	1	0.26543 – 0.24419
4.0 – 4.99	0.196125	0.280965	0.180260	1	0.24401 – 0.22852
5.0 – 5.99	0.186656	0.234800	0.170681	1	0.22839 – 0.21641
6.0 – 6.99	0.178210	0.200841	0.162895	1	0.21630 – 0.20667
7.0 – 7.99	0.170634	0.174558	0.156298	1	0.20658 – 0.19860
8.0 – 8.99	0.165021	0.157143	0.151580	1	0.19852 – 0.19176
9.0 – 9.99	0.159651	0.142017	0.147224	1	0.19170 – 0.18586
10.0 – 11.0	0.155124	0.130004	0.143531	1	0.18636 – 0.18065

Source: Author's conceptualisation. Coefficients of regression model for minimum water content ($\theta_{\min}$) of silty soil and the coefficient of determination R^2.

Table A17: Water content gradient function coefficients and minimum volumetric water content valid for less than 10.5 m depth of single-layer subsoil

h_p(m)	a	b	c	θ_{min}	R^2
0.5	0.401053	0.295672	0.000000	0.40101	0.9999
1.0	0.133733	0.615232	0.219240	0.35343	0.9998
1.5	0.078380	0.704148	0.242277	0.32097	0.9999
2.0	0.054254	0.709670	0.243435	0.29752	0.9999
2.5	0.040437	0.690438	0.240011	0.27963	0.9999
3.0	0.031500	0.663936	0.235442	0.26543	0.9998
3.5	0.025292	0.636172	0.230713	0.25379	0.9997
4.0	0.020779	0.609222	0.226125	0.24401	0.9994
4.5	0.017375	0.583971	0.221804	0.23565	0.9991
5.0	0.014736	0.560604	0.217771	0.22839	0.9988
5.5	0.012647	0.539075	0.214015	0.22199	0.9984
6.0	0.010963	0.519273	0.210521	0.21630	0.9980
6.5	0.009584	0.501037	0.207268	0.21120	0.9975
7.0	0.008440	0.484253	0.204229	0.20658	0.9971
7.5	0.007482	0.468726	0.201386	0.20238	0.9966
8.0	0.006671	0.454333	0.198719	0.19852	0.9961
8.5	0.005977	0.440970	0.196212	0.19498	0.9956
9.0	0.005832	0.428526	0.193850	0.19170	0.9950
9.5	0.004865	0.416906	0.191619	0.18865	0.9945
10.0	0.004415	0.406032	0.189507	0.18581	0.9940
10.5	0.004402	0.395830	0.187503	0.18315	0.9934

Source: Author's conceptualisation. Coefficients of gradient function of water content θ(z) and minimum volumetric water content (θ_{min}) of homogeneous single soil for different ranges of pressure head (h_p) valid for 0-10.5 m subsoil depth.

Table A18: Coefficients of the regression of water content for subsoil depth of 0.1 m

Range of Saturation depth (m)	a	b	c	r^2	Range of $\theta_{(z=0.1)}$
0.1 – 0.19	-0.002876	-8.61779	0.466957	0.999	0.4600
0.2 – 0.49	-1.69490	-0.07368	2.171480	0.999	0.46000 – 0.45225
0.5 – 0.99	0.234565	0.787931	0.254782	1	0.45111 – 0.41417
1.0 – 1.99	0.238299	0.678939	0.240505	1	0.41293 – 0.36232
2.0 – 2.99	0.225857	0.420302	0.203992	1	0.36148 – 0.30211
3.0 – 3.99	0.215778	0.359669	0.194666	1	0.26803 – 0.24603
4.0 – 4.99	0.202861	0.286681	0.181388	1	0.24584 – 0.22990
5.0 – 5.99	0.192009	0.23597	0.171517	1	0.22976 – 0.21750
6.0 – 6.99	0.182882	0.204532	0.163782	1	0.21739 – 0.20756
7.0 – 7.99	0.174560	0.177290	0.157003	1	0.20747 – 0.19934
8.0 – 8.99	0.168101	0.158472	0.151954	1	0.19927 – 0.19240
9.0 – 9.99	0.161569	0.141070	0.146940	1	0.19233 – 0.18641
10.0 – 11.0	0.156559	0.128753	0.143154	1	0.18581 – 0.18114

Source: Author's conceptualisation. Coefficients of the regression models for water content at depth 0.1 m, $\theta_{(z=0.1\ m)}$

Table A19: Water content gradient function coefficients for 0.1 m to 10.5 m depth of single-layer silty subsoil

z_s(m)	a	b	c	$\theta_{(z=0.1)}$	R^2	Range of soil depth
0.5	0.401111	0.295198	0.000000	0.41293	0.9997	$0 \leq z \leq 0.5$
1.0	0.238710	0.384771	0.112415	0.36148	0.999	$0 \leq z \leq 1.0$
1.5	0.097829	0.605815	0.221644	0.32659	0.9992	$0 \leq z \leq 1.5$
2.0	0.061119	0.660624	0.235875	0.30168	0.9995	$0 \leq z \leq 2.0$
2.5	0.0398395	0.695182	0.240842	0.28287	0.9999	$0 \leq z \leq 2.5$
3.0	0.0308859	0.669438	0.236384	0.26804	0.9998	$0 \leq z \leq 3.0$
3.5	0.0256818	0.630860	0.230425	0.25595	0.9997	$0 \leq z \leq 3.5$
4.0	0.0207488	0.608729	0.226400	0.24584	0.9995	$0 \leq z \leq 4.0$
4.5	0.0171172	0.586662	0.222415	0.23723	0.9993	$0 \leq z \leq 4.5$
5.0	0.0143550	0.565472	0.218589	0.22976	0.9999	$0 \leq z \leq 5.0$
5.5	0.0122000	0.545482	0.214968	0.22321	0.9987	$0 \leq z \leq 5.5$
6.0	0.0106979	0.523103	0.211200	0.21739	0.9981	$0 \leq z \leq 6.0$
6.5	0.0090945	0.509353	0.208359	0.21218	0.9978	$0 \leq z \leq 6.5$
7.0	0.0079528	0.493129	0.205355	0.20747	0.9974	$0 \leq z \leq 7.0$
7.5	0.0070037	0.478022	0.202531	0.20319	09969	$0 \leq z \leq 7.5$
8.0	0.0062061	0.463939	0199875	0.19927	0.9964	$0 \leq z \leq 8.0$
8.5	0.0055296	0.450795	0.197371	0.19566	0.9959	$0 \leq z \leq 8.5$
9.0	0.0049509	0.438505	0.195007	0.19233	0.9953	$0 \leq z \leq 9.0$
9.5	0.0047588	0.419167	0.192055	0.18924	0.9946	$0 \leq z \leq 9.5$
10.0	0.0043199	0.408150	0.189920	0.18636	0.9941	$0 \leq z \leq 10.0$
10.5	0.0039352	0.397818	0.187895	0.18366	0.9935	$0 \leq z \leq 10.5$
12	0.0030289	0.370347	0.182398	0.17652	0.9919	$0 \leq z \leq 12.0$
15	0.0019125	0.327291	0.173402	0.16531	0.9887	$0 \leq z \leq 15.0$
18	0.0128494	0.294910	0.166272	0.15679	0.9856	$0 \leq z \leq 18.0$

Source: Author's conceptualisation. Coefficients for θ(z) at depth between 0.1 m and 10.5 m of single-layer silty subsoil

Table A20: Comparison of resistance evaluated from gradient function and hydro-geophysical earthing model

Position of z_s with respect to L_r and $3.5L_r$	**z_s**	**Average water content**		**Soil resistivity**		**Earth rod resistance**	
		Simulation	**Analytical**	**Simulation**	**Analytical**	**Simulation**	**Analytical**
$0 < z_s < L_r$	2	0.4358	0.4357	16.49	16.49	5.10	5.37
$z_s = L_r$	3	0.4133	0.4133	17.60	17.59	5.45	5.73
$L_r < z_s < 3.5L_r$	6	0.3313	0.3323	23.19	23.09	7.18	7.52
$z_s = 3.5L_r$	10.5	0.2235	0.2484	38.59	33.58	11.95	10.94
$z_s \geq 3.5L_r$	12	0.20556	0.2196	43.21	39.51	13.37	12.87
$z_s \geq 3.5L_r$	15	0.1839	0.1914	50.31	48.06	15.57	15.65
$z_s \geq 3.5L_r$	18	0.1703	0.1750	56.93	53.93	17.35	17.56

Source: Author's conceptualisation. Comparison of resistance evaluated from gradient function of water content in the region of influence vertical rod in silty to resistance evaluated from post-simulation from infinite model of subsoil.

Table A21: Coefficients of the expanded Fourier series from the equation of soil suction of three climates

Coefficients U_m	U_m: non-zero evaluations of m = 0, 1, 2, 3, ...		
	Sub – humid	Arid	Semi-Arid
U_0	7.0333	10.3667	8.7000
U_1	0.7958	-0.7958	1.5915
U_2	0.6892	-0.6892	-0.5305
U_3	0.5305	-0.5305	0.3183
U_4	0.3446	-0.3446	-0.2274
U_5	0.1592	-0.1592	0.1768
U_6	-0.1137	0.1137	-0.1447
U_7	-0.1723	0.1723	0.1224
U_8	-0.1768	0.1768	-0.1061
U_9	-0.1378	0.1378	0.0936

Source: Author's conceptualisation.

Table A22: Climatic frequency (n_f) and soil diffusion coefficient (α) for different time scale

Time Scale	n_f (cycle/time)	α (m^2/time)
Second, (s)	32.150E-09	25E-9
Minute (min)	1.9290E-06	1.5E-6
Hour (hr)	1.15741E-04	90E-6
Day (d)	0.0028	0.0022
Month (mon)	0.0833	0.0648
Year (yr)	1.0000	1.5552

Source: Author's conceptualisation.

Table A23: Daily variation of the volumetric water content of silty, sandy clay and clay subsoils in sub-humid, arid, and semi-arid climates

	climate Surface			Volumetric water content (%)								
	Suction (pF)			Sub-humid climate			Arid climate			Semi-Arid climate		
days	Sh	Ad	SAd	ST	SC	CY	ST	SC	CY	ST	SC	CY
0	5.57	3.13	5.66	5.11	12.48	16.99	30.79	29.28	40.64	4.99	12.33	16.73
10	5.63	3.07	5.60	5.03	12.38	16.82	32.99	30.52	42.16	5.06	12.43	16.90
20	5.44	3.26	5.51	5.30	12.73	17.40	23.99	25.47	35.96	5.21	12.61	17.20
30	4.59	4.11	5.46	7.37	14.88	20.92	9.52	16.70	23.74	5.28	12.69	17.35
40	3.40	5.30	5.46	17.06	21.65	31.01	5.55	13.02	17.90	5.28	12.70	17.36
50	2.71	5.99	5.39	41.85	35.53	48.17	4.59	11.79	15.80	5.39	12.83	17.59
60	2.84	5.86	5.21	39.75	34.34	46.76	4.73	11.98	16.14	5.73	13.22	18.23
70	3.24	5.46	5.01	24.97	25.99	36.62	5.28	12.69	17.35	6.17	13.70	19.02
80	3.32	5.38	4.88	19.95	23.19	33.14	5.41	12.85	17.61	6.48	14.03	19.54
90	3.11	5.59	4.80	31.58	29.73	41.19	5.08	12.45	16.93	6.72	14.26	19.93
100	3.00	5.70	4.61	35.48	31.92	43.86	4.94	12.26	16.61	7.31	14.83	20.83
110	3.08	5.62	4.28	32.80	30.41	42.03	5.04	12.39	16.84	8.63	15.98	22.64
120	3.11	5.59	3.96	31.38	29.61	41.05	5.09	12.46	16.95	10.46	17.41	24.82
130	3.05	5.65	3.78	33.81	30.99	42.72	5.00	12.35	16.76	11.86	18.41	26.32
140	3.07	5.63	3.63	33.16	30.61	42.27	5.02	12.38	16.81	13.34	19.40	27.78
150	3.19	5.51	3.22	27.65	27.51	38.48	5.20	12.60	17.19	25.85	26.50	37.24
160	3.21	5.49	2.45	26.65	26.96	37.79	5.23	12.64	17.26	44.33	36.95	49.84
170	3.05	5.65	1.61	33.77	30.96	42.69	5.00	12.35	16.77	45.96	37.96	50.96
180	2.95	5.75	1.24	37.13	32.86	44.99	4.86	12.16	16.45	45.99	37.99	50.99
190	3.05	5.65	1.61	33.77	30.96	42.69	5.00	12.35	16.77	45.96	37.96	50.96
200	3.21	5.49	2.45	26.65	26.96	37.79	5.23	12.64	17.26	44.33	36.95	49.84
210	3.19	5.51	3.22	27.65	27.51	38.48	5.20	12.60	17.19	25.85	26.50	37.24
220	3.07	5.63	3.63	33.16	30.61	42.27	5.02	12.38	16.81	13.34	19.40	27.78
230	3.05	5.65	3.78	33.81	30.99	42.72	5.00	12.35	16.76	11.86	18.41	26.32
240	3.11	5.59	3.96	31.38	29.61	41.05	5.09	12.46	16.95	10.46	17.41	24.82
250	3.08	5.62	4.28	32.80	30.41	42.03	5.04	12.39	16.84	8.63	15.98	22.64
260	3.00	5.70	4.61	35.48	31.92	43.86	4.94	12.26	16.61	7.31	14.83	20.83
270	3.11	5.59	4.80	31.58	29.73	41.19	5.08	12.45	16.93	6.72	14.26	19.93
280	3.32	5.38	4.88	19.95	23.19	33.14	5.41	12.85	17.61	6.48	14.03	19.54
290	3.24	5.46	5.01	24.97	25.99	36.62	5.28	12.69	17.35	6.17	13.70	19.02
300	2.84	5.86	5.21	39.75	34.34	46.76	4.73	11.98	16.14	5.73	13.22	18.23
310	2.71	5.99	5.39	41.85	35.53	48.17	4.59	11.79	15.80	5.39	12.83	17.59
320	3.40	5.30	5.46	17.06	21.65	31.01	5.55	13.02	17.90	5.28	12.70	17.36
330	4.59	4.11	5.46	7.37	14.88	20.92	9.52	16.70	23.74	5.28	12.69	17.35
340	5.44	3.26	5.51	5.30	12.73	17.40	23.99	25.47	35.96	5.21	12.61	17.20
350	5.63	3.07	5.60	5.03	12.38	16.82	32.99	30.52	42.16	5.06	12.43	16.90
360	5.57	3.13	5.66	5.11	12.48	16.99	30.79	29.28	40.64	4.99	12.33	16.73
370	5.63	3.07	5.60	5.03	12.38	16.82	32.99	30.52	42.16	5.06	12.43	16.90
380	5.44	3.26	5.51	5.30	12.73	17.40	23.99	25.47	35.96	5.21	12.61	17.20

Source: Author's conceptualisation. Silty (ST), sandy clay (SC), and clayey (CY) subsoils in sub-humid (Sh), arid (Ad), and semi-arid (SAd) climates.

Table A24: Resistivity of silty, sandy clay, and clayey subsoils in sub-humid, arid, and semi-arid climates.

	silty soil resistivity			Sandy clay soil resistivity			clayey soil resistivity		
days	**sub-humid**	**arid**	**semi-arid**	**sub-humid**	**arid**	**semi-arid**	**sub-humid**	**arid**	**semi-arid**
0	588.80	25.45	638.31	15868.00	302.34	17530.00	159.26	11.48	170.40
10	620.44	23.31	606.42	16926.00	264.78	16456.00	166.40	10.54	163.24
20	520.11	35.14	552.20	13616.00	482.86	14660.00	143.56	15.39	150.93
30	226.29	138.69	528.96	4876.10	2665.50	13902.00	71.53	47.49	145.60
40	55.91	452.58	527.30	873.78	11469.00	13848.00	22.35	127.78	145.21
50	17.33	881.83	493.65	165.42	26119.00	12766.00	7.79	223.33	137.42
60	18.47	780.45	414.80	183.40	22465.00	10299.00	8.33	201.63	118.79
70	33.34	528.77	340.64	450.02	13896.00	8077.00	14.71	145.55	100.73
80	45.00	490.41	301.72	674.29	12663.00	6954.00	18.85	136.66	91.01
90	24.64	599.15	277.23	287.90	16213.00	6264.40	11.12	161.60	84.78
100	21.27	664.12	230.23	229.66	18409.00	4981.10	9.62	176.15	72.57
110	23.48	617.52	165.65	267.62	16828.00	3318.50	10.61	165.74	55.10
120	24.84	596.38	118.01	291.53	16120.00	2184.20	11.21	160.98	41.49
130	22.60	632.49	96.17	252.23	17333.00	1697.40	10.22	169.10	34.98
140	23.16	622.70	80.15	262.24	17002.00	1356.40	10.48	166.90	30.05
150	29.21	553.69	31.86	371.49	14708.00	420.98	13.06	151.27	14.13
160	30.63	543.32	16.15	397.57	14369.00	147.04	13.64	148.90	7.22
170	22.64	631.72	15.45	252.93	17307.00	135.78	10.24	168.92	6.88
180	20.10	700.84	15.44	209.83	19672.00	135.47	9.08	184.26	6.87
190	22.64	631.72	15.45	252.93	17307.00	135.78	10.24	168.92	6.88
200	30.63	543.32	16.15	397.57	14369.00	147.04	13.64	148.90	7.22
210	29.21	553.69	31.86	371.49	14708.00	420.98	13.06	151.27	14.13
220	23.16	622.70	80.15	262.24	17002.00	1356.40	10.48	166.90	30.05
230	22.60	632.49	96.17	252.23	17333.00	1697.40	10.22	169.10	34.98
240	24.84	596.38	118.01	291.53	16120.00	2184.20	11.21	160.98	41.49
250	23.48	617.52	165.65	267.62	16828.00	3318.50	10.61	165.74	55.10
260	21.27	664.12	230.23	229.66	18409.00	4981.10	9.62	176.15	72.57
270	24.64	599.15	277.23	287.90	16213.00	6264.40	11.12	161.60	84.78
280	45.00	490.41	301.72	674.29	12663.00	6954.00	18.85	136.66	91.01
290	33.34	528.77	340.64	450.02	13896.00	8077.00	14.71	145.55	100.73
300	18.47	780.45	414.80	183.40	22465.00	10299.00	8.33	201.63	118.79
310	17.33	881.83	493.65	165.42	26119.00	12766.00	7.79	223.33	137.42
320	55.91	452.58	527.30	873.78	11469.00	13848.00	22.35	127.78	145.21
330	226.29	138.69	528.96	4876.10	2665.50	13902.00	71.53	47.49	145.60
340	520.11	35.14	552.20	13616.00	482.86	14660.00	143.56	15.39	150.93
350	620.44	23.31	606.42	16926.00	264.78	16456.00	166.40	10.54	163.24
360	588.80	25.45	638.31	15868.00	302.34	17530.00	159.26	11.48	170.40
370	620.44	23.31	606.42	16926.00	264.78	16456.00	166.40	10.54	163.24
380	520.11	35.14	552.20	13616.00	482.86	14660.00	143.56	15.39	150.93
390	226.29	138.69	528.96	4876.10	2665.50	13902.00	71.53	47.49	145.60

Source: Author's conceptualisation.

Table A25: Daily variation of ground surface suction and corresponding resistivity of two earthing enhancement materials in sub-humid, arid and semi-arid climates

	Sub-humid climate			Arid climate			Semi-arid climate		
		Resistivity (Ωm)			Resistivity (Ωm)			Resistivity (Ωm)	
Days	Suction (pF)	EEM I	EEM II		EEM I	EEM II		EEM I	EEM II
0	5.57	2.29	8.28	3.13	1.06	3.52	5.66	2.55	9.28
10	5.63	2.45	8.91	3.07	1.06	3.52	5.60	2.38	8.62
20	5.44	1.97	7.03	3.26	1.06	3.52	5.51	2.11	7.59
30	4.59	1.15	3.85	4.11	1.08	3.59	5.46	2.00	7.18
40	3.40	1.06	3.52	5.30	1.70	5.98	5.46	2.00	7.15
50	2.71	1.06	3.52	5.99	4.21	15.45	5.39	1.85	6.60
60	2.84	1.06	3.52	5.86	3.44	12.64	5.21	1.57	5.47
70	3.24	1.06	3.52	5.46	2.00	7.18	5.01	1.36	4.65
80	3.32	1.06	3.52	5.38	1.84	6.54	4.88	1.27	4.31
90	3.11	1.06	3.52	5.59	2.34	8.48	4.80	1.22	4.14
100	3.00	1.06	3.52	5.70	2.69	9.84	4.61	1.15	3.87
110	3.08	1.06	3.52	5.62	2.44	8.85	4.28	1.10	3.65
120	3.11	1.06	3.52	5.59	2.33	8.42	3.96	1.07	3.56
130	3.05	1.06	3.52	5.65	2.52	9.16	3.78	1.07	3.54
140	3.07	1.06	3.52	5.63	2.46	8.95	3.63	1.07	3.53
150	3.19	1.06	3.52	5.51	2.12	7.62	3.22	1.06	3.52
160	3.21	1.06	3.52	5.49	2.07	7.43	2.45	1.06	3.52
170	3.05	1.06	3.52	5.65	2.51	9.14	1.61	1.06	3.52
180	2.95	1.06	3.52	5.75	2.91	10.67	1.24	1.06	3.52
190	3.05	1.06	3.52	5.65	2.51	9.14	1.61	1.06	3.52
200	3.21	1.06	3.52	5.49	2.07	7.43	2.45	1.06	3.52
210	3.19	1.06	3.52	5.51	2.12	7.62	3.22	1.06	3.52
220	3.07	1.06	3.52	5.63	2.46	8.95	3.63	1.07	3.53
230	3.05	1.06	3.52	5.65	2.52	9.16	3.78	1.07	3.54
240	3.11	1.06	3.52	5.59	2.33	8.42	3.96	1.07	3.56
250	3.08	1.06	3.52	5.62	2.44	8.85	4.28	1.10	3.65
260	3.00	1.06	3.52	5.70	2.69	9.84	4.61	1.15	3.87
270	3.11	1.06	3.52	5.59	2.34	8.48	4.80	1.22	4.14
280	3.32	1.06	3.52	5.38	1.84	6.54	4.88	1.27	4.31
290	3.24	1.06	3.52	5.46	2.00	7.18	5.01	1.36	4.65
300	2.84	1.06	3.52	5.86	3.44	12.64	5.21	1.57	5.47
310	2.71	1.06	3.52	5.99	4.21	15.45	5.39	1.85	6.60
320	3.40	1.06	3.52	5.30	1.70	5.98	5.46	2.00	7.15
330	4.59	1.15	3.85	4.11	1.08	3.59	5.46	2.00	7.18
340	5.44	1.97	7.03	3.26	1.06	3.52	5.51	2.11	7.59
350	5.63	2.45	8.91	3.07	1.06	3.52	5.60	2.38	8.62
360	5.57	2.29	8.28	3.13	1.06	3.52	5.66	2.55	9.28
370	5.63	2.45	8.91	3.07	1.06	3.52	5.60	2.38	8.62
380	5.44	1.97	7.03	3.26	1.06	3.52	5.51	2.11	7.59

Source: Author's conceptualisation.

Table A26: Effect of earthing enhancement materials on the daily variation of resistance of vertical earth rod in silty and sandy clay soils under sub-humid and arid climates

Days	silty soil in sub-humid climate			sandy clay soil in sub-humid climate			silty soil in arid climate			sandy clay soil in arid climate		
	Resistance (Ω)											
	w/o EEM	with EEM I	with EEM II	w/o EEM	with EEM I	with EEM II	w/o EEM	with EEM I	with EEM II	w/o EEM	with EEM I	with EEM II
0	186.5	108.1	109.0	5027	2904	2905	8.1	4.8	5.2	96	56	56
10	196.6	113.9	114.8	5362	3098	3099	7.4	4.4	4.8	84	49	49
20	164.8	95.5	96.2	4314	2492	2493	11.1	6.6	6.9	153	88	89
30	71.7	41.6	42.0	1545	892	893	43.9	25.5	25.9	844	488	488
40	17.7	10.4	10.7	277	160	160	143.4	83.1	83.7	3633	2099	2100
50	5.5	3.3	3.7	52	30	31	279.4	162.0	163.6	8275	4780	4782
60	5.9	3.5	3.9	58	34	34	247.3	143.3	144.7	7117	4112	4113
70	10.6	6.3	6.6	143	83	83	167.5	97.1	97.8	4402	2543	2544
80	14.3	8.4	8.7	214	124	124	155.4	90.0	90.7	4012	2318	2318
90	7.8	4.7	5.0	91	53	53	189.8	110.0	110.9	5136	2967	2968
100	6.7	4.0	4.4	73	42	43	210.4	121.9	123.0	5832	3369	3370
110	7.4	4.5	4.8	85	49	49	195.6	113.4	114.3	5331	3080	3081
120	7.9	4.7	5.0	92	53	54	188.9	109.5	110.4	5107	2950	2951
130	7.2	4.3	4.6	80	46	47	200.4	116.1	117.1	5491	3172	3173
140	7.3	4.4	4.7	83	48	49	197.3	114.3	115.3	5387	3112	3113
150	9.3	5.5	5.8	118	68	69	175.4	101.6	102.4	4660	2692	2693
160	9.7	5.8	6.1	126	73	73	172.1	99.7	100.5	4552	2630	2631
170	7.2	4.3	4.6	80	46	47	200.1	116.0	116.9	5483	3168	3168
180	6.4	3.8	4.2	66	39	39	222.0	128.7	129.8	6232	3600	3602
190	7.2	4.3	4.6	80	46	47	200.1	116.0	116.9	5483	3168	3168
200	9.7	5.8	6.1	126	73	73	172.1	99.7	100.5	4552	2630	2631
210	9.3	5.5	5.8	118	68	69	175.4	101.6	102.4	4660	2692	2693
220	7.3	4.4	4.7	83	48	49	197.3	114.3	115.3	5387	3112	3113
230	7.2	4.3	4.6	80	46	47	200.4	116.1	117.1	5491	3172	3173
240	7.9	4.7	5.0	92	53	54	188.9	109.5	110.4	5107	2950	2951
250	7.4	4.5	4.8	85	49	49	195.6	113.4	114.3	5331	3080	3081
260	6.7	4.0	4.4	73	42	43	210.4	121.9	123.0	5832	3369	3370
270	7.8	4.7	5.0	91	53	53	189.8	110.0	110.9	5136	2967	2968
280	14.3	8.4	8.7	214	124	124	155.4	90.0	90.7	4012	2318	2318
290	10.6	6.3	6.6	143	83	83	167.5	97.1	97.8	4402	2543	2544
300	5.9	3.5	3.9	58	34	34	247.3	143.3	144.7	7117	4112	4113
310	5.5	3.3	3.7	52	30	31	279.4	162.0	163.6	8275	4780	4782
320	17.7	10.4	10.7	277	160	160	143.4	83.1	83.7	3633	2099	2100
330	71.7	41.6	42.0	1545	892	893	43.9	25.5	25.9	844	488	488
340	164.8	95.5	96.2	4314	2492	2493	11.1	6.6	6.9	153	88	89
350	196.6	113.9	114.8	5362	3098	3099	7.4	4.4	4.8	84	49	49
360	186.5	108.1	109.0	5027	2904	2905	8.1	4.8	5.2	96	56	56

Source: Author's conceptualisation. Daily variation of resistance of vertical rod with and without earthing enhancement materials (EEM I and EEM II) in silty and sandy clay soils under sub-humid and arid climates.

Appendix B

Appendix B1: Components and forms of energy state of soil water

Total suction ψ [kPa] is expressed in terms of pore water pressure u_w [kPa], pore air pressure u_a [kPa] and osmotic pressure u_π [kPa] as, gravitational pressure u_z

$$\psi = (u_a - u_w) + u_\pi$$

Potential = Force × distance

$$mgd = \rho_w V g l$$

Potential per unit mass, $\mu = gd$ $[N \cdot m \cdot kg^{-1}]$

Potential per unit volume, $\psi = \rho_w gd$ $[N \cdot m^2]$

Potential per unit weight, $H = d$ $[m]$

Pressure head is equivalent to height of water, $H = h = \psi_w / \rho_w g$

where ψ_w, ρ_w and g are the pressure potential, water density and acceleration due to gravity.

Total soil water potential $\psi_T = \psi_P + \psi_z + \psi_s + \psi_a$ $[N \cdot m^2]$

where ψ_P, ψ_z, ψ_s and ψ_a are the pressure, gravitational, osmotic and air pressure potentials.

If ψ_s and ψ_a are negligible, then $\psi_T = \psi_P + \psi_z$

Matric head is the pressure potential is expressed in per unit weight, ψ_T / mg $[m]$

Appendix B2: Chain rule and derivative of the SWRC

Derivative of SWRC

Given that the SWRC function is

$$\theta(h_p) = \theta_r + \frac{1}{\left(1 + \left(\alpha_h |h_p|\right)^n\right)^m}(\theta_s - \theta_r) \qquad m = 1 - \frac{1}{n}, \quad n > 1$$

then the first derivative of SWRC with respect to pressure head is $C(\theta)$ expressed as

$$\frac{\partial \theta}{\partial h_p} = \frac{n^2 \alpha_h \left(\alpha_h |h_p|\right)^{n-1}}{(1-n)\left(1 + \left(\alpha_h |h_p|\right)^n\right)^{\frac{1-2n}{n}}}(\theta_s - \theta_r)$$

The gradient function of water content can be determined from the product

$$\frac{\partial \theta}{\partial z} = \left(\frac{\partial \theta}{\partial h_p}\right)\left(\frac{\partial h_p}{\partial z}\right)$$

$$\frac{\partial \theta}{\partial t} = \left(\frac{\partial \theta}{\partial h_p}\right)\left(\frac{\partial h_p}{\partial t}\right)$$